A STATISTICAL DYNAMIC MODULUS MODEL OF HOT MIX ASPHALT USING JOINT ESTIMATION AND MIXED-EFFECTS ACCOUNTING FOR EFFECTS OF CONFINEMENT, MOISTURE AND ADDITIVES

A DISSERTATION SUBMITTED TO THE GRADUATE DIVISION OF THE UNIVERSITY OF HAWAI‘I AT MĀNOA IN PARTIAL FULFILLMENT OF THE REQUIREMENTS FOR THE DEGREE OF

DOCTOR OF PHILOSOPHY

IN

CIVIL AND ENVIRONMENTAL ENGINEERING

DECEMBER 2016

By

Jose Pablo Corrales

Dissertation Committee:
Adrian R. Archilla, Chairperson
Luis Loria-Salazar
Phillip Ooi
Lin Shen
Peter Flachsbart

Keywords: Asphalt Mixtures, Dynamic Modulus, Modeling

To Calli, Evan and Matteo
Thank you for reminding me of God's love every single day

"Surely your goodness and love will follow me all the days of my life,
And I will dwell in the house of the Lord forever" Psalm 23:6

ACKNOWLEDGEMENTS

First, I would like to thank God for giving me all the traits that I needed to go through this process and succeed. Especially for putting my marvelous wife Calli in my path together with my two major blessings in the entire world, Evan and Matteo. I cannot imagine my life without them in it. Thank you for your unconditional love and patience and for helping me to be a better person.

Second, I would like to express my absolute gratitude to my professor and mentor, Dr. Adrian R. Archilla, who gave me this amazing opportunity and helped me from beginning to end in this journey. Thank you very much for sharing your knowledge and for all your valuable guidance.

To Dr. Luis Loria, thank you very much for accepting to be part of my committee and for your great guidance and friendship. I look forward to working together in more projects.

To my other UH committee members, Dr. Phillip Ooi, Dr. Lin Shen and Dr. Flachsbart, my most sincere gratitude for the trust you deposited in me by accepting to walk this road together.

I would also like to thank my two most amazing lab partners, Bonni Saust and David Ardo, for all the help that I got from them but mainly for their friendship and companionship for long hours. You made my life a lot easier and for that I will always be grateful.

To the people that helped to make this possible by their financial contribution or by supplying all necessary materials: City and County of Honolulu, the University Transportation Center, Grace Pacific, Glover Ltd and Asphalt Hawaii. A special thanks to the Department of Transportation, Airports Division for supporting me inside and outside UH. Particularly to Dennis Lopez and Keith Ishinaga, for their amazing support, patience, friendship and all the trust you put in me.

To my Hawaii Ohana; friends and family that helped us with tons of love all along and made of our visit a fantastic adventure, especially to my outstanding mother in law, Gaylene Nevers, who gave us everything and more and to Nathalie Razo and Matthew Potts and their amazing parents. You have a very special place in heaven guaranteed for being the absolute best.

To my parents, Gerardo and Sandra, who made me the person that I am and taught me to chase my dreams and work hard for them. Thank you for giving me life. Los amo!

Finally, to my UH and XE mates, in whom I found friendship and support along the years, especially the Ph.D. students and alumni that understand this process more than anybody else; thank you Melia, Pasha, Reza, Hui, Lelemia and Ehsan.

ABSTRACT

With the implementation of mechanistic-empirical pavement design methods, dynamic modulus (|E*|) has become the predominant characteristic of Hot Mix Asphalt (HMA) used as the elastic modulus in the computation of stresses and strains in pavement structures.

The predictions of |E*| obtained with the Witczak models currently used in the Mechanistic Empirical Pavement Design Guide (MEPDG) do not account for some HMA characteristics such as polymer modified binders, fibers, confinement and aging effects related to climatic conditions. Therefore, development of models more representative of local materials and conditions are desirable.

In this study, a predictive model for dynamic modulus of HMA was developed taking into consideration several HMA characteristics and testing conditions. 6821 observations of 257 mix specimens from three different laboratory datasets, two from Hawaii and one from Costa Rica, were used to estimate the model parameters. All three data sets contain information about some variables in common such as air voids, binder content, and gradation; however, some datasets contain mix characteristics and testing conditions not available in other datasets such as confinement level, available only in the Hawaiian datasets, and the number of freeze-thaw cycles, available only in the Costa Rican dataset. Important characteristics observed from these datasets include confinement, number of freeze-thaw cycles, binder modifiers (SBS polymers) and mixture additives (e.g. fibers and anti-stripping agents), all of which together with other commonly used variables were found to have statistically significant effects. The model was developed by using joint estimation and mixed-effects techniques. Joint estimation allowed the identification of model parameters available from only some of the databases and the determination of bias parameters. It also resulted in more efficient parameter estimates. The

mixed-effects approach was used to account for unobserved heterogeneities between samples. Using these approaches, together with proper consideration of heteroscedasticity, allowed the estimation of a comprehensive statistical predictive model that satisfies closely all the regression assumptions and that provides accurate values of |E*| for Hawaiian and Costa Rican conditions for any combination of temperature and frequency. These can be used to generate the |E*| inputs that the MEPDG needs to compute |E*| master curves.

TABLE OF CONTENTS

LIST OF TABLES

LIST OF FIGURES

CHAPTER 1: INTRODUCTION AND SUMMARY

1.1 Introduction

In 1996, the Joint Technical Committee on Pavements of the American Association of State Highway and Transportation Officials (ASHTO) initiated the development of the first mechanistic-empirical design guide under the National Cooperative Highway Research Program (NCHRP) Project 1-37A: Guide for the Design of New and Rehabilitated Pavement Structures. As its name suggests, this guide incorporates both mechanistic and empirical methods. The mechanistic approach utilizes analytical calculations to transform pavement influence factors (climate and traffic) and its material properties into critical responses (stress, strain). Afterwards the empirical approach transforms these responses into predicted observed distresses (permanent deformation, fatigue and thermal cracking) and the International Roughness Index (IRI) (Pierce, 2011)

Even though mechanistic-empirical methods were described in the late 1940's as "rational" methods (Hveem and Carmany, 1949), the advancement in computer capabilities regarding storage and speed, newer technologies for pavement evaluation (for both analysis and testing) as well as the creation of the Long Term Pavement Performance (LTPP) database (created to collect the performance of pavements in over 2,000 test sections across the United States and Canada), made possible the reintroduction and development of these methods.

The outcome of this effort was an extensive research document and a software that used these mechanistic-empirical procedures known as the Mechanistic-Empirical Pavement Design Guide, MEPDG (ARA 2004). This software had the advantage of being able to include local climatic conditions, the consideration of the stresses and strains produced by each axle load through the use of load spectra for each axle configuration developed for local conditions (in contrast to the use of Equivalent Single Axle Loads -ESALs- commonly used in empirical methods such as AASHTO 93 (AASHTO, 1993) or even in mechanistically based procedures such as the Asphalt Institute (Asphalt Institute, 2008), which are based on empirical relations of the effects of different load magnitudes developed at the AASHO Road test), and the introduction of a more comprehensive set of required inputs for material properties, making it possible to characterize materials more accurately than by using the structural layer coefficients alone as used in

AASHTO 93 Pavement Design Guide (AASHTO 1993). An illustration of the process followed by the MEPDG is shown in Figure 1.

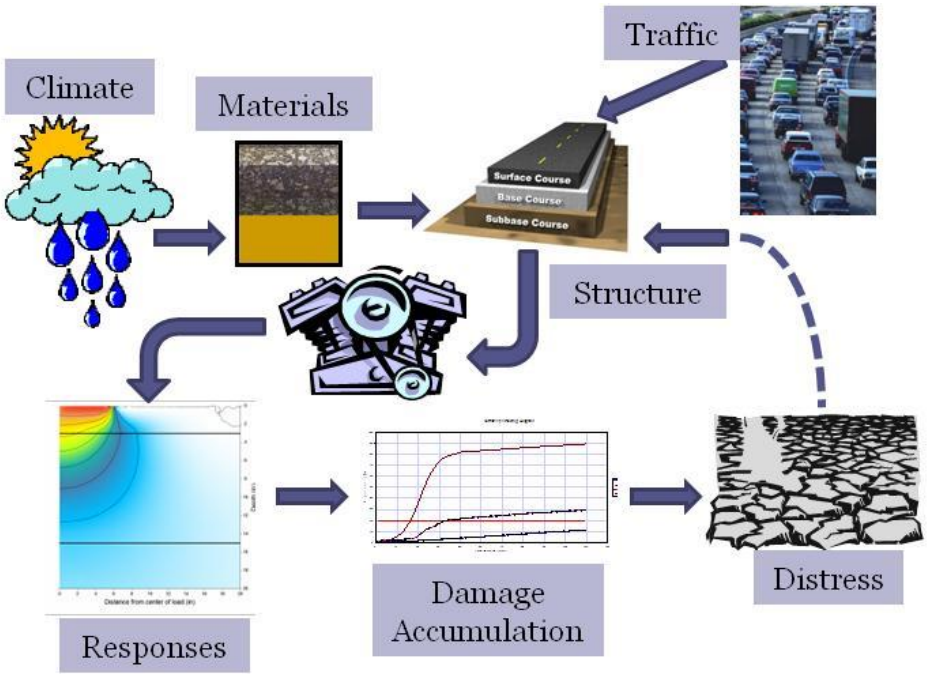

Figure 1. Mechanistic-empirical approach for pavement design.

As can be seen, climate, materials and traffic conditions (influence factors) are introduced in the software (represented by the motor in the middle of the picture) with an initial estimated pavement structure. The mechanistic portion of the software transforms the input factors into strain and stress responses which are used to compute damage accumulation and empirically predict the observed distresses. The design procedure is an iterative one, in which the layer thicknesses are changed until an adequate pavement structure satisfying distress and roughness threshold levels at the end of the design period and at a given reliability level is found.

Some of the most important advantages of the MEPDG include (Pierce, 2011):

- Consideration of a broader range of vehicle types, axle loadings and tire pressures included for analysis,
- Inclusion of material properties more directly related to the performance of pavements,
- Characterization of local materials and climate,
- Improvement of the characterization of existing pavement layers, and
- Improvement of the reliability for the prediction of pavement performance.

With the implementation of the MEPDG, the dynamic modulus (|E*|) test became the test of choice to characterize the stiffness of Hot Mix Asphalt (HMA) in the laboratory. Knowledge of the values of |E*| at different frequencies and temperatures became an essential input for the mechanistic analysis of pavement structures. Currently, most states have implemented or are in the process of calibrating and implementing the MEPDG or other mechanistic-empirical method (Pierce et al. 2014).

The MEPDG is structured into three different levels for its inputs. Level 1 is the most complex one and uses parameters directly measured in the laboratory for the characterization of the pavement materials. Levels 2 and 3 need less data from the lab and instead use models for the prediction of certain material properties. In the case of the dynamic modulus, levels 2 and 3 use one of two models known as the Witczak models, developed through NCHRP 1-37A and NCHRP 1-40D. Although these models were developed with very extensive databases, sometimes their predictions can be imprecise for a given set of materials and climate conditions because of differences in aggregate types with different geological characteristics and the use of different binder types from different sources. In fact, no data from Hawaii were used for the development of these models. Moreover, the use of newer materials and modifiers in the preparation of asphalt mixtures is an aspect that is not accounted for in these models and therefore, the prediction of the behavior of these materials should be studied on a case by case basis.

Consequently, to obtain more accurate values of dynamic modulus for their use on design methods, it is necessary to develop models that are more representative of the conditions of each geographical zone. For this purpose, a laboratory analysis should be performed to determine the influence on |E*| values of the local material characteristics and testing conditions.

This project aims at developing a prediction model for dynamic modulus of asphalt mixtures that takes into consideration different testing conditions, component materials and mixture volumetrics and that provides more accurate values of |E*| throughout the whole range of application in the field (i.e., to predict the behavior of asphalt mixtures for any combination of temperature and frequency with the use of interpolation models know as master curves). To develop the model, |E*| data were collected at the University of Hawaii pavement laboratory (two data sets collected at different times) and at the National Laboratory of Materials and Structural Models at the University of Costa Rica (one data set). Each of the three data sets

contains different characteristics regarding component materials and testing conditions. While all data sets used several different mixture modifiers (e.g. binder modifiers, fibers), the data sets from the University of Hawaii uses different confinement pressures during testing and the data set from Costa Rica includes freeze-thaw conditioning cycles with the objective of capturing the influence of moisture damage on the values of |E*|.

Two statistical approaches are used to develop the model given the characteristics of the data. First, the joint estimation technique is used since data from multiple sources are used. This technique identifies all explanatory variables that are common for all data sets as well as unique variables that have explanatory influence on the model but belong to each data set separately. Through this approach a more robust model can be created. This model relates the data sets through shared characteristics, but also highlight the important features that are unique for each of them. To account for marginal differences between explanatory variables in common between the different databases, the joint estimation approach incorporates bias parameters into the model. The second technique used for the estimation of the model parameters is the mixed-effects approach. Mixed-effects are commonly used for grouped data to describe a response variable by accounting for the correlation between observations within a group (or experimental unit). In the case of the model developed herein, unobserved differences among experimental units (asphalt concrete specimens) due to material differences or sample preparation result in deviations from an overall mean for all samples. The use of the mixed-effects approach is motivated by its capability to account for the variability introduced to the model by unobserved heterogeneity within experimental units.

All samples used for this experiment are representative of common mixtures used in the state of Hawaii and Costa Rica, and for this reason it is expected that the model can be easily implemented in both places. However, a model developed with these characteristics can also be implemented in different regions by adjusting some or all of the model parameters to the corresponding local conditions by following a similar approach or by performing smaller scale studies to determine adjustment factors.

1.2 Research Objectives

The main objective of this study is to estimate a comprehensive predictive model for dynamic modulus |E*| accounting for mixture characteristics commonly used in other studies, such as air voids, effective binder by volume, and gradation, and for other testing and mixture

characteristics such as confinement level, strain level during testing, number of freeze-thaw cycles for simulating moisture sensitivity, and use of anti-stripping agents.

To achieve such ambitious objective, the following two major endeavors were undertaken:

1) A laboratory dynamic modulus database obtained in in this study was combined with a previous one obtained also at the UH pavement laboratory and a third one obtained from LanammeUCR in Costa Rica and merged into a single database with the necessary characteristics for further analysis.
2) The statistical approaches of non-linear mixed effects and joint estimation were applied to this combined database to create a prediction model for dynamic modulus that can be applied in both regions (Hawaii and Costa Rica) for the mechanistic analysis of asphalt pavements.

The resulting model permits the assessment of issues of interests to local authorities, particularly to the Hawaii Department of Transportation Airports Division, such as the comparison of the laboratory performance of different mixtures with unmodified and modified binders with and without the use of synthetic fibers. The model however, opens the possibilities for further studies assessing the effects of factors such as confinement, strain levels, use of anti-stripping agents, and moisture sensitivity.

1.3 Contributions

The model created under this dissertation is expected to predict the values for dynamic modulus of mixtures used in Hawaii and Costa Rica for different mixture characteristics more accurately than the Witzack models. This new model could be used as part of the calibration of a Mechanistic pavement design method for Hawaii and as part of the mechanistic design methods currently being implemented in Costa Rica.

The use of current methods such as the MEPDG or any other design guide without proper calibration can be unreliable for the design of asphalt pavements in Hawaii since they have been calibrated for other locations with different materials and weather characteristics. Costa Rica and Hawaii share a few similarities, specially related to climatic conditions, which makes highway agencies in both places use similar asphalt binders graded using AASHTO methods (AASHTO, 2016). Similar distresses are also observed in both places mainly due to their large annual precipitation. Nevertheless, since not all variables are common to the databases from the two locations (e.g., use of confinement level is available for Hawaii but not for Costa Rica whereas induced moisture damage is available for Costa Rica but not for Hawaii), there is a need to

consider parameters that are unique to each database and to include bias parameters through the joint estimation approach mentioned earlier.

Having the tools to predict the dynamic modulus of asphalt mixtures for these regions will be of great use for the prediction of distresses in pavements with mechanistic-empirical methods and therefore for the selection of appropriate asphalt layer thicknesses. The importance of more accurate tools to predict the dynamic modulus of asphalt materials was noted by Bari, et al. (2006), where an evaluation of the first version of the Witczak model was found to predict values of dynamic modulus that can vary from the measured values by as much as 6 times. This observation led to the development of the modified Witczak model, which was improved with an expanded database and a few changes to its parameters. An over or under-prediction of the dynamic modulus models by a factor of 6 would determine thicknesses that would either be too thin of too thick (respectively). In the first case, an early failure of the pavement would be expected due to a thickness incapable of holding the loads that it was designed for. In the second case, thicknesses larger than necessary, even when they can hold the traffic loads, will still represent an unnecessary over-design implying a very high cost for the local department of transportation and therefore to the users who pay for the roads. Additionally, as mentioned by Zeiada et al. (2014), "the consequence of mis-predicting the pavement distress is a change in the predicted service life". This in turn could have an impact on Quality Control/Quality Assurance analysis when it is included into performance related specifications.

Therefore, the implementation of more accurate prediction models for dynamic modulus is key for a more appropriate asphalt pavement design at all levels. This model can also serve as a starting point for similar models that can be used in other states and countries after the implementation of any necessary calibration procedures to accommodate the characteristics of that location's own asphalt mixture.

1.4 Outline of the dissertation

This dissertation is written in six chapters. Chapters 2 to 6 are organized as follow:

- Chapter 2 presents the theoretical background for the dynamic modulus test as the test of choice for measuring the stiffness of asphalt mixtures. The chapter further explains the use of confinement pressure during testing to better replicate field conditions, and the use of freezing and thawing cycles to induce a severe moisture damage in the mixture. The

final part of this chapter describes some of the most common additives to modify asphalt mixtures that were used during the preparation of the samples tested for this experiment.

- Chapter 3 introduces the statistical approaches that are used to build the prediction model, i.e., joint estimation and mixed-effects. Both approaches are used due to their ability (mentioned earlier) to estimate a model while accounting for differences in data sets and experimental units.
- Chapter 4 describes the three datasets used to create the model. While the first two datasets were produced and gathered in Hawaii, the third dataset was created in Costa Rica. The main characteristics of the materials as well as the testing conditions are discussed in detail in this chapter.
- Chapter 5 details the creation of the prediction model from the initial sigmoidal function (used to define the relationship between |E*| and the frequency (or time) of loading) and through the incorporation of the statistical approaches until the final model was determined.
- Chapter 6 presents the conclusions obtained from this dissertation and some recommendations for the application of the model and further research to be performed in the subject.

CHAPTER 2: BACKGROUND

This chapter presents a synopsis of the dynamic modulus of asphalt mixtures. Section 2.1 begins with the origin of the predictive models that are currently used in the Mechanistic-Empirical Pavement Design Guide (MEPDG), and ends with the calculation of master curves from data collected in the laboratory. After this, the rest of the sections in the chapter provide a discussion about variables included as factors affecting the dynamic modulus of the asphalt mixtures in the predictive model developed in this study. Section 2.2 gives an overview of the use of confinement pressure in the dynamic modulus test, while Section 2.3 gives the background for one of the most recent procedures used to assess the moisture damage in asphalt mixtures. Section 2.4 describes the different mixture modifiers that were used in the samples tested (fibers, binder modifiers, anti-stripping agents.)

2.1 Dynamic modulus of asphalt mixtures

The dynamic modulus (|E*|) measures the stress-strain relationship for an asphalt concrete specimen under a continuous haversine load applied at different combinations of temperature and frequencies. More specifically, |E*| is defined as

$$|E*| = \frac{\sigma_0}{\varepsilon_0} \quad (1)$$

where σ_0 is the peak-to-peak axial stress and ε_0 is the peak-to-peak recoverable axial strain. Another characteristic of the mixture measured along with |E*| is the phase angle, φ, which is the angle needed to be added to the argument of the sine function in the strain sinusoid to simulate the empirically observed difference in time between the occurrence of the peak of the stress and strains sinusoids. Both |E*| and φ are used to predict the time dependent behavior of viscoelastic materials (Archilla, 2013). |E*| has become one of the most important parameters for measuring and comparing the performance characteristics of asphalt mixtures. The MEPDG uses the dynamic modulus as the design stiffness parameter in its linear elastic analyses to compute the strains used in the different transfer functions to predict damage in pavements. Even though the MEPDG is not being used in every state or country, similar design guides are being implemented that include dynamic modulus as the parameter of choice for the same purpose mentioned above. When information about the dynamic modulus of materials is not available for level 1 input, it is estimated through either direct correlation with other material properties, such as the dynamic

shear modulus of the asphalt binder (for level 2 only) or with regression equations developed for this purpose relating the dynamic modulus to several explanatory variables such as air voids, percent passing some sieve sizes, etc. (for both levels 2 and 3). The most commonly used models for these estimations are the Witczak models, developed through the National Cooperative Highway Research Program (NCHRP) studies 1-37A and 1-40D. The first model version was developed by Andrei et al. (1999), using 2750 points from a total of 205 HMA mixtures. This model is shown below in equation (2):

$$log_{10}|E^*| = -1.25 + 0.029\,\rho_{200} - 0.0018(\rho_{200})^2 - 0.0028\,\rho_4 - 0.0048V_a - 0.822\left(\frac{V_{beff}}{V_{beff}+V_a}\right) + \frac{3.872-0.0021\,\rho_4+0.004\,\rho_{38}-0.000017\,(\rho_{38})^2+0.0055\,\rho_{34}}{1+e^{(-0.6033-0.3133\,log(f)-0.3935\,log(\eta))}} \quad (2)$$

where:

|E*| = dynamic modulus of the mix, 10^5 psi,

η = viscosity of the binder at the desired temperature, 10^6 Poise,

f = loading frequency, Hz,

ρ_{200} = % aggregate passing #200 (0.075 mm) sieve,

ρ_4 = cumulative % of aggregates retained on #4 (4.76 mm) sieve,

ρ_{38} = cumulative % of aggregates retained on 3/8 (9.5 mm) sieve,

ρ_{34} = cumulative % of aggregates retained on ¾ (19.5 mm) sieve,

V_a = air voids, % by volume of the mix, and

V_{beff} = effective binder content, % by volume.

The binder viscosity used in this model can be obtained by combining information from traditional tests such as softening point and penetration, viscosity with tube viscometers (absolute viscosity at 140°F (60°C) with the Asphalt Institute or the Cannon-Manning Vacuum Viscometers and kinematic viscosity at 275°F (135°C) with the Zeitfuchs® Cross Arm viscometer) or with more modern tests, such as the Brookfield viscometer that can provide viscosities at a range of temperatures. The second model developed by Bari and Witczak (2006) presents a modified version using 7400 data points from 346 mixtures. This model is shown in equation (3)

$$log_{10}|E^*| = -0.349 + 0.754(|G^*|^{-0.0052}) * \left(6.65 - 0.32\,\rho_{200} + 0.0027(\rho_{200})^2 + 0.011\,\rho_4 - 0.0001\rho_4^2 + 0.006\rho_{38} - 0.00014\rho_{38}^2 - 0.08V_a - 1.06\left(\frac{V_{beff}}{V_{beff}+V_a}\right)\right) + \frac{2.56+0.03V_a+0.71\left(\frac{V_{beff}}{V_{beff}+V_a}\right)+0.012\,\rho_{38}-0.0001\,\rho_{38}^2-0.001\,\rho_{34}}{1+e^{\left(-0.7814-0.5785\,log\left(|G_b^*|\right)+0.8834\,log(\delta_b)\right)}} \quad (3)$$

where:

|E*| = dynamic modulus of the mix, psi,

ρ_{200} = % aggregate passing #200 (0.075 mm) sieve,

ρ_4 = cumulative % of aggregates retained on #4 (4.76 mm) sieve,

ρ_{38} = cumulative % of aggregates retained on 3/8 (9.5 mm) sieve,

ρ_{34} = cumulative % of aggregates retained on ¾ (19.5 mm) sieve,

V_a = air voids, % by volume of the mix,

V_{beff} = effective binder content, % by volume of the mix

$|G_b^*|$ = dynamic shear modulus of binder, psi, and

δ_b = phase angle of binder associated with $|G_b^*|$, degrees.

The $|G_b^*|$ and δ_b values are typically measured at temperatures between 4.4°C and 54.4°C (40°F and 130°F) in increments of around 16.6°C (30°F) using a frequency of 1.59Hz (10 rad/s) with the use of a Dynamic Shear Rheometer. As it will be explained in more detail later, $|G_b^*|$ and δ_b data were not available for all the data sets used for this project and therefore it was not possible to include it in the model. Trying to use available conversions (Bari and Witczack, 2006) to obtain these data has been found to introduce some error in the prediction since many conversions are necessary to predict the required values of |G*| and δ_b (Archilla, 2010). Furthermore, the model has been found to overpredict |E*| even when the |G*| values are directly measured with the dynamic shear rheometer (Robbins and Timm, 2011).

Zeiada et al. (2014) argue that the use of large databases for calibration, such as the ones used for these models, can be a shortcoming since "gross trends, such as the effects of temperature, are captured, but trends with differences across mix types are not" (pp31). The analysis performed by these authors shows that the effects of volumetric changes produce some consistent trends, such as the reduction in |E*| with reduction of air voids. However, while the Witczak model

predicts that the |E*| values will always decrease with an increase in the asphalt content, their laboratory data did not match that trend for most cases. Regarding the aforementioned study, there are two observations that are necessary to point out. First, the trend depicted by the Witczak model regarding asphalt content is expected and was commonly observed in the databases used in this study. Second, the size of the database is not really a problem when trying to capture mixture differences. In fact, it is quite the opposite. The more "valid" data in a database, the higher are the chances of explaining the effect of different factors. Note the emphasis on the word "valid". One of the potential problems with large databases are their higher chances of containing some outliers that may make the explanation of certain effects more difficult. Therefore, it is important to carefully analyze the database for the potential presence of outliers. Another problem is the use of field cross-sectional data (test results for too many different field mixtures with little control of the different factors and without replicates) since in this case important effects may be obscured by for example, high correlations between variables, errors in measurements, self-selection issues, etc. However, when enough points of similar mixtures are included, the trends for a given set of volumetric characteristics might be easier to be identified.

From the evaluation of the predictive characteristics of the Witczak model, Bari et al. (2006), determined that |E*| values estimated with the predictive Equation (2) can vary from the measured values by as much as 6 times. This study led to the modified Witczak model, shown in equation (3), derived with an expanded database to procure the improvement in the prediction of |E*| values. The newer model not only includes more data points but also predicts the dynamic modulus of asphalt mixtures using a set of parameters slightly different from that used in the first model.

Considering, among other things, the potentially large differences between the |E*| values predicted by these models and the actual values, many states and countries have calibrated or are in the process of calibrating the procedures to adjust them for the materials and weather characteristics of the specific region. The availability of material models that better characterize local material performance should result in a more accurate calculation of the pavements' performance period. In this sense, Zeiada et al. (2014) indicate that several models have been proposed over the years, each of them requiring different material properties (e.g. volumetrics) as inputs and using different approaches such as full regression (Witczak model),

micromechanically motivated regression as in the case of the Hirsch model (Christensen et al. 2003), artificial neural networks (Ceylan et al. 2008, Leiva-Villacorta et al. 2013) and other more general regression models (Apeagyei et al. 2012).

The stiffness of HMA is needed over a range of temperatures and frequencies of loading related to the climatic and traffic conditions of the project location; however, in the laboratory the measurement of dynamic modulus is performed at only a few combinations of temperature and frequency specified in the standard testing procedures (AASHTO 2016). For this reason, it is necessary to use an interpolation model that can predict the dynamic modulus values at all temperatures and frequencies. This model is known as "master curve" and it has two main components: a sigmoidal function that defines the shape of the relation between |E*| and the frequency (or time) of loading (Equation (4)), and a second component which defines a shift factor that describes the amount of shifting necessary at different temperatures to match the curve at a reference temperature (Equation (5)). The shift factor can take several functional forms as a function of temperature, T. One example is a quadratic equation as shown in Equation (6). These two models can be used simultaneously to describe the behavior of a mixture at all the frequencies (times of loading) and temperatures of interest. For example, for a given temperature *T*, the shift factor can be computed with Equation (6). This is then used in Equation (5) together with the frequency f to compute a reduced frequency f_r (a fictitious frequency at the reference temperature T_r at which the |E*| is the same as that corresponding to frequency f at temperature *T*). Finally, Equation (4) is used to compute the dynamic modulus at the reduced frequency f_r, corresponding to the actual frequency f and temperature *T*.

$$\log|E^*| = \delta + \frac{\alpha}{1 + e^{\beta+\gamma\left(log\left(\frac{1}{f_r}\right)\right)}} \tag{4}$$

where,

|E*| = dynamic modulus of asphalt mixtures,

f_r = reduced frequency at a reference temperature,

δ = minimum value of log |E*|,

δ+α = maximum value of log |E*|,

β, γ = parameters that describe the shape of the sigmoidal function,

$$a(T) = \frac{f_r}{f} \quad or \quad log\left(\frac{1}{f_r}\right) = log\left(\frac{1}{f}\right) - \log\big(a(T)\big) \tag{5}$$

where,

a(T) = shift factor as a function of the temperature,

f = frequency at the testing temperature,

f_r = reduced frequency at a temperature of reference, and

T = temperature of interest (reference)

As mentioned before, an example of an equation used for computing the shift factor is:

$$log\big(a(T)\big) = AT^2 + BT + C \tag{6}$$

where A, B and C are parameters to be estimated for a given reference temperature T.

One of the most common machines for collecting |E*| laboratory data and the one used in this study, is the Asphalt Mixture Performance Tester (AMPT), shown in Figure 2. To illustrate the use of these equations, an example is provided below with laboratory data collected with the AMPT.

Figure 2. Asphalt Mixture Performance Tester (AMPT) used for dynamic modulus testing

For the dynamic modulus test, the AMPT applies a sinusoidal (haversine) load at different combinations of temperatures and frequencies, and calculates the dynamic modulus as the ratio of the peak-to-peak stress applied and the peak-to-peak recoverable axial strain. The stress is calculated as the deviator force applied over the cross-sectional area of the cylindrical specimen

while the strain is calculated as the average of the three strains measured using three linear variable differential transducers (LVDT) placed at 120 degrees of separation around the sample. Each LVDT is placed between two points separated vertically 70 mm (2.76in) and the strain on each is calculated as the ratio of the deformation of the sample measured axially by each LVDT and their initial length (70 mm). At a given temperature, the process is repeated for several load frequencies, descending from highest to lowest. The temperatures are varied ascending from lowest to highest.

Two methods for the dynamic modulus testing are available as AASHTO standards. The first one, AASHTO T-342 (AASHTO 2016), states that the test should be conducted at -10, 4.4, 21.1, 37.8 and 54°C (14, 40, 70, 100 and 130°F) while using loading frequencies of 0.1, 0.5, 1.0, 5, 10 and 25Hz. This protocol is more commonly used when a Universal Testing Machine (UTM) is used. The second standard, AASHTO PP-61 (AASHTO 2016), which until now has not changed its provisional status (PP: Provisional Practice), is the standard specifically intended for using with an AMPT. This standard recommends the use of three different temperatures to test the asphalt mixture samples. The low and intermediate temperatures, 4°C (39.2°F) and 20°C (68°F) respectively, remain the same for any asphalt grade while the highest testing temperature varies depending on the high temperature performance grade (PG) of the asphalt. A temperature of 40°C (104°F) is recommended as the highest testing temperature for asphalt grades PG64-XX and PG70-XX. In the case of a PG76-XX grade, the maximum testing temperature recommended is 45°C (113°F). This procedure also recommends using the three frequencies of 10, 1 and 0.1Hz for all temperatures with a fourth frequency of 0.01Hz added for the highest testing temperature only.

The first database collected at UH followed the AASHTO T-342 standard regarding testing temperatures and frequencies. This means that even when the AMPT was used, most of the testing was performed at 4 different temperatures, i.e., 4°C, 21°C, 37°C and 54°C (40°F, 70°F, 100°F and 130°F). Besides the fact that the AMPT does not have the capability to reach the lower temperature of -10°C (14°F), this temperature has normally been excluded from testing in more tropical places (such as in Hawaii and Costa Rica) since the behavior of the mixtures at those low temperatures is not a concern for these zones. For this data set, however, several intermediate temperatures were tested at the time, e.g. 14°C, 34°C, 45° (57°F, 93°F, 113°F), with the objective of gathering more information about the available materials. For this same reason,

the frequencies used for this data base included, in several cases, more levels than the ones requested by the standard (i.e. 0.01, 0.2, 2 and 20Hz were added).

In the case of the second database collected at UH and the one collected in Costa Rica, both followed AASHTO PP-61. Regarding testing temperatures, both data sets were gathered at the corresponding temperatures suggested by the standard, i.e. 4°C and 20°C for low and intermediate temperatures and two different high temperatures depending on the asphalt grade. A temperature of 40°C was used for both base binders in the data sets (PG64-22 for UH and PG70-22 for CR) while a temperature of 45°C was applied for the polymer modified binders of both data sets which are classified as PG76-22. Regarding the testing frequencies, the database gathered in Costa Rica followed the exact recommendation of the standard, using three frequencies (10Hz, 1Hz and 0.1Hz) for the low and intermediate temperatures, and four frequencies (10Hz, 1Hz, 0.1Hz and 0.01Hz) for the high temperature. In the case of the datasets collected at UH for this study, 5 frequencies were used (25Hz, 10Hz, 5Hz, 1Hz and 0.1Hz) for the low and intermediate temperatures and a sixth frequency (0.01Hz) was added when testing at the highest temperature.

Error! Reference source not found. shows a typical output from the AMPT after performing d ynamic modulus testing. As can be seen, there are four sinusoidal signals; three of them belong to the LVDTs while the fourth one corresponds to the load applied.

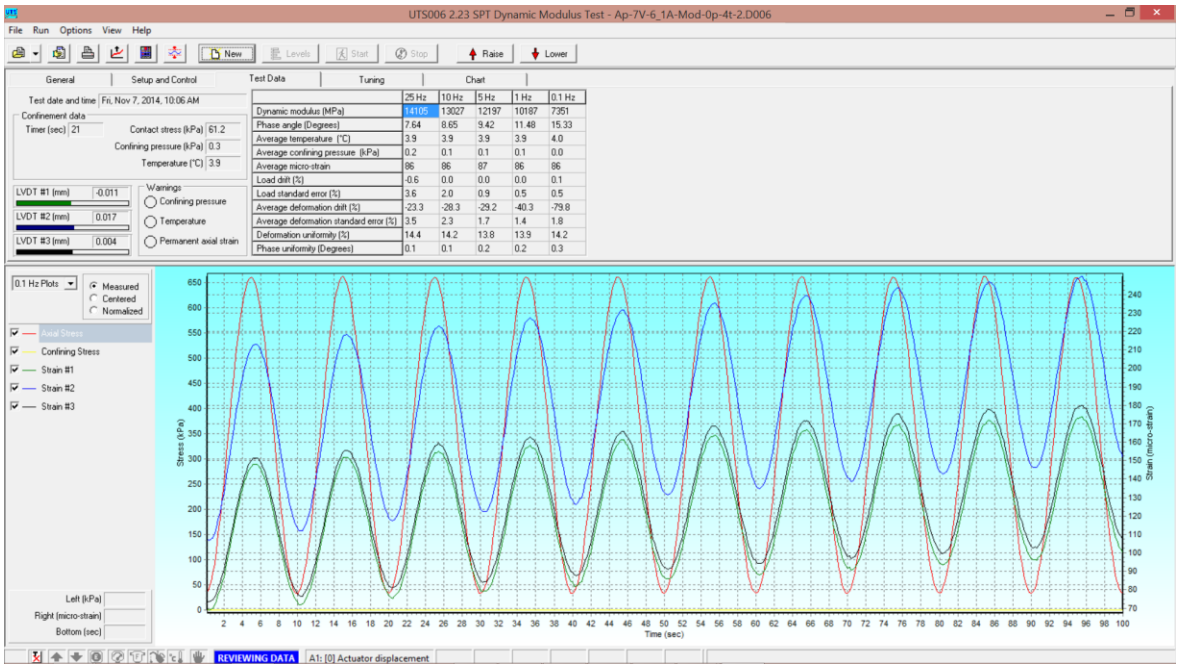

Figure 3. Typical dynamic modulus output from AMPT machine

Paying close attention to the two signals at the top, a horizontal shift can be noted between the peaks of these two signals. The signal at the very top belongs to the load applied, while the second one belongs to one of the LVDT signals, and this shift in time (Δt) is related to the lag in the material's deformation response after a load is applied. This shift in time (Δt) is directly related to the phase angle of the material (φ) by the relation $\Delta t=\varphi/\omega$, where ω is the angular velocity in rad/s. Thus, the phase angle describes the phase lag in radians between the application of a load and the material's response to it. This lag varies between 0 radians (0°) for purely elastic materials, where the strain response after an applied stress is instantaneous, and $\pi/2$ radians (90°) for purely viscous materials. For a more in depth explanation about the phase angle of asphalt material, the reader is directed to the work of Archilla et al. (2014).

Once dynamic modulus has been measured for every frequency at each temperature, the procedure to find the corresponding master curve is applied. As mentioned before, the master curves are interpolation models that can predict the dynamic modulus of a material at any given temperature and frequency. The elastic modulus of asphalt concrete increases with the frequency of loading but at the same time decreases with an increase in temperature (Figure 4). The modulus curves as a function of frequency (inverse of time) change in shape at different temperatures. However, the data points tend to form a smooth curve when shifting the data points to the left or right a distance that depends on the difference between the actual temperature at which the data points were obtained and a reference temperature. This behavior allows for the application of the time-temperature superposition principle, which is used to determine temperature-dependent mechanical properties of linear viscoelastic materials when properties at a reference temperature are known. The principle permits the application of a shift to the curves (e.g., Equation 6) to merge them into a single master curve at a reference temperature, which can then be used for predicting the behavior at any other temperature and frequency of interest by applying the appropriate shift to the frequency based on the temperature of interest.

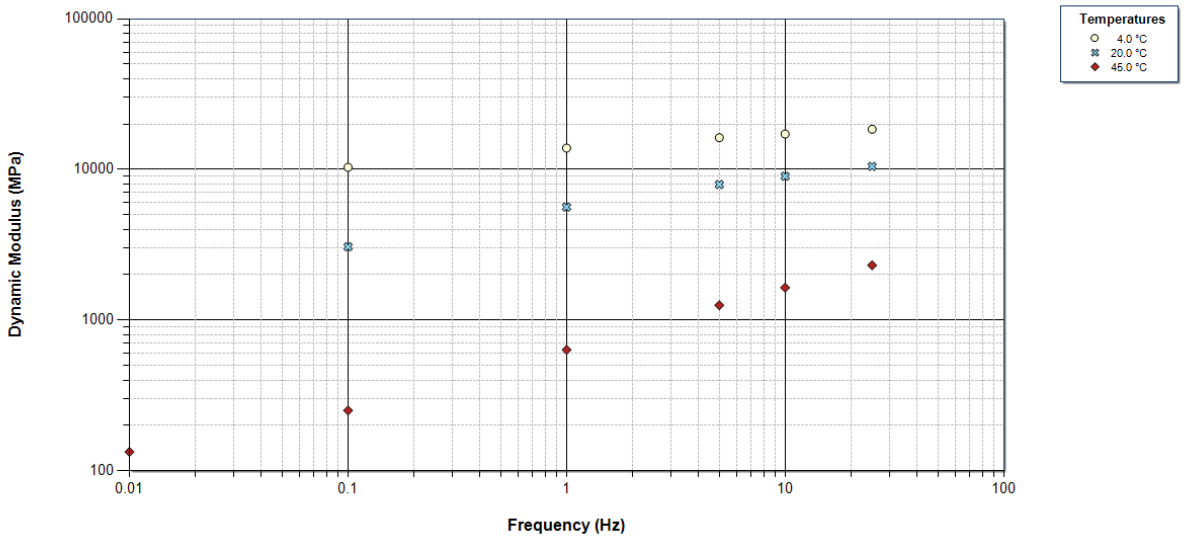

Figure 4. Dynamic modulus as a function of frequency at various temperatures

Figure 5 shows the application of equations 4 to 6, and the horizontal shift that can be observed for the data points, particularly for those at the lowest and highest temperatures for which the shifts are more noticeable (there is a small shift also for the points at 20℃ since the reference temperature used is 21℃) The points obtained at 4℃ (39.2℉) experience a shift in the right direction, while the points obtained at 45°C (113°F) are shifted to the left. The line that fits the points is the master curve of the mixture at a reference temperature of 21℃ (68°F)

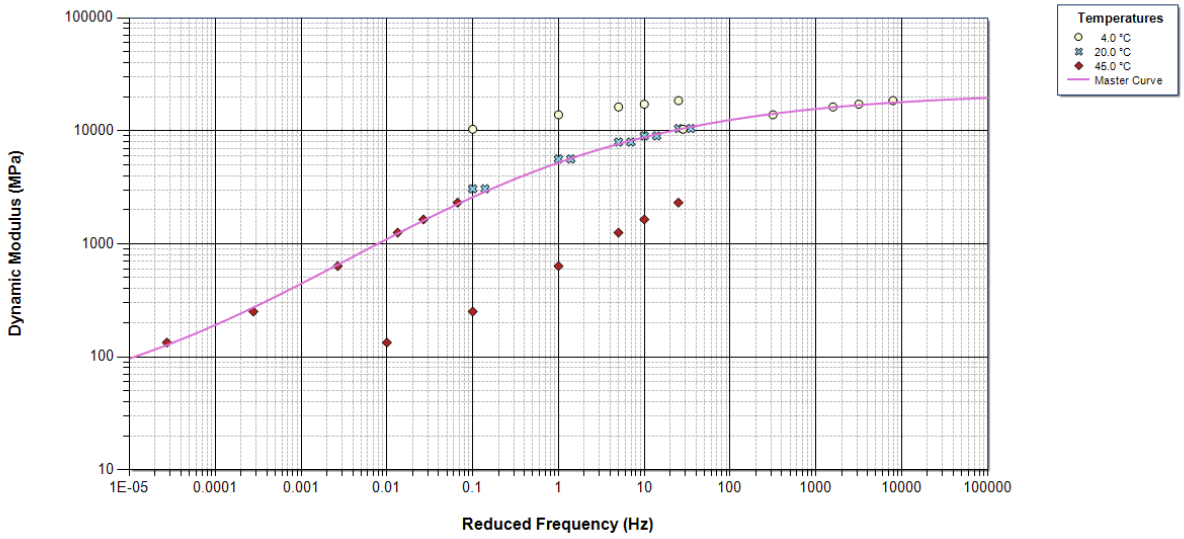

Figure 5. Master curve of asphalt mixtures

The master curves are used as inputs in the MEPDG to determine the behavior of asphalt mixtures at different temperatures and frequencies of loading. Other necessary inputs for the MEPDG, particularly weather and traffic, help define the conditions under which the materials must adequately perform over a design period. The master curves are then used to determine the response (in the form of resilient strains) of the mixtures under these conditions of traffic and weather. The strains calculated for each combination are translated into distresses that affect the pavement's life. Users of the MEPDG can then find the appropriate pavement structure by changing thicknesses until the different distresses do not exceed acceptable thresholds at the end of the design period.

Given the importance of master curves for predicting the performance of asphalt mixtures, it becomes necessary to update, calibrate or develop newer models with the capability of predicting more accurate values of |E*| for the materials available in a region.

2.2 Use of confinement for the dynamic modulus test

Traditionally, dynamic modulus testing has been performed in the laboratory without the application of confining pressure. However, in the field, a large proportion of the zone around the load is subjected to some level of confinement (i.e., with compressive stresses in all directions). Consequently, use of |E*| from confined tests has been reported to simulate field conditions more closely (Shenoy and Romero, 2002).

Several studies have shown that confinement can have an important effect on the measured values of dynamic modulus. Pellinen et al. (2002), while studying the trends of |E*| with bulk-stress (θ) for a given temperature, found that the values of |E*| were directly proportional to the level of confinement at medium to high temperatures. These authors found that at higher temperatures the effect of asphalt content is reduced and the mix behavior is governed mostly by the granular material, which explains why confinement has a larger effect under these conditions. Shenoy and Romero (2002) analyzed WestTrack data and showed that the confined |E*| correlated better than the unconfined |E*| when compared to field performance at the test track. These authors determined that for this laboratory-field comparison, the coefficient of determination R^2 improved from 0.42 using unconfined |E*| to 0.62 with data obtained with 138 kPa (20 psi) confinement and to 0.89 with data for 207 kPa (30 psi) confinement. Shenoy and Romero recommended that an optimum confinement level needs to be found to obtain the best possible correlation.

A challenge for performing confined testing in the laboratory is the additional amount of time required. If testing is performed at several confining pressures, then clearly more time is required for performing the additional frequency sweeps at each temperature and confining pressure combination. In addition, a longer stabilization time is required at each temperature to minimize the effect of the bulk strains induced by confinement. To reduce the testing time, Sotil et al. (2004) proposed a procedure to determine confined master curves from unconfined data and data at only two confined conditions. More recently, Lacroix et al. (2011), proposed a procedure based on rigorous theoretical considerations to estimate confined |E*| from unconfined |E*| measurements at the regular testing temperatures and from measurements of |E*| obtained with at least three different confinement levels at only 54°C (129.2°F). This type of estimation, however, attempts to predict values of confined |E*| at other temperatures and frequencies based solely on assumptions of the behavior of the mixture by using models that do not require any input regarding material characteristics or volumetrics, giving as a result estimations with large errors on the predicted values (close to 20% for that particular study). A few studies (Kim et al. 2009, Zhao et al. 2012) have also concentrated on the development of constitutive relationships to account for the effects of confinement.

Zeiada et al. (2011) performed a study on 26 asphalt mixtures where the effect of confinement is determined in detail for dense, open graded and gap graded mixtures. Their results showed the importance of using confinement, especially for gap and open graded mixtures, where the effect is more noticeable for all combinations of frequency and temperature. For the specific case of dense graded mixtures, the study shows that the biggest influence of confinement is given at high temperatures and low frequencies, while the differences at low and intermediate temperatures are not statistically significant. Additionally, these authors suggested the use of 138 kPa (20 psi) as an optimum confinement level, since after this level, the increases on the values of |E*| were not statistically significant.

In the laboratory, the AASHTO TP 79 standard (2016) for dynamic modulus testing using the AMPT machine, includes the guidelines to perform the experiment with the use of confinement pressure. The level of confinement applied in the lab depends on the capacity of the equipment used. Maximum levels of up to 500 kPa (72.5 psi) have been used with servo hydraulic loading frames and triaxial cells. When using the AMPT, as in this study, the maximum value used has been reduced by half since the AMPT has a 250kPa confining pressure limit.

For this experiment, the second data set from UH was tested specifically with the intention of determining the influence of confining pressure on the dynamic modulus of the asphalt mixture. Four levels of confinement were chosen, 0 kPa, 69 kPa, 138 kPa and 207 kPa (0 psi, 10 psi, 20 psi and 30 psi respectively). The first data set from UH included some testing with confining pressure, particularly for three types of mixtures where a confinement of 100 kPa (14.5 psi) was used. However, the use of confinement was not the focus of the study when that first data base was developed. The inclusion of confinement is an important and novel characteristic of the model developed in this thesis. To date, there appears to be no models for predicting |E*| that account for this effect. Chapter 3 will discuss the statistical tools used to take advantage of the gathered laboratory data to incorporate the effects of confinement on the prediction of |E*| values through the developed model.

2.3 Induced moisture damage during dynamic modulus testing

Moisture damage consists of a loss of strength and durability in asphalt mixtures associated with the effects of moisture (Little and Jones IV, 2003). This damage can be due to a loss of adhesion between the asphalt binder and the aggregates or a loss of cohesion and stiffness of the binder or the mastic which makes them even more susceptible to moisture (Kim and Lutif, 2006).

One of the most common distresses found in asphalt pavements, namely stripping, is described as a loss of integrity of the hot mix asphalt (HMA) which occurs as a result of moisture damage in the mixture.

Stripping can begin from either the top or the bottom of the HMA layer, depending on where the mixture is exposed to moisture. Water runoff on the road surface might generate the distress at the top of the pavement while capillary action from the water table or seepage from surrounding areas would develop a distress that expands from the bottom. When stripping is detected at the top of the HMA layer, it can take different forms such as rutting, shoving or even fatigue or longitudinal cracking (Rae Hunter and Ksaibati, 2002). When the distress initiates at the surface and makes its way to the bottom it is called raveling. In extreme cases, if the pavement surface is not treated at an appropriate time, disintegration of the surface may occur.

There are several tests that can be used to determine the moisture susceptibility of asphalt mixtures:

- ASTM D4867, Effect of Moisture on Asphalt Concrete Paving Mixtures,

- AASHTO T165 (or ASTM D1075), Effect of Water on Compressive Strength of Compacted Bituminous Mixtures,
- AASHTO T324, Hamburg Wheel-Track Testing of Compacted Hot Mix Asphalt, and
- AASHTO T283, Resistance of Compacted Bituminous Mixture to Moisture Induced Damage.

AASHTO T283 is the one that is most commonly used. To induce moisture damage on the asphalt specimens many of these standards rely on conditioning the sample in water baths before or during testing. However, a study conducted by Epps et al. (2000) for the National Cooperative Highway Research Program (NCHRP) determined that the use of a freeze-thaw cycle normally decreases the tensile strength of the asphalt samples when compared with samples that are only soaked in water. The study of Epps et al. did not find statistically significant differences for most of their comparisons between samples tested with and without freeze-thaw cycles. However, when using aggregates considered water-sensitive, the difference in tensile strength between conditioned and unconditioned samples was statistically significant when one freeze-thaw cycle was applied. Thus, their study recommended the use of the freeze-thaw cycle proposed by the AASHTO T283 testing method. The use of one cycle during testing was therefore included to induce more severe moisture damage in asphalt mixtures, independently of the exposure of a geographical zone to natural freezing-thawing conditions.

In both Hawaii and Costa Rica there is no exposure to natural freeze-thaw conditions. Nevertheless, the annual average rainfall is very high, with an average of 2200 mm (86.8 in) for Honolulu, Oahu (Giambelluca et al. 2013) as an example for Hawaiian conditions and 2926 mm (115.2 in) as an average for all Costa Rica (World Bank, 2016). As a comparison, the annual average precipitation for the whole United States is recorded as 715 mm (28.1 in) (World Bank, 2016). Due to this large amount of precipitation, it is only natural that the roads in both places can suffer constant damage from moisture on their roads.

Measuring the moisture susceptibility of asphalt mixtures thus needs a reliable test to prevent all the distresses associated with moisture damage. Even though Superpave® adopted AASHTO T283 for this purpose, several agencies in the United States have reported problems with this test when trying to correlate the laboratory results with field observations (Solaimanian et al. 2003). Experiences from Costa Rica have found that the test can often give false positives or negatives when predicting moisture susceptibility, thus being unable to accurately identify the mixtures

that will perform poorly in the field (Vargas-Nordcbeck et al. 2016). Two limitations have been pointed out by these studies: a) the conditioning procedure does not include dynamic loading which is what actually happens in the field and b) it determines if moisture damage will occur in the field based on a measurement of strength, which is a parameter that is not directly used in pavement design.

For this reason, several studies (Solaimanian et al. 2006 and 2006, Nadkarni, et al. 2009, Vargas-Nordcbeck et al. 2016) have suggested the use of the dynamic modulus to measure the susceptibility of asphalt mixtures to moisture damage. This has the advantage that the dynamic modulus test is an important parameter used directly in mechanistic-empirical pavement design procedures. Furthermore, provided the permanent deformations in the test are limited, the use of the same specimen before and after conditioning eliminates the variability among specimens as a factor.

An experiment conducted by National Laboratory of Materials and Structural Models (LanammeUCR), measured the dynamic modulus of mixtures before and after being conditioned to determine a procedure that could more accurately predict the moisture susceptibility of mixtures in Costa Rica. Since the use of water bath conditioning had shown to not be a good indicator of the moisture susceptibility of mixtures, a more severe approach was followed by applying 1, 3 and 6 freeze-thaw cycles to the mixtures. Their data are used in this document and the effect of freeze-thaw cycles on the dynamic modulus master curves is one of the variables included in the prediction model developed in this study.

2.4 Asphalt mixtures' modifiers

Material modification encompasses a large variety of methods to improve the performance characteristics of the original material. In construction, these modifications can be seen in a large range of materials given that the common objective is to upgrade the quality and behavioral characteristics of the products to meet newer demands. In the case of asphalt mixtures, several factors have contributed to the use of modifiers. Some of the factors worth mentioning are (Kluttz, 2012): a) accommodating an increased demand in traffic, which include heavier loads and bigger volumes, b) satisfying the requirements for Superpave® specifications, and c) economic issues related to higher paving costs, which translates into thinner pavements that need to last longer to delay maintenance.

Although the need for modifiers has long been recognized in the paving industry, the current models used in the MEPDG for the design of pavements do not have the capacity to directly include among its inputs the characteristics of modified mixtures or binders. The only available possibility for level 1 design is to include the laboratory measured values of |E*| of the modified material or the values of |G*| of the binder at level 2. Therefore, newer models that include the expected characteristics and behavior of these materials directly as inputs are needed.
The modifiers that were used for the improvement of the mixtures tested for this research project are discussed in the following sub-sections.

2.4.1 Fibers

Fibers are typically used in asphalt mixtures to improve their performance against permanent deformation and fatigue cracking. Several studies (Bueno et al. 2003, Lee et al. 2005, Kaloush et al. 2010, Bennert 2012) have tested the effects of adding different types of fibers to mixtures and evaluated their performance against unmodified mixtures.
Since for this study synthetic polyolefin/aramid fibers are used to evaluate their effect on the mixtures, the following discussion concentrates on this type of fibers. As reported by McDaniel (2015), to date, the literature regarding the effect of this type of fibers on |E*| is mixed. Kaloush et al. (2010) report significant increases in both dynamic modulus and other performance characteristics. These Arizona State University (ASU) researchers found that the |E*| of mixes modified with synthetic fibers were significantly higher than those of a control mix. At 37.8°C (100°F) and 10Hz, they reported that the modulus of the fiber modified mix was 83% higher than the modulus of the control mix. ASU has conducted several more investigations showing similar results. Gibson and Li (2015) found that a synthetic fiber mix was sometimes softer and sometimes stiffer than the control mix depending on mixture volumetrics, a result that these authors considered sensible because the small strains in the |E*| test do not significantly mobilize tension in the fibers.
On the other hand, according to McDaniel (2015), Bennert reports surprisingly lower dynamic moduli at high temperatures of a plant produced mix with polyolefin/aramid fibers with respect to the mix without fibers. Nevertheless, McDaniel (2015) also indicates that in that study some contamination of the unmodified binder with a polymer modified binder was suspected.
McDaniel (2015) also reports that in another study by Bennert, dynamic modulus test results of two similar plant-produced mixtures with and without fibers showed similar values at all

frequencies but that the mix with fibers had slightly better permanent deformation resistance. While two other studies by Bennert (2012) found some detrimental effects of the fibers under certain testing procedures, they also show little to no improvement on the dynamic modulus of the mixtures tested.

The effect of the addition of fibers was included in one out of the three datasets used for the creation of the predictive model. This factor is considered in the model to predict the behavior of the master curve.

2.4.2 Styrene-Butadiene-Styrene Polymer

Polymer modification is one of the most common procedures performed in the asphalt industry to improve the behavior of asphalt mixtures. Some of the benefits of the polymer modified asphalts (PMA) include improved rutting resistance, less thermal cracking (induced by low temperatures), improved durability and in some cases even an improvement in stripping resistance (Walker 2014).

Even though polymers cover a wide range of modifiers, elastomers (rubbers and elastics) and plastomers (plastics) are the most commonly used (Walker 2014). Two of the most popular elastomers used in the industry are the styrene-butadiene-styrene (SBS) and styrene-butadiene-rubber (SBR). These modifiers are included in the mix to reduce rutting and improve fatigue and thermal cracking resistance (Bahia et al. 2001). Of particular interest is the use of SBS, which was a polymer employed in the three studies used for this research. This elastomer can be added to the mixture in different percentages, depending on the desired performance of the mixture.

The benefits of using polymer modified binders have been documented widely. The Asphalt Institute (AI) quantified the effects of polymer-modified asphalt for reducing pavement distresses (Von Quintus et al. 2003) and determined that in average PMA mixtures can provide an average of 2 to 10 years increase in service life for asphalt pavements. For Hawaii, Archilla (2010) developed a model from unconfined dynamic modulus tests that showed that the dynamic modulus values of polymer modified mixtures were higher than those of the unmodified mixtures at low reduced frequencies.

However, a big problem regarding modified asphalts remains unsolved. Results from the NCHRP Project 09-10 on Superpave protocols for modified binders show that the simplifying assumptions from the Superpave specification AASHTO MP1 (currently AASHTO M320): Standard Specifications for Performance Graded Asphalt Binder (AASHTO 2016), limits its

applicability to the greater part of modified binders analyzed under that study (Bahia et al. 2001). This means that the current AASHTO method is not capable of correctly characterizing the performance of modified binders. Consequently, its effect on the mixture is underestimated (Bahia et al. 2001). The issue can later be transferred into the MEPDG for levels 2 and 3, where limited inputs about the binder are required. Particularly for level 3, where default values are used for binder inputs, the advantages of using modified binders is then lost. In this sense, the use of either level 2 or 3 of the MEPDG limits the ability to accurately predict the distresses in pavements when these types of modified binders are used. As mentioned before, only level 1 of the design guide can capture the advantages of modified mixtures by using laboratory measured data. Including the results of dynamic modulus of mixtures with polymer modified binders in the prediction model developed herein overcomes this limitation.

2.4.3 Elvaloy®Ret

Elvaloy®Ret is the commercial name for a reactive elastomeric terpolymer (RET) that is used to chemically modify asphalt binders. One of the advantages of Elvaloy®Ret is that, unlike most other plastomers and elastomers that are mixed into the asphalt but remain as two separate phases (binder/modifier), this product contains an ingredient that chemically reacts with the asphalt forming a stable, resilient and elastically improved binder (Tarefder and Arifuzzman 2011). Just like in the case of SBS, Elvaloy®Ret can be mixed in different percentages depending on the desired performance, with a range from 0.7% to 2.0% being the recommendation by the manufacturer. However, no more than 2.5% shall be added since the asphalt may gel (Panabaker 2009). The process to modify the asphalt binder with Elvaloy®Ret can take up to 18 hours and for this reason the use of a small percentage of poly-phosphoric acid (PPA), typically ranging from 0.2 to 0.3% of the binder weight, is recommended as a catalyst to reduce the reaction time to close to 1 hour (Panabaker 2009).

Research related to the use of this modifier is also extensive, with some sources claiming a reduction in moisture susceptibility, fatigue cracking and rutting of the mixtures (Kanabar 2010, Tarefder and Arifuzzman 2011, Panabaker 2009). Experiments carried out at UH Manoa (Archilla 2010) found an improvement in the mixture performance by the use of Elvaloy®Ret.

2.4.4 Lime

Lime is the first of two anti-stripping agents that were used in the mixtures from Costa Rica. The benefits of lime can be found widely in the literature and it is one of the most common anti-stripping additives used in the US. From a total of 44 states that experience severe moisture damage on their pavements, 29% of them exclusively use lime as their additive while 15% use either lime or any other liquid agent (Hicks et al. 2003).

Lime improves the binder-aggregate adhesion by reacting chemically with the carboxylic acids in the asphalt and forming insoluble salts that are absorbed at the aggregate surface, which improves the adhesive compatibility between both materials (Little and Jones IV 2003).

A study by Sebaaly (2006) demonstrated that lime not only has a good ability to control water sensitivity but also has the capability to:

- act as a mineral filler, which stiffens the asphalt binder,
- improve the mixture resistance to fracture growth by improving the fracture toughness at low temperatures,
- act as an anti-oxidant, and
- react with clay fines to improve moisture stability and durability.

Moreover, this study determined that lime treatment of asphalt mixtures can increase pavement life by an average of 3 years, which represents an increase of 38% from the expected pavement life (Sebaaly, 2006).

Due to its well-known properties, lime was included in the treatment of the Costa Rican mixtures to evaluate its behavior when cycles of freezing and thawing were applied.

2.4.5 Magnabond

Magnabond is a liquid anti-stripping agent. Most of these modifiers, as in this case, are chemical compounds that contain amines (Rae Hunter and Ksaibati, 2002). These agents work by reducing the surface tension between the aggregates and the binder and therefore promoting an increased adhesion of the two materials. This product was used as an alternative for preventing moisture damage in the mixtures from Costa Rica.

2.4.6 Sasobit

Sasobit is an organic paraffin wax that can reduce the viscosity of the binder at mixing and compacting temperatures. These types of additives are known as asphalt flow improvers (Cooper

2009, Kridan et al. 2011), and are used, among other products and techniques, to create warm mix asphalt (WMA).

The WMA technology has been gaining popularity in the last decade due to the benefit of reduced greenhouse gas emissions and energy consumption during production and paving operations (Jamshidi et al. 2012, Bonaquist 2011). Also, with a reduction of approximately 50°F with respect to the temperatures used for producing conventional HMA mixtures, WMA presents health benefits by reducing the exposure of workers to asphalt fumes as well as benefits for the mixture by reducing binder aging and potentially improving the pavement performance (Bonaquist 2011). Sasobit is the most common wax that has been used in most WMA projects in the United States, typically at a rate of 1.5% by weight of binder, either added to the binder or directly to the mixture (Qin et al. 2015).

Two of the specimens tested in the older UH study were from field collected samples of a mixture that contained Sasobit.

CHAPTER 3: STATISTICAL APPROACH

This chapter presents the two statistical approaches utilized in the estimation of the parameters of the predictive model. As will be explained in detail in chapter 5, the model was developed using the simplest form of the sigmoidal function (presented in chapter 2) as a starting point, and then a non-linear least squares analysis was used to expand the model by including several parameters that characterized the mixtures tested. To integrate the three data sets collected, two different approaches were used to address the potential differences due to material changes, testing conditions, sample conditioning and even sample to sample variations. Section 3.1 introduces the joint estimation approach, while Section 3.2 presents the mixed effects approach. Both approaches will be explained herein in one of their simplest forms and their application will be discussed in chapter 5.

3.1 Joint estimation approach

The joint estimation approach is useful when data from multiple sources are used since it identifies the explanatory variables that are common in all databases and the unique variables for every database that have an explanatory influence on the model (Archilla et al., 2007). This estimation approach has been used by Morikawa et al. (1999) for travel demand modeling and by Archilla (2000), Archilla and Madanat (2001) and Prozzi and Madanat (2004) for pavement deterioration models.

To explain this approach, two different database sources named A and B can be considered. It is then assumed that both databases contain the dependent variable |E*| (which is the variable of interest for this project), and several explanatory variables such as mixture composition, volumetrics, etc. To avoid confusion with the conditional symbol, in the equations that follow |E*| is simply denoted as E*. A model for each of these databases can then be specified as follows:

$$E(E^{*A}|\boldsymbol{x}^A, \boldsymbol{w}) = g^A(\boldsymbol{\beta}^A, \boldsymbol{x}^A, \boldsymbol{\alpha}, \boldsymbol{w}) \quad (7)$$

$$E(E^{*B}|\boldsymbol{x}^B, \boldsymbol{z}) = g^B(\boldsymbol{\beta}^B, \boldsymbol{x}^B, \boldsymbol{\gamma}, \boldsymbol{z}) \quad (8)$$

where,

$E(E^*|\cdot)$ = conditional expectation function of |E*| with a functional form $g(\cdot)$,

E^{*A} = dynamic modulus for model A,

E^{*B} = dynamic modulus for model B,

$\mathbf{x^A}$, $\mathbf{x^B}$ = vector of explanatory variables shared by both models,

$\boldsymbol{\beta^A}$, $\boldsymbol{\beta^B}$ = vectors of model parameters related to $\mathbf{x^A}$ and $\mathbf{x^B}$ respectively,

$\boldsymbol{w}$ = vector of explanatory variables unique to model A,

$\boldsymbol{z}$ = vector of explanatory variables unique to model B,

$\boldsymbol{\alpha}$ = vector of model parameters related to $\boldsymbol{w}$, and

$\boldsymbol{\gamma}$ = vector of model parameters related to $\boldsymbol{z}$,

Depending of the explanatory variables, three scenarios are possible. In the first scenario, all the explanatory variables for both databases are common and both databases can be combined into a single model under the assumption that there is a single underlying data generation process common for both data bases. In this case, the model parameters $\boldsymbol{\alpha}$ and $\boldsymbol{\gamma}$ and the associated variables $\boldsymbol{z}$ and $\boldsymbol{w}$ would not exist. This scenario would be ideal since it results in having more information for developing a single model. A second scenario would represent the opposite situation where two completely different models can be developed from the databases since no common explanatory variables exist. In this case $\boldsymbol{\beta^A}$, $\boldsymbol{\beta^B}$, $\boldsymbol{x^A}$ and $\boldsymbol{x^B}$ do not exist since there is nothing in common between the models. In contrast with the first scenario, nothing is gained by the combined use of the two databases. The third scenario is recognized as a more common situation, where both databases share some explanatory variables but also have some variables that are unique to each source. In this case, some of the estimated parameters are common to both databases and others are unique to one or the other database. The potential advantages of this scenario are that it allows the identification of explanatory variables, which may not be available in some databases and it permits determination of bias parameters to account for the different marginal effects estimated for explanatory variables in common between databases (Archilla, 2007). In terms of the models shown above, the set of common parameters may be different, that is $\boldsymbol{\beta^A} \neq \boldsymbol{\beta^B}$, therefore the relationship between the i^{th} element of the set of parameters of each model can be expressed as $\beta^A_i = \beta^B_i + \delta_i$, where δ_i is a bias parameter. This feature is called *bias correction* and is one of the main advantages of the use of joint estimation (Archilla 2000, Prozzi 2004). Two other advantages are: identification and statistical efficiency. Identification relates to the complementary characteristics of the data sources. For example, one data source may contain explanatory variables not available in the other, thus allowing the identification of the effects of these variables from this single data source. Statistical efficiency is

achieved when a parameter estimate common to all data sources is determined using all available data. Because of the larger sample size, this results in lower variance of the parameter estimate. The motivation for using joint estimation in this study is the use of different materials, additives and testing conditions in the three available data sets.

3.2 Non-linear mixed effects approach

The non-linear mixed-effects approach is used with grouped data (e.g. repeated measures, blocked design, and multilevel data) to describe a response variable as a function of covariates considering the correlation between observations in each group (Pinheiro and Bates, 2000). A mixed-model can be defined as a statistical model which contains both fixed effects and random effects as described shortly. This type of model is useful when several measurements, such as the dynamic modulus values, are made on the same statistical units, such as the cylindrical asphalt samples mixed, compacted and trimmed from different sources for this experiment. Fixed effects are the parameters which can be associated to the entire population or at least with certain repeatable levels of experimental factors (Pinheiro and Bates, 2000). These parameters define a systematic function of the mean response of all samples, which includes an error ε describing the intra-individual variation, allowing for the possibility of heterogeneous within-individual variance as well as within-individual correlation (Davidian and Giltinan, 1995).

On the other hand, random effects are associated with individual experimental units which are drawn at random from an entire population (Pinheiro and Bates, 2000). The differences among experimental units represent a deviation from an overall mean. The inter-individual variation defined by the random effects can be due to variation in testing procedures (Davidian and Giltinan, 1995).

The difference between a fixed-effects model and a random-effects model alone relies on whether it is desired to make inferences about the particular levels of the classification factor defined in the experiment or to make inference about the experimental units from which the levels are drawn respectively (Pinheiro and Bates, 2000).

The idea of a mixed-effects model is therefore to combine both types of effects within one model, with fixed effects parameters explaining the behavior of the population means between a given set of treatments (intra-individual variation) and the random effects representing the variability among testing units (inter-individual variation).

A simple model is used to illustrate the mixed-effects framework. Consider a dependent variable *y* modeled as a simple linear function of a covariate *x* as follows:

$$y_{ij} = \beta_{1i} + \beta_{2i}\, x_{ij} + \epsilon_{ij}\ , \quad \text{with} \quad \beta_{1i} = \left(\bar{\beta}_1 + b_{1i}\right) \quad and \quad \beta_{2i} = \bar{\beta}_2 + b_{2i} \tag{9}$$

where,

y_{ij} = is the j^{th} observation of the dependent variable for the experimental unit *i*,

$\bar{\beta}_1$, $\bar{\beta}_2$ = are the fixed-effects parameters related to the entire population,

b_{1i}, b_{2i} = are random-effects parameters associated with unit *i*; for unit *i* these represent deviations from the population parameters $\bar{\beta}_1$ and $\bar{\beta}_2$, respectively, and

ε_{ij} = is the error term for observation *j* on unit *i;* it is normally assumed as being distributed $N(0, \sigma^2)$, where σ^2 is the variance of ε_{ij}. It is also commonly assumed that these errors are independent and they have constant variance (all these hypotheses need to be corrected if not satisfied).

When the variations from sample to sample (i.e., the b_{1i}'s and b_{2i}'s) are not accounted during model estimation, the random effects b_{1i} and b_{2i} end up being absorbed by the error term ε_{ij}, which are then necessarily correlated for the observations of each unit. This violates one of the assumptions of the classical regression model and thus makes any hypothesis tests on the parameter estimates unreliable. These random effects are the results of unobserved differences from sample to sample. Even though the procedures to create an asphalt mixture and prepare a sample in the laboratory are standardized by the American Association of Highway and Transportation Officials (AASHTO) methods and other standards, it is still expected that variability in the materials, compaction level, material proportioning, etc. from specimen to specimen can affect similarly all the measurements of each specimen. In other words, all the observations for a specimen will tend to differ from the population model in a way that cannot be simply accounted for by an error term with zero mean because, for a given sample, most observations may be on one side or the other of the population model. Similarly, multi-laboratory precision can influence the measurement of the values of dynamic modulus for different samples. The use of the mixed-effects approach for the creation of the prediction model described for this project is motivated by its ability to account for the variability due to unobserved heterogeneity of different experimental units. The mixed-effects approach represents a compromise between two extremes: a) ignoring the unobserved heterogeneity (which may lead to a violation of the

assumptions of the classical regression model), and b) computing separate parameter estimates for each unit, which is not practical unless the interest is in predicting the behavior of just those units. In this compromise the unobserved heterogeneity is accounted for through a few variance parameters of the b_i's random effects. In the context of the previous example, the approach provides estimates of the population parameters $\bar{\beta}_1$ and $\bar{\beta}_2$, the variances and covariance of the random effects b_{1i} and b_{2i} (several assumptions can be made about the appropriate structure of the covariance matrix), the variance of the error term ε_{ij}, and any other parameters that may be needed to correct for heteroscedasticity and correlation. The approach provides a neat evaluation of population parameters and the information about the variability of the random effects can be useful for reliability studies.

As will be explained in more detail in chapter 5, the joint estimation approach was first used for the creation of the model until a good fit was found. At this point, the examination of the model was switched from a nonlinear least squares analysis to the nonlinear mixed-effects analysis approach to look for further improvement by including the associated random effects, which in turn allows a better characterization of the statistical significance of individual parameter estimates because the regression assumptions are satisfied much more closely. All statistical analyses were performed with the use of the free software environment R for Windows.

CHAPTER 4: DATA SOURCES

For the creation of the predictive model, three data sets were gathered with different characteristics not only in origin and materials but also in testing conditions. The consideration of some of these characteristics are what make this model distinctive from other predictive models. This chapter provides a detailed description of each of these data sets and their specific features included in the model. Two of the data sets were obtained at the University of Hawaii, Manoa for two different projects, while the third set was collected at the National Laboratory of Materials and Structural Models of the University of Costa Rica (LanammeUCR). Sections 4.1 and 4.2 cover the data sets collected at UH Manoa, while Section 4.3 describes the data set collected at LanammeUCR. Section 4.4 describes the quality control performed before creating the database. Section 4.5 presents the model's a priori expectations.

4.1 University of Hawaii first data set

The first data set collected at the University of Hawaii, herein called UHO (with the O meaning "old", since it was gathered first), collects the results of 77 laboratory-mixed, laboratory-compacted specimens plus 3 specimens of field mixtures compacted in the laboratory. Regarding the first 77 specimens, these were prepared using two different gradations and three binder types while also varying the binder content and mixture air voids. The materials allowed for different binder content/air voids combinations with actual air voids varying from 2.1% up to 10.4% and binder contents of 5.2%, 5.7%, and 6.2% for gradation A and 4.8%, 5.3%, and 5.8% for gradation B.

The aggregates used for the laboratory mixed specimens are classified as a basaltic limestone from the Makakilo quarry on Oahu. The gradations used for this data set are shown in Figure 6 in a 0.45-power chart. From the two gradations shown, Gradation B was selected at the time for being representative of the gradation used in actual pavement jobs while Gradation A was selected as a variation from Gradation B that could potentially result from changes in stockpiles and/or aggregate feeding procedures at the plant. Both gradations met the Superpave gradation specifications for 12.5 mm Nominal Maximum Aggregate Size (NMAS). It must be noted that many State Mix Type 4 gradations used in Hawaii fall between both these curves.

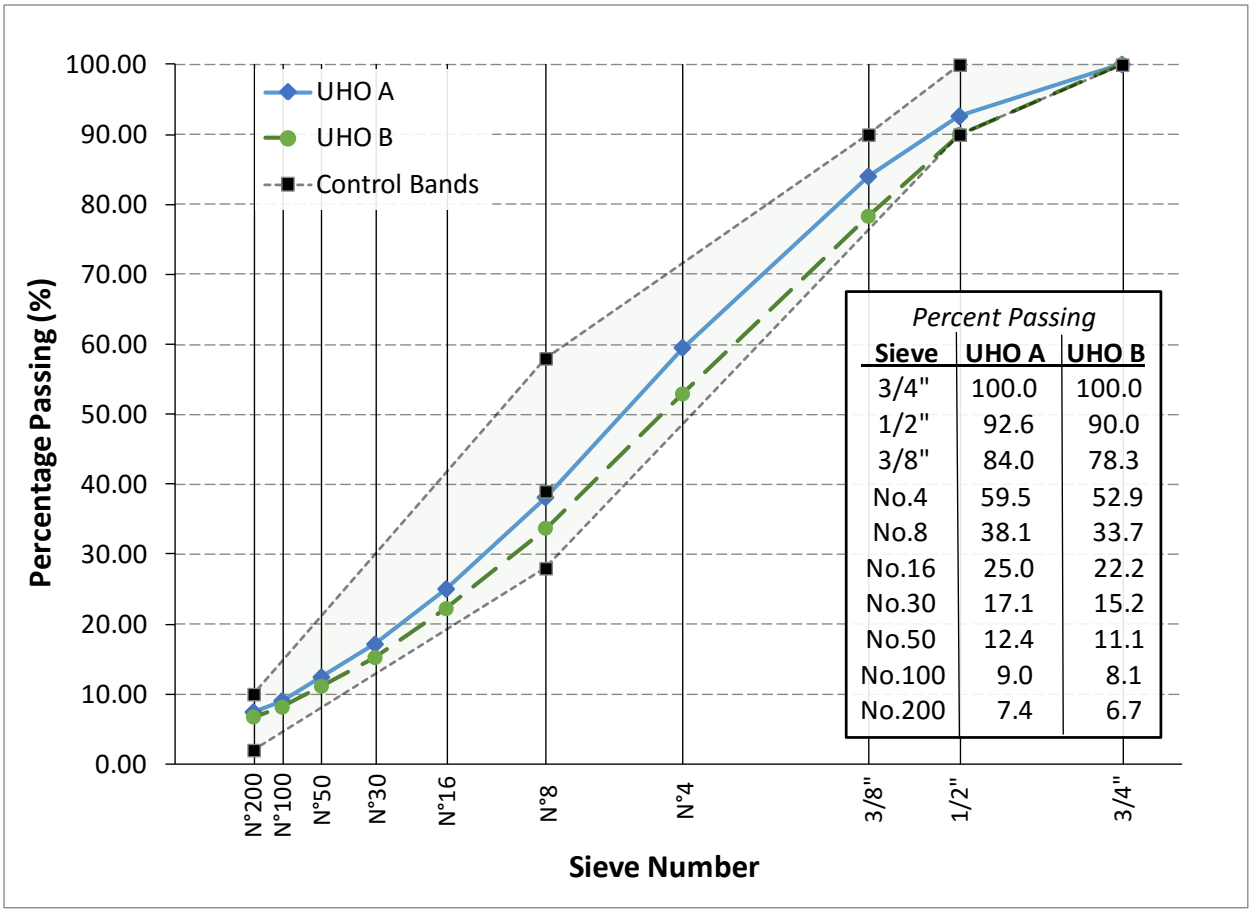

Percent Passing

Sieve	UHO A	UHO B
3/4"	100.0	100.0
1/2"	92.6	90.0
3/8"	84.0	78.3
No.4	59.5	52.9
No.8	38.1	33.7
No.16	25.0	22.2
No.30	17.1	15.2
No.50	12.4	11.1
No.100	9.0	8.1
No.200	7.4	6.7

Figure 6. Gradation curves for the UHO data set

The asphalt binders used to prepare the specimens were a virgin (unmodified) PG64-16 and two polymer modified binders. The PG64-16 binder was the one used at the time in Hawaii for most paving jobs. From the modified binders, one was an SBS modified PG-70-22, commercially available at the time, whereas the second one was obtained by laboratory modification of the PG64-16 binder with a reactive elastomeric terpolymer (RET) sold under the commercial name Elvaloy®Ret. As explained before, to accelerate the reaction of the product with the binder, a small percentage (0.3% by weight of binder) of poly-phosphoric acid (PPA) was used when mixing the Elvaloy®Ret with the binder. This binder was labeled as PG70-XX disregarding the lower temperature bound due to the lack of equipment to perform the testing in the University of Hawaii (UH) pavement laboratory.

In addition to varying the air voids to try to reflect potential field conditions, in that study the optimum binder contents for both gradations were determined following the Superpave mix design procedure. These optimum values were used together with binder contents 0.5% above

and below them. Further analysis from quality assurance records on Oahu, showed the air voids range to be representative of the range found in the field for Type 4 and Superpave 12.5mm mixtures.

From the 3 field mixtures included in this data set, two specimens correspond to a State Mix Type 4 collected from a rehabilitation project on Farrington Highway on Oahu. This mix is a warm mix asphalt (WMA) prepared by using the organic paraffin wax Sasobit in a mixture of a PG64-16 binder with Makakilo quarry aggregates. The last specimen compacted was a 12.5 mm NMAS Superpave mix collected from the asphalt plant, made with the PG64-16 binder and a combination of aggregates from the Kapaa quarry on Oahu (coarse aggregate retained in the 4.75 mm sieve) and the Ameron quarry (fine aggregate passing the 4.75 mm sieve) in Maui. A summary of all these specimens is presented in Table 1 below.

Table 1. Characteristics of UHO data set specimens.

Aggreg. Gradation	Binder Grade	Specimen ID	P_b	G_{mm}	G_{mb}	AV	VMA	VFA	Additive	Test Condition
Type A Gse: 2.994	PG64-16 Gb: 1.019	ADM001C	5.7	2.696	2.623	2.70	13.0	79.2	None	100 kPa Confinement (for specimens in bold)
		ADM001D	5.7	2.696	2.606	3.30	13.6	75.7		
		ADM002	5.7	2.696	2.549	5.50	15.5	64.5		
		ADM002B	5.7	2.696	2.571	4.60	14.7	68.7		
		ADM002C	5.7	2.696	2.556	5.20	15.2	65.8		
		ADM003	5.7	2.696	2.559	5.10	15.1	66.2		
		ADM003B	5.7	2.696	2.497	7.40	17.2	57.0		
		ADM003C	5.7	2.696	2.514	6.80	16.6	59.0		
		ADM004	5.7	2.696	2.425	10.1	19.6	48.5		
		ADM004B	5.7	2.696	2.446	9.30	18.9	50.8		
		ADM005	5.7	2.696	2.446	9.30	18.9	50.8		
		ADM006	5.7	2.696	2.581	4.30	14.4	70.1		
		ADM007	6.2	2.673	2.600	2.70	14.2	81.0		
		ADM008	6.2	2.673	2.614	2.20	13.8	84.1		
		ADM025	5.2	2.720	2.518	7.40	16.0	53.8		
		ADM026	5.2	2.720	2.519	7.40	16.0	53.8		
		ADM027	5.2	2.720	2.472	9.10	17.6	48.3		
		ADM028	5.2	2.720	2.463	9.40	17.9	47.5		

Table 1(Cont'd). Characteristics of UHO data set specimens.

Aggreg. Gradation	Binder Grade	Specimen ID	P_b	G_{mm}	G_{mb}	AV	VMA	VFA	Additive	Test Condition
Type A Gse: 2.989	PG70-XX Gb: 1.019	**ADM009**	5.7	2.692	2.612	3.00	13.4	77.6	Elvaloy®Ret	100 kPa Confinement (for specimens in bold)
		ADM010	5.7	2.692	2.604	3.30	13.6	75.7		
		ADM011	5.7	2.692	2.492	7.40	17.3	57.2		
		ADM012	5.7	2.692	2.500	7.10	17.1	58.5		
		ADM013	5.7	2.692	2.432	9.70	19.3	49.7		
		ADM014	5.7	2.692	2.430	9.70	19.4	50.0		
		ADM015	5.2	2.716	2.519	7.30	16.0	54.4		
		ADM016	5.2	2.716	2.525	7.00	15.8	55.7		
		ADM017	6.2	2.669	2.482	7.00	18.1	61.3		
		ADM018	6.2	2.669	2.516	5.70	17.0	66.5		
Type A Gse: 2.956	PG70-22 Gb: 1.027	ADM019	5.7	2.670	2.597	2.70	13.9	80.6	SBS	None
		ADM020	5.7	2.670	2.607	2.40	13.5	82.2		
		ADM021	5.7	2.670	2.486	6.90	17.5	60.6		
		ADM022	5.7	2.670	2.485	6.90	17.6	60.8		
		ADM023	5.7	2.670	2.427	9.10	19.5	53.3		
		ADM024	5.7	2.670	2.415	9.60	19.9	51.8		
Type B Gse: 2.968	PG64-16 Gb: 1.019	BDM001B	5.3	2.695	2.632	2.30	12.5	81.6	None	100 kPa Confinement (for specimens in bold)
		11CH53	5.3	2.695	2.627	2.50	12.7	80.3		
		BDM002	5.3	2.695	2.542	5.70	15.5	63.2		
		BDM002B	5.3	2.695	2.552	5.30	15.2	65.1		
		BDM002C	5.3	2.695	2.556	5.20	15.1	65.6		
		BDM003	5.3	2.695	2.557	5.10	15.0	66.0		
		BDM004	5.3	2.695	2.437	9.60	19.0	49.5		
		BDM005	5.3	2.695	2.423	10.1	19.5	48.2		
		BDM006	5.3	2.695	2.599	3.60	13.6	73.5		
		BDM007	5.8	2.672	2.597	2.80	14.2	80.3		
		BDM007B	5.8	2.672	2.616	2.10	13.5	84.4		
		BDM008	5.8	2.672	2.607	2.40	13.8	82.6		
		BDM009	4.8	2.718	2.505	7.80	16.3	52.2		
		BDM010	4.8	2.718	2.507	7.80	16.3	52.2		
		BDM011	5.8	2.672	2.408	9.90	20.4	51.5		
		BDM011B	5.8	2.672	2.524	5.50	16.6	66.9		
		BDM012	5.8	2.672	2.414	9.70	20.2	52.0		
		BDM012B	5.8	2.672	2.509	6.10	17.1	64.3		
		BDM013	5.3	2.695	2.440	9.50	18.9	49.7		
		BDM013B	4.8	2.719	2.445	10.1	18.3	44.8		
		BDM014	5.3	2.695	2.445	9.30	18.8	50.5		
		BDM014B	4.8	2.719	2.442	10.2	18.4	44.6		

Table 1(Cont'd). Characteristics of UHO data set specimens.

Aggreg. Gradation	Binder Grade	Specimen ID	P_b	G_{mm}	G_{mb}	AV	VMA	VFA	Additive	Test Condition
Type B Gse: 2.954	PG70-XX Gb: 1.019	BDM015	5.8	2.661	2.383	10.4	21.2	50.9	Elvaloy®Ret	None
		BDM015B	5.8	2.661	2.522	5.20	16.6	68.7		
		BDM016	5.8	2.661	2.484	6.70	17.9	62.6		
		BDM017	5.3	2.684	2.449	8.80	18.6	52.7		
		BDM018	5.3	2.684	2.473	7.90	17.8	55.6		
		BDM019	4.8	2.707	2.512	7.20	16.1	55.3		
		BDM020	4.8	2.707	2.523	6.80	15.7	56.7		
		BDM021	4.8	2.707	2.473	8.60	17.4	50.6		
		BDM022	4.8	2.707	2.482	8.30	17.1	51.5		
		BDM023	5.3	2.684	2.538	5.40	15.7	65.6		
		BDM024	5.3	2.684	2.537	5.50	15.7	65.0		
		BDM025	5.3	2.684	2.627	2.10	12.7	83.5		
		BDM026	5.8	2.661	2.603	2.20	14.0	84.3		
		BDM027	5.3	2.684	2.618	2.50	13.0	80.8		
		11EL53	5.3	2.684	2.623	2.30	12.8	82.0		
		BDM028	5.8	2.661	2.601	2.30	14.0	83.6		
Type B Gse: 2.956	PG70-22 Gb: 1.027	BDM029	4.8	2.712	2.575	5.10	14.0	63.6	SBS	None
		BDM030	5.3	2.688	2.549	5.20	15.3	66.0		
		BDM031	4.8	2.712	2.487	8.30	16.9	50.9		
		BDM033	5.8	2.665	2.610	2.10	13.7	84.7		
		BDM035	5.8	2.665	2.503	6.10	17.3	64.7		
SP 12.5mm Gse: 4.8	PG64-16 Gb: 1.016	H3-E2	6.1	2.501	2.388	4.50	15.9	71.7	None	None
MT IV Gse: 5.159	Warm Mix Gb: 1.016	FARE41	5.9	2.476	2.455	0.90	13.3	93.2	Sasobit	None
MT IV Gse: 5.159	Warm Mix Gb: 1.016	FARE51	5.9	2.476	2.420	2.30	14.6	84.3	Sasobit	None
SP 12.5mm Gse: 4.58	PG64-16 Gb: 1.025	GL1S71	5.2	2.587	2.436	5.80	16.7	65.3	None	None

As explained before, this first data set includes mixtures with several modifiers (i.e., SBS, Elvaloy®Ret, and Sasobit), each of them influencing the behavior of the mixtures in different ways. Changes in dynamic modulus due to the addition of these binder modifiers are not being quantified with the use of the current models of the MEPDG at levels 2 and 3. Therefore, the

introduction of newer models to account for this behavior is needed due to the increasing demand of modified mixtures for different projects around the world.

A second characteristic of this data set that is not commonly taken into consideration is the inclusion of a confining pressure, which as mentioned before, has the objective of simulating field conditions closely. One confinement level of 100 kPa (14.5 psi) was used for a few specimens in this data base, particularly for specimens of the ADM mixture with a PG64-16 binder, the ADM mixture with a PG70-XX binder, and the BDM mixture with a PG64-16 binder. While one other specimen (BDM01) was tested with confining pressures of 50 kPa, 100 kPa, 150 kPa and 200 kPa (7.25 psi, 14.5 psi, 21.75 psi and 29 psi respectively), it was determined that the measurement of the dynamic modulus for these conditions was probably not carried out properly, since this was the first attempt at using confining pressure during dynamic modulus tests at UH. Careful observation of the data points confirmed that the values obtained did not aligned with expected results and therefore these were subtracted from the data set.

This first data set contains 2974 valid points (i.e., points satisfying normal quality control standards such as the load standard error, the deformation uniformity and others statistics required by the AASHTO standards for data quality during dynamic modulus testing.)

4.2 University of Hawaii second data set

The second data set collected at the University of Hawaii consists of 42 laboratory-mixed, laboratory-compacted specimens prepared for a project on the performance of mixtures for the Honolulu International Airport. This data set was called UHN, with the N meaning “new”, due its recent collection. The 42 specimens were prepared by following a Marshall mix design specifically used at the airport and provided by one of the contractors on Oahu. However, to compare the performance of different mixtures, in addition to the unmodified binder, an SBS modified asphalt and synthetic fibers were included, allowing for 4 different combinations, i.e. virgin asphalt (HMA), virgin asphalt with fibers (FHMA), polymer modified asphalt (PMA) and polymer modified asphalt with fibers (FPMA). Each set of specimens was compacted at three target air void levels (4%, 7% and 9%).

The gradation used for this data set is shown in Figure 7 in a 0.45-power chart. The aggregates for these mixtures are basaltic aggregates from the Kapaa quarry in Oahu. As mentioned before, this is a gradation specifically built for the airport with 100% new aggregates. Although the mixtures typically used on the island of Oahu include a percentage of recycled asphalt pavements

(RAP), its use is not allowed for airport pavements in the state of Hawaii. This mixture meets most of the Superpave gradation specifications for a 12.5mm (1/2 in) NMAS. Strictly speaking, its gradation does not meet the requirement of 90% for the 12.5 mm (1/2 in) sieve; however, it is extremely close to the lower bound with a value of 89.9%. While it also meets the gradation requirements for a 19 mm (3/4 in) NMAS, it was felt that it is more representative of a 12.5 mm (1/2 in) NMAS mix.

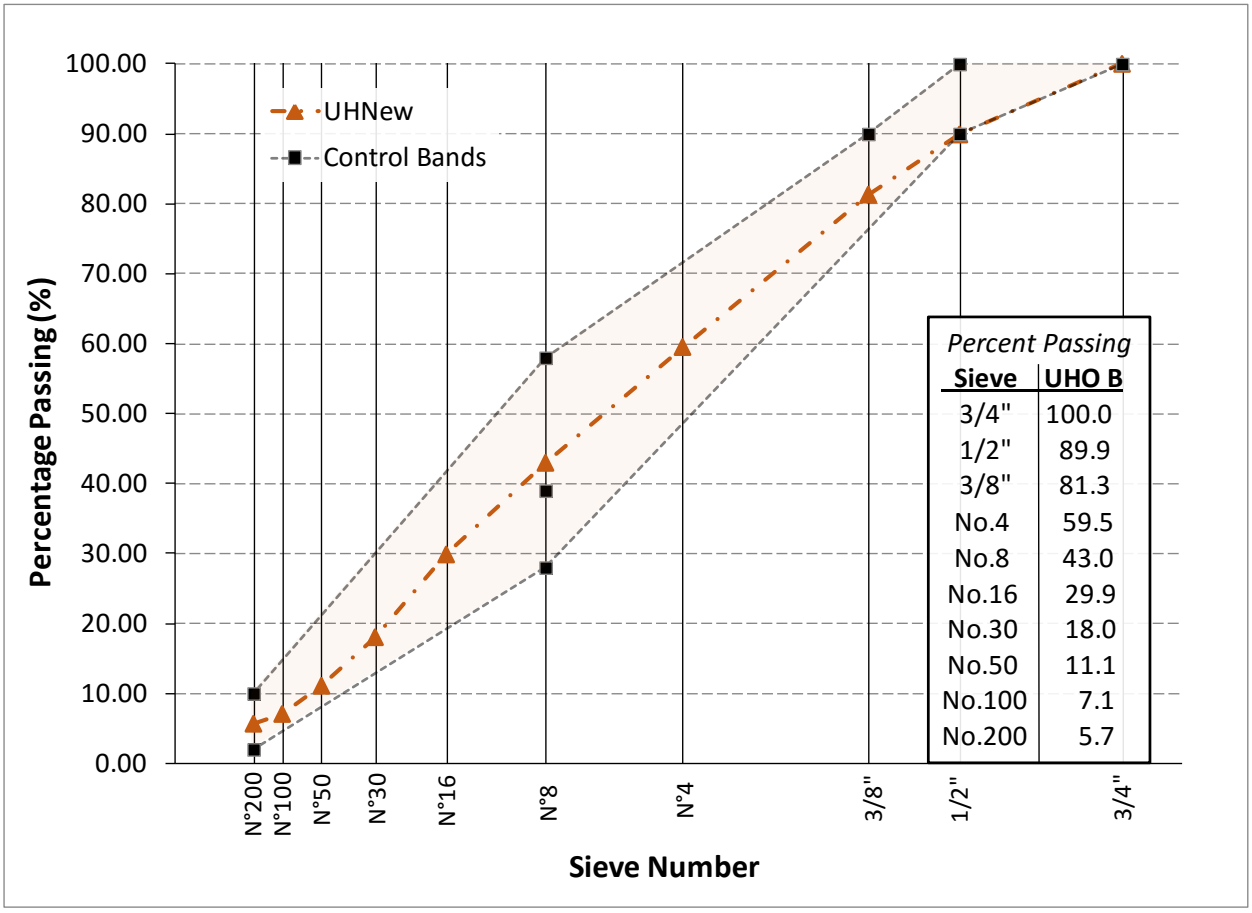

Figure 7. Gradation curves for the UHN data set

For these mixtures, the asphalt binders used were a virgin (unmodified) PG64-22 and an SBS polymer modified PG76-22. The virgin asphalt was imported from Venezuela and was the one being used for everyday jobs in the island until recently. On the other hand, the modified binder is a commercially available binder, modified from the PG64-22 with an SBS at a percentage not disclosed by the producer. The fibers used for this project are a combination of polyolefin and

aramid fibers mixed at a rate equivalent to 1 pound/ton of mix (0.5 g/kg). The fibers were introduced to the mixture per the manufacturer's specifications during the mixing procedure. According to the Marshall mix design provided, the optimum asphalt binder content for these mixtures was 6.1% by total weight of mix (TWM). Three specimens for each of the four mixture combinations were compacted at a target of 4%, 7% and 9% air voids, except for the case of the HMA and FHMA mixtures at 7% air voids, where six specimens were compacted. By testing six specimens instead of three, the coefficient of variation for the mean of the measured dynamic modulus is reduced from 7.5% to 5.3% (AASHTO R62, 2016). The reason behind this decision was to verify the results from the first set of three specimens since these were contrary to a priori expectations (i.e., it was noted that the addition of fibers tended to result in lower dynamic moduli). A summary of the characteristics of the UHN specimens is shown in Table 2.

Table 2. Characteristics of UHN data set specimens.

Aggreg. Gradation	Binder Grade	Specimen ID	P_b	G_{mm}	G_{mb}	AV	VMA	VFA	Additive	Test Condit.
SP 12.5mm Gse: 2.741	PG64-22 Gb: 1.036	HMA-S1-4AV	6.1	2.491	2.388	4.13	15.0	72.5	None	4 Confinement Levels (69 kPa, 138 kPa, 207 kPa)
		HMA-S2-4AV	6.1	2.491	2.402	3.57	14.5	75.4		
		HMA-S3-4AV	6.1	2.491	2.403	3.53	14.5	75.6		
		HMA-S1-7AV	6.1	2.491	2.320	6.86	17.5	60.7		
		HMA-S2-7AV	6.1	2.491	2.324	6.70	17.3	61.3		
		HMA-S3-7AV	6.1	2.491	2.311	7.23	17.8	59.3		
		HMA-S4-7AV	6.1	2.491	2.315	7.07	17.6	59.9		
		HMA-S5-7AV	6.1	2.491	2.313	7.16	17.7	59.6		
		HMA-S6-7AV	6.1	2.491	2.321	6.82	17.4	60.8		
		HMA-S1-9AV	6.1	2.491	2.273	8.75	19.1	54.2		
		HMA-S2-9AV	6.1	2.491	2.270	8.87	19.2	53.9		
		HMA-S3-9AV	6.1	2.491	2.261	9.23	19.6	52.8		
SP 12.5mm Gse: 2.741	PG64-22 Gb: 1.036	FHMA-S1-4AV	6.1	2.491	2.388	4.13	15.0	72.5	Fibers	4 Confinement Levels (69 kPa, 138 kPa, 207 kPa)
		FHMA-S2-4AV	6.1	2.491	2.386	4.22	15.1	72.1		
		FHMA-S3-4AV	6.1	2.491	2.395	3.85	14.8	73.9		
		FHMA-S1-7AV	6.1	2.491	2.305	7.47	18.0	58.5		
		FHMA-S2-7AV	6.1	2.491	2.307	7.39	17.9	58.8		
		FHMA-S3-7AV	6.1	2.491	2.304	7.51	18.0	58.3		
		FHMA-S4-7AV	6.1	2.491	2.307	7.39	17.9	58.8		
		FHMA-S5-7AV	6.1	2.491	2.304	7.51	18.0	58.3		
		FHMA-S6-7AV	6.1	2.491	2.302	7.59	18.1	58.1		
		FHMA-S1-9AV	6.1	2.491	2.258	9.35	19.7	52.4		
		FHMA-S2-9AV	6.1	2.491	2.256	9.43	19.7	52.2		
		FHMA-S3-9AV	6.1	2.491	2.255	9.47	19.8	52.1		

Table 2 (Cont'd). Characteristics of UHN data set specimens.

Aggreg. Gradation	Binder Grade	Specimen ID	P_b	G_{mm}	G_{mb}	AV	VMA	VFA	Additive	Test Condit.
SP 12.5mm Gse: 2.741	PG76-22 Gb: 1.026	PMA-S1-4AV	6.1	2.489	2.399	3.62	14.6	75.3	SBS	4 Confinement Levels (69 kPa, 138 kPa, 207 kPa)
		PMA-S2-4AV	6.1	2.489	2.385	4.18	15.1	72.4		
		PMA-S3-4AV	6.1	2.489	2.400	3.58	14.6	75.5		
		PMA-S1-7AV	6.1	2.489	2.318	6.87	17.5	60.8		
		PMA-S2-7AV	6.1	2.489	2.313	7.07	17.7	60.1		
		PMA-S3-7AV	6.1	2.489	2.313	7.07	17.7	60.1		
		PMA-S1-9AV	6.1	2.489	2.265	9.00	19.4	53.6		
		PMA-S2-9AV	6.1	2.489	2.277	8.52	19.0	55.1		
		PMA-S3-9AV	6.1	2.489	2.276	8.56	19.0	55.0		
SP 12.5mm Gse: 2.741	PG76-22 Gb: 1.026	FPMA-S1-4AV	6.1	2.489	2.403	3.46	14.5	76.2	SBS +Fibers	4 Confinement Levels (69 kPa, 138 kPa, 207 kPa)
		FPMA-S2-4AV	6.1	2.489	2.402	3.50	14.5	76.0		
		FPMA-S3-4AV	6.1	2.489	2.400	3.58	14.6	75.5		
		FPMA-S1-7AV	6.1	2.489	2.319	6.83	17.5	60.9		
		FPMA-S2-7AV	6.1	2.489	2.311	7.15	17.8	59.8		
		FPMA-S3-7AV	6.1	2.489	2.321	6.75	17.4	61.2		
		FPMA-S1-9AV	6.1	2.489	2.277	8.52	19.0	55.1		
		FPMA-S2-9AV	6.1	2.489	2.274	8.64	19.1	54.7		
		FPMA-S3-9AV	6.1	2.489	2.272	8.72	19.2	54.5		

Three different characteristics of this data set are important for estimation of the predictive dynamic modulus model. A first characteristic is the use of a modified asphalt. As discussed in the previous section, the first data set (UHO) also included a modified asphalt and so does the third data set discussed later. However, as explained before, the modification of asphalt binders can be done in many ways with several different modifiers and therefore, each modified binder can (and most likely will) perform in a slightly different way even if the different modified binders have the same binder grade. Thus, inclusion of different modified binders can help to identify the potential differences between different modifiers and/or binders used in different places or in each place over time. Although, this puts some burden on the user to select the most representative binder parameters for a given binder grade (from those estimated from a model using several binders with the same grade but accounting for their differences in performance), it is at least a conscious decision based on something readily available such as the binder grade and often the binder source that may result in similar results to those obtained with models that include a binder characteristic such as viscosity, which is not obtained at temperatures representative of service conditions, or more advanced binder characteristics such as dynamic shear modulus and phase angle, which are usually obtained or available for a single frequency

and at one (or a few) temperatures. At this point it is important to remember that the high temperature of the two modified asphalt binders in the two UH studies is 76°C even though different modifiers and procedures were used to achieve this grade. In other words, the binder grade alone may not be enough to capture the binder effects. For example, even if the same base asphalt, say a PG64-22, is modified with different products such as SBS and Elvaloy®Ret to reach two binders with a final grade of PG76-22, the true grades may be a PG78-22 in one case and a PG80-22 for the other. Since neither of these meet the minimum requirements for a PG82-22 binder, they will both be classified as PG76-22. It is important to note that even if the true grade were the same, the different modifiers may perform slightly different.

Another example relevant for the UHN data set and the data set from Costa Rica described later, is the modification of two different base asphalt binders such as a PG64-22 and a PG70-22 with two different percentages of the same modifier to reach a classification of PG76-22. In fact, this was the case for this study since for the UHN data set, a PG64-22 base was used while in Costa Rica (the third data set) a PG70-22 base was used, with both asphalts achieving a PG76-22 grade by using adequate percentages of the SBS modifier.

A second characteristic of this data set that was considered in the predictive model is the use of synthetic fibers. The use of fibers was one of the required options to be evaluated for their use at the Honolulu airport and therefore they were combined with both the virgin and the modified asphalt mixtures. For this experiment, it was noted that the use of the polyolefin and aramid fibers resulted in general in a slight reduction of the dynamic modulus values. This result will be discussed during the description of the model development.

The third and final characteristic of this data set that is included in the model is the use of confinement pressure. The difference from these results and the ones included in the UHO data set is that for the UHN experiment, four confinement levels were used, i.e. 0 kPa (no confinement), 69 kPa, 138 kPa and 207 kPa (0 psi, 10psi, 20 psi and 30 psi). Also, the use of confinement pressure was part of the experimental plan for this specific data set, and therefore the same confinement levels were used for all specimens in the set instead of just a few samples like in the case of the UHO data set. The inclusion of four levels of confinement for all specimens, temperatures and frequencies, expanded the results to a point where specific trends could be identified and therefore included in the predictive model.

This second data set contains 2430 valid points.

4.3 Costa Rican Data Set

The third data set used for this project was collected in Costa Rica by the National Laboratory of Materials and Structural Models (LanammeUCR), which is a research institution that belongs to the University of Costa Rica. This data set (referred to as CR herein) was collected for a study to determine the behavior of asphalt mixtures when moisture damage was induced. In this case, 12 Superpave mix designs were performed while using two different aggregate gradations (6 mixture designs per aggregate gradation). Twelve specimens per design were mixed and compacted in the laboratory, for a total of 144 asphalt specimens with target air voids of 7%. However, for the 9.5NMAS-HMA-LIME group, one specimen was not tested, therefore data was collected for 143 specimens.

Regarding the aggregates for this data set, these are igneous rocks taken from a quarry in Guapiles, in the northeast part of Costa Rica, province of Limon. This aggregate source is known to show moisture related deterioration in the field (Nordbeck et al. 2016), which made it ideal for their study. The two aggregate gradations used in this project are shown in Figure 8 in a 0.45-power chart. As shown in the figure, these two gradations have different nominal maximum aggregate sizes (NMAS): 9.5 mm (3/8 in) and 12.5 mm (1/2 in). Both gradations meet the Superpave gradation specifications for each NMAS size (though as shown in Figure 8, the 9.5mm NMAS crosses the line joining two of the control points) and were chosen as representative of the combinations commonly used in Costa Rica for everyday paving jobs.

The asphalt binders used in the LanammeUCR study are a virgin PG70-22 (used as base), and another SBS polymer modified PG76-22, modified with 2% SBS by mass of binder. The base asphalt is imported to Costa Rica from the United States and it is used for all regular paving jobs in the country. On the other hand, the modified binder was produced at LanammeUCR to carry out their experiment. The optimum asphalt binder content for these mixtures vary from 5.9% to 7% by total weight of mixture while the air voids vary from 5.65% to 7.93%.

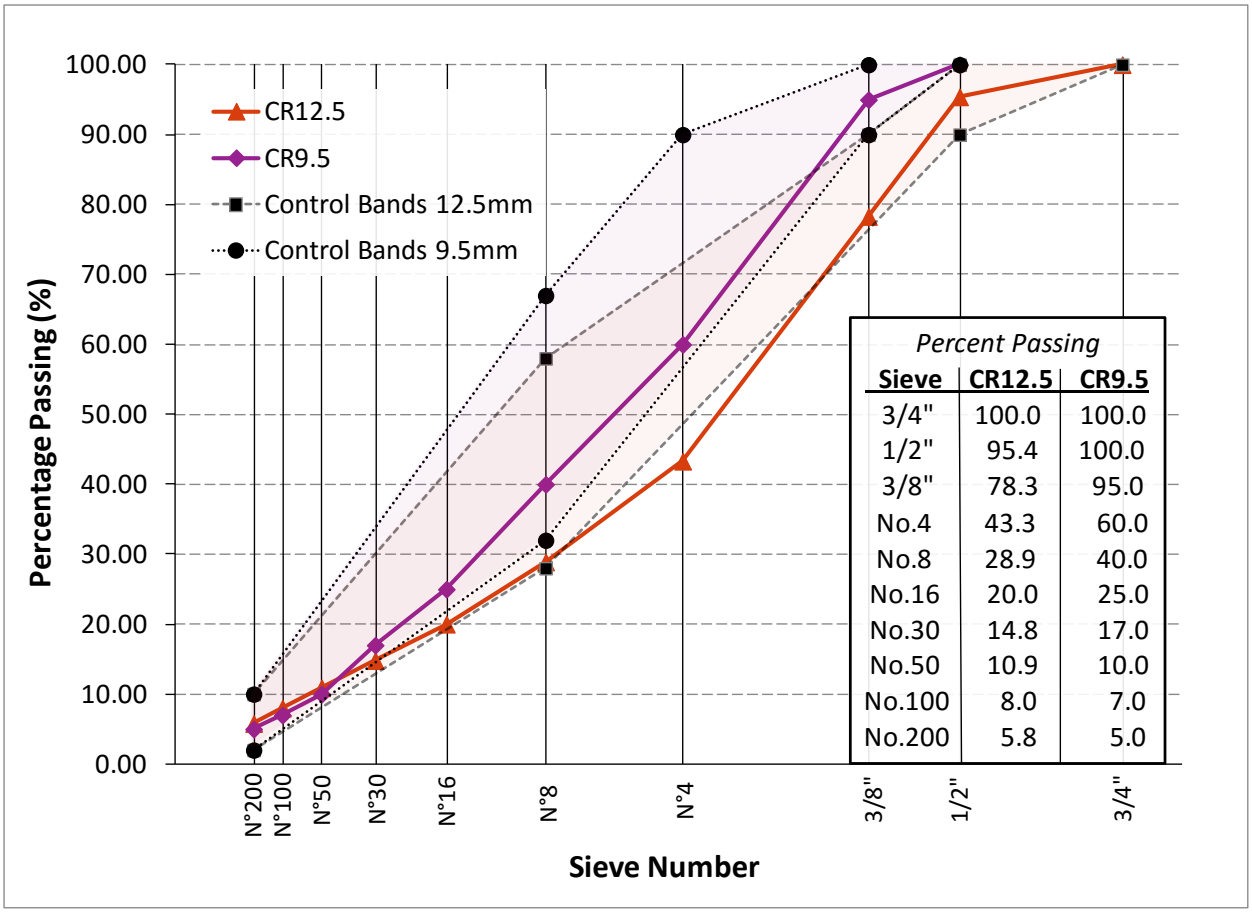

Figure 8. Gradation curves for the CR data set

The experiment carried out by LanammeUCR included for some specimens, the use of a commercial liquid anti-stripping (LAS) agent at a rate of 0.5% by total weight of binder, and for others, the use of hydrated lime at a rate of 1% by total weight of aggregate (hydrated lime is also used to mitigate asphalt stripping). These agents in combination with the two binder grades give a total of 6 mixtures, including a control mix for each of the aggregate sizes. From the 12 specimens compacted for each mixture, 9 specimens were exposed to different freezing and thawing (F-T) cycles, i.e. 1 cycle, 3 cycles and 6 cycles (3 specimens per number of cycles), to induce moisture damage in the mixtures (the remaining 3 specimens were used as a control for each mixture type). As explained before, the use of a water bath to condition the specimens had been shown to be a poor indicator of the susceptibility of the mixtures and therefore a more severe approach was used in this experiment.

A summary of the characteristics for this last data set is shown in Table 3.

Table 3. Characteristics of CR data set specimens.

Aggreg. Gradation	Binder Grade	Specimen ID	P_b	G_{mm}	G_{mb}	AV	VMA	VFA	Additive	Test Condition
9.5 NMAS Gse: 2.691	PG70-22 Gb:1.025	HMA-S1	6.5	2.434	2.275	6.53	17.9	63.6	None	Freeze-Thaw Cycles (0-1-3-6)
		HMA-S2	6.5	2.434	2.276	6.48	17.9	63.8		
		HMA-S3	6.5	2.434	2.268	6.82	18.2	62.5		
		HMA-S4	6.5	2.434	2.261	7.09	18.4	61.5		
		HMA-S5	6.5	2.434	2.273	6.59	18.0	63.3		
		HMAS6	6.5	2.434	2.280	6.31	17.7	64.4		
		HMA-S7	6.5	2.434	2.252	7.47	18.8	60.2		
		HMA-S8	6.5	2.434	2.273	6.60	18.0	63.3		
		HMA-S9	6.5	2.434	2.275	6.53	17.9	63.6		
		HMA-S10	6.5	2.434	2.284	6.17	17.6	65.0		
		HMA-S12	6.5	2.434	2.263	7.02	18.4	61.8		
		HMA-S13	6.5	2.434	2.271	6.72	18.1	62.9		
9.5 NMAS Gse: 2.691	PG70-22 Gb:1.025	L-HMA-S7	6.7	2.427	2.274	6.31	18.2	65.3	Lime	Freeze-Thaw Cycles (0-1-3-6)
		L-HMA-S8	6.7	2.427	2.268	6.54	18.4	64.4		
		L-HMA-S9	6.7	2.427	2.269	6.50	18.3	64.5		
		L-HMA-S10	6.7	2.427	2.266	6.62	18.4	64.1		
		L-HMA-S11	6.7	2.427	2.270	6.44	18.3	64.8		
		L-HMA-S12	6.7	2.427	2.263	6.76	18.6	63.6		
		L-HMA-S13	6.7	2.427	2.235	7.91	19.6	59.6		
		L-HMA-S14	6.7	2.427	2.245	7.47	19.2	61.1		
		L-HMA-S15	6.7	2.427	2.237	7.82	19.5	59.9		
		L-HMA-S16	6.7	2.427	2.255	7.07	18.8	62.5		
		L-HMA-S17	6.7	2.427	2.252	7.17	18.9	62.1		
9.5 NMAS Gse: 2.705	PG70-22 Gb:1.025	MB-HMA-S3	6.5	2.445	2.251	7.93	18.8	57.9	Magnabond	Freeze-Thaw Cycles (0-1-3-6)
		MB-HMA-S5	6.5	2.445	2.259	7.59	18.5	59.0		
		MB-HMA-S7	6.5	2.445	2.254	7.82	18.7	58.2		
		MB-HMA-S8	6.5	2.445	2.255	7.77	18.7	58.4		
		MB-HMA-S9	6.5	2.445	2.265	7.36	18.3	59.8		
		MB-HMA-S13	6.5	2.445	2.277	6.84	17.9	61.7		
		MB-HMA-S14	6.5	2.445	2.272	7.08	18.1	60.8		
		MB-HMA-S15	6.5	2.445	2.275	6.95	18.0	61.3		
		MB-HMA-S16	6.5	2.445	2.277	6.84	17.9	61.7		
		MB-HMA-S17	6.5	2.445	2.273	7.03	18.0	61.0		
		MB-HMA-S18	6.5	2.445	2.285	6.55	17.6	62.8		
		MB-HMA-S19	6.5	2.445	2.284	6.58	17.6	62.7		

Table 3 (Cont'd). Characteristics of UCR data set specimens.

Aggreg. Gradation	Binder Grade	Specimen ID	P_b	G_{mm}	G_{mb}	AV	VMA	VFA	Additive	Test Condition
9.5 NMAS Gse: 2.709	PG76-22 Gb:1.024	PMA-S1	6.5	2.447	2.273	7.12	18.0	60.5	SBS	Freeze-Thaw Cycles (0-1-3-6)
		PMA-S3	6.5	2.447	2.266	7.40	18.3	59.5		
		PMA-S4	6.5	2.447	2.268	7.33	18.2	59.7		
		PMA-S5	6.5	2.447	2.258	7.72	18.5	58.3		
		PMA-S6	6.5	2.447	2.268	7.32	18.2	59.7		
		PMA-S7	6.5	2.447	2.273	7.11	18.0	60.5		
		PMA-S8	6.5	2.447	2.271	7.21	18.1	60.1		
		PMA-S9	6.5	2.447	2.270	7.26	18.1	60.0		
		PMA-S10	6.5	2.447	2.270	7.23	18.1	60.1		
		PMA-S11	6.5	2.447	2.270	7.23	18.1	60.1		
		PMA-S12	6.5	2.447	2.262	7.58	18.4	58.8		
		PMA-S13	6.5	2.447	2.277	6.95	17.9	61.1		
9.5 NMAS Gse: 2.684	PG76-22 Gb:1.024	L-PMA-S4	6.6	2.425	2.250	7.23	18.9	61.8	SBS + Lime	Freeze-Thaw Cycles (0-1-3-6)
		L-PMAS5	6.6	2.425	2.252	7.14	18.8	62.1		
		L-PMA-S6	6.6	2.425	2.264	6.65	18.4	63.9		
		L-PMA-S7	6.6	2.425	2.258	6.89	18.6	63.0		
		L-PMA-S8	6.6	2.425	2.251	7.17	18.9	62.0		
		L-PMA-S9	6.6	2.425	2.259	6.85	18.6	63.2		
		L-PMA-S10	6.6	2.425	2.249	7.26	19.0	61.7		
		L-PMA-S11	6.6	2.425	2.251	7.20	18.9	61.9		
		L-PMA-S12	6.6	2.425	2.253	7.12	18.8	62.2		
		L-PMA-S13	6.6	2.425	2.254	7.05	18.8	62.4		
		L-PMA-S14	6.6	2.425	2.252	7.15	18.9	62.1		
		L-PMA-S15	6.6	2.425	2.253	7.12	18.8	62.2		
9.5 NMAS Gse: 2.704	PG76-22 Gb:1.024	MB-PMA-S7	6.3	2.451	2.280	7.00	17.6	60.2	SBS + Magnabond	Freeze-Thaw Cycles (0-1-3-6)
		MB-PMA-S8	6.3	2.451	2.288	6.66	17.3	61.5		
		MB-PMA-S9	6.3	2.451	2.279	7.02	17.6	60.1		
		MB-PMA-S10	6.3	2.451	2.287	6.70	17.3	61.4		
		MB-PMA-S11	6.3	2.451	2.281	6.96	17.6	60.4		
		MB-PMA-S12	6.3	2.451	2.284	6.84	17.5	60.8		
		MB-PMA-S13	6.3	2.451	2.281	6.96	17.6	60.4		
		MB-PMA-S14	6.3	2.451	2.287	6.71	17.3	61.3		
		MB-PMA-S15	6.3	2.451	2.292	6.50	17.2	62.1		
		MB-PMA-S16	6.3	2.451	2.283	6.85	17.5	60.8		
		MB-PMA-S17	6.3	2.451	2.287	6.68	17.3	61.4		
		MB-PMA-S18	6.3	2.451	2.280	7.00	17.6	60.2		

Table 3 (Cont'd). Characteristics of UCR data set specimens.

Aggreg. Gradation	Binder Grade	Specimen ID	P_b	G_{mm}	G_{mb}	AV	VMA	VFA	Additive	Test Condition
12.5 NMAS Gse: 2.712	PG70-22 Gb:1.025	HMA-S1	7	2.432	2.240	7.90	18.9	58.3	None	Freeze-Thaw Cycles (0-1-3-6)
		HMA-S2	7	2.432	2.257	7.18	18.3	60.8		
		HMA-S3	7	2.432	2.244	7.72	18.8	58.9		
		HMA-S5	7	2.432	2.242	7.81	18.9	58.6		
		HMA-S6	7	2.432	2.262	7.01	18.2	61.4		
		HMA-S7	7	2.432	2.250	7.47	18.6	59.8		
		HMA-S8	7	2.432	2.266	6.81	18.0	62.2		
		HMA-S9	7	2.432	2.240	7.91	19.0	58.3		
		HMA-S10	7	2.432	2.259	7.11	18.3	61.1		
		HMA-S14	7	2.432	2.270	6.65	17.9	62.7		
		HMA-S15	7	2.432	2.274	6.48	17.7	63.4		
		HMA-S16	7	2.432	2.263	6.95	18.1	61.6		
12.5 NMAS Gse:2.689	PG70-22 Gb:1.025	L-HMA-S4	6	2.451	2.282	6.88	16.5	58.4	Lime	Freeze-Thaw Cycles (0-1-3-6)
		L-HMA-S5	6	2.451	2.284	6.80	16.5	58.7		
		L-HMA-S6	6	2.451	2.291	6.50	16.2	59.9		
		L-HMA-S7	6	2.451	2.290	6.56	16.3	59.6		
		L-HMA-S8	6	2.451	2.279	7.01	16.7	57.9		
		L-HMA-S9	6	2.451	2.291	6.50	16.2	59.9		
		L-HMA-S10	6	2.451	2.302	6.07	15.8	61.6		
		L-HMA-S11	6	2.451	2.312	5.65	15.4	63.4		
		L-HMA-S12	6	2.451	2.297	6.27	16.0	60.8		
		L-HMA-S13	6	2.451	2.297	6.25	16.0	60.9		
		L-HMA-S14	6	2.451	2.293	6.41	16.1	60.2		
		L-HMA-S15	6	2.451	2.301	6.09	15.8	61.5		
12.5 NMAS Gse: 2.705	PG70-22 Gb:1.025	MB-HMA-S3	6.5	2.444	2.258	7.61	17.8	57.3	Magnabond	Freeze-Thaw Cycles (0-1-3-6)
		MB-HMA-S4	6.5	2.444	2.278	6.80	17.1	60.3		
		MB-HMA-S5	6.5	2.444	2.264	7.36	17.6	58.2		
		MB-HMA-S6	6.5	2.444	2.272	7.07	17.4	59.3		
		MB-HMA-S7	6.5	2.444	2.255	7.73	17.9	56.9		
		MB-HMA-S8	6.5	2.444	2.263	7.42	17.7	58.0		
		MB-HMA-S9	6.5	2.444	2.281	6.68	17.0	60.7		
		MB-HMA-S10	6.5	2.444	2.281	6.68	17.0	60.8		
		MB-HMA-S11	6.5	2.444	2.280	6.71	17.0	60.6		
		MB-HMA-S12	6.5	2.444	2.273	7.03	17.3	59.4		
		MB-HMA-S13	6.5	2.444	2.282	6.63	17.0	60.9		
		MB-HMA-S14	6.5	2.444	2.291	6.28	16.7	62.3		

Table 3 (Cont'd). Characteristics of UCR data set specimens.

Aggreg. Gradation	Binder Grade	Specimen ID	P_b	G_{mm}	G_{mb}	AV	VMA	VFA	Additive	Test Condition
12.5 NMAS Gse: 2.703	PG76-22 Gb:1.024	PMA-S4	6.5	2.443	2.251	7.87	18.1	56.5	SBS	Freeze-Thaw Cycles (0-1-3-6)
		PMA-S5	6.5	2.443	2.261	7.46	17.7	58.0		
		PMA-S6	6.5	2.443	2.266	7.27	17.6	58.6		
		PMA-S7	6.5	2.443	2.261	7.45	17.7	58.0		
		PMA-S8	6.5	2.443	2.250	7.90	18.1	56.5		
		PMA-S9	6.5	2.443	2.265	7.28	17.6	58.6		
		PMA-S10	6.5	2.443	2.259	7.52	17.8	57.7		
		PMA-S11	6.5	2.443	2.256	7.68	17.9	57.2		
		PMA-S12	6.5	2.443	2.266	7.27	17.6	58.6		
		PMA-S13	6.5	2.443	2.257	7.62	17.9	57.4		
		PMA-S14	6.5	2.443	2.249	7.93	18.2	56.3		
		PMA-S15	6.5	2.443	2.254	7.73	18.0	57.0		
12.5 NMAS Gse: 2.692	PG76-22 Gb:1.024	L-PMA-S4	6.3	2.442	2.283	6.52	16.8	61.2	SBS + Lime	Freeze-Thaw Cycles (0-1-3-6)
		L-PMA-S5	6.3	2.442	2.270	7.04	17.2	59.2		
		L-PMA-S6	6.3	2.442	2.270	7.05	17.3	59.1		
		L-PMA-S7	6.3	2.442	2.276	6.80	17.0	60.1		
		L-PMA-S8	6.3	2.442	2.268	7.10	17.3	58.9		
		L-PMA-S9	6.3	2.442	2.263	7.31	17.5	58.2		
		L-PMA-S11	6.3	2.442	2.289	6.24	16.5	62.2		
		L-PMA-S12	6.3	2.442	2.290	6.24	16.5	62.3		
		L-PMA-S13	6.3	2.442	2.293	6.09	16.4	62.9		
		L-PMA-S14	6.3	2.442	2.286	6.38	16.7	61.7		
		L-PMA-S15	6.3	2.442	2.292	6.12	16.4	62.7		
		L-PMA-S16	6.3	2.442	2.282	6.54	16.8	61.0		
12.5 NMAS Gse: 2.705	PG76-22 Gb:1.024	MB-PMA-S4	5.9	2.467	2.302	6.66	15.7	57.6	SBS + Magnabond	Freeze-Thaw Cycles (0-1-3-6)
		MB-PMA-S5	5.9	2.467	2.308	6.44	15.5	58.5		
		MB-PMA-S6	5.9	2.467	2.305	6.55	15.6	58.0		
		MB-PMA-S7	5.9	2.467	2.297	6.89	15.9	56.7		
		MB-PMA-S8	5.9	2.467	2.306	6.50	15.6	58.2		
		MB-PMA-S9	5.9	2.467	2.298	6.84	15.9	56.9		
		MB-PMA-S10	5.9	2.467	2.293	7.05	16.1	56.1		
		MB-PMA-S11	5.9	2.467	2.300	6.74	15.8	57.3		
		MB-PMA-S12	5.9	2.467	2.291	7.11	16.1	55.9		
		MB-PMA-S13	5.9	2.467	2.287	7.28	16.3	55.2		
		MB-PMA-S14	5.9	2.467	2.300	6.77	15.8	57.2		
		MB-PMA-S15	5.9	2.467	2.295	6.98	16.0	56.4		

In addition to the use of modified binders, as in the other two data sets; the data set from Costa Rica has the peculiarity of including freezing and thawing (F-T) cycles and anti-stripping agents. The effect of the F-T cycles as well as the counter-effect of the anti-stripping agents is expected to be identified from this data set in the predictive model. The use of F-T cycles is detrimental

for the mixture and is used as a surrogate to estimate potential moisture damage in the field. Similarly, the consideration of the anti-stripping agents in the model can also be used to predict their performance benefits when moisture exposure is expected. In fact, these benefits may be observed even without the use of F-T cycles. These characteristics, besides not being included currently in the dynamic modulus predictive model used by the MEPDG, can also help to estimate the potential for damage accumulation over time in zones where high amounts of rain or any other water exposure is expected during the pavement design life. It is important to note that for such use of the model, further research is needed to correlate different F-C cycles to levels of moisture damage exposure in the field. In other words, at this point, a model estimated with these data can only quantify the effects of F-T cycles but without further research it is not yet possible to predict how the modulus would change with moisture exposure in the field.

This third data set completes the entire data base with an additional 1417 valid points.

4.4 Quality control of the data

All data used for developing the model was subjected to a very strict quality control process to make sure that it complied with the data quality statistics requirements from the AASHTO standard (AASHTO 2016). Since the AMPT (Figure 2) was used for testing of all samples in the three data sources, the requirements given by AASHTO TP79 (developed specifically for tests with this machine) were used. Four limits are set in this standard method: a) a load standard error of less than 10%, b) a deformation standard error of less than 10%, c) a deformation uniformity of less than 30% and d) a phase uniformity of less than 3°. Additionally, the peak to peak strain should be kept between 75 and 125 microstrains for an unconfined test and between 85 and 115 microstrains for a confined test. These statistics are included among the outputs of the software for each measurement of |E*|.

Moreover, the data sources were also manually checked for inconsistencies. This means that they were examined to guarantee that the values followed a logical order in their magnitude according to their temperature and confinement level.

The total initial number of data points for each data source were as follows: 3392 points for UHO, 2506 points for UHN and 1430 points for CR. In the case of the UHO data set, close to a third of the data points subtracted (around 130 points) corresponded to values of |E*| with a confinement different from 100 kPa, which was the only confinement level other than zero considered from this data set. Another full sample was excluded from this data set since its

values were much higher than the rest of the samples with similar volumetric characteristics and the same materials. It was also the first sample tested in all the UHO data set. This sample was tested at 5 different confinement levels (0, 50, 100, 150, 200kPa) and therefore its exclusion eliminated close to 100 data points. Another two samples were excluded from this data set since they were field mixtures from the H3 freeway in Oahu that performed very poorly. The last portion of the data excluded from this data set were values of |E*| at intermediate and high temperatures that were higher than other values tested at lower temperatures. It is believed that in these cases, the temperature conditioning time was not appropriate and the samples were tested when the sample was not at the target temperature even though the machine indicated otherwise. From this data set, no values were excluded due to the quality statistics set by the AASHTO standards since this data set (without confinement) was used for a previous study (Archilla, 2010) and those were excluded at that time. In total 418 points were excluded from this data set. In the case of the UHN data set, 26 values were excluded for not complying with the quality statistics defined by AASHTO TP79. Another 55 values were excluded due to inconsistencies in their magnitude for different confinements. These situations were observed only for the highest testing temperature. A typical inconsistency found is, for example, a value of |E*| for a frequency of 0.1Hz or 0.01Hz and a confinement level of 138kPa (20 psi) that was lower than the corresponding value for a confinement level of 69kPa (10 psi) or higher than the corresponding value for a confinement of 207kPa (30 psi). Before eliminating the point, all other values at different frequencies were compared with their counterparts for other confinement levels to make sure that the extracted value had in fact a magnitude problem. A total of 76 values were excluded from this second data set.

Finally, for the CR data set a total of 13 points were excluded. All 13 points corresponded to values that did not meet the quality statistics defined by the AASHTO TP79 standard.

4.5 A priori expectations of the potential effects of different factors

The following chapter explains in detail the development of the predictive |E*| model, its rationale, and the reasonableness of the model parameter estimates. Thus, it is convenient at this point to discuss a priori expectations of the effects that different factors may have on the predicted |E*| values. Most of these expectations are based on simple observations on how certain modifiers or testing conditions may affect the performance of the mix. However, some

others, particularly the effects of confinement, are based on previous research and deserve more explanation.

A summary of prior observations and a priori expectations for the use of confinement, freeze-thaw cycles and the different additives used in the different data sets is shown next:

- Use of confinement pressure: The results from the experiment with the use of confinement were analyzed and presented elsewhere (Corrales-Azofeifa and Archilla, 2016). In general, it was noted that the effect of confinement is quite complex since it has a large influence in the values of |E*| at high testing temperatures but its effect is insignificant for the lower temperatures. Furthermore, the effects at high temperatures are dependent on both binder type and air voids as well as their interaction. As expected, |E*| values increase with the level of confinement at high temperatures. However, they do not increase linearly with confinement level since they typically increase at a decreasing rate. At low air voids levels and high temperatures, increments in confinement level result in significant increments of |E*|. However, the increments were higher for mixes with modified binders than for mixes with unmodified binders. Furthermore, for unmodified mixes the effects of confinement were significantly reduced at 7% air voids at high temperatures and virtually disappear at 9% air voids. On the other hand, for modified mixes, although the effects at higher air voids (7% and 9%) were reduced compared to those at 4% air voids they were still substantial. In other words, the reduction of the sensitivity to confinement level at high temperatures with air voids is much higher for unmodified than for unmodified mixes.
- Use of freeze-thaw cycles: The conditioning of samples with freeze-thaw cycles is performed to induce damage to the asphalt mixtures. Consequently, it was expected that their use will decrease the values of |E*|. The experiments performed in Costa Rica utilized 1, 3 and 6 freeze-thaw cycles. The a-priori expectation was that the damage on the samples would increase with an increase in the number of cycles. However, there was no a priori expectation whether the damage would increase linearly as the number of cycles increase or whether it would increase at a decreasing rate, at an increasing rate, at a variable rate. The results obtained from the Costa Rica experiments with the F-T cycles suggests that the increments do not increase linearly with the number of cycles.

- Use of fibers: The use of fibers as an additive is typically performed in engineering to increase the resistance of mixtures to tensile stresses, as with concrete mixtures. Therefore, it was reasonable to expect that their use in asphalt mixtures would also improve the dynamic modulus. However, it is important to realize that the axial deformations during dynamic modulus testing are so small that are probably not enough to mobilize the fibers in the mix. This may explain why different studies have found contradicting results. It may well be that the effects are mixture dependent. A priori, it was expected that the use of fibers would result in either an increase in the values of |E*| or in the worst case, given the small proportion used in the mix, that the use of fibers would not provide any advantage given the small loads used for dynamic modulus testing. As discussed later, the testing results in this study were opposite to these a priori expectations.
- Use of SBS modifier: The SBS modifier is typically used to reduce rutting (among other things) in asphalt materials (Bahia et al. 2001). The use of this elastomer has typically been proven to improve the elastic behavior of asphalt mixtures. Therefore, it was expected that the use of this product, which is included in all three data sets, would increase the values of |E*|. The improvement on these values would most likely depend on the amount of polymer included in the mixture. Since these percentages are only known for the data set from Costa Rica, a prediction cannot be done in this sense.
- Use of Elvaloy®Ret: The use of Elvaloy®Ret has also been proven to reduce rutting in asphalt materials (Kanabar 2010). More importantly, as part of the analysis for the previous UH study with the same data set, it was shown increase the dynamic modulus of the mixtures at high temperatures and low frequencies and slightly decrease it at low temperatures and high frequencies. Therefore, the expected effect of this polymer was already known prior to this study.
- Use of Sasobit: The use of this organic paraffin wax is intended to reduce the viscosity of the binder at mixing and compacting temperatures to create warm mixtures. However, there is no clear expected influence of this product on the values of |E*|. It could be reasoned that by reducing the mixing and compaction temperatures less aging would be induced to the mixture and therefore there would be an improvement in its behavior. The

older data set from UH includes two samples of this mixture, which may not be enough to explain a distinctive behavior.

- Use of anti-stripping agents: Two anti-stripping agents are used in the Costa Rica database, i.e., lime and Magnabond. Both additives have the main objective of preventing and reducing moisture damage in asphalt mixtures. In the case of lime, it has been found to stiffen the asphalt binder (Sebaaly, 2006), which may be observed as an increase in the values of |E*|. Even though there was not an a priori expectation for the use of these agents when no moisture damage is induced, it was expected that their use would help increase the values of |E*| when the mixtures are subjected to freeze-thaw cycles in comparison with the case where no anti-stripping agent is used.

CHAPTER 5: DEVELOPMENT AND ANALYSIS OF THE MODEL

This chapter presents the process for the development and analysis of the dynamic modulus predictive model. Each of the sections in this chapter discusses a step in the evolution of the model. Section 5.1 discusses the creation of the data base from the three data sets. An explanation of the rationale behind the creation of the initial model is presented in Section 5.2. Later, Section 5.3 and Section 5.4 deal with the use of the joint estimation and the mixed-effects approaches for estimation of the model parameters. Section 5.5 presents the evaluation of the model capability to predict the effects of several variables included in the data sets (e.g. air voids, confinement levels, freeze thaw cycles, and various mixture modifiers).

5.1 Creation of the data base

All the experimental data gathered at UH and LanammeUCR consists of values of |E*| collected for each of the tested specimens at various temperatures and frequencies. This means that for each specimen tested, several points were included in the different data sets depending on the testing conditions utilized. Table 4 presents a summary of the data available for each data set collected.

Table 4. Summary of data available for the three data sets

Source	Total Specimens	Frequency (Hz)	Temperature (°C)	Total Data Points	Data Set Features
UHO	80	25, 20, 10, 5, 2, 1, 0.5, 0.2, 0.1, 0.01	4.4, 10, 14, 21.1, 34, 37.8, 45, 54	2974	Mix modifiers (some confinement)
UHN	42	25, 10, 5, 1, 0.1, 0.01	4, 20, 40, 45	2430	Mix modifiers and confinement
CR	144	10, 1, 0.1, 0.01	4, 20, 40, 45	1417	Mix modifiers and F-T Cycles

Note: Not every combination of frequency and temperature was evaluated for a given specimen in the UHO dataset. The UHO study was started with provisional standards, which led to some experimentation for selecting adequate temperature-frequency combinations.

At this point, it is useful to remember that when both UH data sets were collected, a variation of the AASHTO T-342 and AASHTO PP-61 standards were used regarding the temperatures and frequencies utilized during the testing procedures. In the case of the UHO data set, the testing procedures followed more closely the AASHTO T-342 standard (AASHTO 2016) where

temperatures of -10, 4.4, 21.1, 37.8 and 54°C (14, 40, 70, 100, and 130°F) are required with frequency levels of 0.1, 0.5, 1.0, 5, 10 and 25 Hz. The purpose of selecting additional temperature and frequency combinations beyond those required in the standard was to obtain a better definition of the shape of the master curve for each specimen, though it is now known that using fewer points would have been acceptable. For the UHN data set, the testing protocol followed a modified version of the AASHTO PP-61 standard (AASHTO 2016). In this case, the required temperatures were followed accordingly but the frequencies of 5 Hz and 25 Hz were added to the standard recommended frequencies of 0.1, 1 and 10 Hz for the two lower temperatures (4 and 20°C) and of 0.01, 0.1, 1 and 10 Hz for the higher testing temperature (either 40°C or 45°C depending on the asphalt grade tested). Regarding the data set collected at LanammeUCR, the laboratory protocol followed the AASHTO PP-61 standard to the letter.

To create the data base for the development of the model, each of the values of |E*| (for every combination of temperature and frequency) had to be associated with variables that describe the characteristics of each specimen and its testing conditions. All these variables were initially selected based on their possibility of having an influence on the |E*| values.

The first set of variables includes the volumetric and material characteristics of each tested specimen. These are the type of variables found in the Witczak predictive models and they describe the composition of the mixture at the intra-individual level, i.e. characteristics of the asphalt mixture formula (e.g. aggregate gradation and binder characteristics), and at the within-individual level, i.e. characteristics of the asphalt specimen tested (e.g., air voids and V_{beff}). The second set of variables is related to features of each data set that are accounted for in this specific model. These variables take into consideration the use of freeze-thaw cycles, confinement, fibers and all other mixture modifiers tested across the data sets. These are the variables included in the model with the joint estimation approach. A summary of all the initial variables considered is shown in Table 5. It is important to clarify that the variables related to the asphalt mixture vary from one mix type to the next but remain the same for all samples of a particular mixture. Similarly, all variables related to the specimen vary from one sample to the next but they are constant for all |E*| points of a specific sample.

Table 5. Variables initially considered for developing the model

	Variables
Related to Asphalt Mixture	- Bulk Specific Gravity of Aggregates (G_{sb}) - Percentage of Binder (P_b) - Maximum Theoretical Specific Gravity (G_{mm}) - Specific Gravity of Binder (G_b) - Effective Specific Gravity of Aggregates (G_{se}) - Cumulative % of aggregate retained on ¾" sieve ($\rho_{3/4}$) - Cumulative % of aggregate retained on 3/8" sieve ($\rho_{3/8}$) - Cumulative % of aggregate retained on #4 sieve (ρ_4) - % of aggregate passing #200 sieve (ρ_{200})
Related to Specimens	- Percentage Binder Absorbed (P_{ba}) - Percentage Binder Effective (P_{beff}) - Bulk Specific Gravity of Mixture Sample (G_{mb}) - Air Voids (V_a) - Voids in the Mineral Aggregate (VMA) - Voids Filled with Asphalt (VFA) - Effective Volume of Binder (V_{beff}) - Strains
Related to Data Set Features	- Asphalt Type + UHO: *PG64-16 *PG70-22 *PG70-XX *Warm Mix + UHN *PG64-22 *PG76-22 + CR *PG70-22 *PG76-22 - Fibers (UHN) - Anti-stripping agents (CR) + Lime +Magnabond - Freeze-Thaw cycles (CR) + 1 Cycle + 3 Cycles + 6 Cycles - Confinement (UHN + 69 kPa (UHN) +100kPa (UHO) +138kPa (UHN) +207kPa (UHN)

These variables are either shared by the data sets (mixture and specimen related variables) or belong exclusively to one of them (data set features). Consequently, joint estimation (Section 5.3) is used for the creation of the initial model since it can identify statistical significant explanatory variables for the model from these two groups of variables. In this case, the third scenario discussed earlier in chapter 3 is applicable, where all data sets share explanatory variables (e.g. air voids, effective binder content by volume, and gradation characteristics) while there are other variables that are unique to each data set (e.g., confinement, F-T cycles, and binder type). The three advantages for the use of joint estimation in this model are in more detail:

- Bias correction: This allows the determination of bias parameters to account for marginal effects estimated for parts of the model that are common among the data sets. These marginal effects are a result of small differences on the data sets related to sample preparation (batching, mixing, and compaction) or testing procedures within laboratory (as in the case of UHO and UHN) or among laboratories (when the CR data set is included).
- Identification: This allows the consideration of characteristics that are not observed in all data sets and the estimation of related parameters using the entire database. Variables such as confinement can be included in this way and later used to predict its effect on the dynamic modulus for the other data sets.
- Statistical efficiency: This results in parameter estimates with lower variance since all available data from the three data sets are used. For example, the effect of air voids can be similar for all data sets and therefore one parameter can predict the effect of this variable in the model by incorporating all air void data from all data sets.

Another factor accounted for in the analysis of the data is the fact that several dynamic modulus (|E*|) measurements are determined at different temperatures and frequencies for each specimen. Unobserved factors tend to affect similarly all the observations of a specimen, which leads to correlations of the error terms. These unobserved heterogeneities are ignored in classical regression analysis but can have substantial influence in the reliability of the hypothesis tests performed when evaluating the statistical significance of the model parameters. Therefore, in this study, the mixed-effects approach is used to estimate the model parameters accounting for unobserved heterogeneities.

The three data sets were combined into a single comma delimited file (.csv) with 6821 records for all temperature-frequency combinations. In addition to |E*|, each record contains the associated values for each of the variables shown in Table 5 arranged in columns. The open source software R for statistical analysis was utilized for the development of the model.

5.2 Conception of the initial model

As previously mentioned, the Witczak models developed in the NCHRP 1-37A and the NCHRP 1-40D studies allow the prediction of |E*| values for their use in mechanistic-empirical analysis at design levels 2 and 3. Both models were created by using the sigmoidal function shown in

Equation (4) but changing each of the parameters into more elaborate functions of the characteristics of each mix. To make this clearer, take as an example Equation (2) and Equation (4) rewritten below.

$$log_{10}|E^*| =$$

$$-1.25 + 0.029\,\rho_{200} - 0.0018(\rho_{200})^2 - 0.0028\,\rho_4 - 0.0048V_a - 0.822\left(\frac{V_{beff}}{V_{beff}+V_a}\right) +$$

$$\frac{3.872-0.0021\,\rho_4+0.004\,\rho_{38}-0.000017\,(\rho_{38})^2+0.0055\,\rho_{34}}{1+e^{(-0.6033-0.3133\,log(f)-0.3935\,log(\eta))}} \qquad \text{(2 revisited)}$$

$$\log|E^*| = \delta + \frac{\alpha}{1+e^{\beta+\gamma(log(1/f_r))}} \qquad \text{(4 revisited)}$$

A close examination of these two equations indicates that the second line of Equation (2) is equivalent to δ in Equation (4), that the numerator in the third line of Equation (2) corresponds to the value of α in Equation (4) and that the exponent of e in both equations is equivalent. This last comparison is less obvious, however the term used in Equation (2) is also a shift factor but modeled as a function of temperature through the binder viscosity (η). The MEPDG accounts for the stiffening of the mix over time by modeling the changes in the estimated binder viscosity when using the NCHRP 1-37A model (Archilla et al. 2014). The shift factor used in this approach uses Equation (10) shown below.

$$\log\big(a(T)\big) = c\,(\log\eta - \log\eta_{T_R}) \qquad (10)$$

where

a(T) = shift factor as a function of the temperature

η = binder viscosity, cP (centipoises)

η_{T_R} = binder viscosity at reference temperature, centipoise (cP)

c = model parameter estimated simultaneously with α, β, γ, and δ of Equation (4) for given values of |E*| and viscosity data.

When comparing this shift factor with the one shown in Equation (6), it appears that the use of Equation (10) requires two fewer parameters. However, to predict the binder viscosity as a

function of temperature, the MEPDG includes the following additional two-parameter equation (Equation 11).

$$\log log\, \eta = A + VTS \log T_R \quad (11)$$

where

η = binder viscosity, cP

T_R = temperature, Rankine (temp°F + 459.67)

A = regression intercept and

VTS = regression slope of viscosity temperature susceptibility

The parameters A and VTS are estimated by the MEPDG after the required input data for binder characterization are used at levels 1 and 2. For level 3, the guide provides the values based on the binder grade. The advantage of using a model that requires the binder viscosity is that binder aging, and therefore, mixture aging can be considered directly in the model.

The use of binder characteristics to accommodate for aging effects could be an improvement for the model presented herein. However, a broader data base that includes a wider range of asphalt binders would be necessary to be able to capture the influence of these characteristics in the |E*| values. Additionally, laboratory measurements of viscosity values would also be necessary for all binders included in the model. While some measurements were available for the UHO and CR databases, it was not possible to measure all necessary values for the UHN database.

Furthermore, the use of the model adopted by project NCHRP 1-40D (Equation 3) requires values for the dynamic shear modulus of the binder (|G*|) and its associated phase angle (δ_b) at several frequencies. Values of both |G*| and δ_b were available at a single frequency of 1.59 Hz (10 rad/s) for some of the binders. Thus, to obtain the necessary values at other frequencies, it would have been necessary to use the two values at this single frequency to calculate the parameters A and VTS and then use these estimated parameters to compute the necessary values of |G*| and δ_b at other frequencies. Since estimated values always contains some errors and the data was not available for all binders, using |G*| and δ_b was not an option for this study.

The model developed in this study was also derived using the sigmoidal equation (Equation (4)) as a starting point together with the shift factor specified in Equation (6). Two important changes

were made to the function to accommodate for certain desirable characteristics. The first change is related to the main sigmoidal equation while the second is related to a factor added to the model to account for the use of confinement. Before discussing these in detail, it is necessary to remember how the model parameters are related to features of the sigmoid. As described in Equation (4), the parameter δ is the minimum value of log|E*|, δ+α is the maximum possible value of log|E*|, and the parameters β and γ describe the shape of the sigmoidal function.

The first change introduced to the sigmoidal function is illustrated in Figure 9 where the maximum value of the dynamic modulus |E*| is changed for convenience from $10^{\delta+\alpha}$ to 10^{ρ} (i.e. $\rho=\delta+\alpha$). The procedure to derive the new equation is shown in detail in Equation (12).

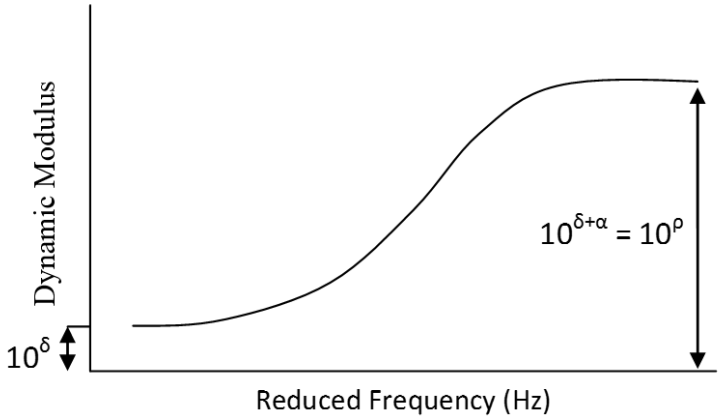

Figure 9. Parameter change in the |E| sigmoidal function*

Given that $\log|E^*| = \delta + \frac{\alpha}{1+e^{\beta+\gamma(log(1/f_r))}}$ *and* $\rho = \delta + \alpha$ therefore,

$$\log|E^*| = \delta + \frac{\rho-\delta}{1+e^{\beta+\gamma(log(1/f_r))}} = \frac{\delta\left(1+e^{\beta+\gamma(log(1/f_r))}\right)+\rho-\delta}{1+e^{\beta+\gamma(log(1/f_r))}} = \frac{\rho+\delta\left(e^{\beta+\gamma(log(1/f_r))}\right)}{1+e^{\beta+\gamma(log(1/f_r))}}$$

$$= \frac{\rho+(\rho-\alpha)\left(e^{\beta+\gamma(log(1/f_r))}\right)}{1+e^{\beta+\gamma(log(1/f_r))}} = \frac{\rho+\rho\left(e^{\beta+\gamma(log(1/f_r))}\right)-\alpha\left(e^{\beta+\gamma(log(1/f_r))}\right)}{1+e^{\beta+\gamma(log(1/f_r))}}$$

$$= \frac{\rho\left(1+e^{\beta+\gamma(log(1/f_r))}\right)-\alpha\left(e^{\beta+\gamma(log(1/f_r))}\right)}{1+e^{\beta+\gamma(log(1/f_r))}} = \rho - \alpha\frac{\left(e^{\beta+\gamma(log(1/f_r))}\right)}{1+e^{\beta+\gamma(log(1/f_r))}}$$

$$\log|E^*| = \rho - \frac{\alpha}{1+e^{-\left(\beta+\gamma\left(log(1/f_r)\right)\right)}} \qquad (12)$$

Notice that Equations (4) and (12) represent the exact same curve when instead of δ the model contains the parameter $\rho = \delta + \alpha$ and the other three parameters ($\alpha, \beta,$ and γ) are the same. However, for the reasons discussed next, Equation (12) is much more convenient for the development of the model in this study. Equation (4) is suitable for modeling the minimum value of |E*| for high temperatures and low frequencies (through the parameter δ) and the increase in modulus from this minimum for other temperature-frequency combinations (through the parameter α). On the other hand, Equation (12) allows for the direct modeling of the maximum of |E*| for low temperatures and high frequencies (through the parameter ρ) and the reduction of the modulus for other temperature-frequency combinations (through the parameter α). Typically, the variability of the log(|E*|) is much higher for low values of |E*| than for higher values. Thus, it is more convenient to model the maximum of the function and how it is affected by some relevant covariates directly and then model the drop from the maximum to the minimum though another function of relevant covariates. As indicated before, usually the drop in log(|E*|) (or α) has higher variability than the maximum (or ρ) and ρ and α are not necessarily highly correlated. On the other hand, if Equation (4) was used, the variability of both δ and α would be high and negatively correlated which would result in a value of ρ with relatively lower variability. Thus, with the use of Equation (4) the identification of factors affecting the model parameters becomes more difficult. This is the main reason why Equation (12) is used here for the development of the predictive model.

Equation (12) is the simplest equation that was used as a starting point for the predictive model together with a quadratic shift factor, repeated here for convenience.

$$log\big(a(T)\big) = AT^2 + BT + C \qquad \text{(6 Revisited)}$$

where,

$$a(T) = \frac{f_r}{f} \quad or \quad log\left(\frac{1}{f_r}\right) = log\left(\frac{1}{f}\right) - \log\big(a(T)\big) \qquad \text{(5 Revisited)}$$

As previously mentioned, the open source statiscal software R was used for estimaing the parameters of the model. With this initial model a first run was carried out as a starting point before adding any other explanatory variables. Figure 10 shows the outcome of this run performed by using the Non-linear Least-Squares (NLS) routine from R, while Figure 11 shows the same result in logarithmic scale as predicted by the model.

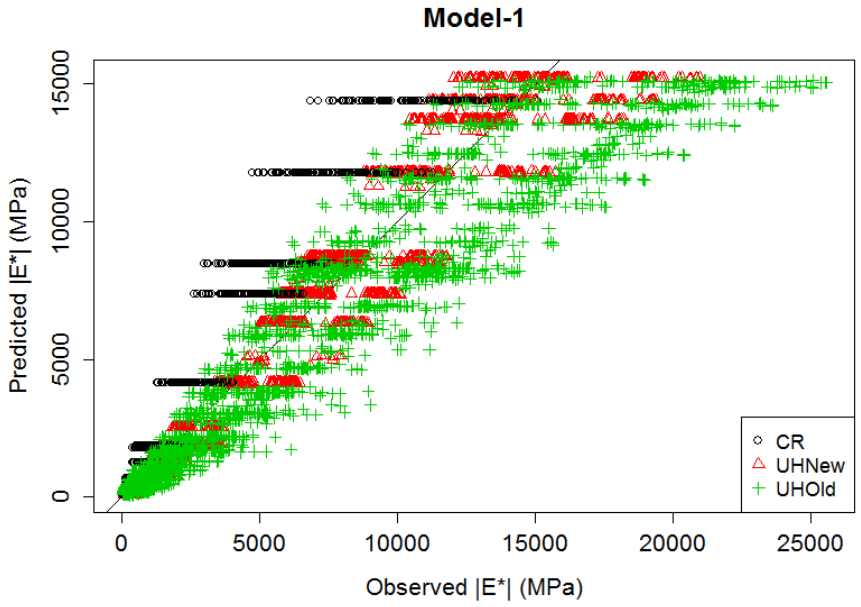

Figure 10. Observed versus predicted values of |E| for the initial model*

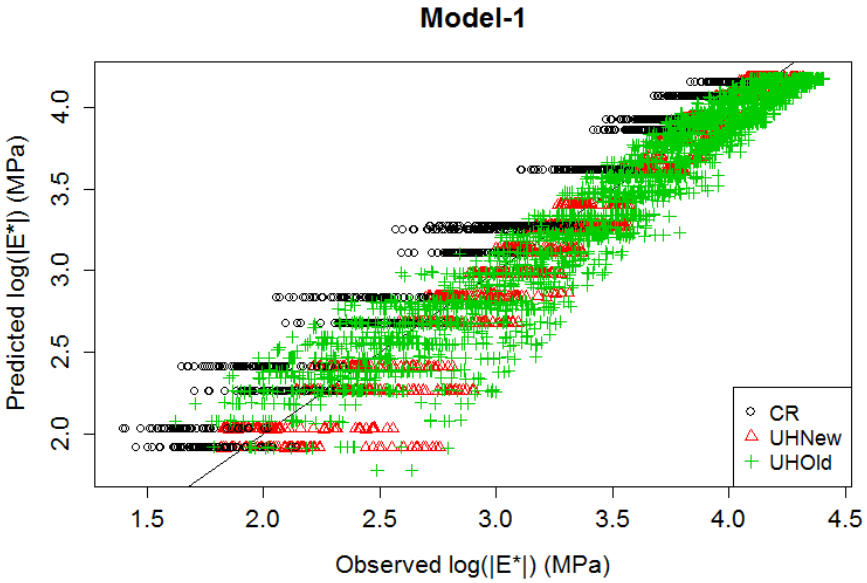

Figure 11. Observed versus predicted values of log|E| for the initial model*

Notice that for this initial model, the use of 6 parameters (ρ, α, β, γ, A and B) is not enough to accurately predict the values of |E*| and capture the different characteristics of each of the data bases. It can be seen in both figures that the values for the UHO dataset seem more uniformly distributed in the vertical axis in comparison with the values for the UHN and CR datasets, where horizontal lines of data points are more evident. It is important to note that there is good

justification for these differences. They are related to fact that temperature and frequency are the only explanatory variables of the estimated model. The UHO data set shown in Table 4, was collected at many more temperatures and frequencies than the other two data sets. Thus, one can expect that there will be a larger density of predicted values. Second, even though the UHO data set was not measured for different testing conditions (such as different confining pressures or freeze-thaw cycles), it still has 3 different binders, one level of confining pressure for a few samples, and a large variability in the sample air voids. For this reason, for all temperatures and frequencies, very diverse values of |E*| can be seen, helping to show this apparent greater dispersion of data points. On the other hand, for the case of the CR and UHN data sets, these were measured at the same 4 temperatures with a slight variation between data sets in the frequencies utilized. In both cases, around half of the values are on each side of the line of equality for each temperature-frequency combination (represented by sets of points aligned horizontally). This means that the model is trying to predict the average value of all measured data for a given frequency-temperature combination since no other difference is made among the data points. Figure 12 illustrates this result more clearly. As an example, in the case of the CR data set, samples were conditioned with 1, 3 or 6 cycles of freezing and thawing (F-T), which increasingly reduces the values of |E*| for all conditioned samples. Additionally, this data set has 12 different mixtures (Table 3). This means that for a given temperature and frequency combination, values of |E*| are gathered for 12 different mixtures and 4 different F-T conditioning levels (0, 1, 3 and 6 cycles), resulting in 48 different values of |E*|. Since three samples were tested for repeatability, a total of 144 points with varying F-T cycles, anti-stripping agents, air voids and other characteristics are being predicted as if they were the same since at this point there are no other variables in the model that can capture these differences.

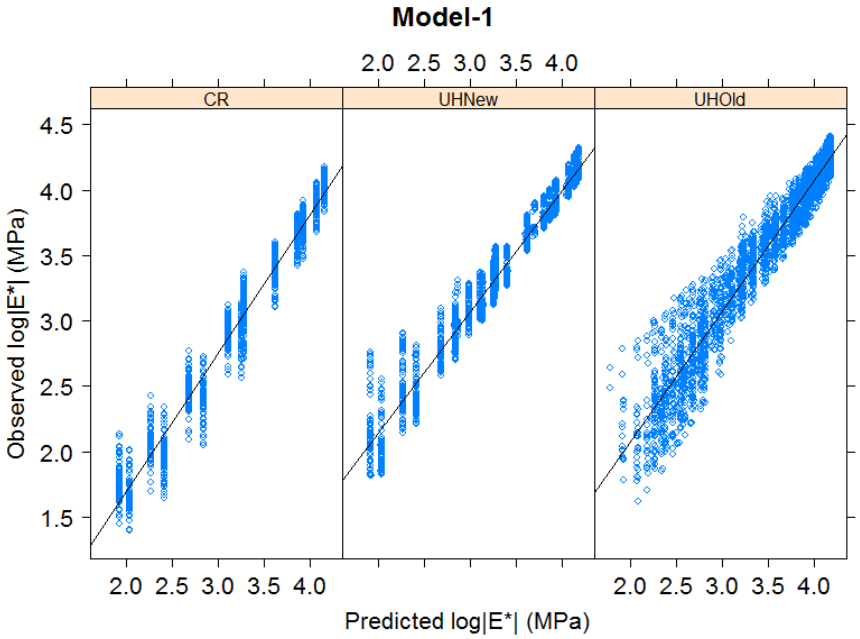

Figure 12. Predicted versus observed values of log|E| (by data set) for the initial model*

Figure 12 makes it easier to recognize that the point alignment patterns are also present in the UHO data base. This is the reason why the better dispersion of the data for the UHO data set was referred as only apparent. Notice that in this particular figure the axes have been inverted showing the points aligned vertically instead of horizontally as was the case in Figure 11. It is easier to see in this figure that the CR data set has a total of 14 levels (the 8th and 9th levels, counted from left to righ, are almost superimposed), since there are 14 combinations of temperatures and frequencies (or equivalently 14 different reduced frequencies), corresponding to the frequencies of 10Hz, 1Hz and 0.1Hz at temperatures of 4°C and 20°C and to frequencies of 10Hz, 1Hz, 0.1Hz and 0.01Hz at the 40°C and 45°C temperatures. The UHN data set presents a similar scenario. In the case of UHO, this is not evident anymore. The number of combinations of temperature and frequency for this last data set is large enough to make the distribution of points look almost as one uniform cloud.

As expected, the inclusion of other expanatory variables related to the different characteristics of the samples and data sets is needed to capture these differences and be able to predict the |E*| values more accurately than with model 1.

Most of the additional explanatory variables will be introduced as linear terms affecting each of the six parameters in model 1 (i.e. α, β, γ, ρ, A and B). However, confinement level presents a

unique challenge since it varies substantially with frequency and temperature combinations (it has practically no effect at low temperature/high frequencies but the modulus can double with increases in confinement at high temperature/low frequencies). With this in mind, the second change to the base model is the addition of a factor with a functional form developed specifically to account for the effects of confinement and the different sensitivity to air voids observed in unmodifieed and modified mixes. At this point, it is convenient to remember that in the test, the maximum principal stress σ_1 (the vertical stress) is related to the minor principal stress or confining stress σ_3 and the deviatoric stress σ_d by $\sigma_1 = \sigma_3 + \sigma_d$.

The functional form of the confinement factor α_{cf} (α confinement factor) that is added as a mutiplicative factor to α in Equation (12) is shown in Equation (13). Since α_{cf} decreases with σ_3, it makes the numerator of the term subtracting ρ (i.e., $\alpha_{cf} \cdot \alpha$), and hence the whole term subtracting ρ, smaller for higher confinement levels. For convenience, it is assumed that the confinement factor is defined by a sigmoidal function with a value of 1 when the confinement level used is $\sigma_3 = 0$ as shown in Figure 13.

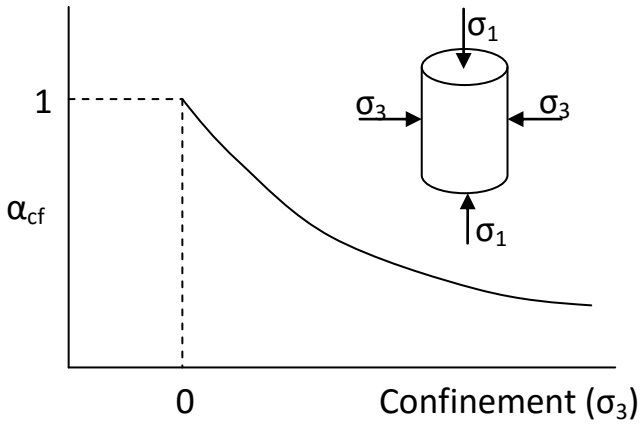

Figure 13. Graphical explanation of factor α_{cf}

The reason for choosing a sigmoidal function instead of another function with a maximum of 1 is to allow for the potential inclusion of conditions that make the modulus even lower than the unconfined modulus (which would imply values of α that are larger than that correponding to the unconfined conditions or $\alpha_{cf}>1$). For example, preliminary results of |E*| testing in tension at the UH pavement laboratory as well as other studies indicate that at temperatures of 40°C and frequencies of 0.1 Hz and 0.01 Hz the modulus can be as low as one half or one third that for the

unconfined conditions, thus requiring an alpha factor α_{cf} greater than 1. (Note that it is not yet clear what would be the best definition of the function for tensile conditions, which is beyond the scope of this thesis).

As indicated before, a sigmoidal function is considered as a starting point:

$$\alpha_{cf} = \rho_{conf} - \frac{\alpha_{conf}}{1 + e^{\left(\beta_{conf} + \gamma_{conf} * \sigma_3\right)}} \tag{13}$$

Similar to the sigmoidal function that represents the variation of |E*| with reduced frequency, equation (13) above gives the variation of α_{cf} with σ_3. In equation (13), ρ_{conf}, α_{conf}, β_{conf}, and γ_{conf} are the model parameters.

Given the imposition that for σ_3 = 0 the factor α_{cf} must equal 1, then

$$1 = \rho_{conf} - \frac{\alpha_{conf}}{1 + e^{\left(\beta_{conf} + \gamma_{conf} * 0\right)}} \xrightarrow{yields} \rho_{conf} = 1 + \frac{\alpha_{conf}}{1 + e^{\left(\beta_{conf}\right)}}$$

Therefore, equation (13), can be simplified to

$$\alpha_{cf} = \left(1 + \frac{\alpha_{conf}}{1 + e^{\left(\beta_{conf}\right)}}\right) - \frac{\alpha_{conf}}{1 + e^{\left(\beta_{conf} + \gamma_{conf} * \sigma_3\right)}} \tag{14}$$

To simplify this equation further and avoid over specification of the |E*| model, the parameter β_{conf} was set to zero. Note that contrary to what is shown in Equation (12), no negative sign was included in the exponent of *e*. Thus, the parameter γ_{conf} in equation (14) should be negative for this equation to represent the effects of confinement shown in Figure 13.

To understand the use of Equation (14) imagine that the confinement pressure (σ_3) is zero. In this case, the first term in parentheses is 1 + 0.5 and the second term is 0.5, thus giving (1 + 0.5) – 0.5 = 1. Therefore, there is no change in the general factor α of the main Equation (12) when the confinement level is σ_3=0.

When confinement is greater than zero, the following analysis applies. For simplification purposes call the exponent (γ_{conf} σ_3) simply *x* and remember that γ_{conf} is negative. For negative values of the exponent *x*, e^x varies between 0 and 1. The larger the value of confinement, the more negative is the exponent *x*, and therefore e^x is a smaller value (closer to 0). Having a

smaller denominator as the confinement increases, results in a larger value for the subtracting factor in Equation (14) (i.e. $\alpha_{conf}/(1+e^{(\gamma c*\sigma 3)})$). This in turn results in a smaller value for the parameter α_{cf}. Therefore, the larger the confinement pressure, the smaller the value of α_{cf}. Since α_{cf} is included as a multiplication factor to the overall α factor in Equation (12), the higher the confinement, the smaller is the overall α factor (since $\alpha \cdot \alpha_{cf}$ is smaller). Consequently, the predicted values of |E*| at high temperatures/low frequencies are higher as the confinement pressure increases (since a smaller α is subtracted from ρ). This is reflected in an overall shift of the master curve upwards, which is the typical behavior observed with confinement in laboratory tests. This behavior will be illustrated later during the analysis of the final model.

Through the incorporation of this second change to Equation (12), a more involved equation was created to account for the effects of confinement in the |E*| values of the mixtures.

$$\log|E^*| = \rho - \frac{\alpha\left[\left(1+\frac{\alpha_{conf}}{1+e^{(0)}}\right) - \frac{\alpha_{conf}}{1+e^{(\gamma_{conf}*\sigma_3)}}\right]}{1+e^{-\left(\beta+\gamma\left(log\frac{1}{f_r}\right)\right)}} \quad (15)$$

As shown later, the term α also contains a term related to confinement. The reason for this is that although the term α_{cf} is capable of producing the expected drop with confiment level, it is also used to capture the different sensititivity to air voids for mixes prepared with unmodified and modified binders by incorporating dummy variables for the type of binder in α_{cf}. However, it will also be seen that the estimated factor α_{cf} tends to be lower for higher air voids, which by itself would produced unreasonable results. Hence, there is a need to account for the effect of confinment in α as well to counteract this issue. As will be shown, this combination of factors produces results that match extremelly well the trends observed with the combination of confinement, air voids, and binder type.

It is also possible to show the $\log(1/f_r)$ in a more general form as a function of the $\log(1/f)$ and the shift factor log(a(T)) shown in Equation (6). At the reference temperature, the shift factor has a value of 0 since no shifting is necessary. Choosing 21.1°C (70°F) as the reference temperature and solving Equation (6) allows for the determination of C in terms of the other two parameters A and B. After applying these changes to Equation (15), it was possible to obtain the following equation.

$$\log|E^*| = \rho - \frac{\alpha * \left[\left(1 + \frac{\alpha_{conf}}{1 + e^{(0)}}\right) - \frac{\alpha_{conf}}{1 + e^{(\gamma_{conf} * \sigma_3)}}\right]}{1 + e^{-\left(\beta + \gamma\left(log\left(\frac{1}{f}\right) - (A * T^2 + B * T - (A * (21.1)^2 + B * (21.1))\right)\right)}} \quad (16)$$

This equation is the base of the final model obtained for predicting the |E*| values of asphalt mixtures, since all terms (ρ, α, β, γ, A and B) will be presented as combinations of several characteristics of the different mixtures included in the complete data base. All the variables shown previously in Table 5, were included progressively within the different terms and hypothesis tests were performed at each stage to define which variables were statistically significant for the prediction of the |E*| values. As an example, the parameters ρ_{AV} (parameter for ρ related to air voids), α_{AV} (parameter for α related to air voids) and so on, were included to evaluate the effect of the air voids in the model.

The inclusion of all explanatory variables that were common for all data bases was performed together with the inclusion of the explanatory variables related to only one of the data bases using the joint estimation approach explained next.

5.3 Joint estimation

The joint estimation approach was used to assess two situations. First, to be able to incorporate bias parameters to account for the overall bias of either the UHO or CR datasets with respect to the UHN dataset, and second, to allow for the incorporation of the explanatory variables that are unique to each data set and identification of their effects. In both cases the approach followed was the same and consisted in the inclusion of several dummy variables in the model.

Dummy variables are used in regression analysis as a way to assign two or more distinct values to an independent variable (Pyndyck and Rubinfeld, 1991). By taking a value of 1, if a given effect is present in the model or a value of 0 if the effect is absent, dummy variables can divide one population into several subgroups and measure the differences among them (Ben-Akiva and Lerman, 1985). If a dummy variable is associated with a given characteristic or condition within the entire data base, this characteristic is only included in the prediction of the value of |E*| for the mixtures that possess this feature. As an example, several dummy variables were associated with the use of the different asphalt binder grades. In particular, the variable D_{PG76CR} is associated with the use of the PG76-22 binder in the CR data set. This dummy variable

multiplies the parameters α_{PG76CR} and ρ_{PG76CR} associated with the use of this binder and takes a value of 1 when it is necessary to predict the |E*| value of mixtures using this binder and 0 if not.

5.3.1. Intermediate Non-Linear Regression Model

The use of the dummy variables gives the model the necessary flexibility to accommodate for the different aspects that need to be captured. To illustrate this statement, the observed vs. predicted values for an intermediate model without the introduction of any bias parameters are shown in Figure 14. This figure is the equivalent of Figure 11 for the initial model.

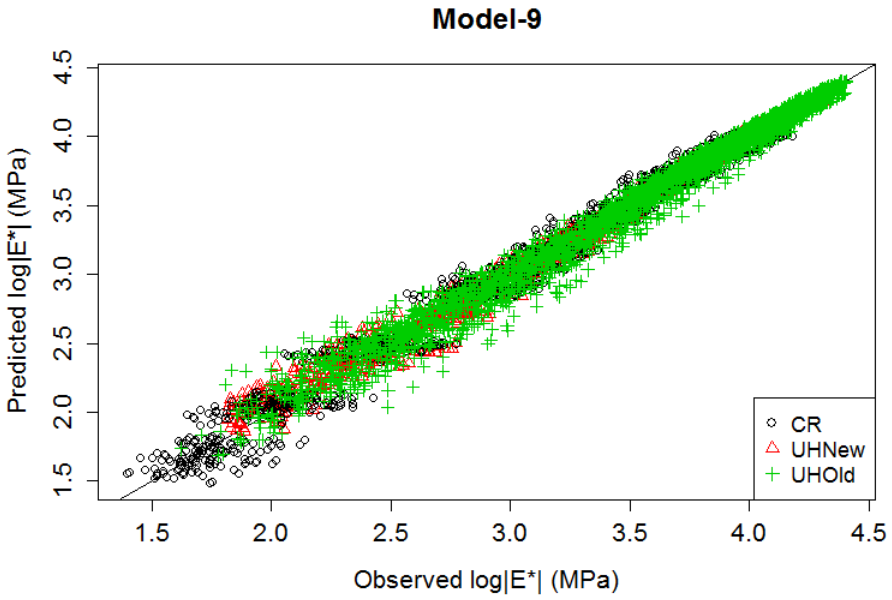

Figure 14. Observed versus predicted values of log|E| for model-9*

The results for this model are shown because it illustrates the effects of including some dummy variables and the factor α_{cf} in its simplest form (as shown in Equation (14)) to consider the effect of confinement. Table 6 shows the parameters and the implicitly affected variables used in this preliminary model. All factors have as a minimum a constant parameter.

Table 6. Parameters included in model 9 for each factor

Factor ρ		Factor α		Factors β, γ, A, B	
Parameter	Variable affected	Parameter	Variable affected	Param.	Var.Affec
ρ_C	1	α_C	1		
ρ_{AV}	Air voids	α_{AV}	Air voids		
ρ_{Vb}	Eff. Binder Vol.	α_{Vb}	Eff. Binder Vol.		
ρ_{R38}	Retained in 3/8" sieve	$\alpha_{PG64UHO}$	PG64-16 UHO binder	β_C	1
ρ_{R4}	Retained in No.4 sieve	$\alpha_{PG76UHN}$	PG76-22 UHN binder	γ_C	1
$\rho_{PG64UHO}$	PG64-16 UHO binder	α_{Elv}	Elvaloy modif. binder	A_C	1
ρ_{Elv}	Elvaloy modif. binder	α_{PG76CR}	PG76-22 CR binder	B_C	1
ρ_{PG76CR}	PG76-22 CR binder	$\alpha_{PG70UHO}$	PG70-22 UHO binder		
$\rho_{PG70UHO}$	PG70-22 UHO binder	α_{PG70CR}	PG70-22 CR binder		
ρ_{PG70CR}	PG70-22 CR binder	$\alpha_{cf\_}\alpha_{conf}$	Confinement (14)		
		$\alpha_{cf\_}\gamma_{Conf}$	Confinement (14)		

As an example, the factor ρ is a summation of the multiplication of each of the factor's parameters with the corresponding variable, as shown next:

$$\rho = \rho_C + \rho_{AV} \cdot AV + \rho_{Vb} \cdot V_{beff} + \rho_{R38} \cdot R_{38} + \rho_{AV} \cdot R_4 + \rho_{PG64UHO} \cdot D_{PG64UHO} + \rho_{Elv} \cdot D_{Elv} + \rho_{PG76CR} \cdot D_{PG76CR} + \rho_{PG70UHO} \cdot D_{PG70UHO} + \rho_{PG70CR} \cdot D_{PG70CR}$$

Note that the constant can be interpreted as another parameter multiplying a variable that is always 1.

As can be seen in Table 6, at this stage, there are no variables related to the parameters β, γ, A and B other than a constant for each of them (hence the sub-index C for the corresponding parameters). However, in the case of ρ and α, besides the constant for each term (ρ_C, α_C), there are several terms related to the mixture characteristics. Specifically, the variables for air voids (ρ_{AV}, α_{AV}) and effective binder content by volume (ρ_{Vb}, α_{Vb}) appear in both terms, while variables for the percentages of aggregate retained in the 3/8" and number 4 sieve sizes are only included in the ρ factor (ρ_{R38}, ρ_{R4}). Most parameters related to gradation were later eliminated from the model due to near multi-collinearity problems as explained later when presenting the final model.

In the case of asphalt type, it is expected that binders that come from different sources or that were produced at different times can have slight differences in their behavior even if they have the same grade. For example, although there are two binders classified as PG76-22 and two classified as PG70-22, it is expected that their performance would not be identical. Therefore, to account for the effect of a particular binder on each of the model terms (ρ, α, β, etc.), the dummy variable associated with that binder was multiplied by a parameter specific to that binder for the specific term considered. For example, for model 9 described in Table 6, when predicting the |E*| value of a mixture from the CR data set with a PG76-22 binder, the only binder-related ρ that stays in the model is ρ_{PG76CR} and the only binder related α included is α_{PG76CR}. The dummy variable for the PG76-22 binder from CR, which multiplies the parameter ρ_{PG76CR}, takes on a value of 1 whereas the dummy variables for all other binders take on a value of 0. This approach allows the model to capture the differences in the major model terms (ρ, α, β, etc.) caused by different binders. Of course, to avoid over specification (multi-collinearity) of the model, the dummy for one of the asphalt binders needs to be excluded. In this case, the dummy of the PG64-22 binder from the UHN study was used as the reference binder and therefore its dummy was excluded from the model. Thus, the parameter for a specific binder such as ρ_{PG76CR} for the PG76-22 in the CR study represents the increase in ρ relative to the ρ corresponding to the PG64-22 binder from the UHN study with all else equal. It is important to note here that the above interpretation needs to be changed slightly when bias parameters for each term are included for a given database. The discussion of this issue is postponed until bias parameters are considered.

In addition to the variables considered in ρ and α, this intermediate model 9 had two statistically significant parameters related to the effect of confinement in the term α_{cf}, named herein $\alpha_{cf\_}\alpha_{conf}$ and $\alpha_{cf\_}\gamma_{conf}$. However, other than this term α_{cf}, the model is still a relatively simple extension of the sigmoidal model of equation (12).

Returning to Figure 14, it is evident that including just a few key variables related to volumetrics, gradation and binder type greatly improves the fit of the model in comparison with a more general version like model 1 previously shown.

Figure 15 below shows the predicted versus observed values of log(|E*|) for model 9 for each of the three data sets analyzed. Again it is clear that the inclusion of variables for the parameters ρ, α, and α_{cf} improve the fit of the model with respect to the more general model.

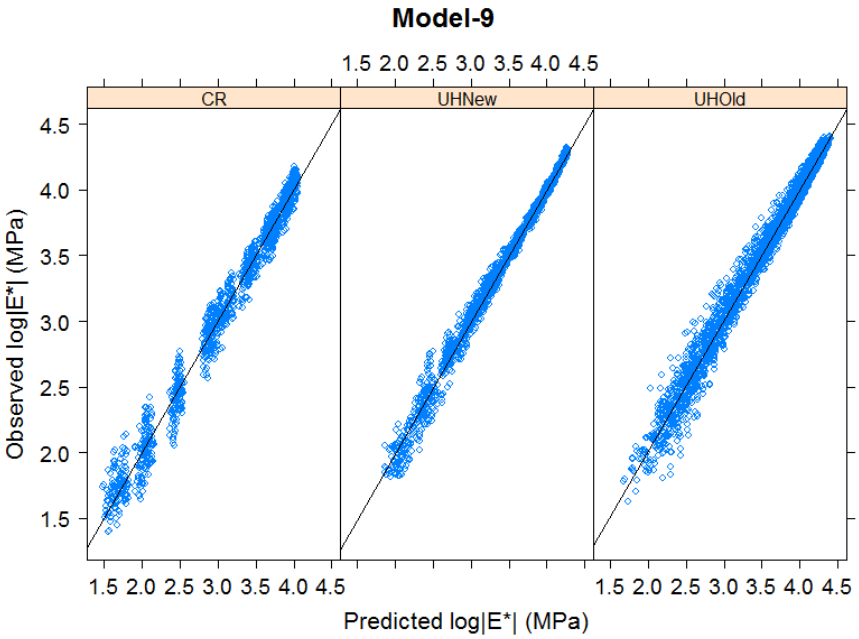

Figure 15. Predicted versus observed values of log|E| (by data set) for the initial model*

It is interesting to note that for the UHN data set, the line patterns previously observed are not noticeable anymore. The fact that this model includes, in addition to the aforementioned characteristics, the α_{cf} factor related to the confinement level helps in reducing the variability. A second point of interest from this figure is that the line patterns are still somehow visible for the CR data set. This is due to the inexistence of some of the most important variables that describe this data set, such as the inclusion of F-T cycles or the use of anti-stripping agents. A more uniform distribution of the data along the measured range will be presented for the last model obtained after the use of the joint estimation approach only.

5.3.2. Final Non-Linear Regression Model with Bias Parameters

After including all variables that were thought to have an influence in the prediction of the |E*| values for the complete database and discarding all variables that were found not to have statistical significance with a 10% significance level, the last model which uses joint estimation was obtained. It is important to clarify that the final model still needs the consideration of the mixed-effects approach. Also, it must be noted that the results presented below include some

parameters that are not statistically significantly different from zero. These parameters were left in this intermediate model either for discussion purposes about some bias parameters or because the model contained higher other terms of the variable related to the specific parameter.

A total of 105 individual parameters obtained using the nonlinear least squares (NLS) routine are included in this model. The lists of all parameters together with its estimated values, standard errors, t-statistics, and p-values from the statistical analysis are presented in Table 7 through Table 12. The parameters were separated by each of the main terms (ρ, α, β, γ, A and B) for practical reasons. Notice that the final number of parameters varies for each of the data sources since either some of them do not belong to the specific source or they are included only in one source as bias parameters.

The UHN data set was selected as the base case for data sets. In other words, bias parameters were used for the other data sources to account for potential differences in response between the data sources. Bias parameters for the constants in the terms and some other parameters (e.g., ρ_{AV2_UHO} and ρ_{Str_CR}) were considered. All variations from the base characteristics were included in the model using dummy variables. The reason why bias parameters were not included for most characteristics in a data source is that the effects of those characteristics from the specific data source are like those of the base case. Thus, based on statistical significance, the effect can be accounted for by a single parameter. In fact, as discussed later when the final model is estimated with mixed-effects, except for the constant terms no other bias parameters are found to be statistically significantly different from zero.

A final observation about the tables is that the first column for parameter number combines the base parameter with the bias parameter when applicable. This reduces the number of parameters for a specific data source to 75 as shown below.

The introduction of bias parameters for the terms ρ, α, β, γ, A and B requires a re-interpretation of the meaning in this study of some binder parameters. Recall that the bias parameters are intended to capture unobserved differences between seemingly identical samples from two different sources and that the binder parameters (with the dummy variables defined in this study) are intended to capture the difference in behavior arising from the use of a binder different from the base binder (the PG64-22 of the UHN study). Unfortunately, there is no PG64-22 binder in either the CR or UHO data sets. For the CR data set the closest binder is a PG70-22, which is a

high temperature grade higher than that in the UHN study. Thus, the inclusion of bias parameters for the CR data set together with dummies for the two binders resulted in over-specified models (that is, in models where both the bias parameter and some binder parameters competed to capture the same binder effect, in addition to other unobserved differences). Similar issues were found with the UHO data set. Furthermore, with the consideration of bias parameters, the lowest graded binders in each of the non-base data sets (PG70-22 in the CR data set and PG64-16 in the UHO data set) were generally not statistically significant anymore. Thus, a decision had to be made about whether bias parameters should be included for the non-base data sets or whether binder dummies should be used for all asphalt binders in the terms of the |E*| equation (of course, if statistical significant results were found and excluding the PG64-22 base binder of UHN). In this study, preference was given to the use of bias parameters since this accounts not only for differences in binder effects but also for any other unobserved differences between data sets. Thus, in the final model presented below, a base binder was considered for each data set: the PG64-22 in the UHN data set, the PG64-16 in the UHO data set, and the PG70-22 in the CR data set. No dummy variables were included for these binders. Instead, only dummy variables for other binders were considered. Now since the bias parameters are also capturing the differences between the bases binders, for a given data set, the interpretation of the parameter multiplying the dummy for a binder needs to be re-interpreted as the increase or decrease in the term if the binder corresponding to the dummy variable is used instead of the base binder for the data set.

For all the parameters included in Table 7 through Table 12 shown next, most of the sub-indices are self-explanatory. However, to avoid confusion, Table 13 presents a summary of all of them.

Table 7. Parameters of the model included in the ρ factor (NLS model)

Param. No.	Parameter	Parameter Estimate	Standard Error	*t* value	*p* value	Included in
1	ρ_C	4.3633	0.0952	45.852	<0.0001	All
	ρ_{CR}	0.4210	0.1355	3.107	0.00190	CR
2	ρ_{Vb}	-0.0433	0.0026	-16.411	<0.0001	All
3	ρ_{AV}	0.0058	0.0037	1.574	0.11543	All
4	ρ_{AV2}	-0.0026	0.0004	-7.160	<0.0001	All
	ρ_{AV2_UHO}	-0.0007	0.0002	-2.870	0.00412	UHO
5	ρ_{R38}	-0.0175	0.0036	-4.794	<0.0001	All
6	ρ_{R4}	0.0231	0.0035	6.595	<0.0001	All
	ρ_{R4_CR}	-0.0074	0.0013	-5.879	<0.0001	CR

Table 7 (Cont'd). Parameters of the model included in the ρ factor (NLS model).

Param. No.	Parameter	Parameter Estimate	Standard Error	*t* value	*p* value	Included in
7	ρ_{Str}	-0.0007	0.0001	-5.153	<0.0001	All
	ρ_{Str_CR}	-0.0029	0.0011	-2.700	0.00695	CR
8	ρ_{Elv}	-0.0388	0.0068	-5.721	<0.0001	UHO
9	ρ_{PG76CR}	0.1506	0.0112	13.484	<0.0001	CR
10	ρ_{Fib}	-0.0015	0.0009	-1.723	0.08484	UHN
11	ρ_{Lime}	0.0543	0.0030	18.228	<0.0001	CR
12	ρ_{MB}	0.0193	0.0028	6.796	<0.0001	CR
13	ρ_{D1C}	-0.0627	0.0094	-6.705	<0.0001	CR
14	ρ_{D3C}	-0.0780	0.0091	-8.560	<0.0001	CR
15	ρ_{D6C}	-0.0783	0.0093	-8.449	<0.0001	CR

Table 8. Parameters of the model included in the α factor (NLS model).

Param. No.	Parameter	Parameter Estimate	Standard Error	*t* value	*p* value	Included in
16	α_{Fib}	0.0159	0.0038	4.232	<0.0001	UHN
17	α_{cf}_α	-0.8501	0.2003	-4.244	<0.0001	UHN/UHO
18	$\alpha_{cf}\_\alpha_{PG76}$	2.8005	0.2346	11.935	<0.0001	UHN/UHO
19	$\alpha_{cf}\_\alpha_{AV}$	0.0531	0.0090	5.909	<0.0001	UHN/UHO
20	$\alpha_{cf}\_\alpha_{AV\_PG76}$	-0.0957	0.0118	-8.139	<0.0001	UHN/UHO
21	α_{cf}_γ	-0.0084	0.0008	-10.166	<0.0001	UHN/UHO
22	α_{C}	-44.7812	16.9822	-2.636	0.00838	All
	α_{UHO}	39.7408	16.9705	2.341	0.01922	UHO
	α_{CR}	38.1560	17.0404	2.239	0.02518	CR
23	α_{AV}	10.1825	1.3885	7.333	<0.0001	All
	α_{AV_CR}	-9.4740	1.4251	-6.647	<0.0001	CR
	α_{AV_UHO}	-9.6382	1.3890	-6.938	<0.0001	UHO
24	α_{AV2}	-0.1084	0.0129	-8.431	<0.0001	All
	α_{AV2_CR}	0.0539	0.0243	2.215	0.02676	CR
	α_{AV2_UHO}	0.0926	0.0128	7.209	<0.0001	UHO
25	α_{Vb}	3.6453	1.4919	2.443	0.01458	All
	α_{Vb_CR}	-3.7062	1.4990	-2.472	0.01344	CR
	α_{Vb_UHO}	-3.5135	1.4919	-2.355	0.01855	UHO
26	α_{AV*Vb}	-0.8225	0.1150	-7.153	<0.0001	All
	α_{AV*Vb_CR}	0.8254	0.1170	7.054	<0.0001	CR
	α_{AV*Vb_UHO}	0.7955	0.1150	6.915	<0.0001	UHO
27	α_{Str}	-0.0078	0.0006	-13.031	<0.0001	All
	α_{Str_CR}	0.0092	0.0033	2.805	0.00505	CR
	α_{Str_UHO}	0.0048	0.0006	7.971	<0.0001	UHO

Table 8 (Cont'd). Parameters of the model included in the α factor (NLS model).

Param. No.	Parameter	Parameter Estimate	Standard Error	*t* value	*p* value	Included in
28	$\alpha_{PG76UHN}$	-0.3780	0.1027	-3.682	0.00023	UHN
29	α_{Elv}	-1.1113	0.0327	-33.975	<0.0001	UHO
30	$\alpha_{PG70UHO}$	-0.8293	0.0644	-12.880	<0.0001	UHO
31	α_{R38}	-0.3006	0.0190	-15.847	<0.0001	All
32	α_{R4}	0.2841	0.0177	16.036	<0.0001	All
33	α_{Conf}	-0.0062	0.0011	-5.720	<0.0001	UHN/UHO
	α_{Conf_PG76}	0.0128	0.0015	8.463	<0.0001	
34	α_{Conf2}	1.00E-05	2.54E-06	3.937	<0.0001	UHN/UHO
	α_{Conf2_PG76}	3.26E-05	9.41E-06	3.461	0.00054	
35	α_{D1C}	-0.3011	0.0320	-9.408	<0.0001	CR
36	α_{D3C}	-0.3349	0.0307	-10.905	<0.0001	CR
37	α_{D6C}	-0.3139	0.0320	-9.811	<0.0001	CR

Table 9. Parameters of the model included in the β factor (NLS model)

Param. No.	Parameter	Parameter Estimate	Standard Error	*t* value	*p* value	Included in
38	β_{C}	-2.5564	0.1840	-13.896	<0.0001	All
	β_{UHO}	1.8391	0.2382	7.722	<0.0001	UHO
39	β_{P200}	0.2576	0.0334	7.719	<0.0001	All
	β_{P200_CR}	-0.0561	0.0254	-2.207	0.02728	CR
	β_{P200_UHO}	-0.3433	0.0393	-8.740	<0.0001	UHO
40	$\beta_{PG76UHN}$	0.1391	0.0216	6.428	<0.0001	UHN
41	β_{Elv}	0.4114	0.0224	18.329	<0.0001	UHO
42	β_{PG76CR}	0.0679	0.0184	3.685	0.00023	CR
43	$\beta_{PG70UHO}$	0.5628	0.0305	18.471	<0.0001	UHO
44	β_{Lime}	-0.1606	0.0159	-10.126	<0.0001	CR
45	β_{MB}	-0.0828	0.0147	-5.637	<0.0001	CR
46	β_{D1C}	-0.1453	0.0244	-5.968	<0.0001	CR
47	β_{D3C}	-0.1692	0.0244	-6.941	<0.0001	CR
48	β_{D6C}	-0.1904	0.0239	-7.965	<0.0001	CR
49	β_{Conf}	-3.89E-04	6.85E-05	-5.670	<0.0001	UHN/UHO
	$\beta_{Conf\_PG76UHN}$	-5.29E-04	1.25E-04	-4.235	<0.0001	UHN
50	β_{AV}	-0.0499	0.0059	-8.422	<0.0001	All
	β_{AV_CR}	0.0648	0.0194	3.340	0.00084	CR
	β_{AV_UHO}	0.0373	0.0065	5.727	<0.0001	UHO

Table 10. Parameters of the model included in the γ factor (NLS model)

Param. No.	Parameter	Parameter Estimate	Standard Error	*t* value	*p* value	Included in
51	γ_C	0.1764	0.0199	8.882	<0.0001	All
	γ_{UHO}	-0.1365	0.0174	-7.838	<0.0001	UHO
	γ_{CR}	-0.1898	0.0271	-7.004	<0.0001	CR
52	γ_{P200}	0.0542	0.0032	17.132	<0.0001	All
53	γ_{PG76CR}	-0.0440	0.0035	-12.500	<0.0001	CR
54	$\gamma_{PG70UHO}$	0.0239	0.0115	2.079	0.03760	UHO
55	γ_{Lime}	-0.0413	0.0073	-5.635	<0.0001	CR
56	γ_{D1C}	0.4827	0.0684	7.060	<0.0001	CR
57	γ_{D3C}	0.5642	0.0727	7.759	<0.0001	CR
58	γ_{D6C}	0.5324	0.0717	7.422	<0.0001	CR
59	$\gamma_{Con\_PG76UHN}$	2.19E-04	7.99E-05	2.743	0.00609	UHN
60	γ_{AV}	-0.0073	0.0023	-3.212	0.00132	All
	γ_{AV_CR}	0.0131	0.0036	3.668	0.00025	CR
	γ_{AV_UHO}	0.0134	0.0023	5.755	<0.0001	UHO

Table 11. Parameters of the model included in the A factor (NLS model)

Param. No.	Parameter	Parameter Estimate	Standard Error	*t* value	*p* value	Included in
61	A_C	1.91E-03	6.41E-05	29.742	<0.0001	All
62	A_{Vb}	-1.22E-04	5.71E-06	-21.433	<0.0001	All
63	A_{PG76CR}	-4.46E-04	3.62E-05	-12.315	<0.0001	CR
64	$A_{PG70UHO}$	-3.07E-04	7.70E-05	-3.987	<0.0001	UHO
65	A_{WMA}	2.47E-04	5.18E-05	4.760	<0.0001	UHO
66	A_{Conf}	0.0019	0.0004	4.478	<0.0001	UHN/UHO
67	A_{MB}	0.7370	0.0895	8.236	<0.0001	CR
68	A_{D1C}	0.1252	0.0433	2.894	0.00382	CR
69	A_{D3C}	0.0828	0.0445	1.857	0.06325	CR
70	A_{D6C}	0.0898	0.0435	2.063	0.03913	CR

Table 12. Parameters of the model included in the B factor (NLS model)

Param. No.	Parameter	Parameter Estimate	Standard Error	*t* value	*p* value	Included in
71	B_C	-0.1562	0.0017	-93.656	<0.0001	All
	B_{CR}	-0.0080	0.0021	-3.773	0.00016	CR
	B_{UHO}	-0.0050	0.0011	-4.786	<0.0001	UHO
72	B_{PG76CR}	0.0291	0.0031	9.425	<0.0001	CR
73	$B_{PG70UHO}$	0.0245	0.0051	4.796	<0.0001	UHO
74	B_{Conf}	2.52E-04	9.61E-05	2.616	0.00891	UHN/UHO
75	B_{MB}	0.1422	0.0198	7.168	<0.0001	CR

Table 13. List of sub-indices used for the parameter description

Sub index	**Meaning**	**Sub index**	**Meaning**	**Sub index**	**Meaning**
C	Constant	Vb	Eff. Binder Vol.	PGXX	Asphalt grade
CR	Costa Rica	Vb2	(Eff. Binder Vol.)^2	Elv	Elvaloy®Ret
UHO	UHO	Conf	Confinement	Lime	Lime
AV	Air Voids	Conf2	(Confinement)^2	MB	Magnabond
AV2	(Air Voids)^2	R38	Retained in 3/8" sieve	D1C	1 F-T cycles
Str	Strains	R4	Retained in No.4 sieve	D3C	3 F-T cycles
Fib	Fibers	P200	Passing No. 200	D6C	6 F-T cycles

In the previous model, there are combinations of sub-indices that indicate the interaction of two or more characteristics. This is the case for example of $\alpha_{PG76UHN}$, where the sub-indices express that the α is included for the case of the PG76-22 from the UHN data set. In the case where it only reads PG76, this means that the parameter applies for all binders in all data sets that possess that asphalt grade. As an example, one of the most complex indices included in the model is $\alpha_{cf}\_\alpha_{AV\_PG76}$. The initial α_{cf} means that this parameter belongs to the confinement factor described in Equation (14), while the α_{AV_PG76} points at the specific parameter of this equation. Finally, AV and PG76 indicate that the parameter multiplies the interaction of air voids with a PG76-22 binder dummy. That is, it accounts for the effects of air voids in the parameter α of the factor α_{cf} but only for PG76-22 binders.

The model is presented below as a single equation but it could be re-written for each data set considering only the parameters related to the specific set. However, since this model is intended to be used as a prediction model for any mixture with similar characteristics, it is presented as a single equation with the use of several dummy variables (D_i). As explained before, these will take a value of 1 when a given characteristic is included in the model or 0 otherwise. Given that each of the terms ρ, α, β, γ, A and B is a long combination of several characteristics of the mixture, writing the model in one piece was not possible, and therefore, after revisiting Equation 16, each of the terms is written below as a combination of all statistically significant variables. In addition to the variables presented in Table 7 through Table 12, the dummy variables (D_i) and other properties of the mixtures included in the model are as follows.

In the case of the dummy variables, all of them have identical sub-indices similar to the ones shown in Table 13. All other variables related with mixture characteristics that are included in the model are as follows.

- AV: Air voids (by volume of the mix) (%),
- V_{beff}: Effective binder content (by volume of the mix) (%),
- $Ret_{3/8}$: Cumulative percent of aggregate (by weight) retained on the 3/8" sieve (%),
- Ret_4: Cumulative percent of aggregate (by weight) retained on the No. 4 sieve (%),
- P200: Percent of aggregate (by weight) passing through the No.200 sieve (%),
- μs: microStrain measured during |E*| testing at the particular temperature/frequency combination (μs),
- σ_3: Confinement pressure applied to the sample during testing (%)

$$\log|E^*| = \rho - \frac{\alpha * \alpha_{cf}}{1+e^{-\left(\beta+\gamma\left(log\left(\frac{1}{f}\right)-(A*T^2+B*T-(A*(21.1)^2+B*(21.1))\right)\right)}} \quad \text{where,} \quad \text{(16 Revisited)}$$

$$\rho = \left[\left(\rho_C + \rho_{CR}D_{CR} + \rho_{Vb}V_{beff} + \rho_{AV}AV + \left(\rho_{AV2} + \rho_{AV2_{UHO}}D_{UHO}\right)AV^2 + \rho_{R38}Ret_{3/8} + \left(\rho_{R4} + \rho_{R4_{CR}}D_{CR}\right)Ret_4 + \left(\rho_{Str} + \rho_{Str_{CR}}D_{CR}\right)\mu s + \rho_{Elv}D_{Elv} + \rho_{PG76CR}D_{PG76CR}\right) * (1 + \rho_{Fib}D_{Fib}) * (1 + \rho_{Lime}D_{Lime} + \rho_{MB}D_{MB}) * (1 + \rho_{D1C}D_{D1C} + \rho_{D3C}D_{D3C} + \rho_{D6C}D_{D6C})\right] \quad (17)$$

$$[\alpha_{cf}] = (1 + \alpha_{Fib}D_{Fib}) * \left[\left(1 - D_{Conf} + D_{Conf}\right)\left\{\left(1 + \frac{\alpha_{cf\_\alpha} + \alpha_{cf\_\alpha_{PG76}}(D_{PG76UHN}+D_{Elv}) + \left(\alpha_{cf\_\alpha_{AV}} + \alpha_{cf\_\alpha_{AV_{PG76}}}(D_{PG76UHN}+D_{Elv})\right)AV}{1+e^0}\right) - \frac{\alpha_{cf\_\alpha} + \alpha_{cf\_\alpha_{PG76}}(D_{PG76UHN}+D_{Elv}) + \left(\alpha_{cf\_\alpha_{AV}} + \alpha_{cf\_\alpha_{AV_{PG76}}}(D_{PG76UHN}+D_{Elv})\right) * AV}{1+e^{\alpha_{cf\_\gamma}\sigma_3}}\right\}\right] \quad (18)$$

$$\alpha = \left[\left(\alpha_C + \alpha_{CR}D_{CR} + \alpha_{UHO}D_{UHO} + \left(\alpha_{AV} + \alpha_{AV\_CR}D_{CR} + \alpha_{AV\_UHO}D_{UHO}\right)AV + \left(\alpha_{AV2} + \alpha_{AV2\_CR}D_{CR} + \alpha_{AV2\_UHO}D_{UHO}\right)AV^2 + \left(\alpha_{Vb} + \alpha_{Vb\_CR}D_{CR} + \alpha_{Vb\_UHO}D_{UHO}\right)V_{beff} + \left(\alpha_{AVVb} + \alpha_{AVVb\_CR}D_{CR} + \alpha_{AVVb\_UHO}D_{UHO}\right)AV \cdot V_{beff} + \left(\alpha_{Str} + \alpha_{Str\_CR}D_{CR} + \alpha_{Str\_UHO}D_{UHO}\right)\mu s + \alpha_{PG76UHN}D_{PG76UHN} + \alpha_{Elv}D_{Elv} + \alpha_{PG70UHO}D_{PG70UHO} + \alpha_{R38}Ret_{3/8} + \alpha_{R4}Ret_4 + \alpha_{Conf}\sigma_3 + \alpha_{Conf2}{\sigma_3}^2 + \alpha_{Conf\_PG76}(D_{PG76UHN} + D_{Elv})\sigma_3 + \alpha_{Conf2\_PG76}(D_{PG76UHN} + D_{Elv}){\sigma_3}^2\right) * (1 + \alpha_{D1C}D_{D1C} + \alpha_{D3C}D_{D3C} + \alpha_{D6C}D_{D6C})\right] \quad (19)$$

$$\beta = \left(\beta_C + \beta_{UHO}D_{UHO} + \left(\beta_{AV} + \beta_{AV\_CR}D_{CR} + \beta_{AV\_UHO}D_{UHO}\right)AV + \left(\beta_{P200} + \beta_{P200\_CR}D_{CR} + \beta_{P200\_UHO}D_{UHO}\right)P200 + \beta_{PG76UHN}D_{PG76UHN} + \beta_{Elv}D_{Elv} + \beta_{PG76CR}D_{PG76CR} + \beta_{PG70UHO}D_{PG70UHO}\right) * (1 + \beta_{Lime}D_{Lime} + \beta_{MB}D_{MB}) * (1 + \beta_{D1C}D_{D1C} + \beta_{D3C}D_{D3C} + \beta_{D6C}D_{D6C}) * \left(1 + \beta_{Conf}\ \sigma_3 + \beta_{Conf\_PG76UHN}D_{PG76UHN}\ \sigma_3\right) \quad (20)$$

$$\gamma = \left(\gamma_C + \gamma_{UHO}D_{UHO} + \gamma_{CR}D_{CR} + \left(\gamma_{AV} + \gamma_{AV\_CR}D_{CR} + \gamma_{AV\_UHO}D_{UHO}\right)AV + \gamma_{P200}P200 + \gamma_{PG76CR}D_{PG76CR} + \gamma_{PG70UHO}D_{PG70UHO}\right) * (1 + \gamma_{Lime}D_{Lime}) * (1 + \gamma_{D1C}D_{D1C} + \gamma_{D3C}D_{D3C} + \gamma_{D6C}D_{D6C}) * \left(1 + \gamma_{Conf\_PG76UHN}D_{PG76UHN}\ \sigma_3\right) \quad (21)$$

$$A = \left(A_C + A_{Vb}V_{beff} + A_{PG76CR}D_{PG76CR} + A_{PG70UHO}D_{PG70UHO} + A_{WMA}D_{WMA}\right) * \left(1 + A_{Conf}\sigma_3\right) * (1 + A_{MB}D_{MB}) * (1 + A_{D1C}D_{D1C} + A_{D3C}D_{D3C} + A_{D6C}D_{D6C}) \quad (22)$$

$$B = (B_C + B_{CR}D_{CR} + B_{UHO}D_{UHO} + B_{PG76CR}D_{PG76CR} + B_{PG70UHO}D_{PG70UHO}) * \left(1 + B_{Conf}\ \sigma_3\right) * (1 + B_{MB}D_{MB}) \quad (23)$$

The observed vs. predicted plots for this model, obtained using the non-linear least squares routine (NLS) in R with the inclusion of the joint estimation approach are shown in Figure 16 in regular scale and Figure 17 in a logarithmic scale.

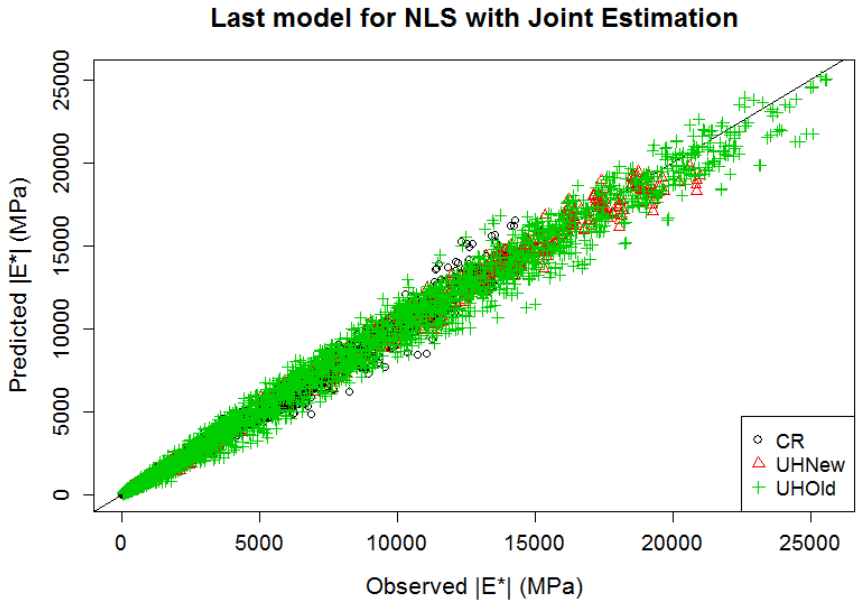

Figure 16. Observed versus predicted values of |E| for the last NLS model*

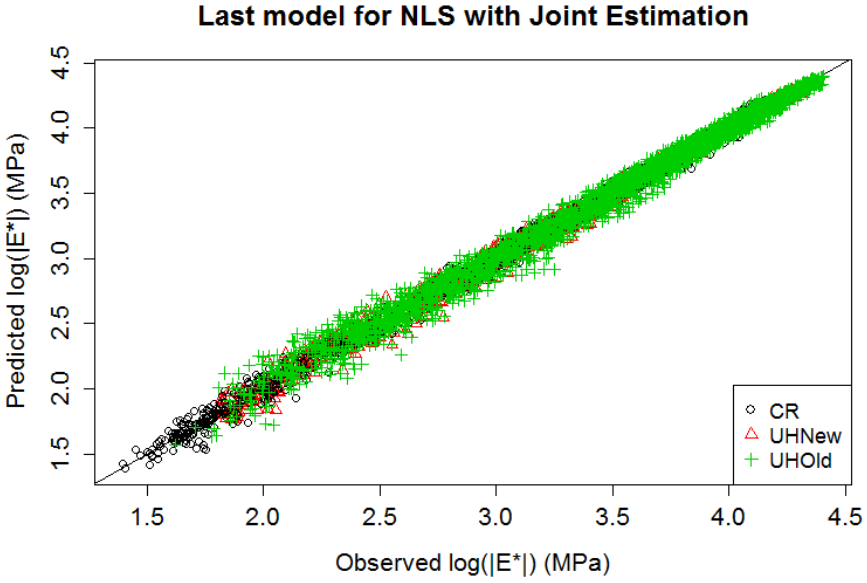

Figure 17. Observed versus predicted values of log|E| for the last NLS model*

When observing these two plots, an improvement in the fit of the model with respect to the previously shown figures is noticeable. The addition of statically significant variables that

influence the behavior of the mixtures allowed for achieving an improved standard error of the estimate (σ_{est}), which can be used as an indicator of the goodness of fit for non-linear models. The nonlinear least squares (NLS) routine employed to develop this model estimates the model parameters by minimizing the sum of squares of the residuals (SS_{Res}). The value of σ_{est} is then calculated using the SS_{Res}. Smaller values of σ_{est} indicate more accurate predictions. In the case of the initial model (Model-1) σ_{est}=0.191, while in the case of the intermediate model shown (model-9) σ_{est}=0.0811. Even when this reduction in σ_{est} by the addition of a few variables seems to be a good improvement, it is necessary to remember that the intermediate model still needed several variables to be able to capture the characteristics of all three data sets. The last model for the NLS fit illustrated above has an σ_{est}=0.0539, which is the minimum value achieved after over 50 different models were tested.

Typically, to indicate the goodness of fit of a model, the coefficient of determination (R^2) is the statistic of choice. However, the use of R^2 should be limited to the fitting of linear models for the following reasons. In the case of linear models, the sum of the variation of the regression plus the variation of the error is equal to the total variation. In other terms, the total sum of squares (SS_{Tot}) is equal to the sum of the regression sum of squares (SS_{Reg}) and the sum of squares of residuals (SS_{Res}). R^2 is simply the ratio of the regression sum of squares (SS_{Reg}) and the total sum of squares (SS_{Tot}). For linear models, R^2 always falls between a value of 0 and 1 which indicates the fraction of the variation in the data that is explained by the independent variable in the regression equation. In the case of nonlinear models, the sum of SS_{Reg} and SS_{Res} is not equal to SS_{Tot} and R^2 can no longer be interpreted as the fraction of the total variation explained by the model. Although goodness of fit is important, the satisfaction of the assumptions in which the model is based is also of great importance. When the assumptions are not satisfied, statistical results such as t-statistic and p-values are unreliable and therefore variables can be kept or excluded from the model erroneously.

The improvement in the goodness of fit is more noticeable in Figure 18, where the predicted versus observed values are shown for all data sets separately. Not only is the variation much smaller in this case but also there are no traces of the line-patterns shown previously for Model 1 and Model 9, indicating that the differences within data points are being captured and addressed better.

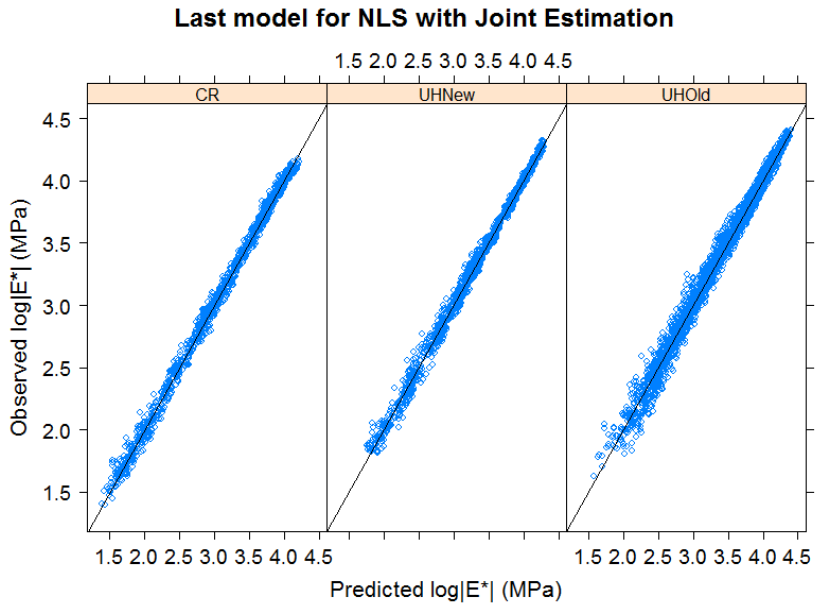

Figure 18. Predicted versus observed values of log|E| (by data set) for the last NLS model*

As discussed before, after the development of the model, it is necessary to verify the assumptions on which it was based. This will be discussed in more detail for the final model after the consideration of the random effects in the mixed-effects approach. However, three figures are shown at this point to show how the main assumptions are assessed. Figure 19 shows the standardized residuals, versus the predicted values of |E*| by source. A standardized residual is defined as the residual divided by its standard deviation.

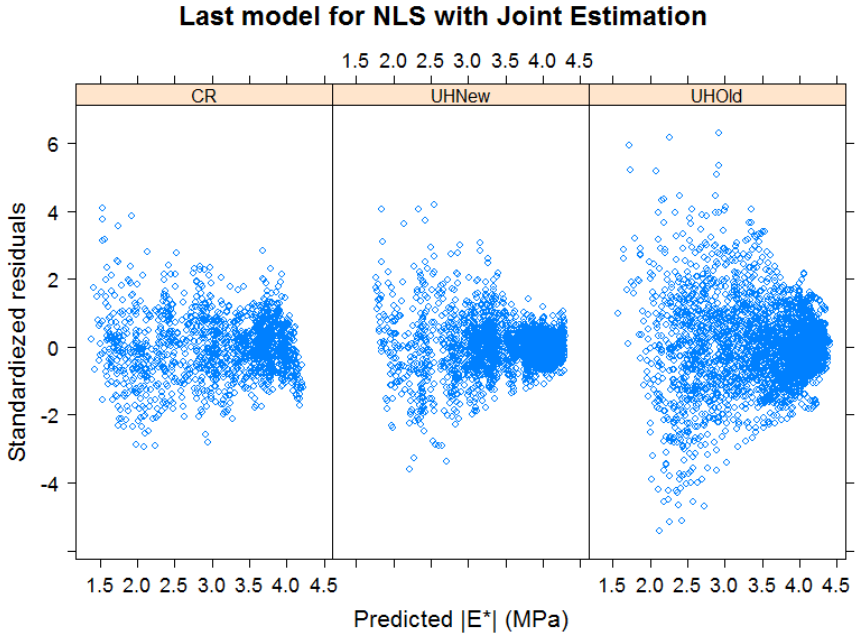

Figure 19. Standardized residuals versus predicted values for the NLS fit

In the figure, it is clear that the residuals do not have constant variance. Instead, they form a conical pattern. Also, there are differences in the range of the residuals, particularly for the UHO data set for which there is a wider spread than for the other two data sources. This invalidates one of the assumptions of the least-squares regression (i.e., homoscedasticity).

As illustrated by this figure, each data set appears to have a somewhat different variance that decreases differently with the predicted value. This is a classic example of heteroskedasticity. Although the parameter estimates are still unbiased, when heteroskedasticity is present but it is not accounted for, it produces inefficient parameter estimates (i.e., parameter estimates with large variation and unreliable test of hypothesis results).

Figure 20 presents a normal quantile-quantile plot of the standardized residuals. In this type of plot, the residuals should plot as a straight line if they follow the assumed distribution for hypothesis testing, which is asymptotically normal in this case (except for the extremes where a few outliers always produce some departures from a straight line). Clearly, the residuals for the three data sets depart from a straight line showing that the assumption that they have a normal distribution is not met either. Because of this, the statistical results are again unreliable.

Figure 20. Quantile-Quantile plot of the standardized residuals for the NLS fit

The last plot of this section, Figure 21, shows box and whiskers plots of the residuals of the NLS fit for each of the 265 samples tested. Due to the large number of samples it is not possible to clearly identify the boxes and whiskers (the boxes are not noticeable but instead they appear as

solid lines covering the interquartile range whereas the lengths of the whiskers represent 1.5 times the corresponding inter-quantile range and appear as dotted lines.) Nevertheless, it is simple to identify the black points which represent the median of the |E*| values for every sample tested. The hollow dots represent points identified as outliers. It can be seen from this figure that the residuals are distributed around the value of 0; however, it can be noted that there are differences in the distribution by data source: UHN: samples 1-42, CR: samples 43-186, UHO: samples 187-265, separated by horizontal lines. This supports the statement made above about each data base having its own variance of the residuals. Also, there are unobserved heterogeneities at the sample level that cannot be captured by the parameters currently describing the model. Note that the range of residuals for some samples do not even include zero (which means that all residuals from those samples are either all positive or all negative, which violates the assumption of independence of the error terms). It is vital to understand that the fact that the model does not comply with the assumptions on which it is based means the validity of the t-statistics and p-values and thus of the whole model may be questionable. This is the motivation for the use of the mixed-effects approach explained next.

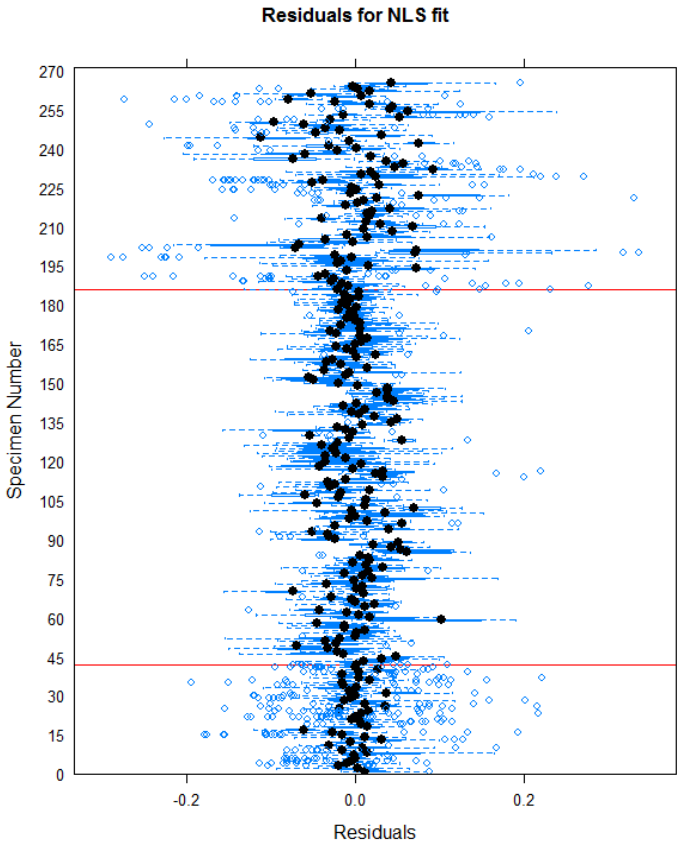

Figure 21. Boxplot of residuals for NLS fit by sample

5.4 Incorporation of non-linear mixed-effects

The mixed effects approach was used in the development of the predictive model to consider the correlation between the errors of the observations at the within-individual level (i.e. within samples) induced by the random effects. By including random effects, it is possible to identify for each tested sample, a deviation from an overall mean, due to unobserved heterogeneities in the samples.

To obtain this final model, the nonlinear mixed effects (NLME) routine available in the software R was used. When using this routine, several arguments are required for the desired analysis. The initial model used for this approach was the last model shown in the previous section obtained through the NLS routine. The model was corrected after the inclusion of the random effects to exclude all parameters that became not significant and after the significance of some other parameters was re-assessed. Parameters that are not statistically significant after the consideration of the random effects were probably capturing variation that was likely due to within-sample variability when using the non-linear least squares approach. Several parameters were removed from the model as shown later in the discussion.

From the list of arguments that can be included on the NLME routine, two are of fundamental importance to run the routine:

- Random: describes in a two-sided formula, the random effects that are desired in the model and their corresponding grouping structure.
- Weights: describes the desired within group heteroscedasticity structure.

For this model, the random argument selected was a two-sided formula of the form *krho_C+kalpha_C ~1*, which indicates that two random effects are included in the model, one for the parameter ρ_C and a second one for α_C. The 1 on the right-hand side of the formula indicates that a single effect is included for each parameter. Furthermore, the NLME routine can model these random effects with positive-definite matrices (pdMat) with several patterns of variance-covariance (Pinheiro and Bates, 2000). For this model, the particular pdMat utilized was the pdSymm structure, which defines a general symmetric positive-definite matrix. In terms of the random parameters being included, the pdSymm implies a matrix where the diagonal shows the variance of each of the random effects and all other *i, j* positions in the matrix show the covariance of the i^{th} and j^{th} random effects. This type of matrix assumes that there may be some correlation between the random effects.

In the case of the weights, the NLME routine requires the definition of the within group variance structure using classes of variance functions (varFunc). From the available varFunc classes, the varExp was used for developing the model. VarExp uses an "exponential function of the variance covariate", which allows for an increase or decrease of the model's variance with respect to the variance covariate (Pinheiro and Bates, 2000). The specific structure used for this model was *varExp (1, form = ~fitted(.)-1|Source)*; which specifies a variance covariate given by the obtained fitted values minus 1 and includes a stratification at the Source level of the data base (i.e. UHN, CR, UHO). By including this within group variance at the source level, heteroscedasticity is being accounted for in the model. This implies that the dispersion of the residuals is different for each source, which in turn allows for an improved distribution of the model's residuals in comparison with the NLS fit. The specific variance structure chosen as well as the number of random parameters was the result of experimentation between several variance structures (power, exponential, and other combinations) such that a balance could be achieved between residuals satisfying the regression assumptions and avoidance of over specification of the model. The subtraction of 1 to the fitted values in the variance structure was found to produce better results than the default exponential variance structure.

The final model developed with the NLME routine includes a total of 56 statistically significant parameters. A complete list of these is shown next in Table 14 through Table 19. These tables present the same information as Table 7 through Table 12, organized also by the different terms for practical reasons.

Each of the tables contains for each parameter its estimate, its standard error and the *t-statistic* and *p*-values from the statistical analysis. The parameter number from column one combines the base parameter with the bias parameters. By counting these combinations as one parameter, the model is reduced to 46, compared to the 75 parameters from the NLS fit. It is important to notice that the parameters β_{UHO} and γ_{CR} included in the tables were not found to be statistically significant. These terms were retained at this point for discussion purposes only. The parameter will be excluded from the final model presented later. The exclusion of both parameters does not affect the significance of any other parameters since in the case of β_{UHO}, its *p*-values is 0.9904, meaning that the parameter is not statistically different from zero while in the case of γ_{CR} the *p*-values is 0.1126, meaning that it is not statistically significantly different from zero at 10% significance level which was set as the limit to include parameters.

Table 14. Parameters of the model included in the ρ factor (NLME model)

Param. No.	Parameter	Parameter Estimate	Standard Error	*t* value	*p* value	Included in
1	ρ_C	4.9040	0.0386	127.055	<0.0001	All
	ρ_{CR}	-0.0790	0.0111	-7.137	<0.0001	CR
	ρ_{UHO}	0.0809	8.16E-03	9.915	<0.0001	UHO
2	ρ_{Vb}	-0.0338	3.09E-03	-10.909	<0.0001	All
3	ρ_{AV}	-0.0229	1.51E-03	-15.163	<0.0001	All
4	ρ_{Str}	-3.44E-04	5.00E-05	-6.884	<0.0001	All
5	ρ_{Elv}	-0.0331	8.37E-03	-3.952	<0.0001	UHO
6	ρ_{PG76CR}	0.0433	6.86E-03	6.313	<0.0001	CR
7	ρ_{Lime}	0.0260	1.56E-03	16.695	<0.0001	CR
8	ρ_{MB}	0.0112	1.61E-03	6.962	<0.0001	CR
9	ρ_{D1C}	-0.0108	2.14E-03	-5.073	<0.0001	CR
10	ρ_{D3C}	-0.0199	2.14E-03	-9.301	<0.0001	CR
11	ρ_{D6C}	-0.0221	2.31E-03	-9.555	<0.0001	CR

Table 15. Parameters of the model included in the α factor (NLME model)

Param. No.	Parameter	Parameter Estimate	Standard Error	*t* value	*p* value	Included in
12	α_{cf}_α	0.3670	0.0919	3.996	<0.0001	UHN/UHO
13	$\alpha_{cf}\_\alpha_{PG76}$	0.1934	0.0396	4.884	<0.0001	UHN/UHO
14	$\alpha_{cf}\_\alpha_{AV}$	0.0192	4.54E-03	4.223	<0.0001	UHN/UHO
15	$\alpha_{cf}\_\alpha_{AV\_PG76}$	-0.0119	3.23E-03	-3.671	0.0002	UHN/UHO
16	$\alpha_{cf}\_\alpha_{Fib}$	-0.0233	6.85E-03	-3.398	0.0007	UHN
17	α_{cf}_γ	-6.22E-03	3.91E-04	-15.901	<0.0001	UHN/UHO
18	α_C	1.8521	0.1693	10.942	<0.0001	All
	α_{CR}	-0.7498	0.1180	-6.353	<0.0001	CR
	α_{UHO}	0.3082	0.1198	2.573	0.0101	UHO
19	α_{AV}	0.2966	0.0170	17.405	<0.0001	All
20	$\alpha_{PG76UHN}$	-0.7190	0.0900	-7.992	<0.0001	UHN
21	α_{Elv}	-1.4970	0.0846	-17.705	<0.0001	UHO
22	$\alpha_{PG70UHO}$	-0.5199	0.1202	-4.323	<0.0001	UHO
23	α_{R4}	0.0166	2.54E-03	6.516	<0.0001	All
24	α_{Conf}	-8.17E-04	3.70E-04	-2.208	0.0273	UHN/UHO
25	α_{Fib}	0.1291	0.0775	1.665	0.0960	UHN

Table 16. Parameters of the model included in the β factor (NLME model)

Param. No.	Parameter	Parameter Estimate	Standard Error	*t* value	*p* value	Included in
26	β_C	-1.2153	0.0223	-54.414	<0.0001	All
	β_{CR}	0.4121	0.0233	17.681	<0.0001	CR
	β_{UHO}	-2.47E-04	0.0205	-0.012	0.9904	UHO
27	$\beta_{PG76UHN}$	0.1771	0.0130	13.606	<0.0001	UHN
28	β_{Elv}	0.4477	0.0149	30.067	<0.0001	UHO
29	$\beta_{PG70UHO}$	0.3559	0.0274	12.969	<0.0001	UHO
30	β_{D6C}	-0.0556	0.0129	-4.303	<0.0001	CR
31	β_{Conf}	9.99E-04	6.98E-05	14.318	<0.0001	UHN/UHO
32	$\beta_{Conf\_PG76UHN}$	1.87E-04	5.82E-05	3.215	0.0013	UHN
33	β_{AV}	-0.0589	2.99E-03	-19.707	<0.0001	All

Table 17. Parameters of the model included in the γ factor (NLME model)

Param. No.	Parameter	Parameter Estimate	Standard Error	*t* value	*p* value	Included in
34	γ_C	0.4143	0.0165	25.098	<0.0001	All
	γ_{CR}	0.0107	6.71E-03	1.587	0.1126	CR
	γ_{UHO}	-0.0379	5.38E-03	-7.047	<0.0001	UHO
35	γ_{P200}	0.0110	2.74E-03	4.021	<0.0001	All
36	γ_{PG76CR}	-0.0330	3.80E-03	-8.702	<0.0001	CR
37	γ_{D1C}	0.0293	0.0127	2.309	0.0210	CR
38	γ_{D3C}	0.0298	0.0129	2.312	0.0208	CR
39	γ_{D6C}	0.0458	0.0135	3.381	0.0007	CR
40	γ_{AV}	-7.14E-03	6.63E-04	-10.781	<0.0001	All
41	γ_{Fib}	-0.0112	0.0022	-5.102	<0.0001	UHN

Table 18. Parameters of the model included in the A factor (NLME model)

Param. No.	Parameter	Parameter Estimate	Standard Error	*t* value	*p* value	Included in
42	A_C	9.03E-04	4.01E-05	22.555	<0.0001	All
	A_{CR}	-4.54E-05	1.80E-05	-2.519	0.0118	CR
	A_{UHO}	7.82E-05	1.56E-05	5.020	<0.0001	UHO
43	A_{Vb}	-1.74E-05	3.62E-06	-4.798	<0.0001	All
44	A_{Conf}	1.46E-07	3.53E-08	4.148	<0.0001	UHN/UHO

Table 19. Parameters of the model included in the B factor (NLME model)

Param. No.	Parameter	Parameter Estimate	Standard Error	*t* value	*p* value	Included in
45	B_C	-0.1591	5.33E-04	-298.569	<0.0001	All
	B_{CR}	3.31E-03	9.47E-04	3.497	0.0005	CR
	B_{UHO}	-9.33E-03	8.46E-04	-11.037	<0.0001	UHO
46	$B_{PG70UHO}$	8.37E-03	1.02E-03	8.196	<0.0001	UHO

At this point it is convenient to assess the adequacy of the parameters' sign within the model and to the extent possible, the reasonableness of their magnitude. In some cases, a specific sign is expected for a parameter given the observed behavior in the laboratory or a priori expectations, while in some other cases, further discussion is necessary to determine the specific effects of a given parameter.

5.4.1. Discussion of parameters in ρ

Since ρ represents the maximum possible value of the log(|E*|), then all positive parameters increasing the value of the term ρ increase the values of log(|E*|), and because of the monotonicity of the logarithmic function, of |E*| as well. On the other hand, all negative parameters reduce the value of ρ and therefore the values of log(|E*|) and |E*|. To show this behavior, Figure 22 presents the dynamic modulus master curve corresponding to the characteristics of a specimen (taken as a base case) selected from the sample of specimens in this study together with the master curves that result from a small change with respect to the base case in the value of ρ. As previously mentioned, the master curve predicts the elastic behavior of asphalt mixtures for any combination of temperature and frequency. The final model was utilized to create these curves by keeping all parameters constant except for ρ and making this factor vary around the range of possible predicted values.

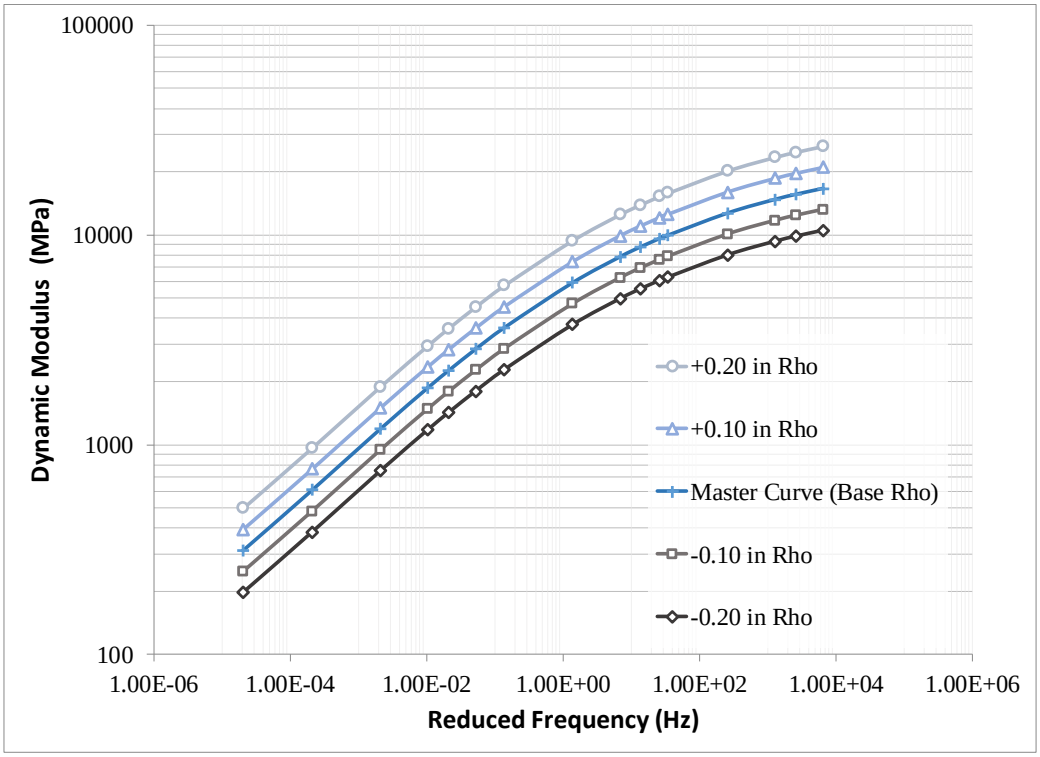

Figure 22. Effect of factor ρ on the behavior of the master curves

Analyzing all parameter estimates from Table 14, the estimate of ρ_C, 4.904, is positive, while the estimate of the bias parameter for the Costa Rican data set ρ_{CR} has a negative value (-0.0790), which means that the maximum values of |E*|, all else being equal, are lower for the CR data set in comparison to the other two data sets (see the discussion for α below for further clarification about this parameter). The estimate of the UHO bias parameter (0.0809) shows the opposite behavior by having a positive value, which means that with all else equal, the |E*| values of specimens in this data set are higher than those from the UHN data set with identical characteristics. The estimate of the parameter associated with air voids, ρ_{AV}, is negative (-0.0229), which means that an increase in air voids reduces the maximum value of |E*|. This is the exact behavior seen in the laboratory, where mixtures with lower air voids percentages have higher values of |E*| for all temperatures and frequencies tested. The estimate of the parameter ρ_{Vb} (-0.0338) related to the effective binder content has a negative sign, which means that an increase in the effective binder content results in a reduction of |E*|, all other things being equal. This behavior is also expected from the point of view of the mixture composition. Higher asphalt contents result in thicker asphalt film thicknesses around the aggregate particles and less stiff mixtures because of the lower stiffness of the binder relative to the aggregate. The estimate of

the strain parameter, $\rho_{Str,}$ is negative (-3.44E-04). This indicates that in general the higher the strains the lower are the values of |E*|. This is a very interesting result since the dynamic modulus test standards require to keep the strains within a certain range, typically between 75 to 125 μstrains for unconfined tests (AASHTO, 2016). This is required to keep the material within its linear viscoelastic range and to obtain repeatable moduli measurements. However, while performing some experiments with dynamic modulus in tension with stress-controlled tests in research currently being conducted at the UH Pavement Laboratory, in which the resulting strains are not always close to the target strains, it was noticed that the |E*| of a sample could vary significantly with variations in the peak-to-peak measured strain. It was also noted, particularly for the UHN data set, that there could be variations with strain even within the relatively narrow test ranges required in the standards. This was the motivation for considering the effect of strain in the model and the results obtained confirm the observation that the strain level can affect the measured modulus significantly, even within the ranges specified by the standards. While performing the testing for this study, it was generally observed that higher measured strains result in lower values of |E*|. Thus, it may be desirable to reduce the peak-to-peak strain range allowed for testing to reduce the variability in measuring |E*|.

Parameters ρ_{Elv} and ρ_{PG76CR} are related to the behavior of two specific type of binders. The estimate of the first parameter, ρ_{Elv}, is negative (-0.0331), which means that the maximum value of |E*| of mixtures prepared with the PG70-XX from the UHO data set (which was modified with Elvaloy®Ret) is reduced relative to the value obtained with the PG64-16 from the UHO study (the asphalt binder selected as base). This is consistent with the results of Archilla (2010), who found similar results with the UHO data set, and indicates that the ElvaloyRet© modified binder may provide some advantages to prevent cracking at low temperatures and high frequencies for thick pavement structures (under those conditions, the strain induced by a given load is not affected much by the relatively low change in the stiffness of the mix but the resistance to cracking can be higher for the lower modulus mixes). In contrast, for mixtures prepared with the PG76-22 binder from Costa Rica the corresponding parameter estimate (ρ_{PG76CR} = 0.0433) is positive, meaning that mixtures prepared with this binder have higher maximum values of |E*| than those prepared with the base asphalt PG70-22 of the CR study (remember the earlier discussion about excluding dummy variables of a base binder for each data set).

The parameter estimates for ρ_{D1C}, ρ_{D3C} and ρ_{D6C} also have intuitively correct signs and values (-0.0108, -0.0199, and -0.0221, respectively). First, it is observed that all three of them have negative signs, meaning that by using F-T cycles, the values of |E*| are reduced. Second, the values become more negative as the F-T cycles increase from 1 to 6, meaning that the |E*| values are progressively reduced with an increased number of F-T cycles. However, the reduction is not proportional to the number of cycles. For example, increasing the F-T cycles from 0 to 1 results in a reduction of ρ of -0.0108, but when the number of cycles increases from 1 to 3 and from 3 to 6 the resulting reductions are of -0.0091 and -0.0022, respectively. Thus, as the number of cycles increases, the reductions in the maximum of log(|E*|) become progressively smaller even when the number of cycles increments are increasingly larger. Note that this effect could also have been accounted for with a function of the number of cycles (e.g., with a quadratic function that has the same number of parameters). Nevertheless, in this study, it was preferred to account for this through dummy variables since this permits the identification of the effects of F-T cycles without making assumptions about the functional form, which can only be speculated with only three levels of F-T cycles.

The next two parameters, ρ_{Lime} and ρ_{MB}, have both positive signs meaning that the inclusion of any of these anti-stripping agents to the mixture increases the |E*| values on samples with no F-T cycles. However, from the values of the parameters, it is concluded that the addition of Lime (0.0260) result in a bigger increase of log(|E*|) than with the addition of Magnabond (0.0112). Also, when considering the use of anti-stripping together with F-T cycles, the net effect with the use of lime is an increase of |E*| irrespective to the number of F-T cycles. On the other hand, with Magnabond, the net effect is still a modulus reduction with 3 and 6 F-T cycles.

The last five parameters discussed from the ρ list (i.e. ρ_{Lime}, ρ_{MB}, ρ_{D1C}, ρ_{D3C} and ρ_{D6C}) are explanatory variables that are exclusive to the CR data set. However, as mentioned before, by including these parameters in the model it is possible to predict the effects on |E*| of a mixture from either the UHN or UHO data sets with the inclusion of these characteristics, if the assumption of similar mix behavior is accepted.

5.4.2 Discussion of parameters in α

Regarding α, it is necessary to remember that its multiplication with α_{cf} of Equation (14) represents the reduction from the maximum to the minimum of the value of log |E*| in Equations (15) or (16). Therefore, α is mostly responsible for the predicted values in the lower part of the

curve. Remember that for very low values of the reduced frequency in Equation (15) for the calculation of log(|E*|) the product $\alpha \cdot \alpha_{cf}$ is subtracted from the factor ρ. Consequently, a higher α results in a lower minimum value of the predicted log(|E*|) and this, in turn, drags the whole curve down (depending on the reduced frequency, the value subtracted from ρ varies from 0 at very high reduced frequencies to $\alpha \cdot \alpha_{cf}$ at very low reduced frequencies). Likewise, a lower α results in a smaller reduction in the values of |E*| and on curves with higher minimum values of |E*|. This is the behavior shown in Figure 23. From this figure, it is evident that the greater impact of α is on the lower part of the curve.

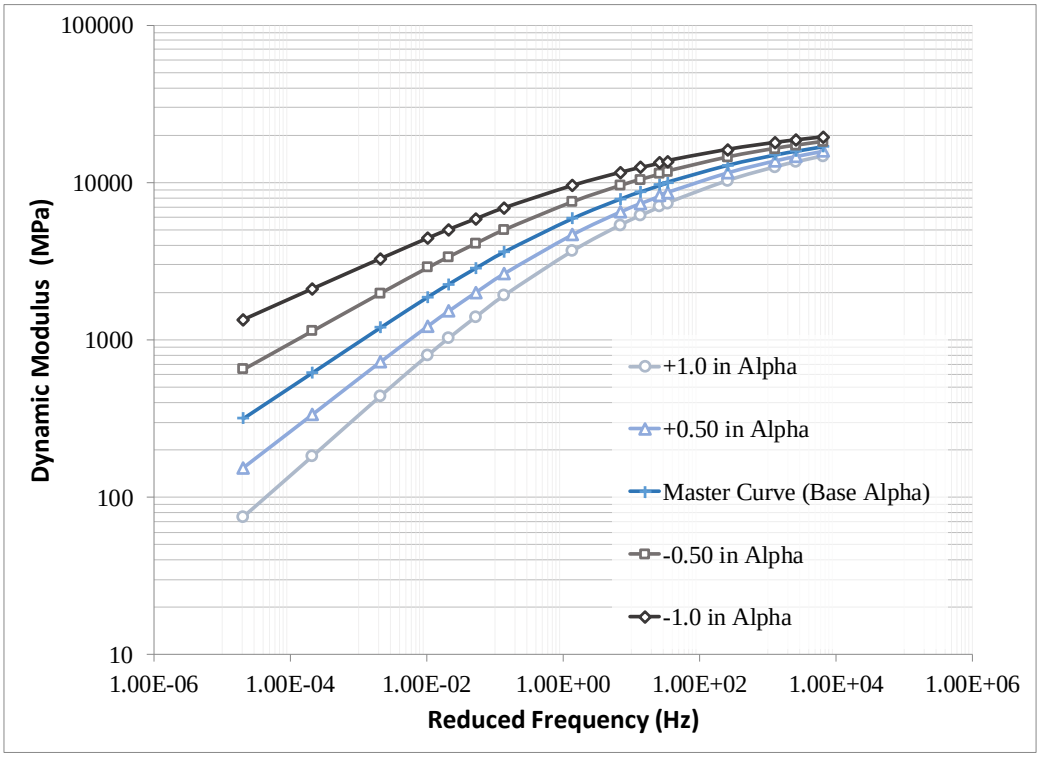

Figure 23. Effect of factor α on the behavior of the master curves

By analyzing each of the parameters related to the prediction of α, it is seen that the constant α_C has a positive value of 1.8521, which is as expected since a positive value needs to be subtracted from ρ to reduce the values of |E*|. As in the case for ρ, the bias parameters for this factor also have opposite signs for the CR and UHO datasets. The bias parameter for CR (-0.7498) is negative, which implies a reduction in the value of α relative to that for UHN and therefore an increase of the minimum value of |E*|, with all else equal. Recall that the estimate of the bias parameter ρ_{CR} was also negative (-0.0790), implying a smaller maximum value of |E*| when all else is equal. Thus, when both results are put together it can be concluded that for the Costa

Rican dataset the difference (max |E*| - min |E*|), all else equal, is smaller than those observed in the UH studies. This is not surprising considering that the base asphalt binder in the Costa Rican study is a PG70-22 as opposed to the PG64-22 used as base in the UHN study. Thus, not all else can be made equal in the two datasets since the two binders differ by a full grade and thus the bias parameter captures in big part the difference between base binders (the "all else equal" must be taken as with all the model inputs equal in this case).

The UHO bias parameter for α (0.3082) is positive. Therefore, the minimum value of |E*| is smaller than that corresponding value for UHN, with all the other input variables equal. Note that in this case the difference (max |E*| - min |E*|) is larger than for UHN, but not as dramatic as the difference for the Costa Rican data set. This is also likely due to differences in the binders. Although the binders in the UHN and UHO studies have the same maximum grade (PG64), the sources were most likely different.

The estimate for α_{AV} (0.2966) is positive. Consequently, higher air voids in the mixture lead to higher estimates of α and therefore to larger estimated reductions in the values of |E*|. This is consistent with the laboratory results in this study and elsewhere, where it is commonly seen that the mixtures with low air voids perform better in dynamic modulus testing than mixtures with high air voids. Recall also that the estimate of parameter ρ_{AV} (-0.0229) also meant that higher air voids reduce the maximum |E*| values. Thus, higher air voids appear to have a compounding effect of lowering the maximum value |E*| and making the reduction from that maximum with reduced frequency also larger.

The α factor contains three statistically significant parameter estimates related to binder type: $\alpha_{PG76UHN}$, α_{Elv} and $\alpha_{PG70UHO}$ with values of -0.7190, -1.4970, and -0.5199, respectively. All three of them have a negative sign. This means that the use of any of these binders makes α smaller and the minimum value of |E*| larger relative to the values for the base binder of the corresponding data set. This is again a very reasonable result since all these binders are modified binders. Both the PG76-22 from the UHN data set and the PG70-22 from the UHO data set were modified with an SBS polymer while the PG70-XX from the UHO data set was modified with Elvaloy®Ret (hence its sub index). Therefore, it is expected that their minimum values are still higher than for the corresponding base binders (PG64-16 for UHO and PG64-22 for UHN). It is interesting however, that the effect of the PG76-22 from Costa Rica was not found to be statistically significant since it was also modified with an SBS polymer. It also interesting that

the estimate for $\alpha_{PG70UHO}$ of -0.5199 is of the same order as the estimate of the bias parameter for Costa Rica, α_{CR}, of -0.7498. In a sense, both parameters capture the differences in α caused by using a PG70-22 instead of the PG64-22 of the UHN study. Considering that α_{CR} may also be capturing other differences such as gradation, compaction method, mixing procedures, density measurements, etc., the differences between the two parameters appear reasonable.

The only statistically significant gradation related parameter in α is α_{R4}, which is the parameter for the percentage of material retained on the No.4 sieve size. The estimated value for this parameter is 0.0166. As discussed earlier, the inclusion of parameters related to gradation is commonly seen in predictive models such as the Witczak prediction models shown in Chapter 2. Thus, the a priori expectation was that the parameters related to several of the gradation variables should be statistically significantly different from zero. However, it is important to realize that despite the large amount of information from the three data sets available for this study, there are basically 5 different gradations (two for UHO, one for UHN, and two for CR) plus a few more from the few field collected mixes. Furthermore, the percent passing a given sieve size is typically highly correlated to the percent passing other sieve sizes. Thus, the combination of little variation of the gradations in each data set with high correlation between the variables representing the gradations makes it difficult to identify several gradation related parameters for the three databases combined and virtually impossible for each database individually. Indeed, initial attempts at identifying parameters for each database using mixed-effects were fruitless because the model was over specified. Attempts were also made to include other gradation parameters common to the three data sets. For example, in attempts with models with three gradation parameters related to the percent retained in the 3/8" sieve size, the percent retained in the No. 4 sieve size, and the percentage passing the No. 200 sieve size (P200), it was found that the parameter for the P200 was not statistically significant and that the parameters corresponding to the other two variables were statistically significant but had almost identical values with opposite signs. An analysis of the variance-covariance matrix of the parameter estimates indicated that these were highly negatively correlated (~ -0.99). Consequently, even though apparently statistically significant results for additional parameters were obtained in some situations, engineering judgment had to be used to eliminate some of these parameters to avoid over specification of the model. When parameters related to the material retained in the 3/8" sieve size or No. 4 sieve size were found significant within one of the major parts of the model

(ρ, α, β, etc.), the one related to the No.4 sieve size was retained while the one related to the 3/8" sieve size was eliminated. The reasoning behind this is that the number No. 4 sieve size is commonly utilized as the separation between the coarse and fine material, and therefore it could be used as an indication of the effects of coarser or finer gradations in the values of |E*| of a mixture. As expected, very little degradation was noted in the predictive ability of the model when the parameters related to the retained in the 3/8" sieve size were eliminated.

The next statistically significant parameter in α is α_{Conf}, which multiplies the confinement utilized during testing of the samples (in kPa). The estimated value of this parameter (-8.17E-04) has an expected negative sign. That is, higher confinement levels make α smaller and the minimum of |E*| larger. However, this parameter captures only a small but statistical significant part of the confinement effect that is proportional to the confinement level. As discussed at the end of chapter 4, a previous study based on the UHN data (Corrales-Azofeifa and Archilla, 2016) noted that there is a complex interaction of the confinement level, air voids, and asphalt type. Specifically, it was noted that for the polymer modified mixes, the benefits of higher confining stresses were observed for all levels of air voids. Although the benefits at the higher air voids were smaller, they were still substantial. On the other hand, for the unmodified mixes, large benefits observed at 4% air voids decreased slightly at 7% and virtually disappeared at 9%. As the air voids level was increased, not only the dynamic modulus decreased but so did the effect of confinement level. Consistent with the findings from other studies, it was also found that increasing the confining level increased the dynamic modulus. However, it did so at a decreasing rate. Based on the above observations, it is clear that a single linear term in confinement cannot capture the effects observed in that study. For this reason, the second multiplicative factor (α_{cf}) was added to the model to capture these effects more closely.

Finally, the last statistically significant parameter in α is α_{Fib}, which is related to the use of fibers in the mixture. The value of this parameter is 0.1291. It was noted in the laboratory that the addition of synthetic polyolefin/aramid fibers resulted in a consistent reduction of the |E*| values for all conditions tested. The reduction was observed regardless of the binder used to prepare the mix. This is consistent with the sign of this last parameter which increases the value of α, creating a reduction in the values of |E*|.

The second multiplicative part of α is termed α_{cf}. This factor was shown in Equation (14) and a brief explanation of its rationale was provided therein. However, a plot of the variation of α_{cf} with confinement level (Figure 24) is used to illustrate its role in accounting for confinement.

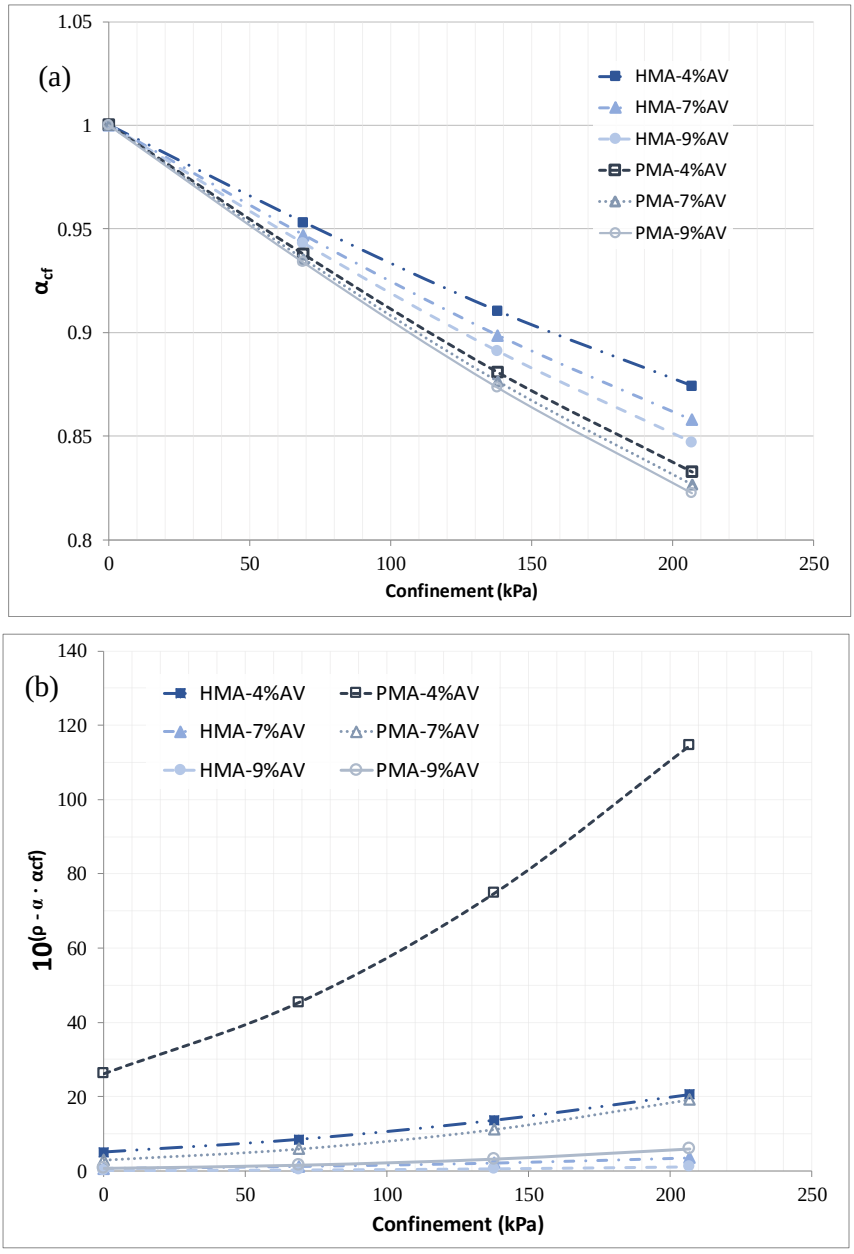

Figure 24. Effect of α_{cf} with varying confinement level

(a)Effect of a_{cf} alone (b) Effect of a_{cf} on minimum value of $|E^*|(10^{(\rho-\alpha\cdot\alpha cf)})$

Notice that figure (24a) shows realizations of the curve shown in Figure 13 based on the estimated parameters and different binder types and air voids levels. Clearly, an increase of the confinement level reduces α_{cf} and thus the term $\alpha_{cf}\cdot\alpha$, which implies a smaller maximum drop of

|E*| with reduced frequency for higher confinement levels. With no confinement, α_{cf} takes a maximum value of 1 (i.e., in this situation, α_{cf} has no effect on the overall values of |E*|) and decreases non-linearly with confining stress.

The more general effects of other parameters in the α_{cf} factor are not as obvious and therefore it is necessary to remember that from Equation (14), when β_{conf} =0 (as assumed in this study to avoid over specification of the model), the equation can be rewritten as

$$\alpha_{cf} = \left(1 + \frac{\alpha_{conf}}{2}\right) - \frac{\alpha_{conf}}{1 + e^{\left(\gamma_{conf}\,\sigma_3\right)}} = 1 - \alpha_{conf}\left(\frac{1}{1 + e^{\left(\gamma_{conf}\,\sigma_3\right)}} - \frac{1}{2}\right) \quad (24)$$

It is easy to see that for any given confinement level utilized, the term in parenthesis on the right side of the equal sign in Equation (24) is greater than zero since the denominator that includes σ_3 is smaller than 2, e.g. for σ_3=138kPa (20psi) the term $1 + e^{\left(\gamma_{conf}\,\sigma_3\right)}$= 1.42. Thus, larger positive values of α_{conf} result in smaller α_{cf} values and, therefore, larger minimum values of |E*|.

Based on this analysis, it is now easier to explain the reasonableness of the results of the parameters in α_{cf} in Table 15. The first and easier parameter to explain is $\alpha_{cf\_}\gamma$, whose estimate is as expected negative (-6.22E-03). Thus, the model does indeed predict a decrease of α_{cf} and an increase of |E*| with increasing confinement levels.

The estimate of parameter $\alpha_{cf\_}\alpha$ is positive (0.3670), which as expected, indicates that α_{cf} is smaller than 1 for any confinement level above zero (with smaller values as σ_3 increases). The parameter $\alpha_{cf\_}\alpha_{PG76}$ affects both the PG76-22 and the Elvaloy®Ret modified asphalts from the UHN and UHO data sets, respectively. Its parameter estimate (0.1934) is again positive, which results in even larger values of α_{conf}, and thus in even smaller values of α_{cf} and correspondingly larger values of |E*| with all else equal. This is consistent with the observations of the previous study (Corrales-Azofeifa and Archilla, 2016), where larger benefits of confinement were observed for the mixes with modified binders.

In the case of the parameters related to air voids, $\alpha_{cf\_}\alpha_{AV}$ and $\alpha_{cf\_}\alpha_{AV\_PG76}$, the estimate of the first one is positive (0.0192) and the estimate of the second is negative (-0.0119) (Note also, that their sum, which determines the effect for modified binders, is positive). In the first case, an increment in the air voids content will create a smaller value of α_{cf} and therefore a larger value of |E*|. It may be tempting to conclude that this is not reasonable behavior since it is typically

observed that higher air voids lead to lower |E*|, but it must be remembered that α_{cf} is intended to capture the complex interaction of air voids, asphalt type, and confinement (not just air voids) and that ρ and α also contain terms related to air voids. What the above results are indicating is that the variation of α_{cf} with confinement is smaller for mixes with higher air voids regardless of the type of binder as indicated by the positive parameters for both unmodified and modified mixes ($\alpha_{cf\_}\alpha_{AV} > 0$ and $\alpha_{cf\_}\alpha_{AV} - \alpha_{cf\_}\alpha_{AV\_PG76} > 0$, respectively) but that mixes with modified binders are less sensitive to air voids (less variation with confinement level) than the mixes with unmodified binders since $\alpha_{cf\_}\alpha_{AV} >> \alpha_{cf\_}\alpha_{AV} - \alpha_{cf\_}\alpha_{AV\_PG76}$, which is exactly the behavior illustrated in Figure (24a) where the curves for modified binders for varying air voids are closer than the ones for unmodified binders. The effect depicted in figure (24b) is one that was also noted in the previous study (Corrales-Azofeifa and Archilla, 2016), where the minimum values of |E*| depend highly on the confinement level, with higher values of |E*| as the confinement level increases. Also, the combined effect of ρ and $\alpha \cdot \alpha_{cf}$ define higher values of the minimum |E*| for modified binders and smaller differences on the |E*| values as the air voids increase.
The last parameter included in the α_{cf} factor is the $\alpha_{cf\_}\alpha_{Fib}$. The negative sign of this parameter estimate (-0.0233) indicates that when using fibers the minimum value of |E*| is reduced in confined tests. This is the same effect discussed before for the α_{Fib}, which in this case means that the use of fibers reduces the values of |E*| even more relative to a mix without fibers when confinement is used, offsetting in part some of the benefits of confinement.

5.4.3 Discussion of parameters in β and γ

The beta and gamma parameters are more difficult to interpret since they define mostly the shape of the curve. Also, both parameters are within the exponent of *e* in the denominator of Equation (16), which makes their effect less obvious. However, by making plots of their variation along their range of possible values, it is possible to illustrate their effect on |E*|. Figure 25 and Figure 26 show the effect of the variation of both parameters on the master curves.
From Figure 25, it is seen that smaller values of the factor β shift the curve to the left (remember that ρ determines the maximum of |E*| and that $\rho - \alpha$ determines the minimum of |E*| and that these are unaffected by a change in β). In effect, this means that smaller values of β increase the values of |E*| across all frequencies. However, the increment is not uniform as it varies from zero at reduced frequencies approaching zero, it reaches a maximum at some intermediate reduced

frequency, and it returns to zero as the reduced frequency tends to infinity (this is not obvious from Figure 25 since only a practical range of reduced frequencies are shown). Conversely, higher values of β result in smaller values of |E*| (again, the reduction is not uniform with reduced frequency).

The estimate of parameter β_C (Table 16) is -1.2153, which does not have a particular interpretation. Based on the previous analysis, for a given reduced frequency, a positive parameter estimate (other than the estimate of the constant) results in a lower estimated value of |E*| (relative to the value estimated with only β_C) whereas a negative parameter estimate results in a larger prediction of |E*|.

The estimates of the bias parameters for the factor β are β_{CR} = 0.4121 and β_{UHO} = 2.47E-04. Their magnitudes differ significantly, which is not entirely surprising since the base binder in the UHO and UHN studies have the same high temperature grade (PG64) (the low temperature grade has little relevance for Hawaii's climate); hence the low value of the bias parameter for UHO, which indicates that the difference in β for specimens of equal characteristics in the UHN and UHO data sets is very small and not statistically significantly different from zero as evidenced by its very large p-value = 0.9904 (a discussion for the other non-statistically significant parameter γ_{CR} will follow shortly). The fact that most bias parameters are statistically significant means that in general all three data sets have statistically significant differences in the shape of the master curves. The reason why these parameters were not deleted from the table was to be able to show which of the bias parameters were significant. On the other hand, as discussed before for ρ and α, the larger and statistically significantly different from zero value of β_{CR} may be capturing the fact that a PG70-22 is the base binder in the CR data set. This estimate implies that the predicted values of |E*| are lower for a specimen in the CR data set than the predicted values for a specimen with all else equal in the UHN data set. This discussion illustrates the difficulty in assessing the reasonableness of the parameter estimates in a non-linear model. So far, the bias parameters for the CR data set tend to decrease ρ, increase α, and increase β. The final effect (which also depends on the bias parameters for A and B), is the result of all these changes simultaneously.

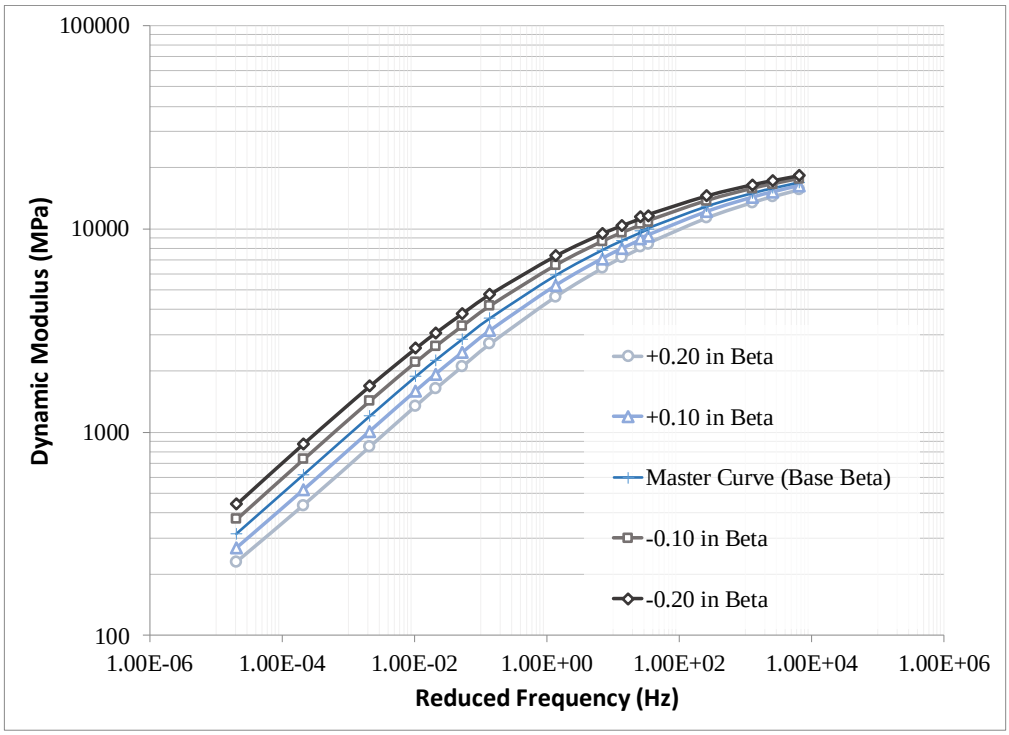

Figure 25. Effect of factor β on the behavior of the master curves

Continuing with the analysis of the parameters affecting β, once again, three parameters related to the same three binders analyzed before are statistically significantly different from zero. All three parameters, $\beta_{PG76UHN}$, β_{Elv} and $\beta_{PG70UHO}$, have positive signs which means that using any of these binders will reduce the values of |E*| non-uniformly over the practical range of reduced frequencies. Again, it is important to remember that when any of these binders are utilized then most of the other terms of the sigmoidal function (ρ, α, γ, A, and B) will move at the same time, thus changing the overall shape and level of the sigmoidal function. A decrease in β is more related to how the curve makes a transition from the maximum to the minimum value, thus compensating at intermediate reduced frequencies some of the changes at the maximum and minimum values. This is also the case for the parameter estimates of β_{Conf} = 9.99E-04, $\beta_{Conf\_PG76UHN}$ = 1.87E-04, which are both related to the confinement level and are both positive. In contrast, the estimates of β_{D6C} = -0.0556 and β_{AV} = -0.0589 are both negative. Thus, it is apparent that changes that tend to make a mixture stiffer at intermediate reduced frequencies (such as using modified binders and applying confinement with and without modified binders) tend to increase β whereas changes that tend to make a mixture less stiff at intermediate reduced frequencies (such as the application of many F-T cycles and high air voids) have the opposite

effect and tend to decrease it. It is important to emphasize that the resulting effects on |E*| need be analyzed together with the effects of the same variable in the other parameters. The different effects work together to change the shape and level of the master curve.

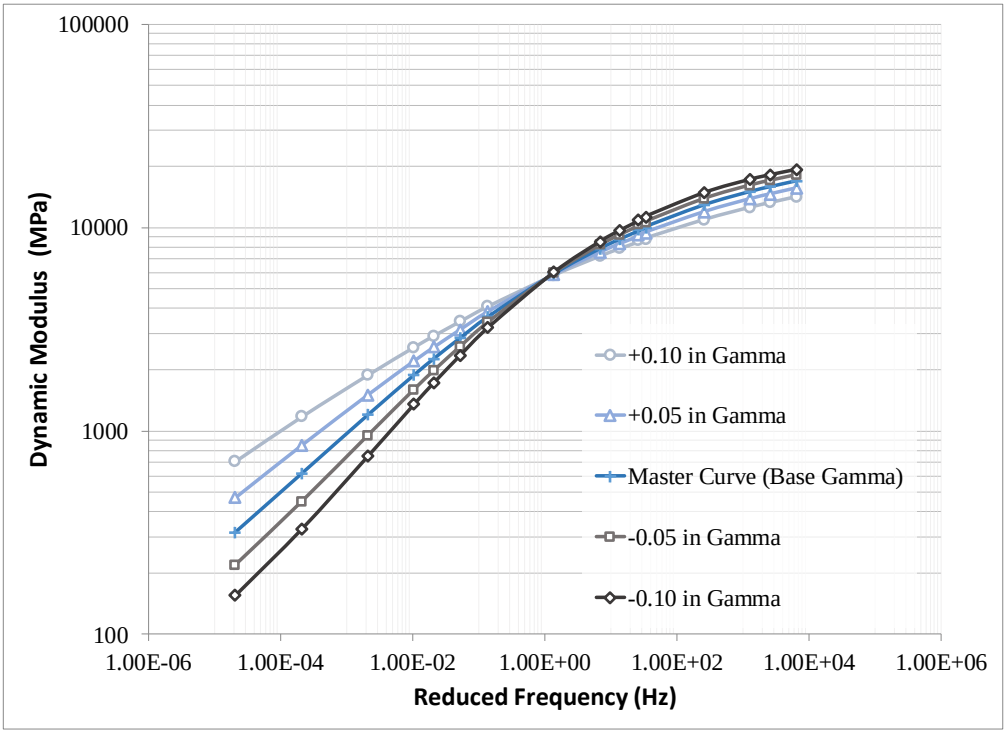

Figure 26. Effect of factor γ on the behavior of the master curves

The effect of γ is as complex as that of β. As seen in Figure 26, a positive change in the value of γ with all the other terms fixed (ρ, α, β, A, and B) makes the values of |E*| decrease for high reduced frequencies and increase for low reduced frequencies. Of course, the opposite happens for a decrease in γ. Consequently, as seen in the figure, γ affects the maximum slope of the master curve at intermediate temperatures. The estimate of the constant $\gamma_C = 0.4143$ is positive, which as in the case of β_C, does not have an interpretation other than together with other parameters it helps defining the shape of the curve. The estimates of the bias parameters for γ, $\gamma_{CR} = 0.0107$ and $\gamma_{UHO} = -0.0379$, have opposite signs. In this case, the magnitudes of the bias parameters are of the same order which means that both parameters recognize a difference from the base case (PG64-22 from UHN). While the bias parameter for CR increases the value of γ, the one for UHO decreases it. This is considered quite reasonable since it means that a master curve for a mix with the base binder from CR (PG70-22) has a lower maximum slope than one

prepared with the base binder from UHN (a PG64-22) (assuming that a big component of the bias factor in this case is related to the differences in binders. Of course, other factors may be playing a role as well.) In other words, it is reasonable to expect a smaller slope for binders with higher grades that are typically less temperature/frequency susceptible (and hence less reduced frequency susceptible). However, γ_{CR} is the second bias parameter that was eliminated from the model since in this case it was not statistically significantly different from zero at 10% significance level (p-value =0.1126). On the other hand, a mix with the UHO PG64-16 has a larger slope than a mix with the PG64-22 in the UHN study. In this case, the high temperature grade between the two binders is the same. Although the low temperature grade is not quite relevant for Hawaii's environmental conditions, in general, a higher low temperature grade is indicative of a lower quality, more temperature susceptible binder (higher maximum slope). Therefore, the above result (smaller γ and higher slope of the curve for UHO than for UHN) once again coincides with a priori expectations.

One parameter related to gradation is statistically significant in γ, γ_{P200}, which is related to the percentage of material passing the No. 200 sieve size. Its estimate, 0.0110, is positive which implies that higher P200 values (within the range of values in this study) result in lower maximum slopes. This appears to capture the asphalt mastic stiffening effect that results from higher P200 values.

The only parameter related to binder type in γ, γ_{PG76CR}, appears with a negative sign (its estimate is -0.0330). This would indicate a higher maximum slope in comparison to the base binder PG64-22 and also that the modified binder of the CR data set has the opposite effect than its base binder (PG70-22). It is interesting to see also that only the modified binder from Costa Rica appears in γ while only the modified binders from UHO and UHN appear in β. Apparently, their effects can only be captured in one or the other term.

The estimates of the three parameters related to freeze-thaw cycles, $\gamma_{D1C} = 0.0293$, $\gamma_{D3C} = 0.0298$, $\gamma_{D6C} = 0.0458$, are all positive, indicating that F-T cycles reduce the maximum slope of the master curves or, in other words, flatten the master curves. Recall that statistically significant effects of F-T cycles were also found in ρ and that they tended to lower the whole master curve. Thus, with lower maximum values of |E*| one would expect the curves to be flatter as well. Finally, it is seen that the estimates increase monotonically with the number of cycles though the increments are much larger from 0 to 1 cycles (0.0293) and from 3 to 6 cycles (0.0160) than

from 1 to 3 cycles (0.0005), which implies a substantially nonlinear effect in which the first cycle has a substantial effect in flattening the curve, the following 2 cycles have little effect, and then the effects increase once again with more cycles. However, a more complete study with more F-T cycle levels would be needed to verify if this is the case. The important point is that the parameter estimation results in this study appear to be reasonable.

The last two statistically significant parameters in γ are γ_{AV}, which is related to air voids and γ_{Fib}, related to the use of fibers in the mixture. Both estimates are negative, γ_{AV} = -7.29E-03 and γ_{Fib} = -0.0112, which implies steeper master curves or curves with a more sudden drop with reduced frequency. This again appears intuitively correct in both cases. In the first case (for γ_{AV}) at low temperatures/high frequencies, the binder is quite stiff and collaborates significantly with the aggregate structure to determine the stiffness of the mix (though with higher air voids, the stiffness is still reduced as seen in the discussion of ρ). On the other hand, at high temperatures and low frequencies, the stiffness of the mix approaches that of aggregate. Air voids affect what happens under the above conditions and those effects were already discussed in ρ, α, and β. Now, with higher air voids, the aggregate structure can become more unstable under loading when the temperature is risen and one would expect that with lower aggregate interlock the drop in the stiffness can be more sudden, which is consistent with the negative sign of the parameter estimate. In the case of γ_{Fib}, the negative sign means that the addition of fibers also creates a more sudden transition from the high to lower frequencies, which is also consistent with the effect of fibers observed in the α factor according to which the addition of fibers lowers the minimum values of |E*|. Therefore, the transition needs to have a higher maximum slope

5.4.4 Discussion of parameters in A and B

To conclude the analysis of the model parameters, Figure 27 and Figure 28 are included to show the effect of the variation in A and B on the logarithm of the shift factor. Both plots show similar behavior.

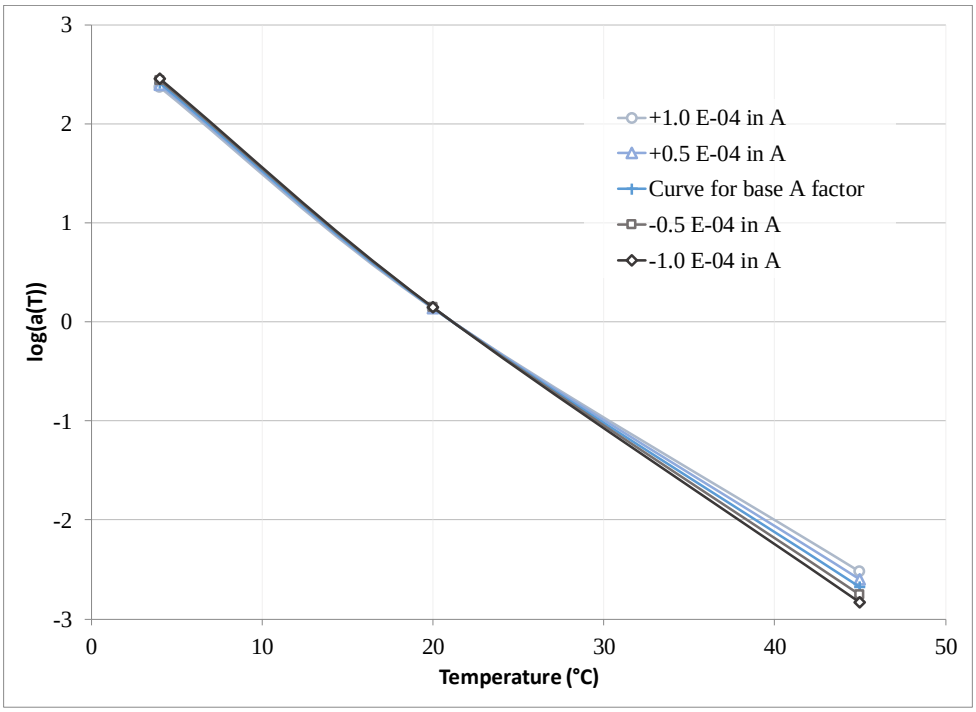

Figure 27. Effect of factor A on the log of the shift factor a(T).

In general, parameters that increase the value of A (which is the parameter affecting the square of temperature in the log(*a*(T) equation) result in less shifting, while parameters that decrease the value of A result in larger changes in the log of the shift factors, thus expanding the range of reduced frequencies in both directions for a given experiment.

As shown in Figure 28, parameter B, which is the parameter of the linear term in the log(*a*(T)) equation, has the opposite effect (i.e., larger B values lead to more shifting and vice-versa.)

As with other terms, the estimates of the constants (A_C = 9.03E-04 and B_C = -0.1591) do not have a direct interpretation other than that they yield reasonable values when they are modified with other terms such as bias factors and terms accounting for air voids and confinement. However, it is important to note that the estimate of B_C, which may be modified only by bias factors or the dummy for the PG70-22 binder from UHO, compares quite well with typical values of this parameter.

Both estimates of the bias parameters for the CR data set (A_{CR} = -4.54E-05 and B_{CR} = 3.31E-03), indicate that the master curves of the CR data set require more shifting with respect to the UHN curves, while the opposite is true for the master curves of UHO (A_{UHO} = 7.82E-05 and B_{UHO} = -9.33E-03).

Air voids and confinement also appear to have a statistically significant effect on the shift factor through the A term but in opposite directions. Their parameter estimates are A_{Vb} = -1.74E-05 and A_{Conf} = 1.46E-07. Thus, higher air voids appear to lead to more shifting while higher confinement appear to result in less shifting.

Finally, an effect of the PG70-22 binder in the UHO data set was detected in B. The parameter estimate is $B_{PG70UHO}$ = 8.37E-03, which indicates that mixes prepared with this binder require (all other things equal) slightly less shifting.

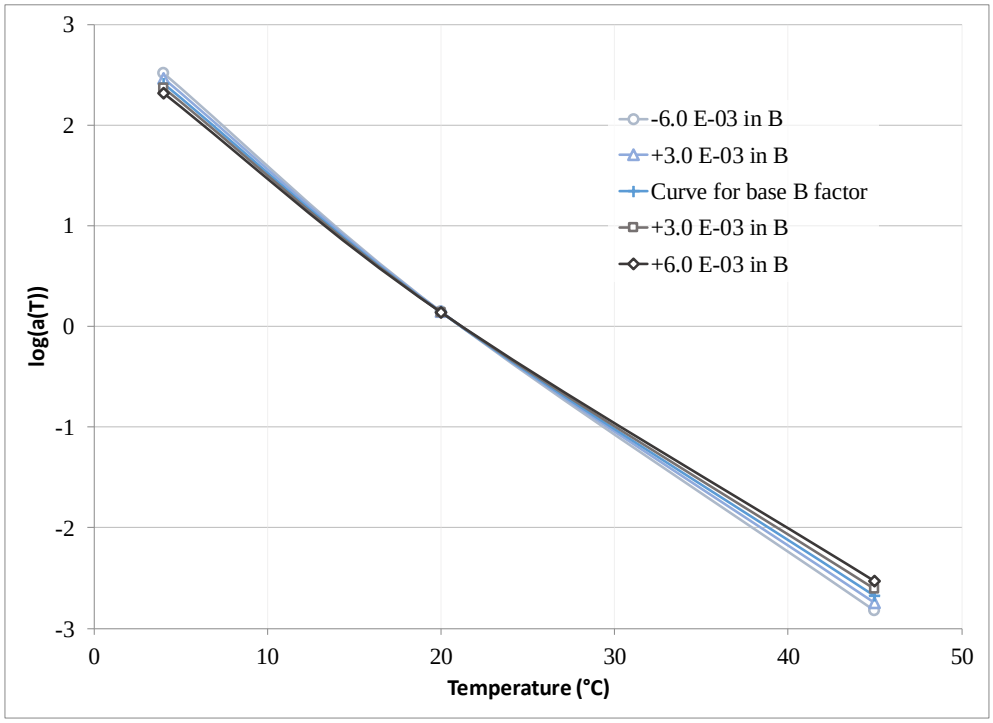

Figure 28. Effect of factor B on the log of the shift factor a(T).

5.4.5 Final statistical assessment of the model

The model discussed in the previous sections was modified slightly by excluding β_{UHO} and γ_{CR} since these are not statistically significant. Remember that this final model has the same structure as the NLS fitted model since it was developed using precisely the final model specification estimated with the NLS routine while using the joint estimation approach to pool the information from the different data sets and the mixed-effects approach to account for unobserved heterogeneity. The same explanation that was given to understand the NLS fitted model also applies in this case. All sub-indices are identical for all parameters and the dummy variables (D_i) were used to include both bias parameters and explanatory variables that are unique for one of the data sets (i.e. UHN, CR, UHO).

$$\log|E^*| = \rho - \frac{\alpha\ \alpha_{cf}}{1+e^{-\left(\beta+\gamma\left(log\left(\frac{1}{f}\right)-(A\,T^2+B\,T-(A\,(21.1)^2+B\,(21.1))\right)\right)}}$$ where, (16 Revisited)

$$\rho = \left[\left(\rho_C + \rho_{CR}\,D_{CR} + \rho_{UHO}\,D_{UHO} + \rho_{Vb}\,V_{beff} + \rho_{AV}\,AV + \rho_{Str}\,\mu s + \rho_{Elv}\,D_{Elv} + \rho_{PG76CR}\,D_{PG76CR}\right)(1 + \rho_{Lime}\,D_{Lime} + \rho_{MB}\,D_{MB})\,(1 + \rho_{D1C}\,D_{D1C} + \rho_{D3C}\,D_{D3C} + \rho_{D6C}\,D_{D6C})\right] \quad (25)$$

$$\alpha_{cf} = \left[\left(1 + \frac{\alpha_{cf\_}\alpha + \alpha_{cf\_}\alpha_{PG76}(D_{PG76UHN}+D_{Elv}) + \alpha_{cf\_}\alpha_{Fib}D_{Fib} + \left(\alpha_{cf\_}\alpha_{AV} + \alpha_{cf\_}\alpha_{AV_{PG76}}(D_{PG76UHN}+D_{Elv})\right)AV}{1+e^{0}}\right) - \frac{\alpha_{cf\_}\alpha + \alpha_{cf\_}\alpha_{PG76}(D_{PG76UHN}+D_{Elv}) + \alpha_{cf\_}\alpha_{Fib}D_{Fib} + \left(\alpha_{cf\_}\alpha_{AV} + \alpha_{cf\_}\alpha_{AV_{PG76}}(D_{PG76UHN}+D_{Elv})\right)AV}{1+e^{\alpha_{cf\_}\gamma*\sigma_3}}\right] \quad (26)$$

$$\alpha = \left(\alpha_C + \alpha_{CR}\,D_{CR} + \alpha_{UHO}\,D_{UHO} + \alpha_{AV}\,AV + \alpha_{PG76UHN}\,D_{PG76UHN} + \alpha_{Elv}\,D_{Elv} + \alpha_{PG70UHO}\,D_{PG70UHO} + \alpha_{R4}\,Ret_4 + \alpha_{Conf}\,\sigma_3 + \alpha_{Fib}\,D_{Fib}\right) \quad (27)$$

$$\beta = \left(\beta_C + \beta_{CR}\,D_{CR} + \beta_{AV}\,AV + \beta_{PG76UHN}\,D_{PG76UHN} + \beta_{Elv}\,D_{Elv} + \beta_{PG70UHO}\,D_{PG70UHO} + \beta_{Conf}\,\sigma_3 + \beta_{Conf_{PG76UHN}}\,\sigma_3\,D_{PG76UHN}\right)(1 + \beta_{D6C}\,D_{D6C}) \quad (28)$$

$$\gamma = (\gamma_C + \gamma_{UHO}\,D_{UHO} + \gamma_{P200}\,P200 + \gamma_{AV}\,AV + \gamma_{PG76CR}\,D_{PG76CR} + \gamma_{Fib}\,D_{Fib})\,(1 + \gamma_{D1C}\,D_{D1C} + \gamma_{D3C}\,D_{D3C} + \gamma_{D6C}\,D_{D6C}) \quad (29)$$

$$A = \left(A_C + A_{CR}\,D_{CR} + A_{UHO}\,D_{UHO} + A_{Vb}\,V_{beff} + A_{Conf}\,\sigma_3\right) \quad (30)$$

$$B = (B_C + B_{CR}\,D_{CR} + B_{UHO}\,D_{UHO} + B_{PG70UHO}\,D_{PG70UHO}) \quad (31)$$

The exclusion of parameters β_{UHO} and γ_{CR} from the model produced negligible changes in the values of the other parameter estimates. Analysis of variance performed between the model shown in the previous section and the one without these two parameters gives a p-value=0.8833 which in this case means that the models are not statistically significantly different and thus the exclusion of those bias parameters did not have any major effect in the model (more correctly, the hypothesis that both parameters are jointly equal to zero cannot be rejected). Furthermore, there are no changes in the significance of the other parameters. Table 20 through Table 25 show the final parameter estimates after excluding these two non-statistically significant parameters. These are the final parameter estimates that should be use to perform estimations with the model.

Table 20. Parameters of the model included in the ρ factor (NLME final)

Param. No.	Parameter	Parameter Estimate	Standard Error	*t* value	*p* value	Included in
1	ρ_C	4.9058	0.0387	126.911	<0.0001	All
	ρ_{CR}	-0.0691	9.27E-03	-7.460	<0.0001	CR
	ρ_{UHO}	0.0814	8.02E-03	10.146	<0.0001	UHO
2	ρ_{Vb}	-0.0339	3.10E-03	-10.938	<0.0001	All
3	ρ_{AV}	-0.0230	1.51E-03	-15.191	<0.0001	All
4	ρ_{Str}	-3.55E-04	4.96E-05	-7.143	<0.0001	All
5	ρ_{Elv}	-0.0331	8.39E-03	-3.951	<0.0001	UHO
6	ρ_{PG76CR}	0.0426	6.81E-03	6.248	<0.0001	CR
7	ρ_{Lime}	0.0259	1.55E-03	16.708	<0.0001	CR
8	ρ_{MB}	0.0112	1.61E-03	6.956	<0.0001	CR
9	ρ_{D1C}	-0.0117	2.07E-03	-5.681	<0.0001	CR
10	ρ_{D3C}	-0.0208	2.07E-03	-10.034	<0.0001	CR
11	ρ_{D6C}	-0.0228	2.27E-03	-10.043	<0.0001	CR

Table 21. Parameters of the model included in the α factor (NLME final)

Param. No.	Parameter	Parameter Estimate	Standard Error	*t* value	*p* value	Included in
12	α_{cf}_α	0.3643	0.0919	3.964	<0.0001	UHN/UHO
13	$\alpha_{cf}\_\alpha_{PG76}$	0.1925	0.0389	4.945	<0.0001	UHN/UHO
14	$\alpha_{cf}\_\alpha_{AV}$	0.0192	4.46E-03	4.309	<0.0001	UHN/UHO
15	$\alpha_{cf}\_\alpha_{AV\_PG76}$	-0.0119	3.23E-03	-3.679	0.0002	UHN/UHO
16	$\alpha_{cf}\_\alpha_{Fib}$	-0.0232	6.85E-03	-3.387	0.0007	UHN
17	α_{cf}_γ	-6.24E-03	3.95E-04	-15.803	<0.0001	UHN/UHO
18	α_C	1.8413	0.1567	11.749	<0.0001	All
	α_{CR}	-0.6594	0.0977	-6.751	<0.0001	CR
	α_{UHO}	0.3089	0.0820	3.769	0.0002	UHO

Table 21 (cont'd). Parameters of the model included in the α factor (NLME final)

Param. No.	Parameter	Parameter Estimate	Standard Error	*t* value	*p* value	Included in
19	α_{AV}	0.2934	0.0164	17.870	<0.0001	All
20	$\alpha_{PG76UHN}$	-0.7133	0.0860	-8.291	<0.0001	UHN
21	α_{Elv}	-1.4846	0.0784	-18.946	<0.0001	UHO
22	$\alpha_{PG70UHO}$	-0.5114	0.1178	-4.342	<0.0001	UHO
23	α_{R4}	0.0167	2.54E-03	6.591	<0.0001	All
24	α_{Conf}	-8.29E-04	3.66E-04	-2.266	0.0235	UHN/UHO
25	α_{Fib}	0.1298	0.0773	1.680	0.0931	UHN

Table 22. Parameters of the model included in the β factor (NLME final)

Param. No.	Parameter	Parameter Estimate	Standard Error	*t* value	*p* value	Included in
26	β_{C} β_{CR}	-1.2145 0.3931	0.0186 0.0179	-65.282 21.965	<0.0001 <0.0001	All CR
27	$\beta_{PG76UHN}$	0.1764	0.0116	15.231	<0.0001	UHN
28	β_{Elv}	0.4459	0.0137	32.615	<0.0001	UHO
29	$\beta_{PG70UHO}$	0.3547	0.0271	13.086	<0.0001	UHO
30	β_{D6C}	-0.0554	0.0127	-4.367	<0.0001	CR
31	β_{Conf}	1.00E-03	6.61E-05	15.166	<0.0001	UHN/UHO
32	$\beta_{Conf\_PG76UHN}$	1.86E-04	5.69E-05	3.268	0.0011	UHN
33	β_{AV}	-0.0583	2.92E-03	-19.972	<0.0001	All

Table 23. Parameters of the model included in the γ factor (NLME final)

Param. No.	Parameter	Parameter Estimate	Standard Error	*t* value	*p* value	Included in
34	γ_{C} γ_{UHO}	0.4177 -0.0386	0.0162 4.82E-03	25.844 -8.013	<0.0001 <0.0001	All UHO
35	γ_{P200}	0.0107	2.71E-03	3.943	<0.0001	All
36	γ_{PG76CR}	-0.0316	3.55E-03	-8.887	<0.0001	CR
37	γ_{D1C}	0.0381	0.0116	3.281	0.0010	CR
38	γ_{D3C}	0.0386	0.0118	3.263	0.0011	CR
39	γ_{D6C}	0.0544	0.0125	4.340	<0.0001	CR
40	γ_{AV}	-7.09E-03	6.62E-04	-10.711	<0.0001	All
41	γ_{Fib}	-0.0118	2.17E-03	-5.458	<0.0001	UHN

Table 24. Parameters of the model included in the A factor (NLME final)

Param. No.	Parameter	Parameter Estimate	Standard Error	*t* value	*p* value	Included in
42	A_C	9.06E-04	4.00E-05	22.657	<0.0001	All
	A_{CR}	-4.62E-05	1.80E-05	-2.563	0.0104	CR
	A_{UHO}	7.60E-05	1.51E-05	5.039	<0.0001	UHO
43	A_{Vb}	-1.76E-05	3.62E-06	-4.858	<0.0001	All
44	A_{Conf}	1.44E-07	3.47E-08	4.137	<0.0001	UHN/UHO

Table 25. Parameters of the model included in the B factor (NLME final)

Param. No.	Parameter	Parameter Estimate	Standard Error	*t* value	*p* value	Included in
45	B_C	-0.1591	5.32E-04	-299.122	<0.0001	All
	B_{CR}	3.03E-03	9.30E-04	3.259	0.0011	CR
	B_{UHO}	-9.32E-03	8.26E-04	-11.281	<0.0001	UHO
46	$B_{PG70UHO}$	8.38E-03	1.02E-03	8.193	<0.0001	UHO

To illustrate the overall adequacy of the model with the final parameter estimates shown in the previous tables, the following analysis is performed.

When using the NLME routine, it is possible to show the results for all levels of nesting utilized in the model. In this case, a default level of 1 will show the within-group fitted values, i.e. with the inclusion of random effects, while a level of 0 will show the population fitted values, i.e. taking into account only the fixed effects.

To illustrate the differences between models with and without random effects, both plots for levels 0 and 1 are shown below. Figure 29 and Figure 30 show the |E*| values in a regular scale, while Figure 31 and Figure 32 show the plots in logarithmic scale.

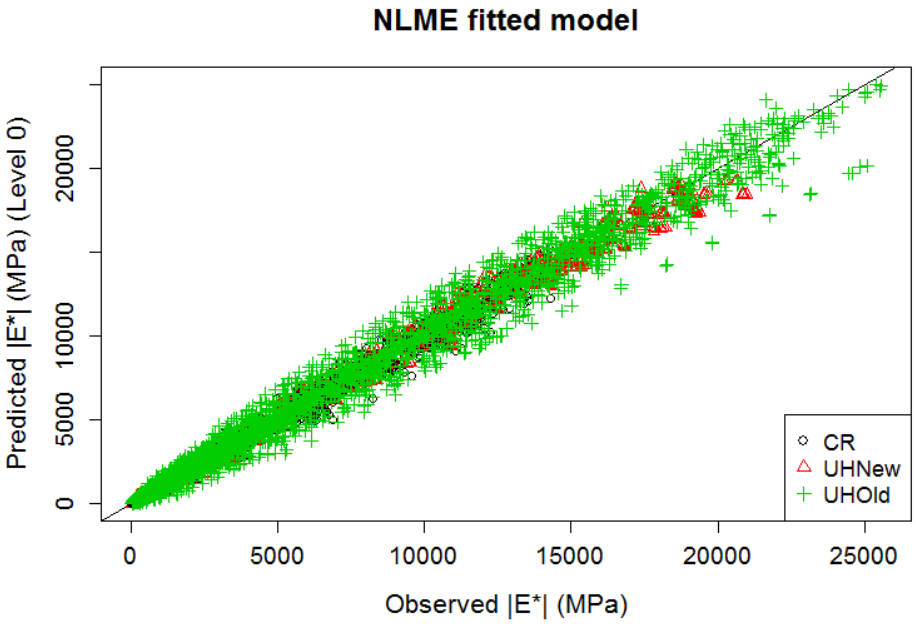

Figure 29. Observed versus predicted values of |E| for the NLME model (level 0)*

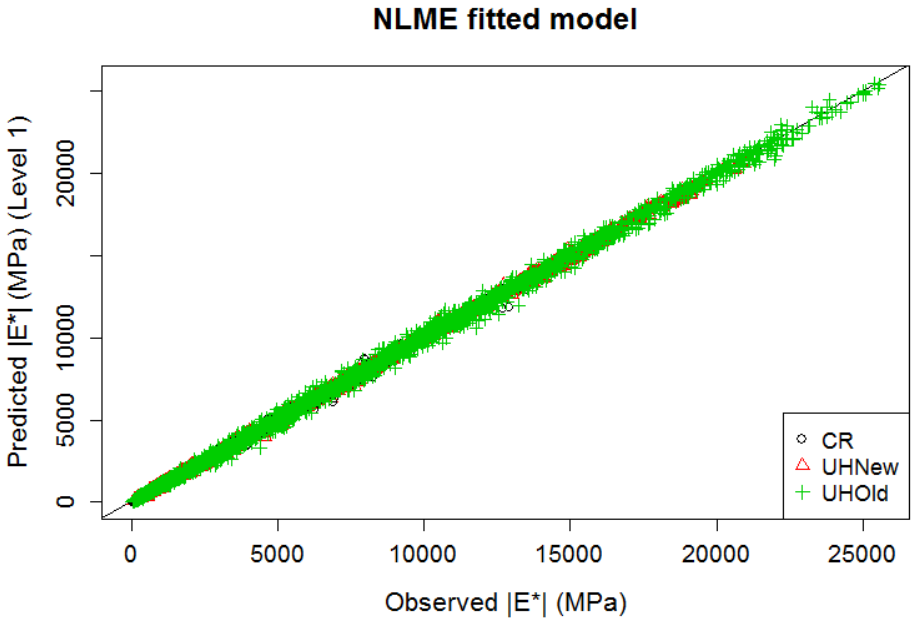

Figure 30. Observed versus predicted values of |E| for the NLME model (level 1)*

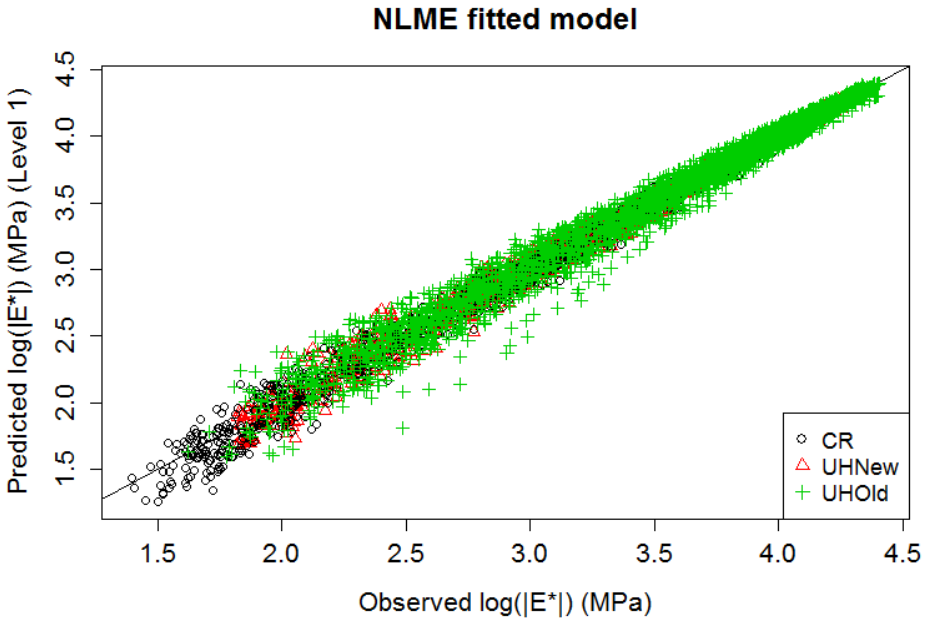

Figure 31. Observed versus predicted values of log|E| for the NLME model (level 0)*

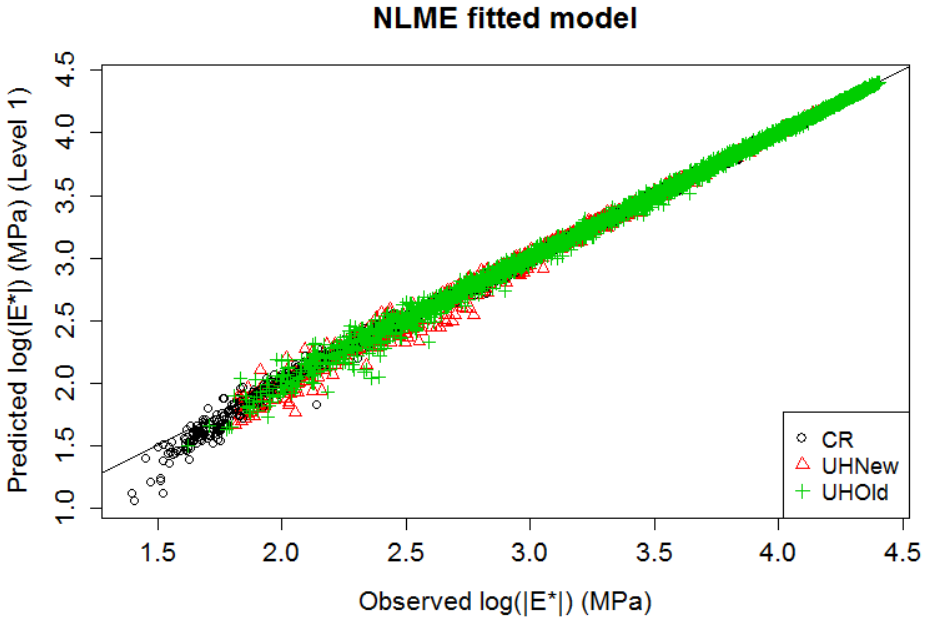

Figure 32. Observed versus predicted values of log|E| for the NLME model (level 1)*

From these plots, it is seen that the model that includes mixed-effects explains the data much better than the model with only fixed effects. This is to be expected since the predictions with the random effects from the mixed-effects approach essentially correspond to a model with two more parameters that are specific for each specimen (one for ρ and one for α, in this study). However, the purpose of using mixed-effects for estimation is not to obtain a better fit than with a non-linear least squares regression model but to satisfy the assumptions in which the model is based, which as discussed before simply it could not be achieved with non-linear least squares regression. This is of fundamental importance for the validity of all statistical significance tests. Note that the predictions with fix-effects produce lower fits than those with non-linear least squares regression since the latter specifically minimizes the sum of square residuals and therefore no other approach would do better than this.

It is also important to note that the random effects are a byproduct of the estimation approach but that they are not used to estimate the fix-effects of the model. The only additional parameters used during estimation are the parameters of the variance-covariance matrix of the random effects (which, allowing for random effects only in ρ and α, are just three parameters including two for the variance of each random effect and one for the covariance of the two) and the heteroscedasticity parameters in the stratified variance of the error terms.

The estimated standard deviation of the random effects for ρ_C is 0.03369 with an approximate 95% confidence interval of (0.03066,0.03703), which shows the parameter to be statistically different from zero at a 5% significance level. This estimate is small compared to the estimate of ρ_C of 4.9058. On the other hand, as expected, the estimated standard deviation of the random effects of α_C of 0.27244 is much higher both in absolute terms and relative to the parameter estimate of α_C of 1.8413. Its estimated 95% confidence interval is (0.24586, 0.30190), which also indicates the estimated standard deviation of the random effects of α_C is statistically different from zero at a 5% significance level. This is again not surprising since several factors make the measurements with conditions leading to low $|E^*|$ values more difficult. For example, the applied loads are much smaller compared to the load cell capacity and therefore the measurements are more prone to have relatively larger errors.

Finally, the estimate of the correlation between the random effects of ρ_C and α_C is 0.4205 with a 95% confidence interval of (0.2962,0.5308), which again shows that this estimate is statistically

significantly different from zero. This indicates that these random effects are moderately and positively correlated.

Thus, the superiority of the mixed-effects model is not judged based on the fits but instead is judged with anova and likelihood tests. A summary of the results of these tests is shown on Table 26. It is important to remember that the use the joint estimation approach was necessary to merge the three data sets gathered for this project, however, the model needed to be improved to satisfy the assumptions on which it was based.

Table 26. Results of anova and likelihood ratio tests

	Model	df	AIC	BIC	logLik	Test	L.Ratio	p-value
NLME fit	1	63	-31907.0	-31476.9	16016.49			
NLS fit	2	106	-20393.8	-19670.0	10302.88	1vs2	11427.2	<.0001

The table shows the values of the Akaike Information Criterion (AIC) ($-2\text{logLik} + 2n_{par}$) and the Bayesian Information Criterion (BIC) ($-2\text{logLik} + n_{par}\log(N)$) which measure the relative quality of statistical models. logLik is the model log likelihood function, n_{par} is the number of model parameters, and N is the number of observations. These two criteria help discerning whether it is worthwhile or not to add a certain number of parameters to improve a model's fit. In general, models with lower values (algebraically) of AIC and BIC are preferred. Therefore, based on the AIC and BIC criteria, it is concluded that the NLME fit is superior than the NLS fit. The same conclusion is reached using the log-likelihood ratio test. The small p-value of less than 0.0001 for this test indicates that the model with the substantially larger log likelihood value (the model estimated with NLME) should be preferred to the model estimated with NLS, thus confirming the results of the other two criteria.

Figure 33 and Figure 34 show the predicted versus observed values of |E*| by data source in regular scale, for levels 0 and 1 respectively. Figure 35 and Figure 36 show the same information but in logarithmic scale. From these plots, it is seen that the model fit the data from all three sources well and that there are no big deviations from the 45° equality line.

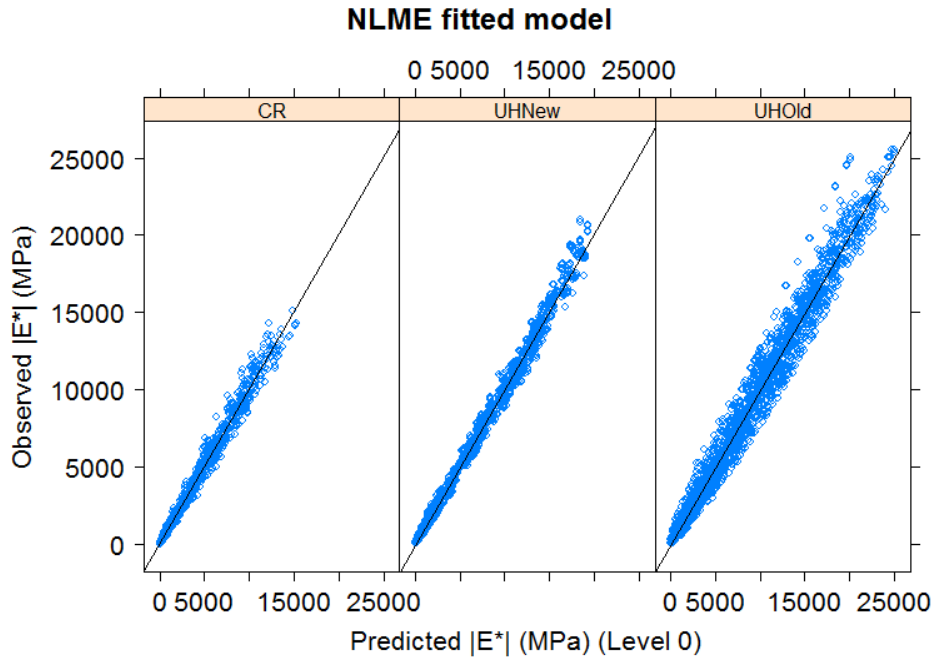

Figure 33. Predicted versus observed values of |E| (by data set) NLME model level=0*

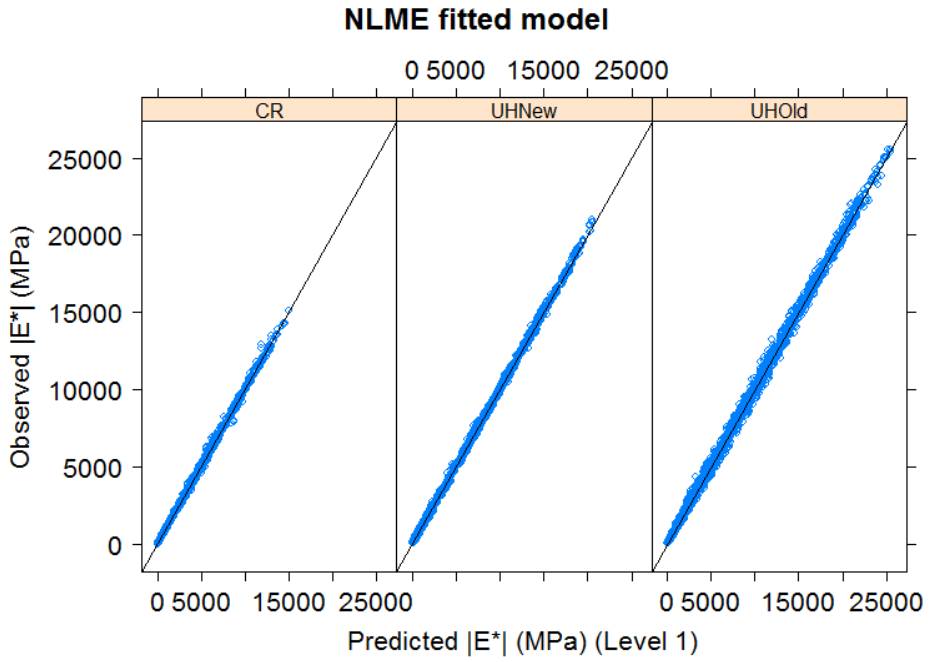

Figure 34. Observed versus observed values of |E| (by data set) NLME model level=1*

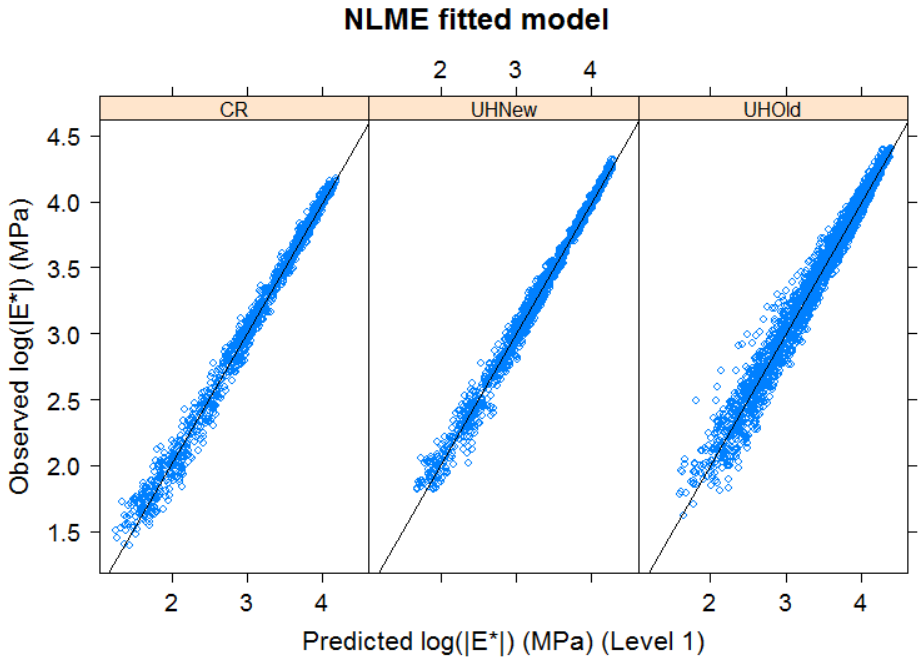

Figure 35. Observed versus observed values of log|E| (by data set) NLME model level=0*

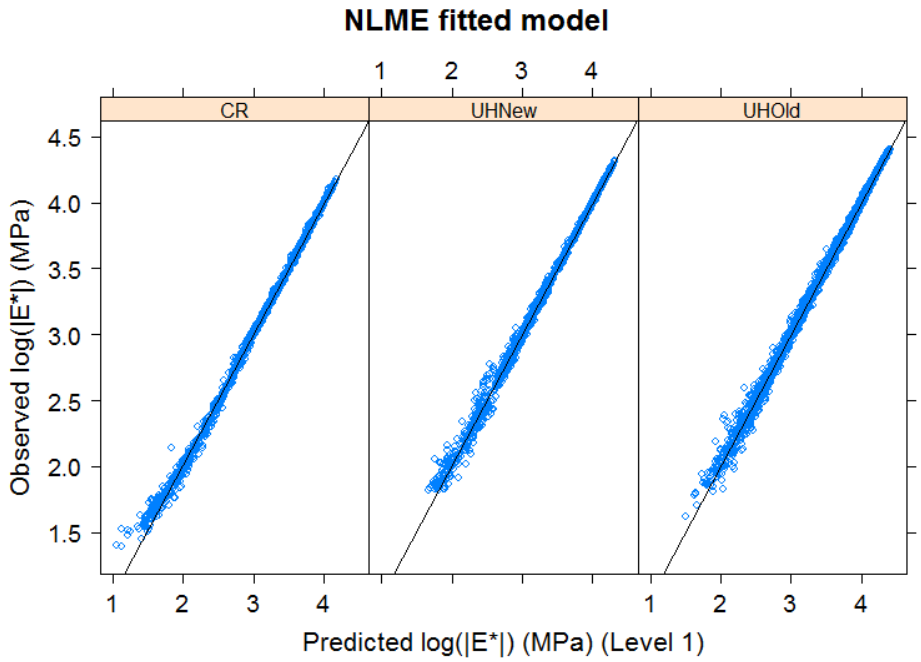

Figure 36. Observed versus observed values of log|E| (by data set) NLME model level=1*

The next step in the analysis is to assess the assumption of the within-group errors. Recall that an exponential structure was used to model variability of the standard deviation of the residuals with the fitted value. Specifically, the following form available in R was used: *varExp (1, form = ~fitted(.)-1|Source)*; which specifies a variance covariate given by the obtained fitted values

minus 1 and includes a stratification at the source level of the data base (i.e., UHN, CR, UHO). Using this model, the estimate of the standard error of the residuals is 0.3313, which corresponds to situations in which the estimated value of log(|E*|) -1 = 0. The 95% confidence interval for this estimate is (0.3028, 0.3625). The estimated parameters of the exponential function accounting for heteroscedasticity are -1.2644, -1.2000, and -1.0640 for the UHN, CR, and UHO strata, respectively. The corresponding 95% confidence intervals are (-1.3034, -1.2255) for UHN, (-1.2410, -1.1589) for CR, and (-1.1005, -1.0275) for UHO. Once again, these indicate that all these parameters are statistically significantly different from zero.

Figure 37 shows the corresponding estimated variation of the residuals with the fitted value of the log(|E*|) estimated as $\sigma_\varepsilon^2 e^{\left(\lambda_i(\log\widehat{(|E*|)}-1)\right)}$, where $\sigma_\varepsilon^2 = 0.3313^2$ and where λ_i equals the heteroscedasticity parameter estimate for data source i (i.e, -1.2644, -1.2000, and -1.0640 for UHN, CR, and UHO, respectively.) This is consistent with previous graphs that show the highest variability for UHO, the lowest for UHN, and intermediate variability for CR. The figure also illustrates that the actual variability of the residuals is in general much lower than the value 0.33, varying from about 0.2 for the lowest fitted values in the database (which are typically prone to contain significant errors), to about 0.1 for fitted values of 2, and to values of about 0.005 for fitted values of about 4.5.

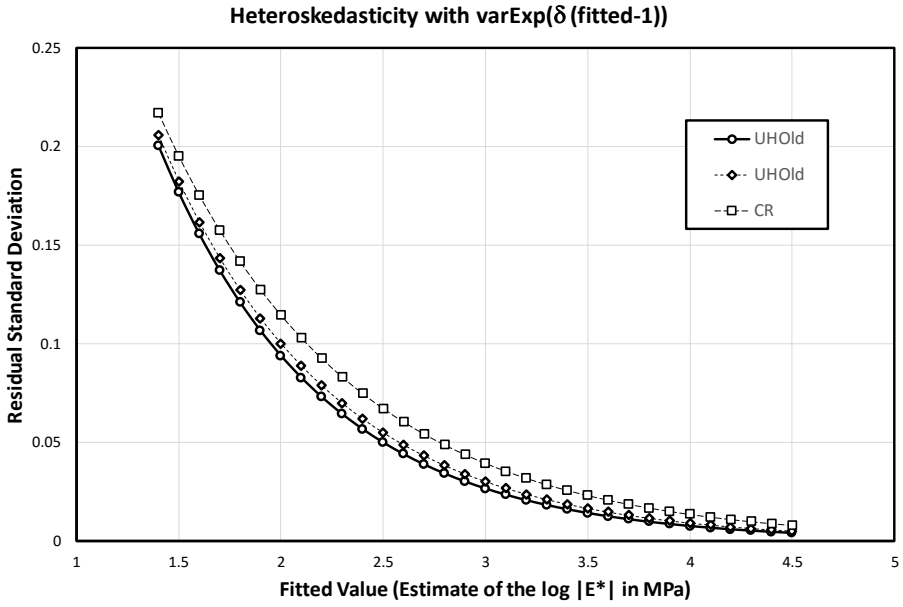

Figure 37. Variation of the estimated standard error of the residuals with fitted values

Figure 38 shows the standardized residuals versus fitted values for each data source. This figure confirms that the variance assumptions are approximately correct since the standardized residuals are approximately uniformly distributed around zero (zero population mean) and show relatively constant variation with the fitted values (except for a slight increase for the CR data set, no other noticeable trends or patterns are seen in the residuals). Furthermore, their variability is similar for all data sources (the number of standardize residuals outside the range of -2 to 2 is around 5%). All these observations support the assumption of independence of the error terms for all three data sets and indicates that the variance function selected produces acceptable corrections for heteroscedasticity. As indicated above, a slight increasing variation pattern is noted for the CR data set, which indicates that the correction for heteroscedasticity is slightly higher than desired for this data set. Nevertheless, the impression of an increasing pattern is mostly driven by about 10 to 20 of the 1417 residuals in the CR data set. Consequently, it was considered that further improvements were not needed.

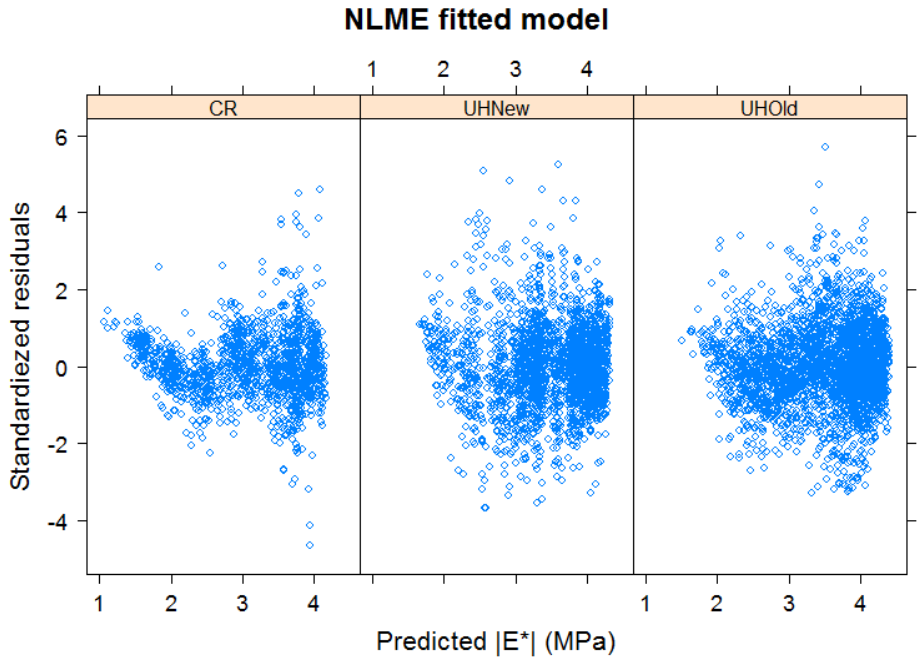

Figure 38. Standardized residuals versus predicted values for the NLMEfit

Figure 39, 40 and 41 address the normality of the error term with quantile-quantile plots of the standardized errors for each data set. In this type of plot, the points for normally distributed errors align themselves in a straight line. From these figures, it is seen that the normality assumption is acceptable since only some deviations from normality are seen at the extremes of the curve (a normal occurrence with outliers, particularly for such large data sets). For the CR

data set, the residuals within two standard deviations form a remarkably linear pattern, which indicates that the model manages to capture the behavior of this data source quite well. For the other two sources, a very slight curvature is still present though it is acceptable. In any case, the normality assumption is much more closely satisfied than for the non-linear least squares fits, thus providing more validity to all the hypothesis tests about parameter estimates.

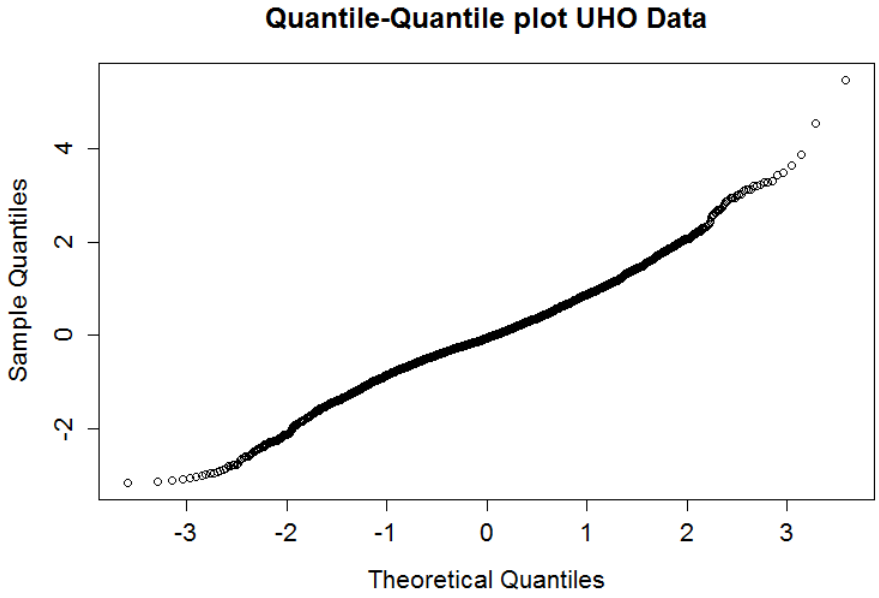

Figure 39. Quantile-Quantile plot of the residuals for UHO source with an NLME fit

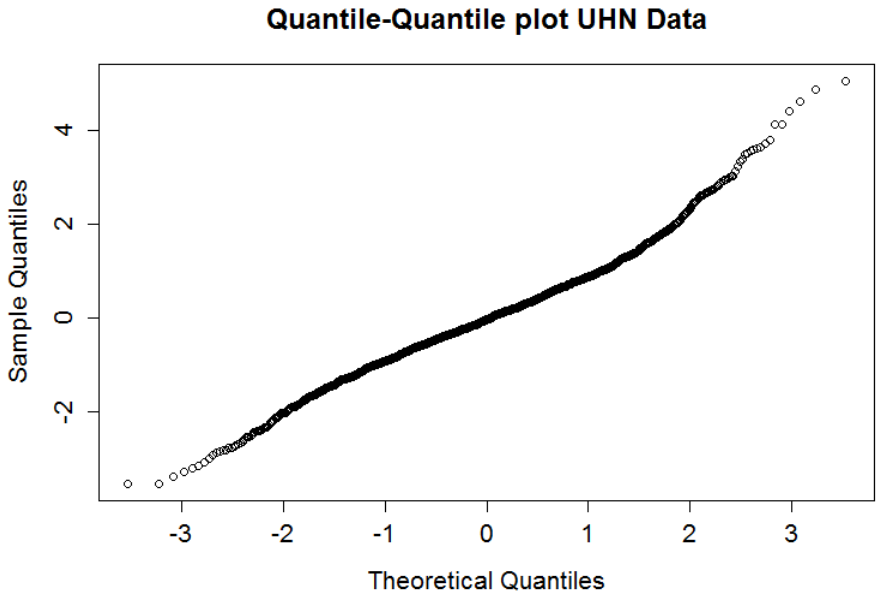

Figure 40. Quantile-Quantile plot of the residuals for UHN source with an NLME fit

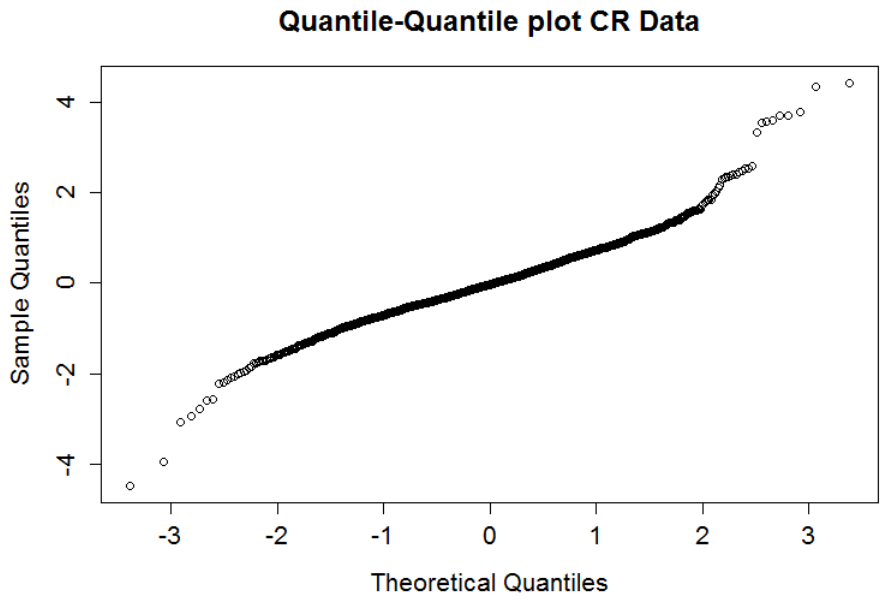

Figure 41. Quantile-Quantile plot of the residuals for CR source with an NLME fit

In regards to the assumptions for the errors, one last figure is included to show their variability for individual samples. Figure 42 shows the sample residuals for each of the samples tested. The improvements in comparison to the NLS fit is noticeable. By allowing for random effects in the model, it was possible to capture the deviations from the overall mean and thus better model the data generation process. By comparing this figure with Figure 21, it is possible to observe that the differences in the distribution of the errors from source to source were significantly reduced and that the random effects could capture unobserved heterogeneities between specimens and eliminate them from the error term.

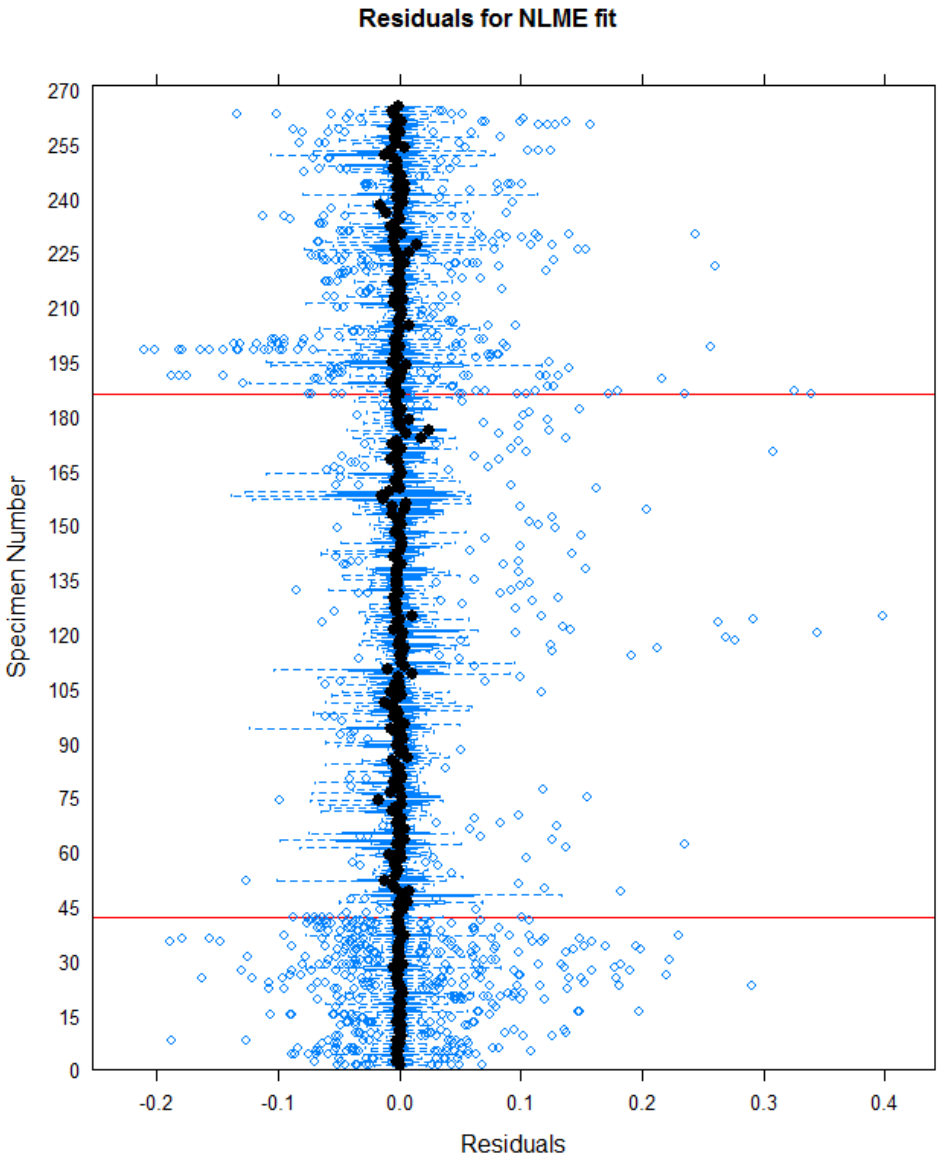

Figure 42. Boxplot of residuals for NLME fit by sample

Finally, Figure 43 shows a quantile-quantile plot of the random effects. It can be noted that except for a few outliers, in general the distributions have straight patterns. Therefore, the assumption of the normality of the random effects made for model estimation is also empirically verified.

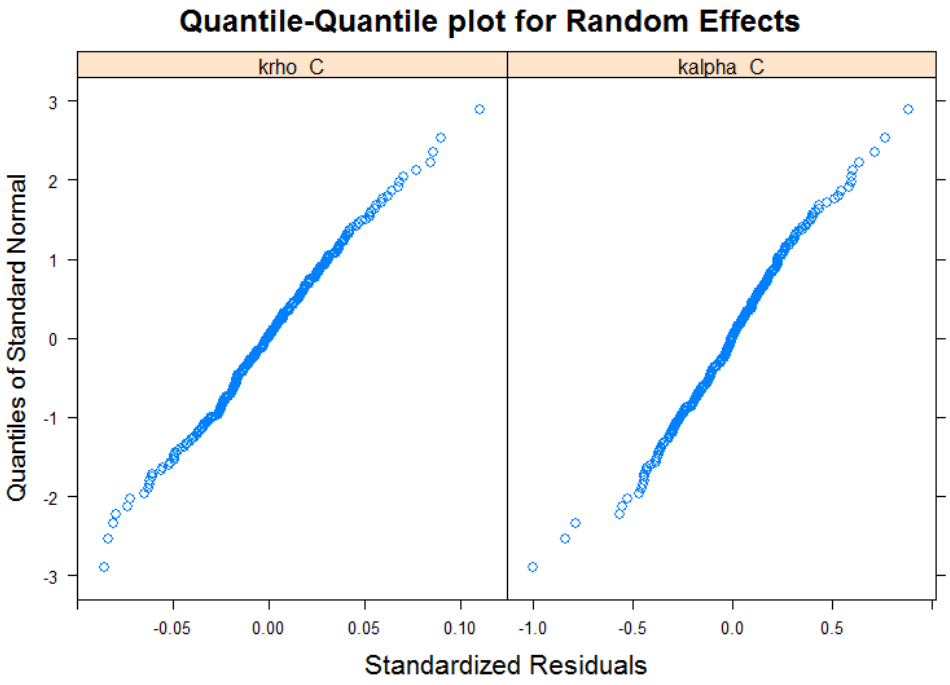

Figure 43. Quantile-Quantile distribution of the random effects

As seen above, the model is satisfactory from a statistical point view. The next section evaluates its capabilities to fit the data and capture all the different characteristics that were included from the different sources from an engineering point of view.

5.5 Evaluation of the final model

This last section deals with the assessment of the model in terms of its reasonableness to account for several characteristics. Several figures are presented showing how the model approaches the laboratory measured values. Other plots are shown to illustrate the sensitivity of the model predictions when certain variables are varied. In most cases, when presenting each of the groups of plots, the first sample in the data base that contains the desired characteristic was chosen. This means that for example, in the first sub-section for the prediction of dynamic modulus with varying air voids, the first sample with 4% air voids, 7% air voids and 9% air voids were taken from the UHN data set. This was done to avoid a possible bias due to a preference to present the best results. Continuing with this example, when presenting the capabilities of the model to predict master curves for different air void levels, one or more samples are chosen from the first block of plots to show these capabilities.

The plots that show how the model approaches the laboratory measured values have 3 sets of data. First, points are included to show the laboratory measured values and then two lines are included to show the predictive characteristics of the model at two different levels. Level 0 shows the population fitted values, meaning that the model uses only fixed effects for prediction (this is how the model will most often be used in practice). This level is shown with long-dashed (green) lines. On the other hand, level 1 shows the within-group fitted values, meaning that random effects are included in the model. This level is shown with a dotted (red) line.

5.5.1 Prediction of dynamic modulus with varying air voids

To show the capability of the model to capture the effect of air voids, samples with virgin asphalts were chosen from all three data sets. The reasoning behind this is that these are the "simpler" samples in any of the data sets, meaning that no other characteristics such as modifiers, confinement level, etc., are included and therefore the model does not need to capture them. The first group of plots shown belongs to the UHN data set. As explained before, the first sample in the data set with 4% air voids (UH-HMA-S1-4AV) was chosen for the characteristics used as input to the model together with the characteristics of the first sample with 7% air voids (UH-HMA-S1-7AV) and the characteristics of the first sample with 9% air voids (UH-HMA-S1-9AV). The sample S2 with 7% air voids was picked at random to complete a set of 4 plots since no more air void levels are included in the UHN data set.

The results are shown in Figure 44 and indicate that the predictions at both levels are quite accurate. The title of each plot includes the air void level of the sample along with the number appearing before AV.

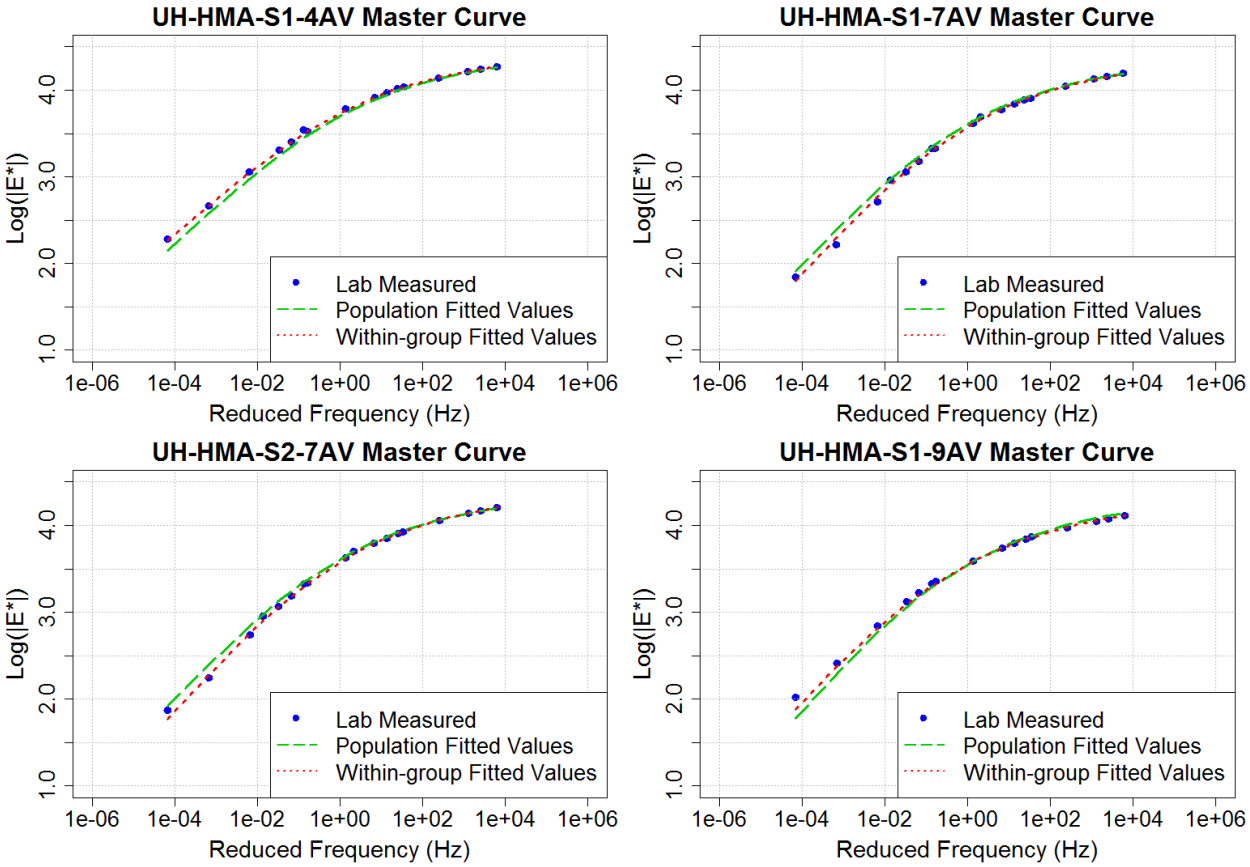

Figure 44. Model capability to capture air void effects for UHN data set

In the case of the CR data set only one level of 7% air voids was targeted and for this reason Figure 45 shows only two plots. Both plots belong to samples mixed with a PG70-22, the base asphalt used in Costa Rica, but they have different gradations. The one on the left-hand side has a 9.5 mm nominal maximum aggregate size (NMAS) gradation while the one on the right-hand side has a 12.5 NMAS gradation.

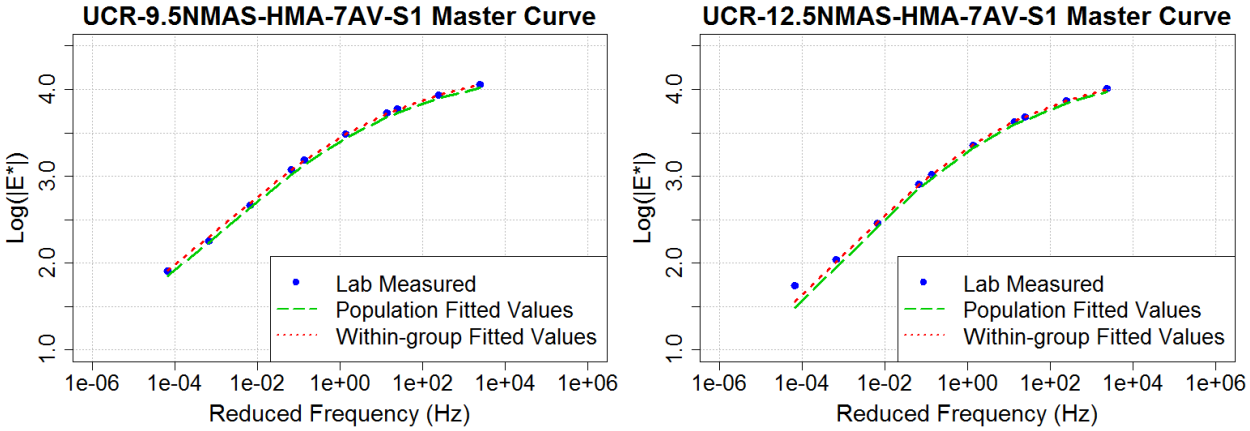

Figure 45. Model capability to capture air void effects for CR data set

The two samples chosen are also the first sample of every set (notice the S1 in the sample name). The figure shows that the model can also capture the shape of the master curves of basic CR mixtures with 7% air voids.

Since the UHO data set has the wider range of air voids, 4 different air void levels were chosen to show the model capability to capture those differences. From the available range of air voids for the base binder type (PG64-16), the lowest (2.1%) and highest (10.2%) air void levels were chosen together with two other samples with more typical air void levels (~4% and ~7%). In Figure 46, the top left sample, BDM007B, has the lowest percentage of air voids, while the bottom right sample, BDM014B, has the highest percentage. From the other two, ADM006 on the top right-hand side has 4.3% air voids, and the bottom left sample, ADM003C has 6.8% air voids.

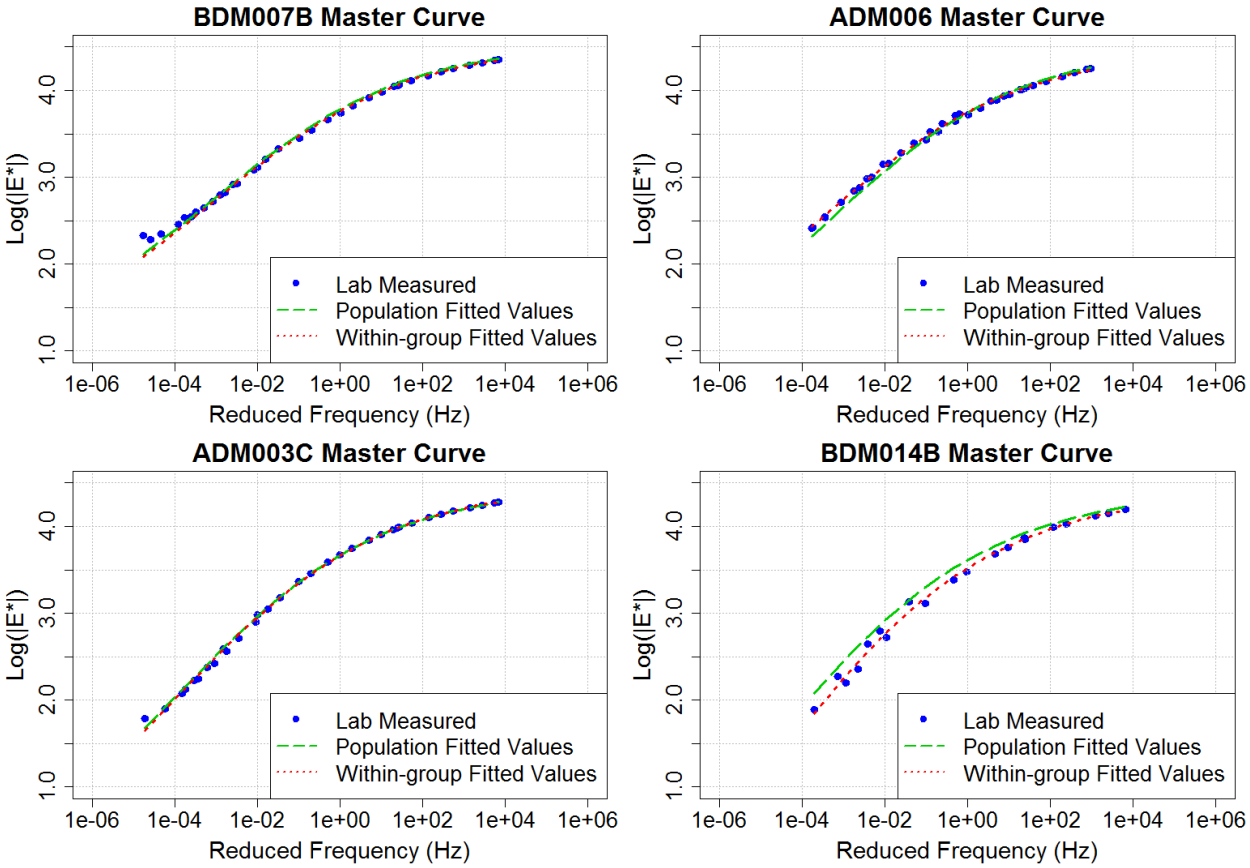

Figure 46. Model capability to capture air void effects for UHO data set

Independently of the variability on the air void level, Figure 46 shows that the model is capable of capturing the effects of all these air void levels quite accurately, even without the consideration of the random effects.

Four samples were chosen at random to further analyze the capability of the model to differentiate master curves by changes in air void levels. Two were selected from the UHN data set (UH-HMA-S1-4AV and UH-PMA-S3-4AV), one from the CR data set (UCR-9.5NMAS-HMA-7AV-S4) and one from the UHO data set (ADM006) to predict the master curves, when all other characteristics are fixed and only the air void percentage varies for three levels, i.e. 4%, 7% and 9%. Figure 47 shows the results obtained.

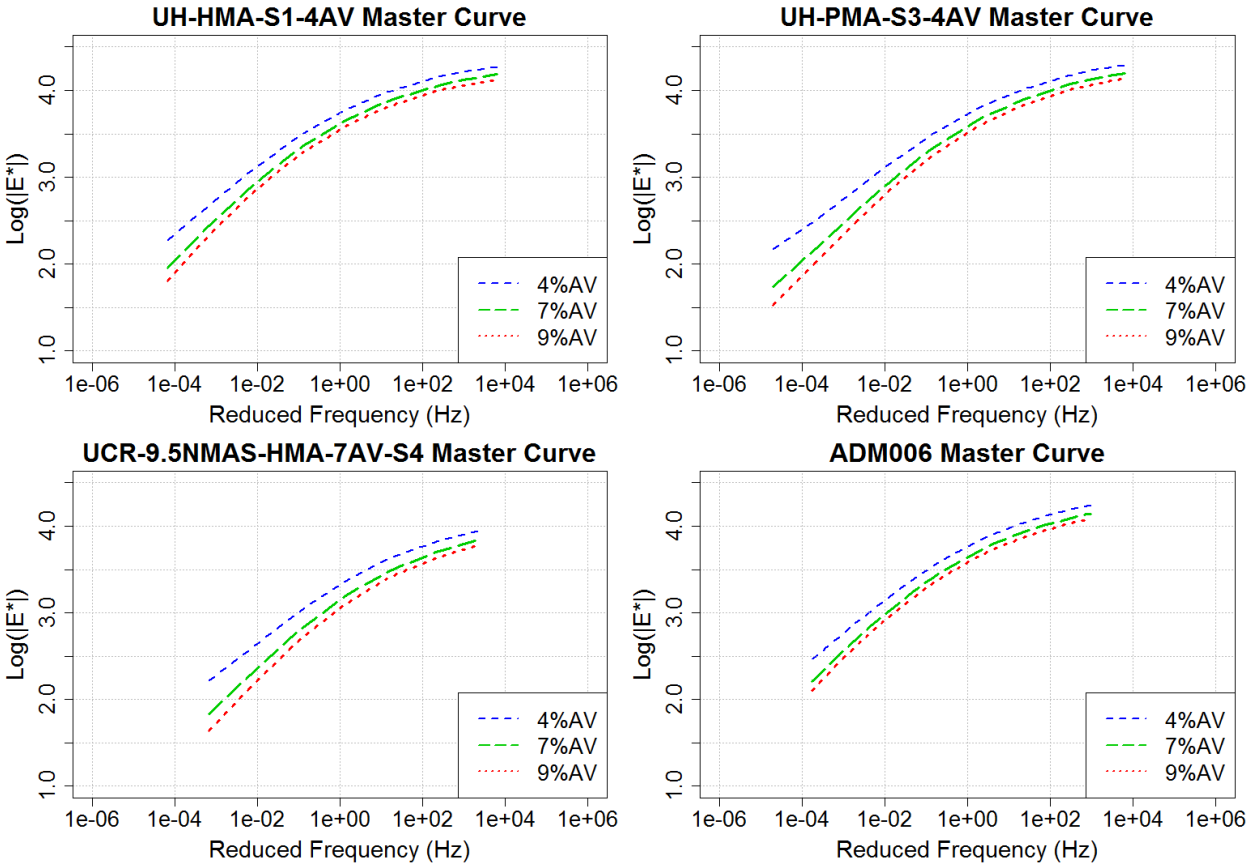

Figure 47. Variation of master curve with 3 levels of air voids

From this figure, it is possible to conclude that the model is capable not only of capturing the trends but also differentiate them in the right order noticed in the laboratory, with higher air voids having lower values of |E*| for all temperatures and frequencies tested but with the difference growing for low reduced frequencies.

5.5.2 Prediction of dynamic modulus with varying confinement levels

Regarding the capabilities of the model to capture the effect of confinement, a similar analysis was performed for samples with base binder type and different confinement levels. Figure 48 shows the result of this analysis. Note that again the first sample from the UHN data set was used (UH-HMA-S1-4AV). With this sample, three levels of confinement are used, 69kPa, 138kPa, and 207kPa (10psi, 20psi, and 30psi respectively). A confinement of 0kPa is not shown in the figure since it was illustrated by default in other figures shown before. However, it will be illustrated in the next figure for comparison purposes. The top left plot shows the results for a confinement pressure of 69kPa, the top right corresponds to a confinement of 138kPa, and the plot at the bottom left-hand side corresponds to a confinement of 207kPa. The fourth plot shown at the bottom right-hand side corresponds to the first sample from the UHO data set that includes confinement. The only positive confinement available and shown for the UHO data set is 100kPa (14.5psi).

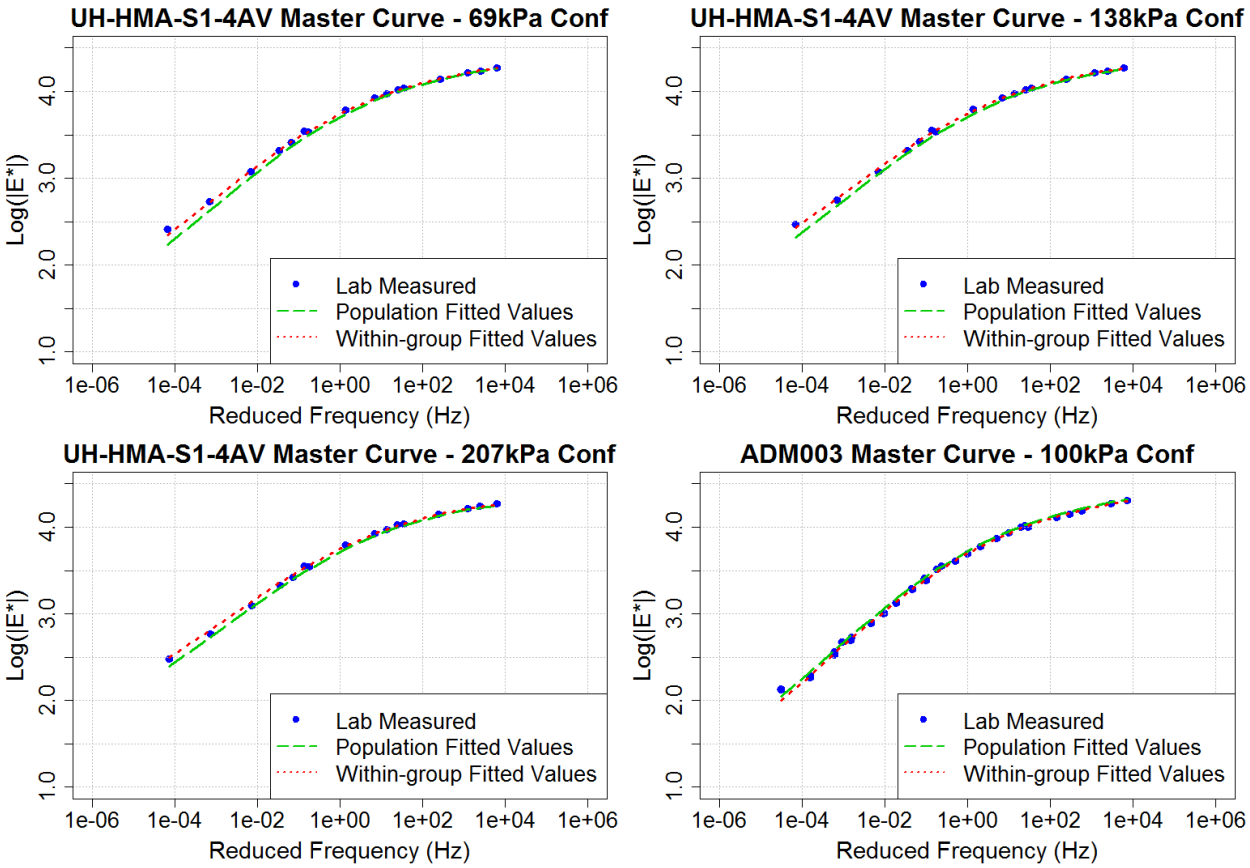

Figure 48. Model capability to capture the effect of confinement

The plots in this figure show that the model is also capable of accurately capturing the effects of confinement at all levels, even if the differences are small as it seems to be for this case. Another way to verify this capability is by drawing the master curves when all variables are kept constant and only the confinement level is varied. This is shown in Figure 49 for a sample chosen from the UHN data set with the five levels of confinement. This particular sample was not chosen at random. A sample with modified binder was selected to illustrate the larger effect of confinement seen in these samples. This figure confirms the capability of the model to differentiate among levels of confinement since the predicted behavior is similar to that observed in the lab (i.e., no differences at large reduced frequencies but important differences at low reduced frequencies, with higher levels of confinement leading to higher values of |E*|). Notice that for this figure the vertical axis shows the values of |E*|.

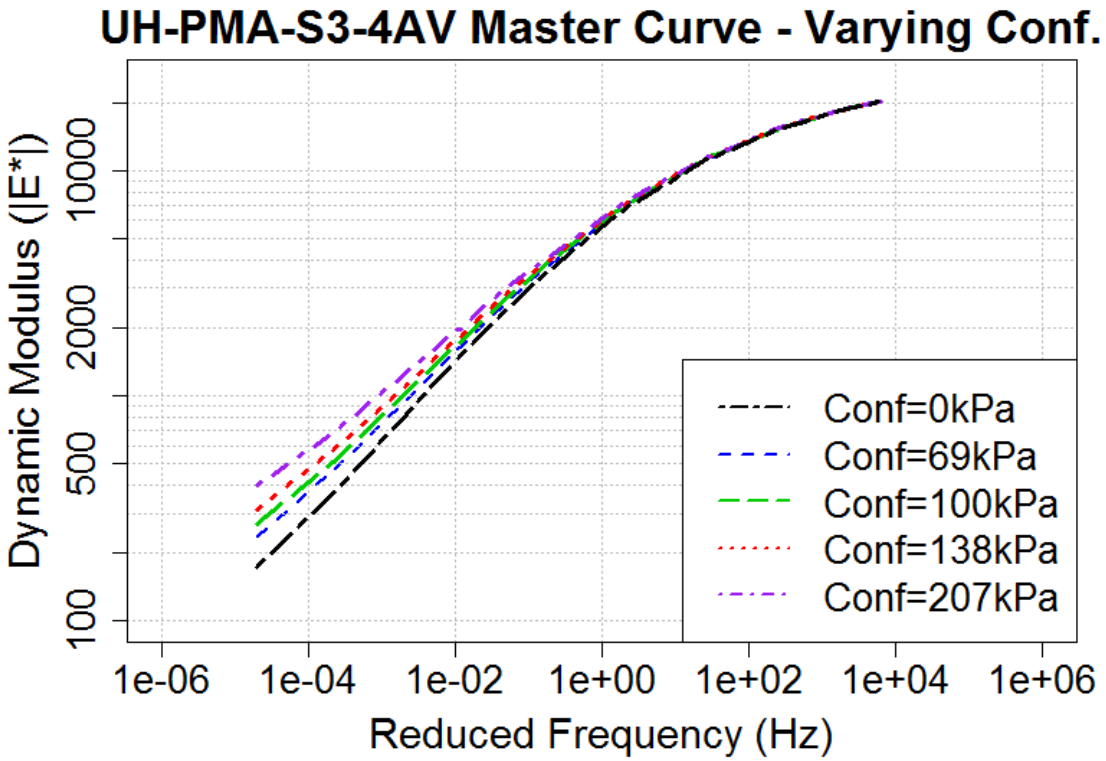

Figure 49. Variation of dynamic modulus with 5 levels of confinement

5.5.3 Prediction of dynamic modulus with varying freeze-thaw cycles

The next characteristic analyzed is the use of freeze-thaw (F-T) cycles. This is a feature of the model that was extracted from the CR data set. As a reminder, three levels of F-T cycles were included, i.e. 1 F-T, 3 F-T and 6 F-T cycles. To illustrate the model capability to identify the

differences among F-T cycles, four samples were taken from the data base with these characteristics. Contrary to the inclusion of confinement, where one sample was used for all confinement levels, in the case of F-T cycles, samples were conditioned for only one of this number of cycles and discarded after testing. Therefore, the first sample from the data base that has a given number of F-T is not S1. Also, there was no particular order in the number of F-T cycles applied to the samples, so it is not possible to say that for all of the 12 mixtures tested, sample 3, for example, was conditioned with 1, 3 or 6 F-T cycles.

The above explanation is offered to justify the sample number for each of the plots shown in Figure 50. To select these samples, the exact same approach was used, were from the 12.5NMAS-HMA-7AV set of samples, the first one to have 0, 1, 3 or 6 F-T cycles was chosen. The order followed in Figure 50 is as follows. At the top, on the left-hand side the plot corresponds to a sample with no F-T cycles (S3), and on the right-hand side the sample has 1 F-T cycle (S14). At the bottom, on the left-hand side, a sample with 3 F-T cycles is shown (S5), while on the right-hand side the sample has 6 F-T cycles (S8).

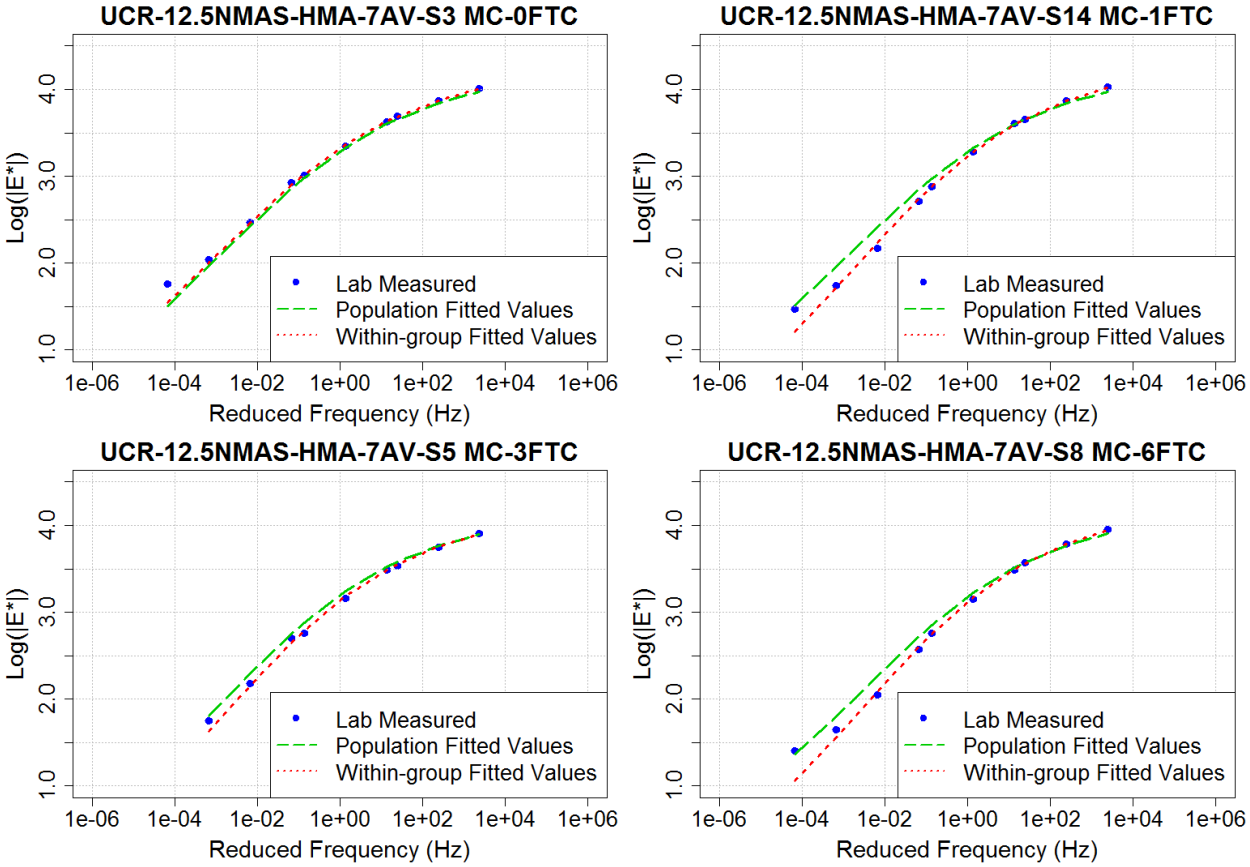

Figure 50. Model capability to capture the effect of freeze-thaw cycles

As seen in Figure 50, the model is able to predict the reductions in the |E*| values with increments on the number of F-T cycles applied to the samples. To compare the differences in the master curve with different number of F-T cycles, Figure 51 shows the first sample from the previous figure (UCR-12.5NMAS-HMA-7AV-S3) with all levels of F-T cycles. Even when this sample was tested with no F-T cycles, the model is able to predict the behavior of the curve for all other F-T cycles levels. Notice that as expected, the model is able to show that the values of |E*| are reduced when F-T cycles are increased. It is also interesting to see that, consistent with the discussion of the parameter estimates, the curves for 1 and 3 cycles are relatively closer to each other than to the other two curves.

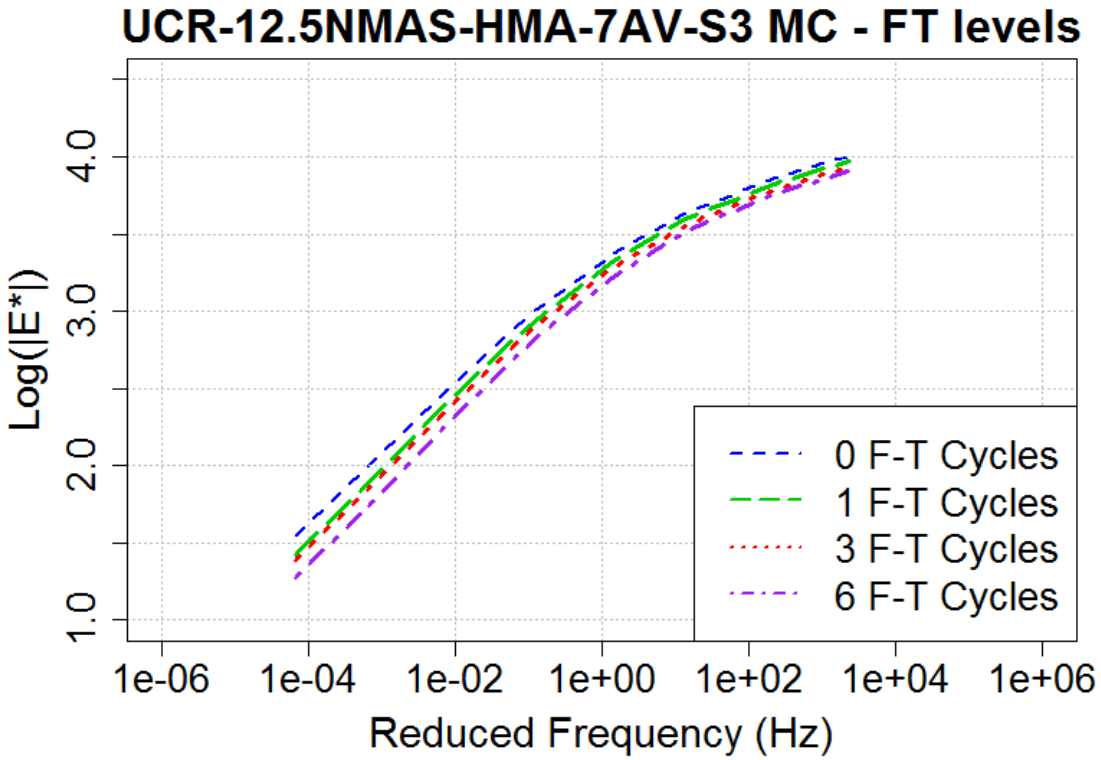

Figure 51. Variation of dynamic modulus with 4 levels of freeze-thaw cycles

5.5.4 Prediction of dynamic modulus with varying mixture modifiers

This last section presents the capabilities of the model to predict the effects of modifiers in the asphalt mixtures. Recall from chapter 2 that the following list of modifiers are found in the three data sets:

- Fibers: For the UHN data set.
- Styrene-Butadiene-Styrene (SBS): Found in all three data sets.
- Elvaloy®Ret: For the UHO data set (PG70-XX).

- Sasobit: For the UHO data set (Warm Mix).
- Lime: Anti-stripping or the CR data set.
- Magnabond: Anti-stripping or the CR data set.

With all these products in mind, a similar analysis is presented to illustrate how the model approaches the laboratory data points and how it can differentiate the effects of one product over the other. First, the effect of the fibers is analyzed, followed by the effect of binder modifiers and finishing with the effect of anti-stripping agents used to counteract the effect of the F-T cycles previously analyzed.

Regarding the use of fibers, it is necessary to remember that after using the mixed-effects approach it was determined that the effect of fibers was significant in the factors α and γ. Particularly for the α factor, the effect of fibers was statistically significant in both the main α and the factor α_{cf} related to the sensitivity to the confinement with air voids and binder type. The model could capture that for both terms the addition of fibers produces a decrease in |E*| values, particularly for lower reduced frequencies and higher temperatures. To show this combined effect, the first specimens with fibers mixed with virgin (F-HMA) and modified (F-PMA) binders are shown in Figure 52 with and without the use of confinement.

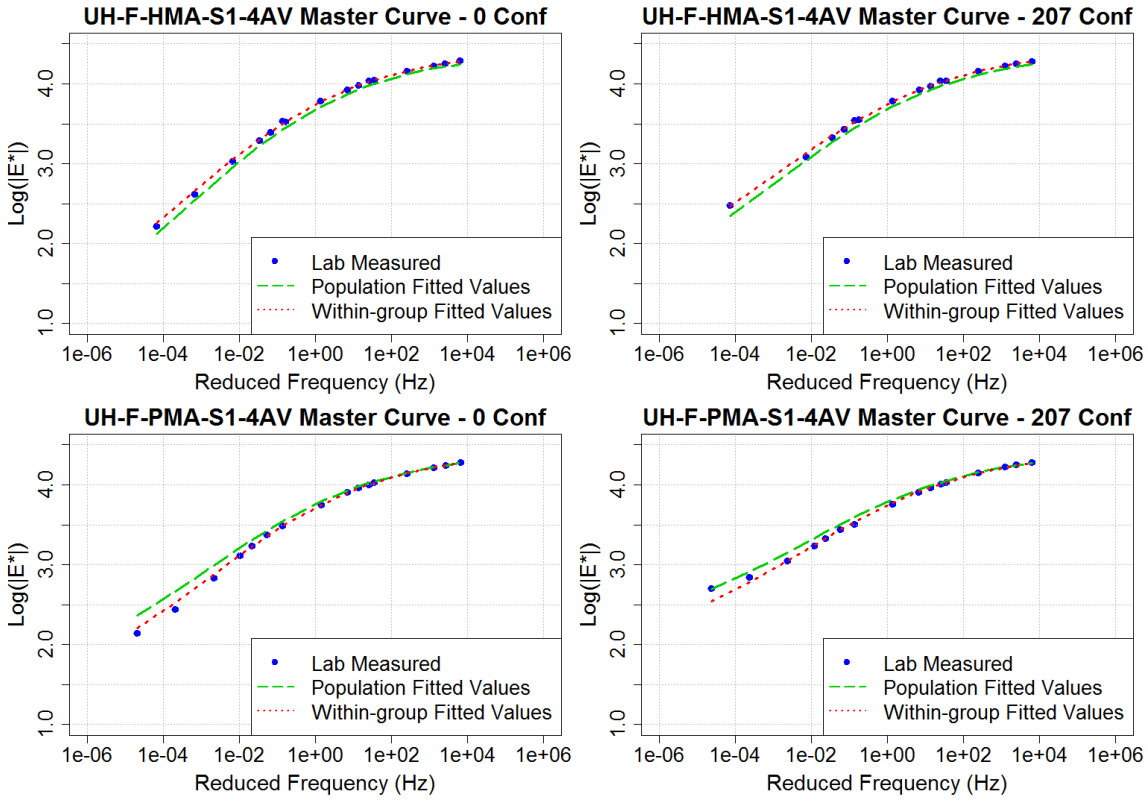

Figure 52. Model capability to capture the effect of polyolefin/aramid fibers

The plots on the top correspond to the mixtures with virgin binder and fibers (F-HMA) without confinement (left-hand side) and with a confinement of 207kPa (30psi – right hand side). The two plots in the bottom show the mixtures with modified binder and fibers (F-PMA) also for a no confinement condition (left-hand side) and with a confinement of 207kPa (right-hand side). All plots show that both levels of the model (level 1 and level 0), with and without the consideration of random effects can accurately capture the effects of the combined interaction of fibers and confinement.

Figure 53 shows the difference in master curves with and without fibers. To create this plot, a sample of a mixture prepared with virgin binder (PG64-22) and fibers (F-HMA) at 7% air voids was used while introducing changes in its characteristics by using the model. This means that by changing some of the dummy variables, the sample was also modeled as a mix with virgin binder with no fibers (D_{Fib}=0), as mix with a polymer modified binder with fibers ($D_{PG76UHN}$=1, $D_{PG64UHN}$=0 and D_{Fib}=1), and as a mix with polymer modified binder without fibers ($D_{PG76UHN}$=1, $D_{PG64UHN}$=0 and D_{Fib}=0). Each sample was additionally modeled without any confinement and with a confinement level of 207kPa (30psi). The idea of this plot is to test the capability of the model to capture the differences in master curves with and without fibers but also with different confinement levels since, as mentioned before, the effect of fibers is also included in the factor α_{cf}. Note that this plot shows the values of |E*| instead of the log(|E*|) on the vertical axis. The figure reflects the behavior observed at the laboratory, where the addition of fibers lowers the values of |E*|. The behavior is more noticeable at lower reduced frequencies. The curves with fibers are shown as continuous lines and the curves of the sample with the same characteristics but without fibers are shown as non-continuous lines on top of these. The lowest (blue) curves show the virgin asphalt sample with and without the use of fibers and no confinement. The next two (green) curves from bottom to top show the virgin asphalt sample with and without fibers with a confinement of 207kPa. The next two (red) curves show a polymer modified sample with and without fibers and no confinement, and the top two (purple) curves show a polymer modified sample with and without fibers with a confinement of 207kPa.

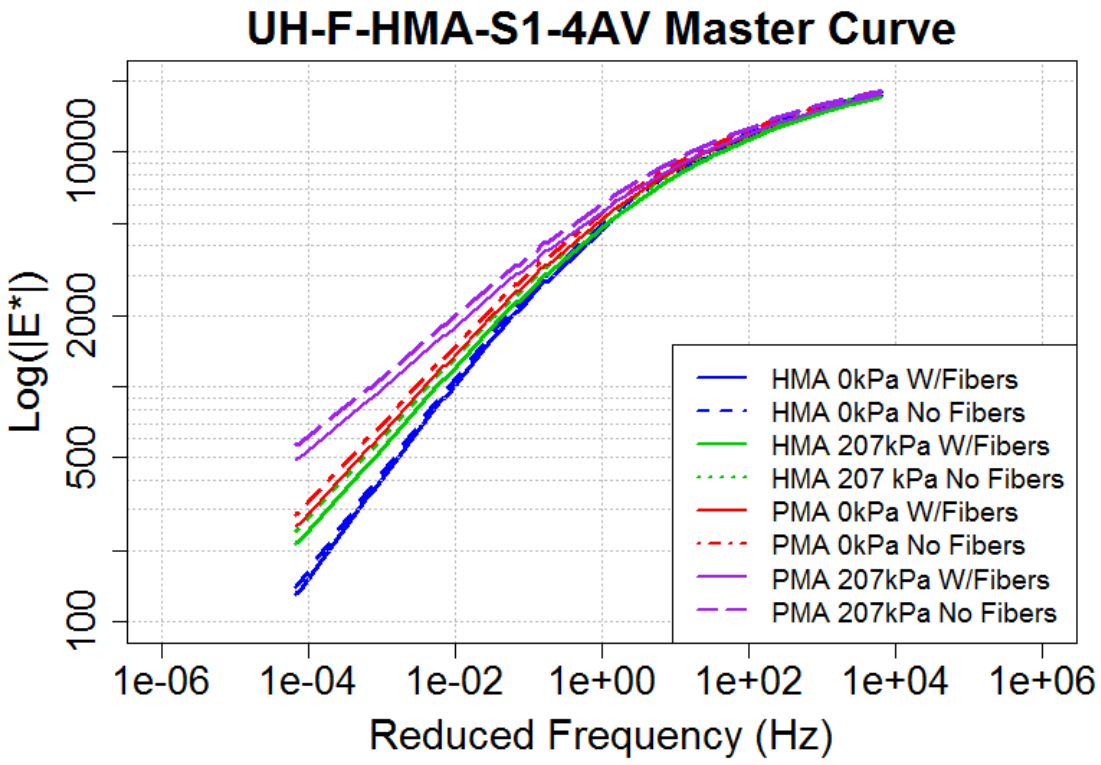

Figure 53. Variation of master curves with and without the use of fibers

Regarding asphalt binder modifiers, the same type of analysis was performed for the three products found in the data base (i.e. SBS, Elvaloy®Ret and Sasobit). Each of the modifiers is presented separately to illustrate the capability of the model to capture the specific effects.

In the case of the SBS, 4 plots are shown in Figure 54. Since this modifier was used in all three sources, a plot from the UHN data set is shown on the top left-hand side (UH-PMA-S1-7AV) while a plot from the UHO data set is shown on the top right-hand side (ADM019). Two plots from the CR data set are shown in the lower part. From the CR data set, the plot on the left-hand side has a 9.5NMAS gradation and the one on the right-hand side has a 12.5NMAS gradation.

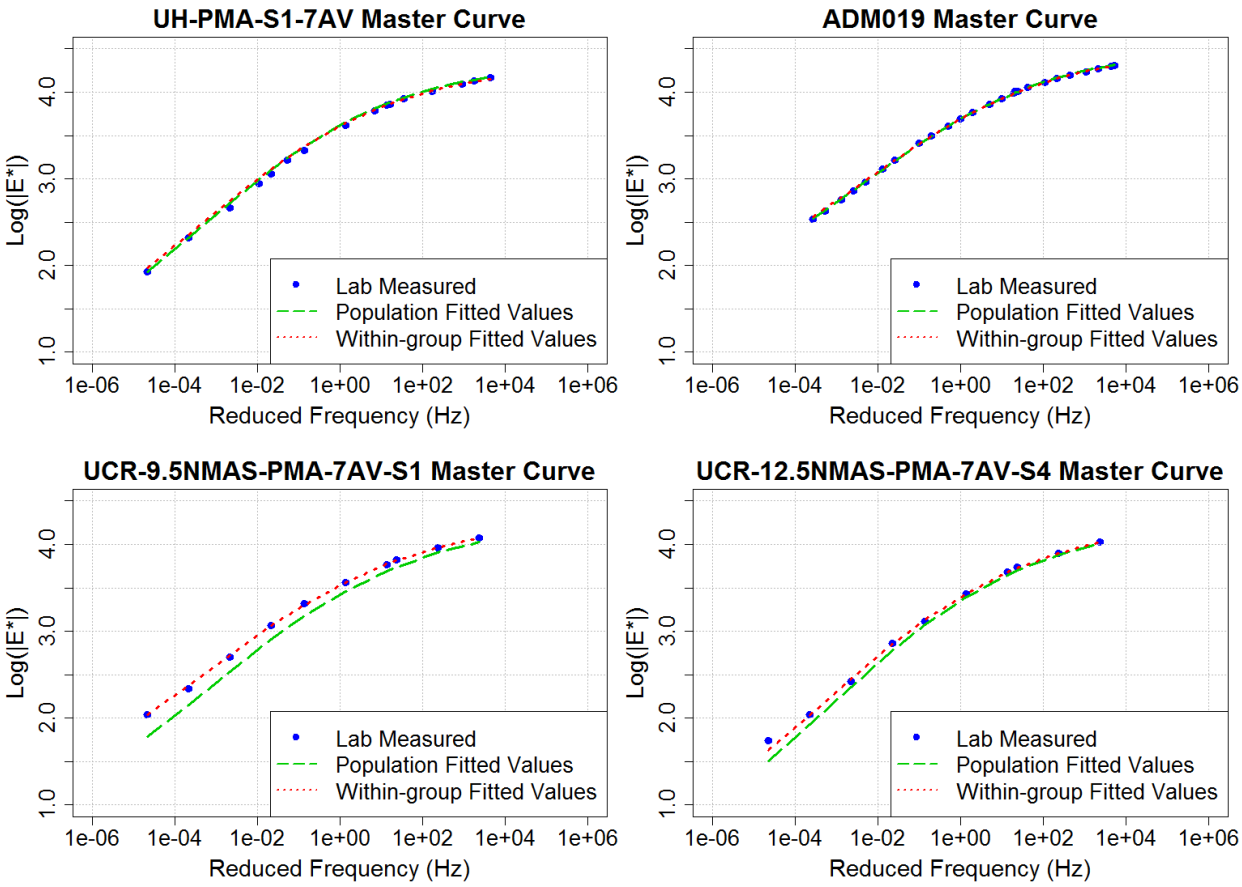

Figure 54. Model capability to capture the effect of the SBS binder modifier

It is clear from this figure that the model is capable of predicting the effect of each of the binders. It is important to remember that even though all these binders were modified with the same polymer, each binder was modified with different percentages, and therefore the model needed to capture the differences between the different binders. This was the reason to include each binder type with a dummy variable in several of the model factors instead of a single variable for all binders modified with SBS.

For the binder with Elvaloy®Ret, which was a PG64-16 binder modified with 1.0% by weight of binder of Elvaloy®Ret at the UH pavements laboratory, the grade of the asphalt was not fully determined (hence the denomination PG70-XX). Since the behavior of the mixtures prepared with this binder was substantially different from the others, dummy variables were included to capture its effect. Figure 55 below shows the model predictions for a couple of specimens with this binder. The two plots selected correspond to the first sample from the UHO data set with a type A gradation (ADM009) and a type B gradation (BDM015). By looking at these two plots,

an important observation is made. The model with fixed effects alone manages to capture the tendency of the curve; however, its predictions are not as good for these two examples.

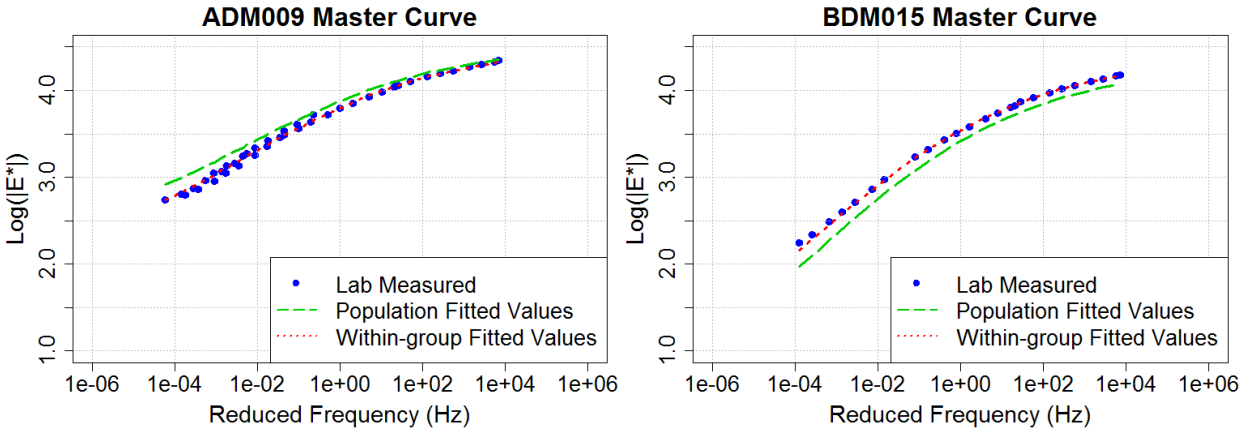

Figure 55. Model capability to capture the effect the of Elvaloy binder modifier

In this regard, it is important to point out that overpredictions for a sample tend to be compensated by under predictions for other samples. Seeing these plots side by side one can notice that on the left-hand side the model with fixed effects is over-predicting the values of |E*| while on the right-hand side, the model is under-predicting these values. This means that the model with fixed-effects might sometimes over-predict and some other times under-predict but on average the model captures the behavior of the particular feature. A problem would be if the model only manages to either under-predict or over-predict the values every time in which case it would be desirable to review the model to verify that there are no important variables missing. This tendency of the model with only fixed effects is observed for other characteristics of the samples (see Figures 44, 46, 50 as examples). A full set of plots is offered in the appendix of this document for further review. This particular observation was made at this point, due to the more obvious pattern seen for these two plots.

For the last binder additive, Sasobit, it is shown in Figure 56 that even when the model with random effects can capture the behavior of the values of |E*|, the model with fixed effects only is not able to accurately predict this behavior. This was expected since neither the NLS nor the NLME fitted models were able to identify variables related to this binder type (introduced as WMA for Warm Mix Asphalt). In the case of the NLS model only one variable related to the factor A, included in the shift factor was significant but was later excluded when the mixed-effects approach was used since it became not significant. This means that no statistically

significant difference between this type of mixture and a mixture with a base binder type PG64-22 was identified even though it is visually evident that the differences are substantial and that Archilla (2010) had identified significant parameters related to this mix. The reason for this lies in the competing needs for identification of the bias parameters, the random effects variance-covariance parameters, and other model parameters and that only two samples are available with these characteristics. Consequently, there is not enough information to capture a significant difference of the factor since the parameters considered for this additive competed with the two random effects and the bias parameters for statistical significance. It is important to note that in the Archilla (2010) study no bias parameters were estimated and a single random effect was used, which explains why significant results were obtain in that study with practically the same UHO data set. Since this is a sample size problem, it could be solved with additional samples prepared with Sasobit. However, the two samples where created with mix from a field project and therefore it was not possible to create additional replicates.

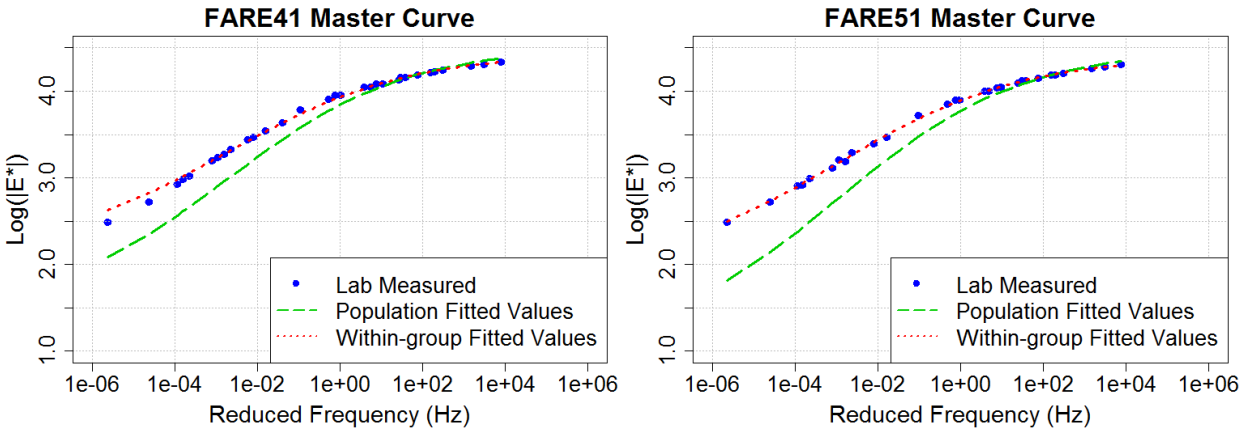

Figure 56. Model capability to capture the effect of the Sasobit binder modifier

A last plot with the effects of all binder modifiers is shown as mentioned before. This plot was made using the characteristics for one sample from UHN data set (UH-PMA-S1-4AV) assuming that everything but the binder type was constant for the sample. By switching the values of the dummy variables, from 1 to 0 for the original binder type of the sample and from 0 to 1 for the desired binder type it is easy for the model to add or delete the associated parameters and calculate the |E*| values for each case. Figure 57 shows these curves. From this figure, it is observed that all three SBS modified binders from the UHN (PG76-22UHN), the CR (PG76-22CR) and the UHO data set (PG70-22UHO) behave quite similar for high and intermediate

reduced frequencies, while for lower reduced frequencies the model can capture some differences. The SBS modified from UHO seems to produce the higher modulus, followed by the one from UHN, while the SBS modified from CR, seems to produce the lowest values of |E*|. It is also observed that the binder that seems to perform the best is the Elvaloy®Ret modified binder from the UHO data set. The last curve in the figure is that of a PG64-22UHN binder which is used as comparison since the model was developed with this binder as a base. The mixtures with Sasobit (Warm Mix) was not included for the reasons discussed above.

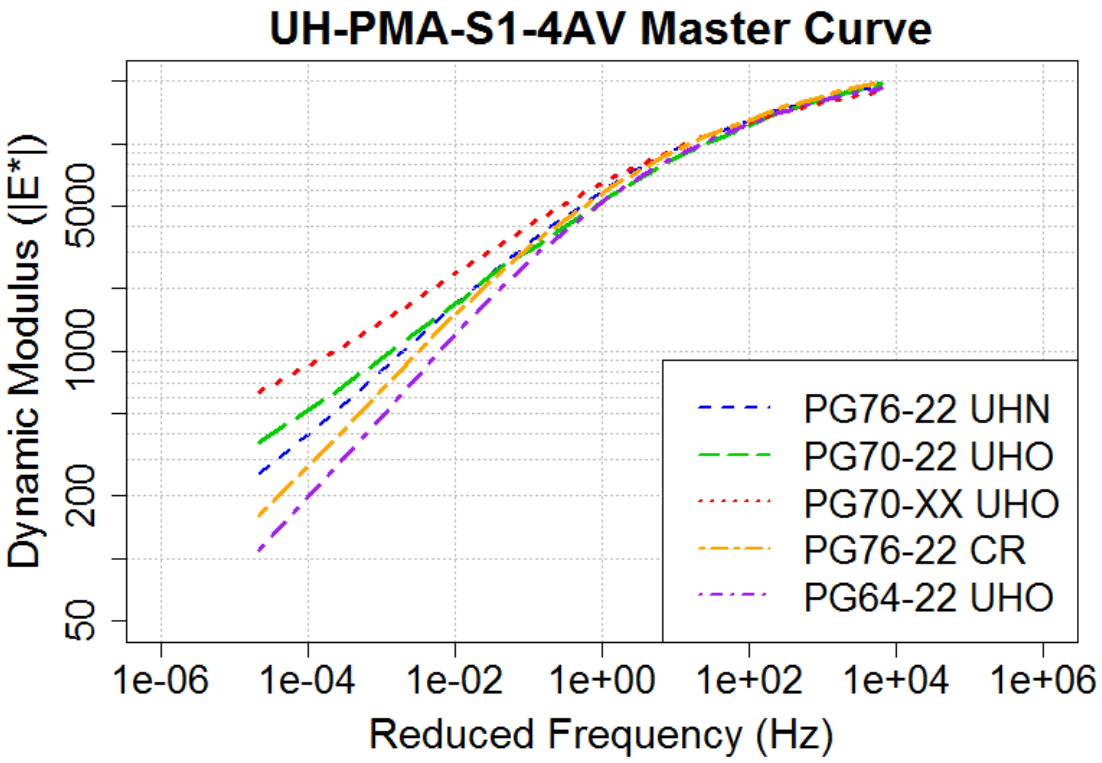

Figure 57. Variation of master curves for all modified binders in the data base

The last characteristic to verify for the predictive capabilities of the model is the use of anti-stripping agents. For each of the two agents utilized i.e. lime and Magnabond, two plots are shown to see how the model approaches the observed data points.

Starting with lime, two plots are shown here for both gradations used in the CR data set. The sample on the left-hand side was the first sample found in the data set that uses lime with a 9.5NMAS gradation, while the sample on the right-hand side is also the first sample for a 12.5NMAS gradation. None of these samples include F-T cycles so that the ability of the model to capture the lime effects alone is evaluated. As shown in Figure 58, the model approaches the

values accurately, particularly in the case of the 9.5NMAS gradation sample. In the other case, the model with random effects captures both the values and tendency of the curve, while the model with fixed effects only, slightly over predicts the values but still manages to follow the tendency quite well.

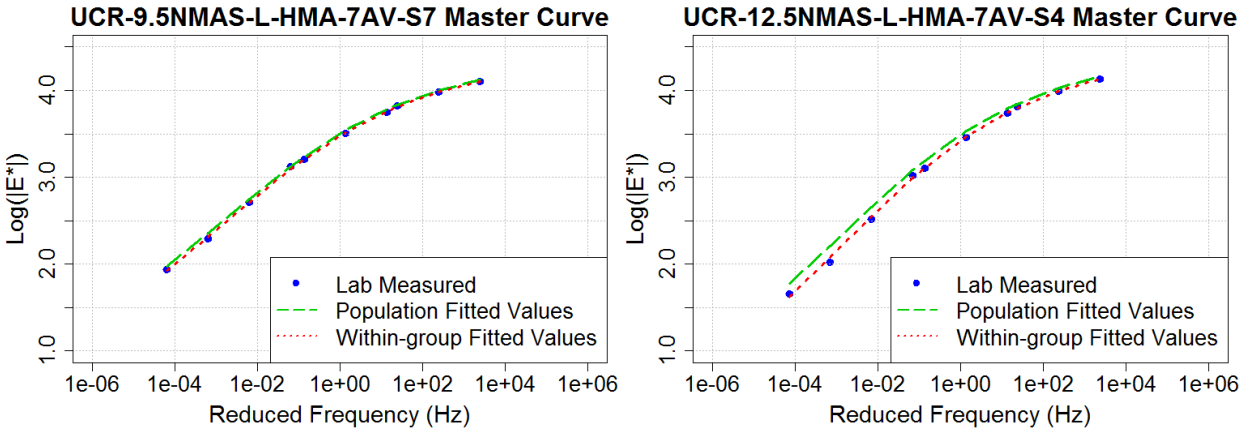

Figure 58. Model capability to capture the effect of the anti-stripping agent Lime

For the case of Magnabond, the plots shown in Figure 59 show again the first samples for a 9.5NMAS gradation (left-hand side) and a 12.5NMAS gradation (right-hand side) that were found in the data base. Again, for these samples, no F-T cycles are included to verify the capacity of the model to capture the effect of Magnabond alone.

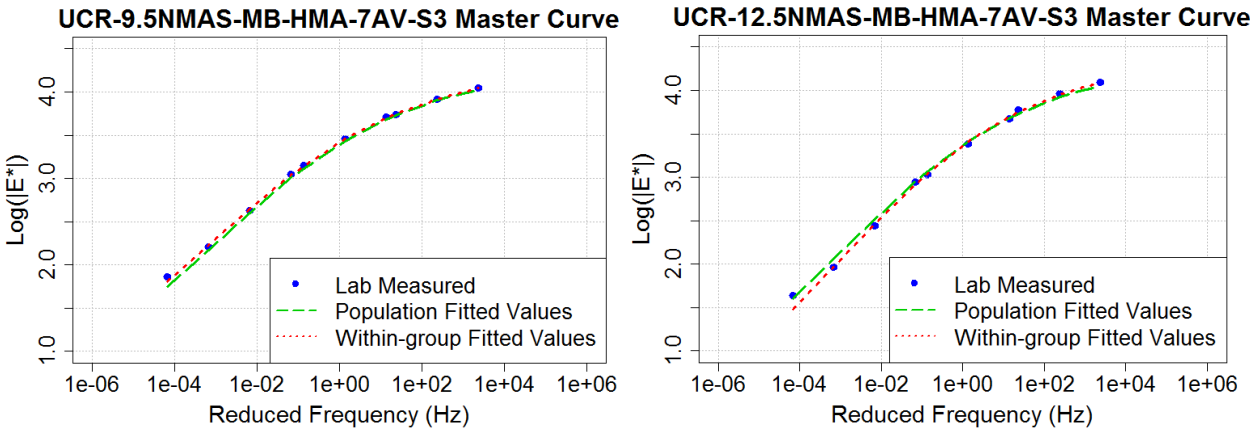

Figure 59. Model capability to capture the effect of anti-stripping Magnabond

In this particular example, the model with and without random effects manages to predict the tendency and values of the curve more accurately than the examples used for the lime. This is not necessarily the case for all samples as can be seen in the appendix. The over and under predicting

tendency of the model with no random effects is seen in this example also, with the model slightly under-predicting the lower part of the curve on the left-hand side and slightly over predicting the values of |E*| on the right-hand side. Nevertheless, it is important to point out that the predictions are in general quite accurate.

Figure 60 shows the effect of using lime (long dashes (green) line) and Magnabond (short dashes (blue) line) on the master curve of a sample. This sample was mixed originally with lime (as can be seen in the L of the name). Dummy variables were changed to reflect the use of Magnabond and also a master curve when no anti-stripping agent is used (continuous (purple) line). The general tendency is that the use of Lime is superior at improving the values of |E*| for all samples tested. Also, the use of both anti-stripping agents increase the values of |E*| even when no moisture damage is induced to the sample

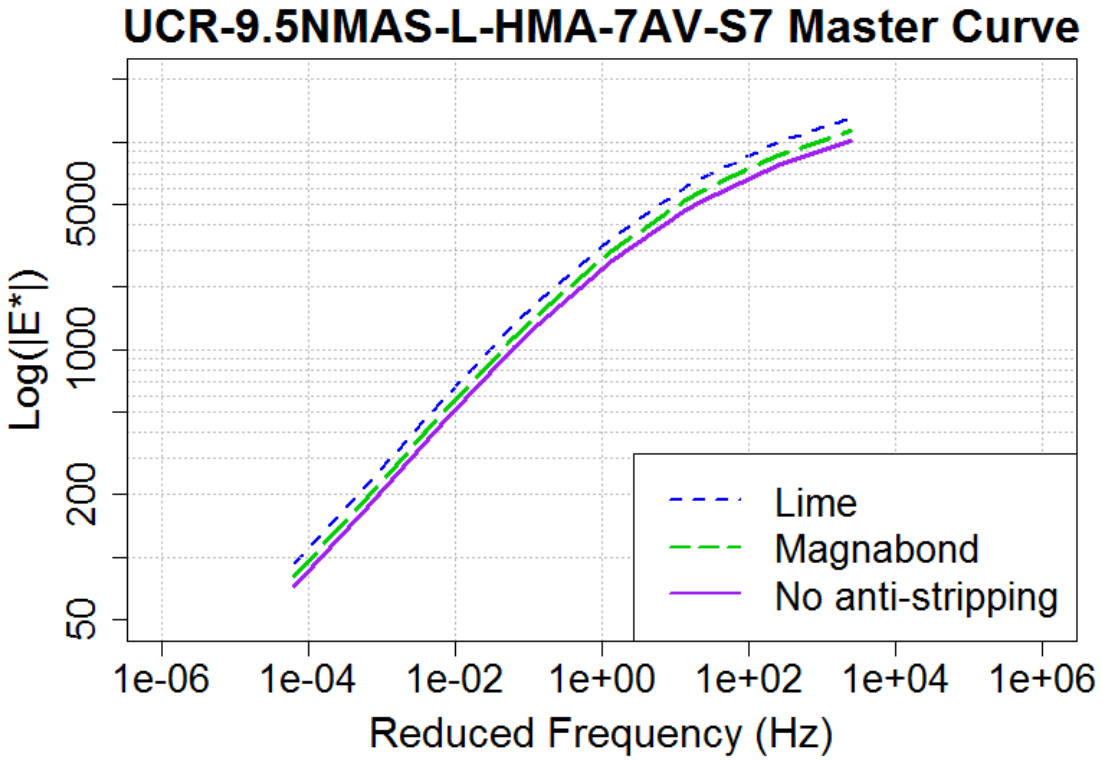

Figure 60. Variation of master curves for the use of different anti-stripping agents

Before finalizing this chapter, two more plots are shown to test the capabilities of the model to combine some features. This was shown earlier in Figure 52 for a combination of fibers and

confinement, however to include another example, combinations of anti-stripping agents and F-T cycles were selected to show how the model captures the two effects at once.

Figure 61 shows on the right left-hand side a plot for a sample with Magnabond and 3 F-T cycles (Sample 14). It is seen that both levels of the model are able to capture both effects with accuracy, even though the model with fixed effects only, is slightly over predicting the values, but follows perfectly the tendency of the curve.

Furthermore, on the right hand side, three effects are captured by the model, that is, the effect of Lime, 6 F-T cycles and additionally the use of a polymer modified binder (PMA sample 10). The model again is able to capture all these effects accurately with a slight under-prediction from the model with fixed effects only.

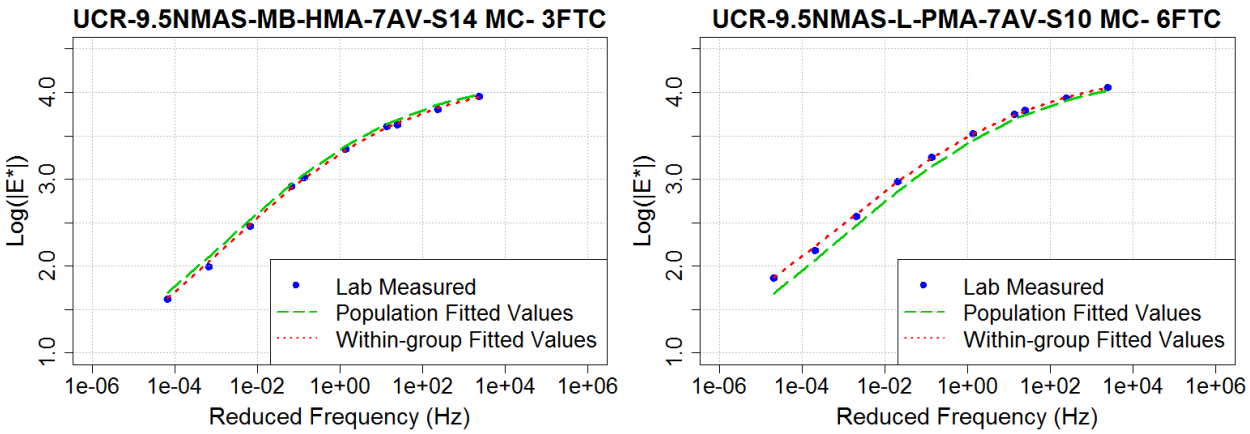

Figure 61.Combined effect of anti-stripping agents and FT Cycle on master curves

Even with some under or over predictions for the model with no random effects, the fit of the model is considered of high-quality. With the inclusion of the random effects, it was shown that the model is capable of capturing the effects of all features included in the data base on the shape of the master curves with very high precision, though it is important to emphasize that the main goal of the consideration random effects is to obtain more reliable statistical results (specifically, testing the statistical significance of the model parameters and thus more closely capturing the marginal effects of the different factors without spurious results).

After performing this analysis of the capabilities of the model a final section of conclusions and recommendations will summarize the usefulness and contributions from this project, while opening the possibilities for further research and potential improvements.

CHAPTER 6: CONCLUSIONS AND RECOMMENDATIONS

6.1 Conclusions

This dissertation presented a predictive model for dynamic modulus of asphalt mixtures that considers several additives and non-conventional testing characteristics such as confinement and freeze-thaw cycles. The model was created based on three different data sets, two of them collected at the University of Hawaii, Manoa and the last one collected at the National Laboratory of Materials and Structural Models of the University of Costa Rica (LanammeUCR). Because of variability from specimen to specimen, the model was developed to account for unobserved heterogeneities at the specimen level and differences in the data bases. The most important conclusions derived from the development of the model are as follows:

- The model includes among its required inputs common mixture characteristics e.g. air voids, gradation-related variables, and effective binder content, which can be found in other models such as the Witczak model. However, the model also includes several other inputs that capture the effects of some other testing and conditioning characteristics that are not found in other models such as confinement levels, freeze thaw cycles, and strains.
- The effect on dynamic modulus of all the characteristics included in the model are:
    - In general, the two binder modifiers, i.e. Styrene-Butadiene-Styrene (SBS) and Elvaloy®Ret, were found to significantly increase the performance of the mixtures. The mixtures containing Elvaloy®Ret were found to perform better overall, while the model captured an improved behavior for all three mixtures modified with SBS (i.e., PG76-22UHN, PG76-22CR and PG70-22 UHO) when compared to the base binder case. In the case of a third additive, Sasobit, which is the wax used to produce warm mix asphalt, no statistically significant differences were found with the mixed-effects approach due to insufficient number of specimens and data points, even when there was an obvious positive effect at high temperature/low frequencies.
    - The use of the anti-stripping agents, lime and Magnabond, was found to increase the values of |E*| in general and to reduce the moisture damage of the samples with freezing and thawing conditions. Lime was found to provide a higher increase in the |E*| values than Magnabond.

- The effects of freezing and thawing cycles were accurately captured by the model as reductions in the values of |E*|. As expected, moisture damage in the mixture (reduction of |E*| values) increases with an increased number of freeze-thaw cycles. This tendency is however nonlinear. Even though the reduction in modulus is monotonic, the magnitude of the predicted reduction is relatively high with only 1 cycle, it decreases from 1 to 3 cycles, and increases again from 3 to 6 cycles.
- The model was able to capture a reduction in the values of |E*| with the use of fibers. This effect was not only captured in the factor α and γ, but also within the confinement factor α_{cf} which indicates that when applying confinement, the use of fibers will further lower the values of |E*| in comparison with the use of no confinement. This is one of the most important results obtained since this means that the differences between a mix with and without fibers is statistically significant. This further confirms the qualitative assessment found in a previous study with the UHN data set (Corrales-Azofeifa and Archilla, 2016)
- The effect of confinement was also captured by the model through the introduction of a factor α_{cf} with a sigmoidal behavior. As mentioned before, increments on the confinement level always increase the values of |E*| but they are also substantially affected by both air voids and binder type. Mixtures with polymer modified binders benefit the most with confinement at all air voids levels whereas the benefits for unmodified mixes are realized only for the lower air voids (~4%), they are substantially decreased at approximately 7% air voids and they virtually disappear at around 9% air voids. The model is able to capture these complex interactions. The confinement level factor gives the model the flexibility to calculate the effect of any level of confinement desired within the range available in the data sets.

- The model was developed using the joint estimation and the mixed-effects statistical approaches. The joint estimation approach was used to estimate a joint model for three different data sources. The use of this technique allowed for a gain in efficiency in the estimation of model parameters common to different data sets since all available data were used to determine their significance, thus achieving a lower variance. A major

advantage of developing the model with joint estimation is the consideration of explanatory variables that belong to a single source in the model specification. This allows for the use of these characteristics for prediction with the other data sets by properly accounting during estimation for biases in some of the data sources arising from unobserved differences between data sources. These biases, accounted through a set of bias parameters, allow for the consideration of the differences in a data set relative to another data set. By applying this approach, the use of fibers, different binder modifiers (i.e. SBS, Elvaloy®Ret), anti-stripping agents, freeze-thaw cycles and confinement pressure were included in the model and their effects were captured accurately. On the other hand, the use of the mixed-effects approach allowed for an improvement in the efficiency of the parameter estimates through the consideration of random variation for some model parameters. For this model, two random effects were included (one for ρ_C and one for α_C) together with a symmetric variance-covariance function that allow for correlation between them. In addition, the assumption of the within-group variance structure as an exponential function was found appropriate to model the heteroscedasticity found for the error terms.

- The model presented is useful for the calculation of |E*| values of mixtures for Hawaii and Costa Rica. One of the most important things for the implementation of mechanistic-empirical methods is the development of material libraries that can be used as input without the need for testing. The model presented in this dissertation takes into consideration local materials for both Hawaii and Costa Rica and provides several advantages over a more generic model like the Witczak model, which was created with information and materials from other regions in the continental United States. Therefore, this model can be used to develop pseudo level 1 input data as an alternative to the use the default MEPDG models for levels 2 and 3. This means that the model can be used to generate the |E*| values required at level 1, as if the samples were tested in the laboratory. The use of the model presented as pseudo level 1 input would have the advantage of providing better prediction of the values of |E*| than the models for levels 2 and 3 and therefore improve the design outcome from the MEPDG. The model could also be used in a guide created for more tropicalized conditions as are the cases of both Costa Rica and Hawaii.

- The default models for levels 2 and 3 of the MEPDG have limited capacity to account for differences in binders and/or the inclusion of other modifiers such as fibers or anti-stripping agents. This means that two mixtures with very different characteristics can be analyzed by the MEPDG as if there were no important differences among them. Therefore, this model comes as an improvement for the prediction of the effects of these additives and modifiers while also providing the tools for the development of other similar models that consider materials and products from different regions.

6.2 Model Limitations

Even though it is believed that the prediction model developed in this study represents an improvement from other models that are currently used for design of asphalt pavements, it also has some limitations that are important to point out

- The model includes a total of 46 parameters which can be considered excessive in comparison to simpler models such as the Witczak model. However, this is expected since there are many characteristics included in this model that are not included in the simpler models such as confinement, freeze-thaw cycles and several additives and each of these characteristics can typically affect several of the main model factors (ρ, α, β, γ, A and B). In fact, even with this large number of parameters, the model estimated with mixed-effects approach is more parsimonious that the model estimated with non-linear least squares that had several more statistically significant parameters (75 in total). However, as shown in Chapter 5, the lack of compliance with the regression assumptions (something that is rarely seen being checked in the literature) made those tests of hypothesis questionable as shown in chapter 5. Despite the large number of parameters, creating a program facility with the few needed inputs can make use of this model relatively simple.
- By using the joint estimation approach, it is assumed that the all explanatory variables that belong to one data source can be applied to the other data sources. For example, it is assumed that the influence of lime captured from the CR data set is the same when lime is applied to mixes in the UHN or UHO data sets. These assumptions can be validated by performing small scale studies for each case. If the behavior predicted by the model deviates too much from the results of the study, some re-calibration may be necessary.

- Due to the large variability in materials and additives, the model might not be able to include exactly the desired characteristics. For example, when using a PG76-22 from a different region than Hawaii or Costa Rica, the effects of this other binder may differ from those captured in this study. Nevertheless, the model can still be use to evaluate its applicability for this newer material. It is believed that even if the model cannot predict the exact influence of the additive or material included, it is capable to at least predict an expected trend, which is an advantage over the use of a model that does not include any of these characteristics.
- As with any regression model, it is dangerous to use in extrapolations. Consequently, the model should be used for mixes with dense gradations that differ substantially from those used in this study or for open graded and gap graded mixes.

6.3 Recommendations

The model presented in this study accurately captures the effects of mixture characteristics and testing conditions from all data sets. Furthermore, by using joint estimation and mixed-effects, it was possible to closely satisfy the regression estimation assumptions. However, additional benefits can be realized with additional research efforts. The following are recommendations for such studies:

- The techniques used in this study, joint estimation and mixed-effects, can be used in other studies for developing models with similar specifications that account for local conditions and/or other material characteristics not considered here.
- It is recommended to test the capabilities of other binder characteristics, such as viscosity and dynamic shear modulus |G*| to accurately capture the binder properties and compare these capabilities with the ones shown by the model presented in this dissertation. From a more practical point of view, it may be more efficient to relate binder performance to a material property such as the dynamic shear modulus than to associate the performance to a given grade since variations from region to region and even among binder providers are likely to be observed. For example, the PG76-22 from UHN and the PG76-22 from CR, were found to have slightly different behaviors and therefore a dummy variable had to be added for each of them. Thus, the use of binder grades can result in the use of too many dummy variables, potentially affecting the ease

of use the model. In the case of this dissertation, the binder data were not available for all binders and for this reason the binder effects were included more generally as binder grade parameters.

- The model developed in this study needs validation to test its capabilities to accurately predict the values of dynamic modulus for mixtures with similar characteristics. The data sets gathered for this project contained two or three replicates (in most cases) for each testing condition and therefore it was decided to use all of them for model estimation to improve the quality of the parameter estimates instead of putting one replicate aside for later validation. It is recommended to perform this verification when additional data from Costa Rica and Hawaii becomes available.
- Although the developed predictive model for |E*| can capture well the effects of freeze-thaw cycles and anti-stripping agents, to take full advantage of this capability it is necessary to relate the number of freeze-thaw cycles to the actual degradation of the mixes in the field.
- Finally, to evaluate the effect of confinement in the state of the stresses and strains in a pavement structure (particularly at high temperatures) it is necessary to implement the model as a constitutive model in a finite element program. This may be quite challenging since the direction of the minor principal stress changes with the position of the element in the pavement. Furthermore, since |E*| values in tension are significantly lower than the unconfined compressive moduli at high temperatures, the consideration of tensile moduli should also be considered in an updated version of this model and in the finite element implementation for those conditions.

APPENDIX

This appendix presents the master curves of all 265 samples tested for this study. All plots are presented in the same way as they were presented in Chapter 5, where 3 sets of data are provided. The (blue) points show the laboratory measured values. Long-dashed (green) lines show the data at level 0 for the population fitted values (i.e. using only fixed effects) which illustrates how the model will be used in practice. Lastly, dotted (red) lines are used to show the data at level 1 for the within-group fitted values (i.e., including random effects).

Notice that for the case of the first 42 plots, which illustrate de data of the UNH data set, there are 4 red and 4 green lines for each plot and instead of one point at each frequency there are normally 4 points also (except for points that were excluded due to quality control). Each of these lines represents one confinement level, i.e. 0kPa, 69kPa, 138kPa, and 207kPa (0, 10, 20, 30psi). The lower line represents the no confinement case and they go up as the confinement level increases for both levels (0 and 1) as can be seen from these plots.

This is also the case for some of the plots of the UHO data set. Particularly for ADM002, ADM003, ADM004, ADM005, ADM006, ADM007, ADM009, ADM010, BDM002, BDM003, BDM004, BDM005, BDM006, BDM007 for which a confinement level of 100kPa (14.5psi) was used.

In the case of the CR data set, since no confinement testing was used in that particular experiment, these only show the two lines for level 0 and level 1 explained before.

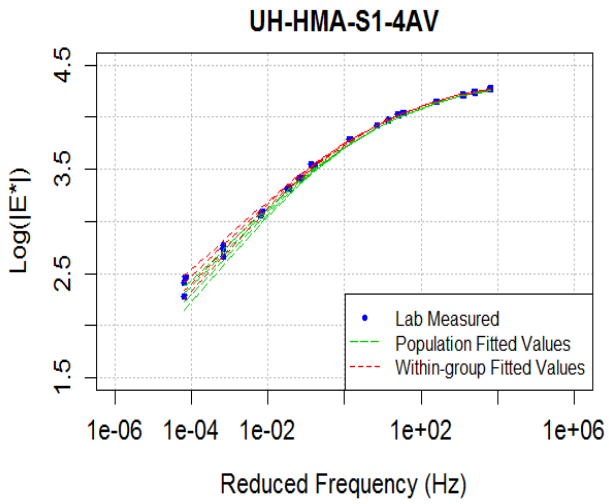
UH-HMA-S1-4AV
Log(|E*|)
Reduced Frequency (Hz)
Lab Measured
Population Fitted Values
Within-group Fitted Values

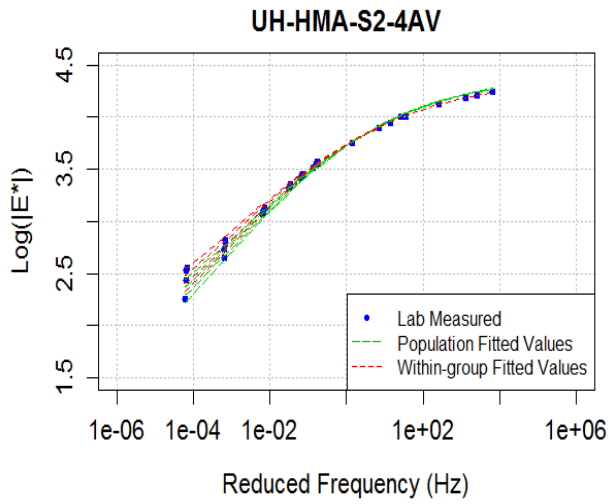
UH-HMA-S2-4AV
Log(|E*|)
Reduced Frequency (Hz)
Lab Measured
Population Fitted Values
Within-group Fitted Values

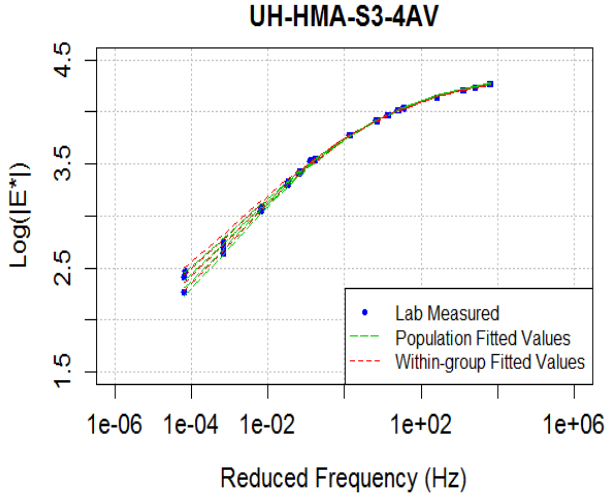
UH-HMA-S3-4AV
Log(|E*|)
Reduced Frequency (Hz)
Lab Measured
Population Fitted Values
Within-group Fitted Values

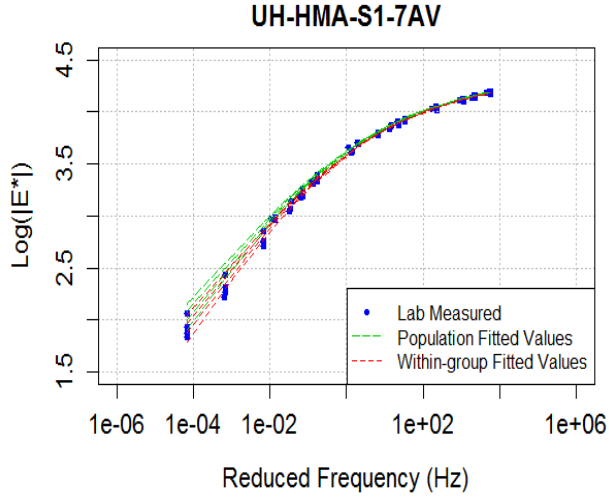
UH-HMA-S1-7AV
Log(|E*|)
Reduced Frequency (Hz)
Lab Measured
Population Fitted Values
Within-group Fitted Values

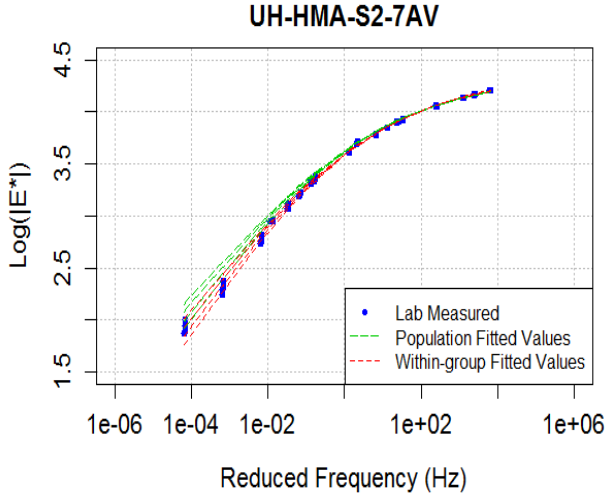
UH-HMA-S2-7AV
Log(|E*|)
Reduced Frequency (Hz)
Lab Measured
Population Fitted Values
Within-group Fitted Values

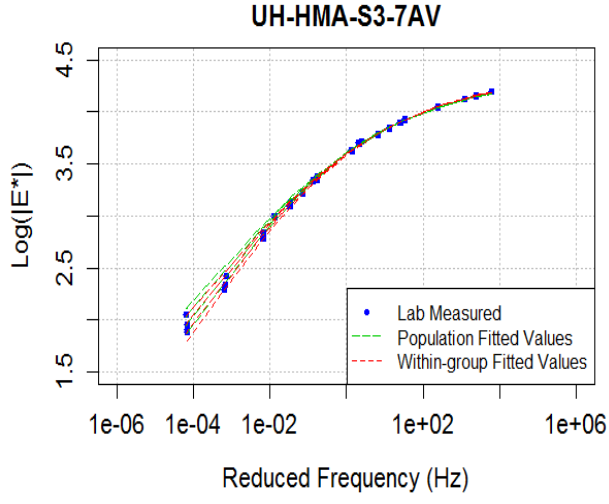
UH-HMA-S3-7AV
Log(|E*|)
Reduced Frequency (Hz)
Lab Measured
Population Fitted Values
Within-group Fitted Values

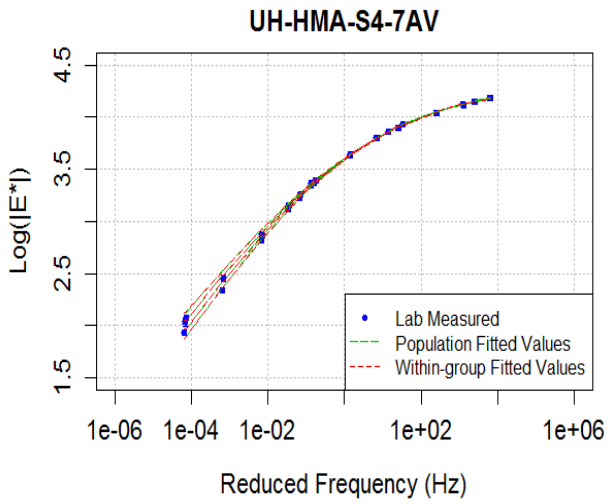
UH-HMA-S4-7AV
Log(|E*|)
1.5
2.5
3.5
4.5
1e-06
1e-04
1e-02
1e+02
1e+06
Reduced Frequency (Hz)
Lab Measured
Population Fitted Values
Within-group Fitted Values

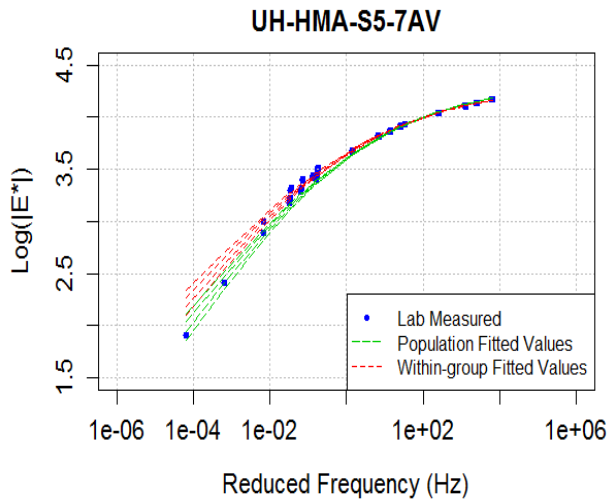
UH-HMA-S5-7AV
Log(|E*|)
1.5
2.5
3.5
4.5
1e-06
1e-04
1e-02
1e+02
1e+06
Reduced Frequency (Hz)
Lab Measured
Population Fitted Values
Within-group Fitted Values

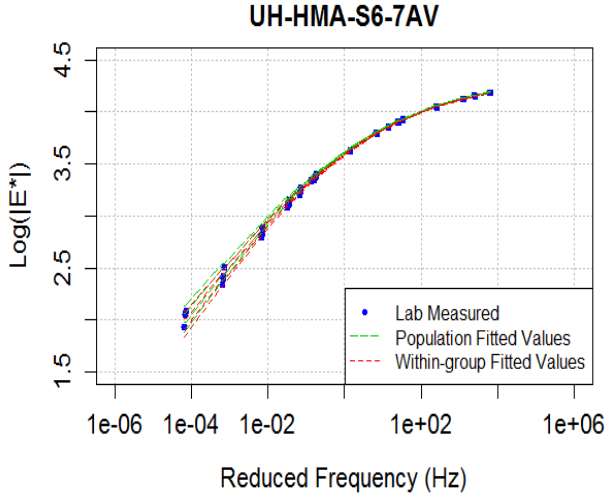
UH-HMA-S6-7AV
Log(|E*|)
1.5
2.5
3.5
4.5
1e-06
1e-04
1e-02
1e+02
1e+06
Reduced Frequency (Hz)
Lab Measured
Population Fitted Values
Within-group Fitted Values

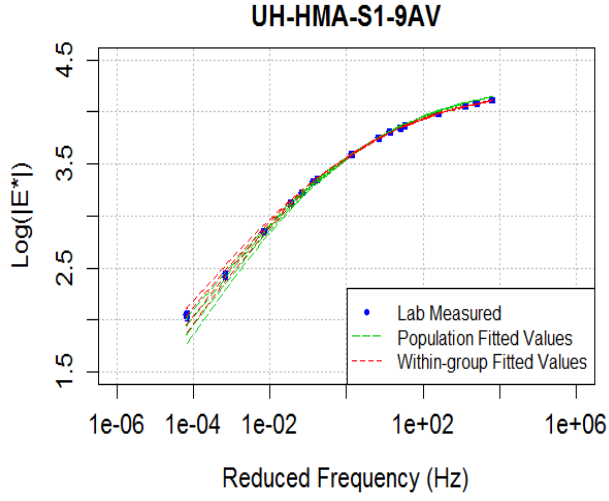
UH-HMA-S1-9AV
Log(|E*|)
1.5
2.5
3.5
4.5
1e-06
1e-04
1e-02
1e+02
1e+06
Reduced Frequency (Hz)
Lab Measured
Population Fitted Values
Within-group Fitted Values

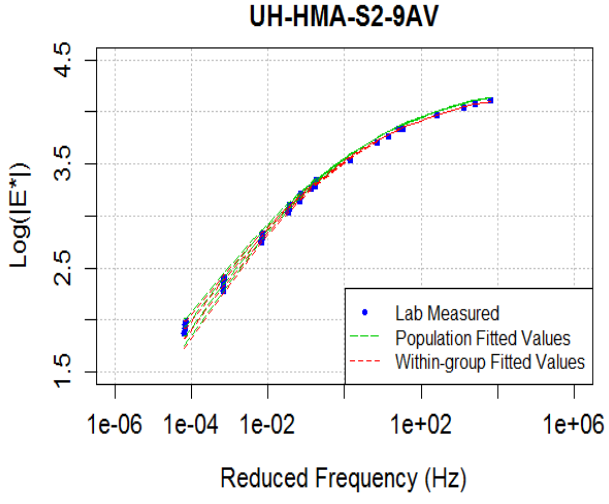
UH-HMA-S2-9AV
Log(|E*|)
1.5
2.5
3.5
4.5
1e-06
1e-04
1e-02
1e+02
1e+06
Reduced Frequency (Hz)
Lab Measured
Population Fitted Values
Within-group Fitted Values

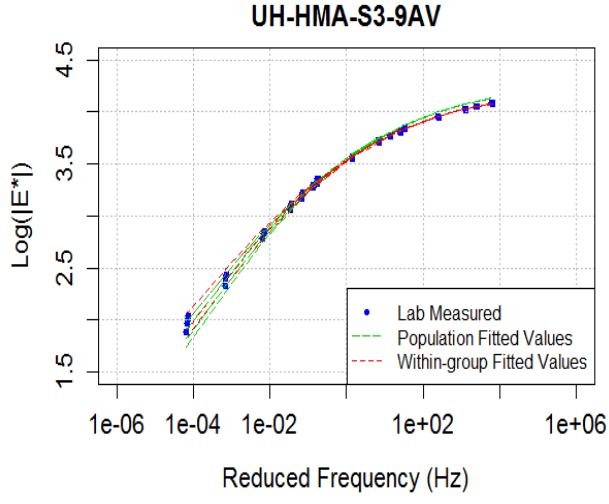
UH-HMA-S3-9AV
Log(|E*|)
1.5
2.5
3.5
4.5
1e-06
1e-04
1e-02
1e+02
1e+06
Reduced Frequency (Hz)
Lab Measured
Population Fitted Values
Within-group Fitted Values

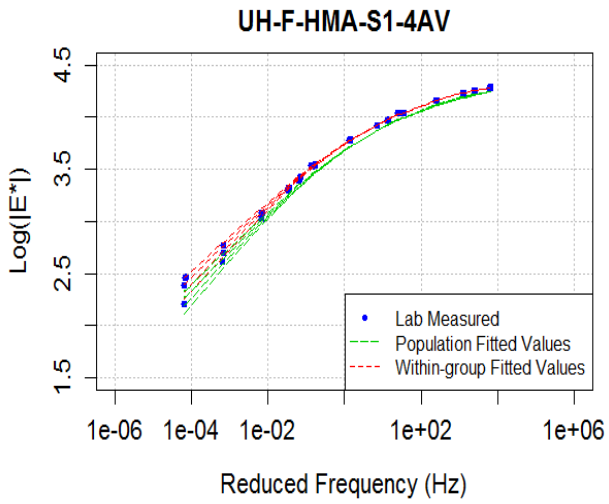
UH-F-HMA-S1-4AV
Log(|E*|)
4.5
3.5
2.5
1.5
1e-06
1e-04
1e-02
1e+02
1e+06
Reduced Frequency (Hz)
Lab Measured
Population Fitted Values
Within-group Fitted Values

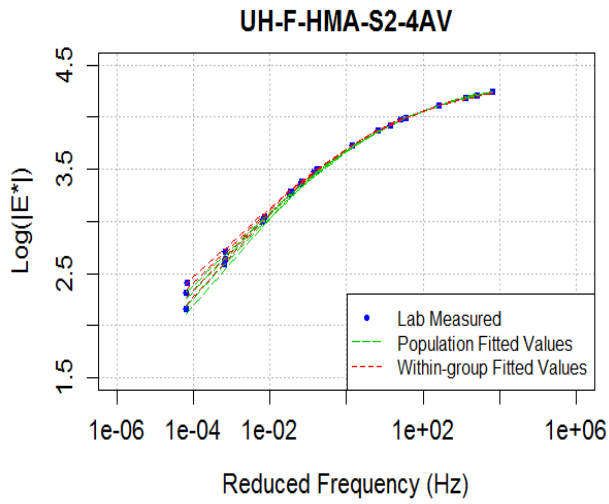
UH-F-HMA-S2-4AV
Log(|E*|)
4.5
3.5
2.5
1.5
1e-06
1e-04
1e-02
1e+02
1e+06
Reduced Frequency (Hz)
Lab Measured
Population Fitted Values
Within-group Fitted Values

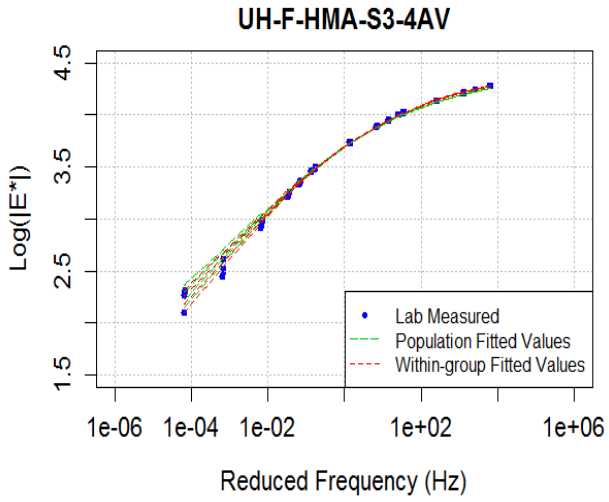
UH-F-HMA-S3-4AV
Log(|E*|)
4.5
3.5
2.5
1.5
1e-06
1e-04
1e-02
1e+02
1e+06
Reduced Frequency (Hz)
Lab Measured
Population Fitted Values
Within-group Fitted Values

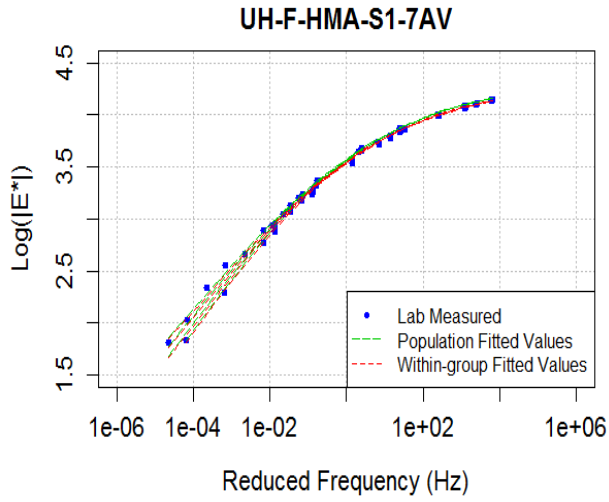
UH-F-HMA-S1-7AV
Log(|E*|)
4.5
3.5
2.5
1.5
1e-06
1e-04
1e-02
1e+02
1e+06
Reduced Frequency (Hz)
Lab Measured
Population Fitted Values
Within-group Fitted Values

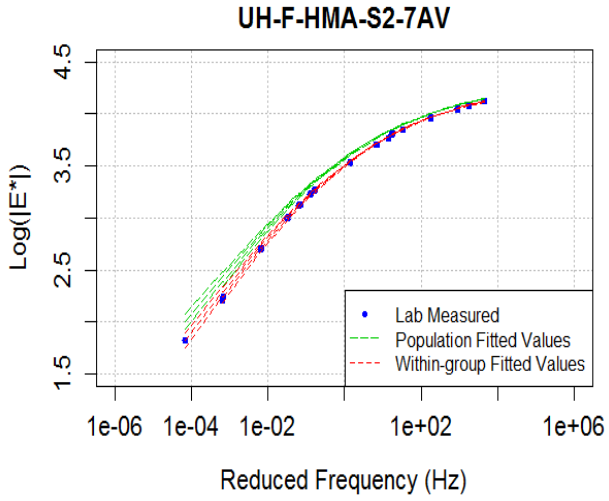
UH-F-HMA-S2-7AV
Log(|E*|)
4.5
3.5
2.5
1.5
1e-06
1e-04
1e-02
1e+02
1e+06
Reduced Frequency (Hz)
Lab Measured
Population Fitted Values
Within-group Fitted Values

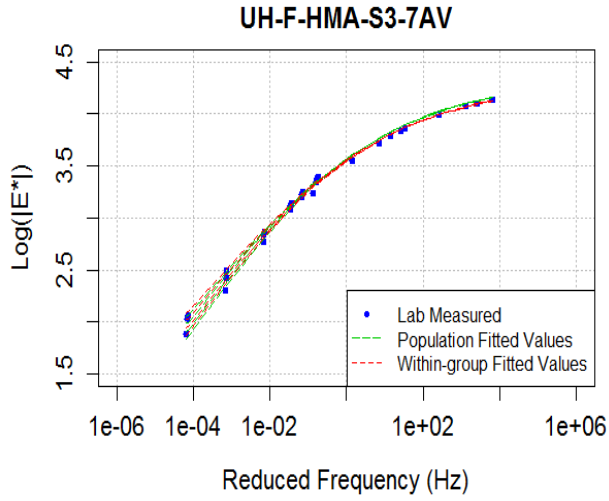
UH-F-HMA-S3-7AV
Log(|E*|)
4.5
3.5
2.5
1.5
1e-06
1e-04
1e-02
1e+02
1e+06
Reduced Frequency (Hz)
Lab Measured
Population Fitted Values
Within-group Fitted Values

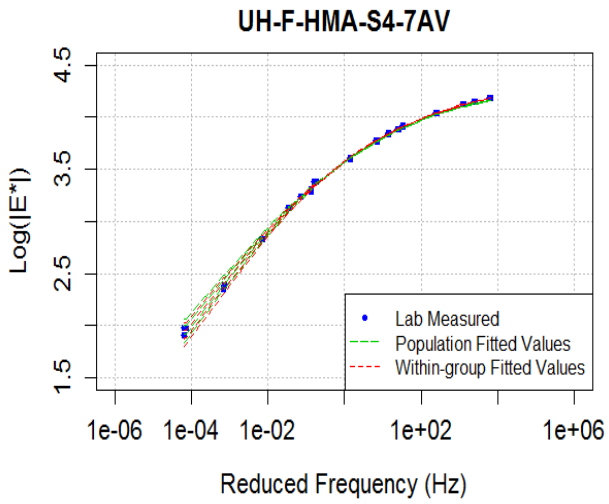
UH-F-HMA-S4-7AV
Log(|E*|)
4.5
3.5
2.5
1.5
1e-06
1e-04
1e-02
1e+02
1e+06
Reduced Frequency (Hz)
Lab Measured
Population Fitted Values
Within-group Fitted Values

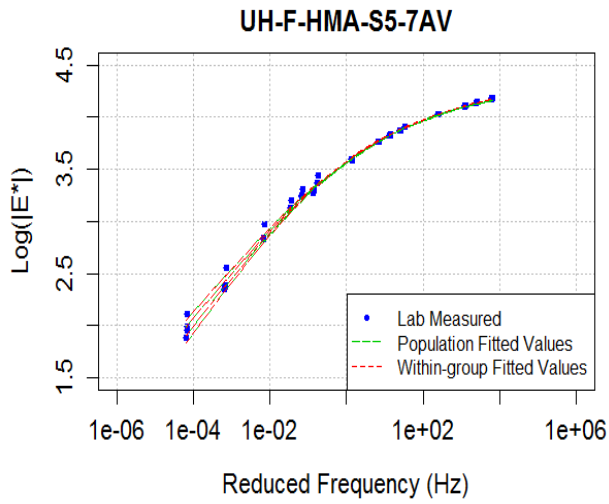
UH-F-HMA-S5-7AV
Log(|E*|)
4.5
3.5
2.5
1.5
1e-06
1e-04
1e-02
1e+02
1e+06
Reduced Frequency (Hz)
Lab Measured
Population Fitted Values
Within-group Fitted Values

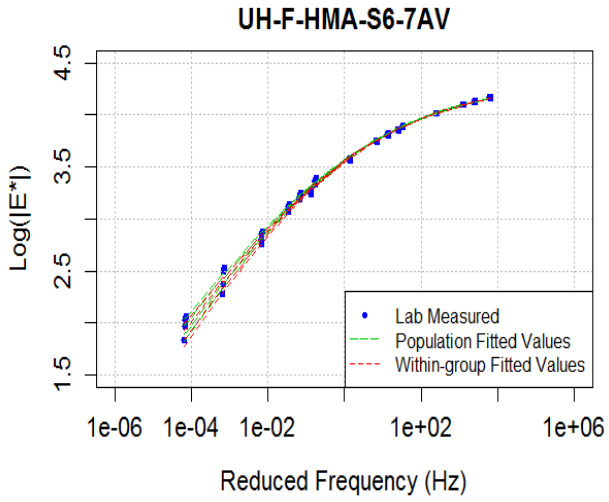
UH-F-HMA-S6-7AV
Log(|E*|)
4.5
3.5
2.5
1.5
1e-06
1e-04
1e-02
1e+02
1e+06
Reduced Frequency (Hz)
Lab Measured
Population Fitted Values
Within-group Fitted Values

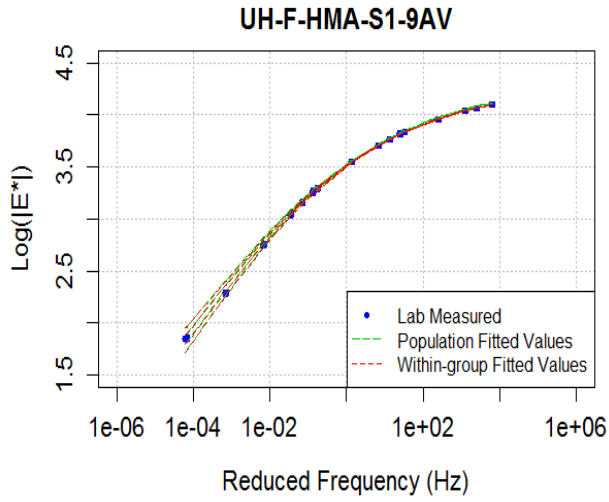
UH-F-HMA-S1-9AV
Log(|E*|)
4.5
3.5
2.5
1.5
1e-06
1e-04
1e-02
1e+02
1e+06
Reduced Frequency (Hz)
Lab Measured
Population Fitted Values
Within-group Fitted Values

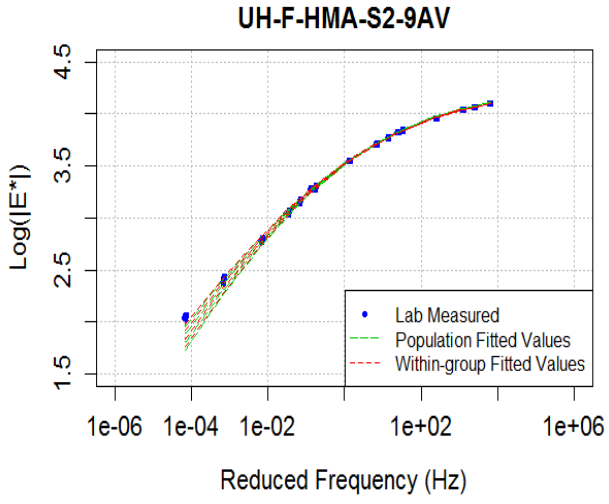
UH-F-HMA-S2-9AV
Log(|E*|)
4.5
3.5
2.5
1.5
1e-06
1e-04
1e-02
1e+02
1e+06
Reduced Frequency (Hz)
Lab Measured
Population Fitted Values
Within-group Fitted Values

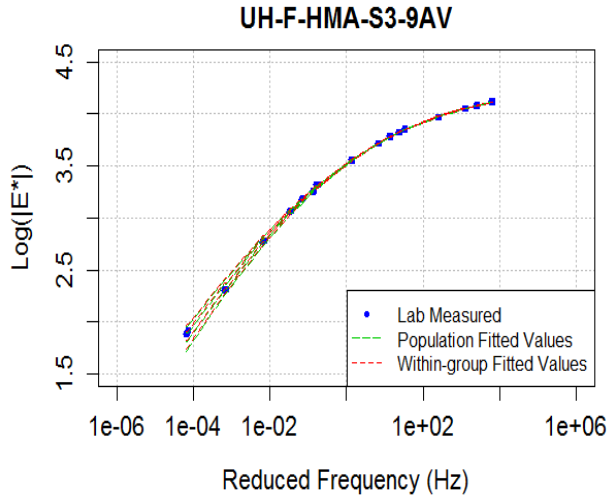
UH-F-HMA-S3-9AV
Log(|E*|)
4.5
3.5
2.5
1.5
1e-06
1e-04
1e-02
1e+02
1e+06
Reduced Frequency (Hz)
Lab Measured
Population Fitted Values
Within-group Fitted Values

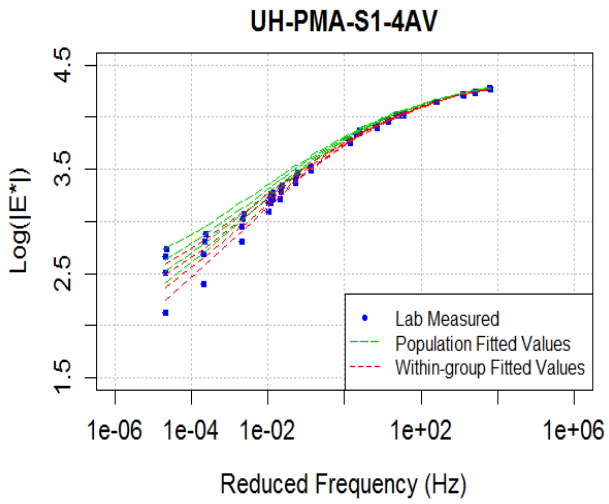
UH-PMA-S1-4AV
Log(|E*|)
Reduced Frequency (Hz)
Lab Measured
Population Fitted Values
Within-group Fitted Values

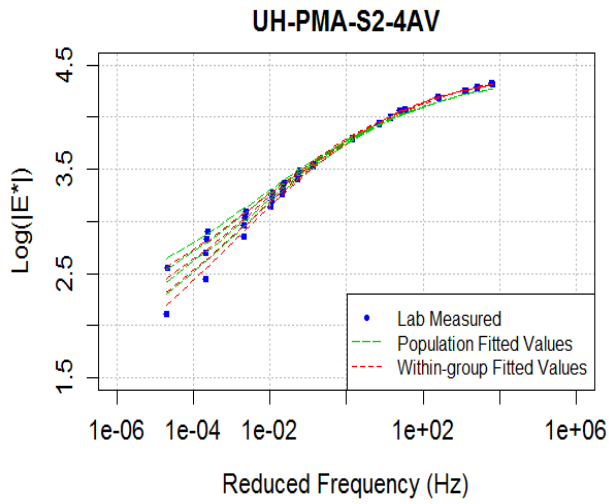
UH-PMA-S2-4AV
Log(|E*|)
Reduced Frequency (Hz)
Lab Measured
Population Fitted Values
Within-group Fitted Values

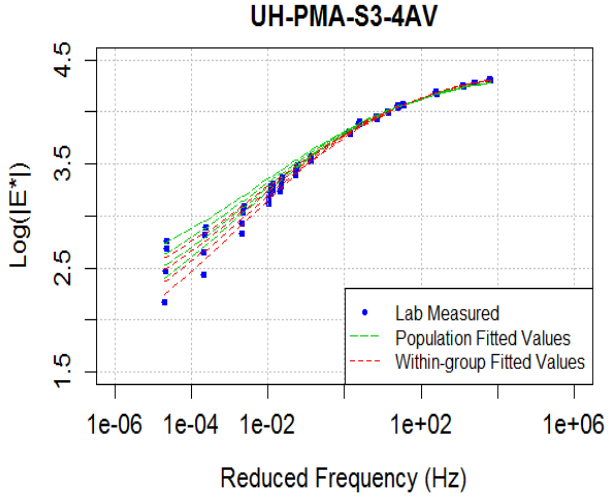
UH-PMA-S3-4AV
Log(|E*|)
Reduced Frequency (Hz)
Lab Measured
Population Fitted Values
Within-group Fitted Values

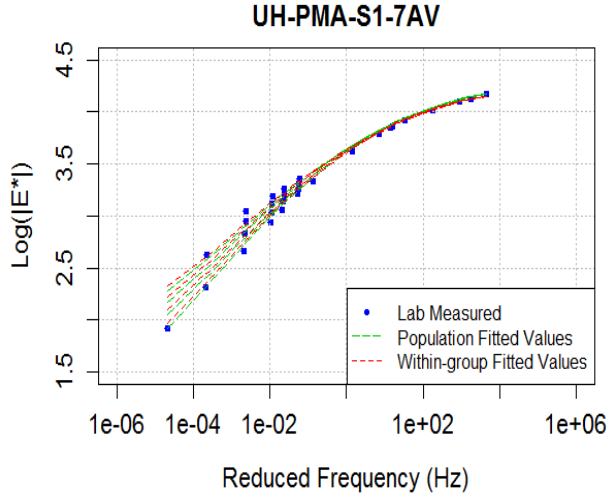
UH-PMA-S1-7AV
Log(|E*|)
Reduced Frequency (Hz)
Lab Measured
Population Fitted Values
Within-group Fitted Values

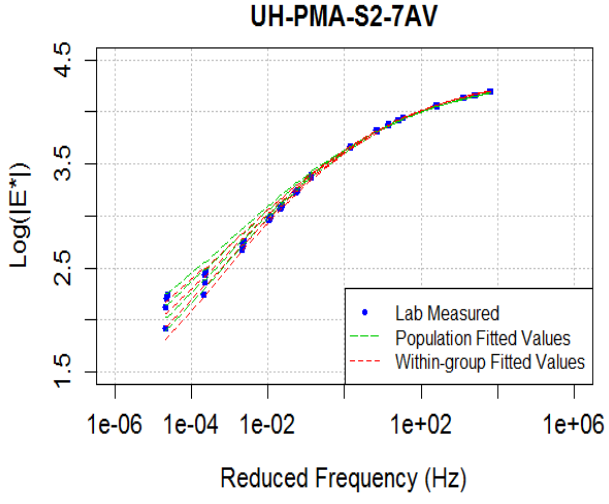
UH-PMA-S2-7AV
Log(|E*|)
Reduced Frequency (Hz)
Lab Measured
Population Fitted Values
Within-group Fitted Values

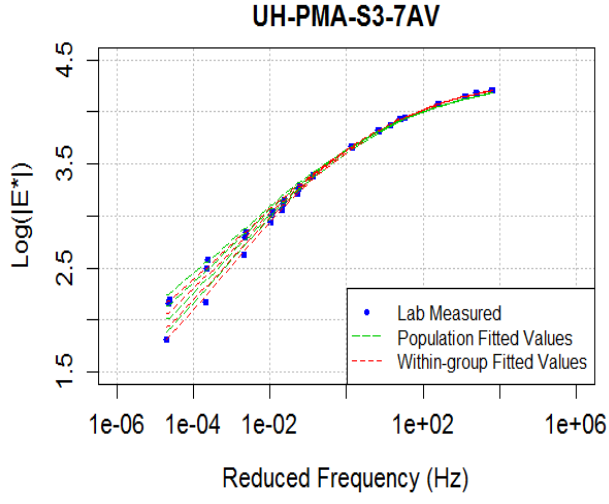
UH-PMA-S3-7AV
Log(|E*|)
Reduced Frequency (Hz)
Lab Measured
Population Fitted Values
Within-group Fitted Values

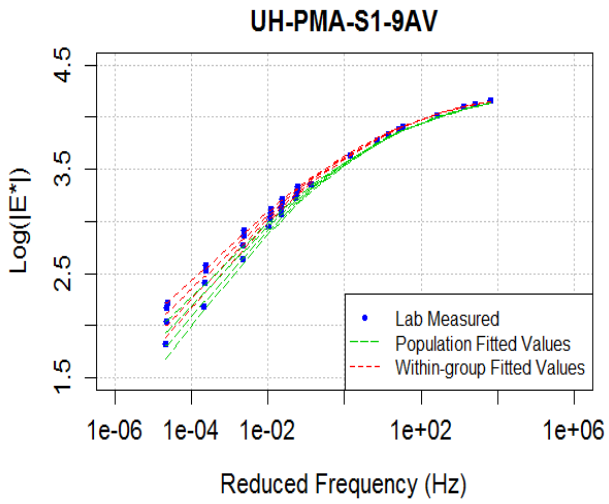
UH-PMA-S1-9AV
Log(|E*|)
Reduced Frequency (Hz)
Lab Measured
Population Fitted Values
Within-group Fitted Values

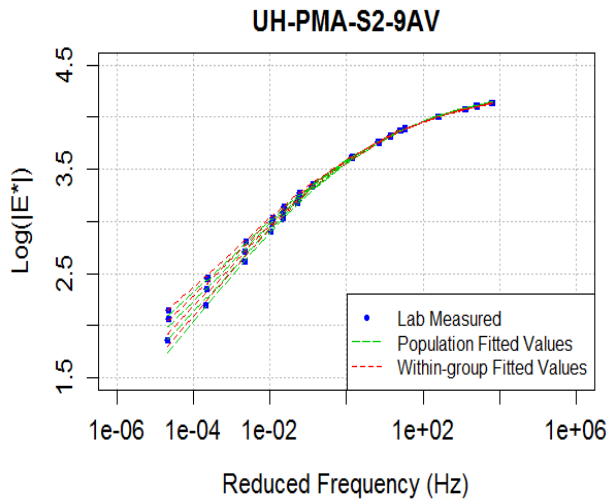
UH-PMA-S2-9AV
Log(|E*|)
Reduced Frequency (Hz)
Lab Measured
Population Fitted Values
Within-group Fitted Values

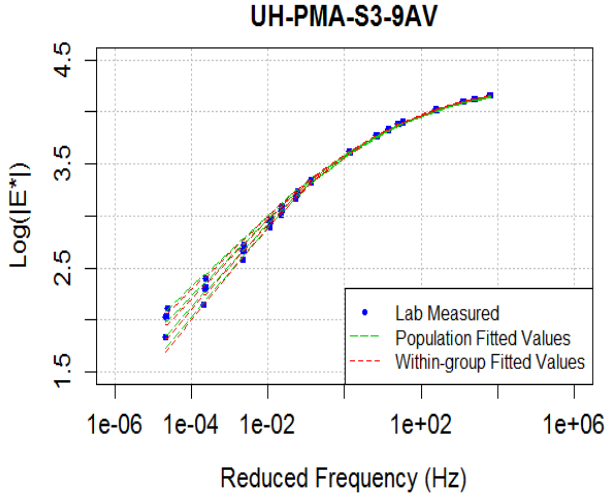
UH-PMA-S3-9AV
Log(|E*|)
Reduced Frequency (Hz)
Lab Measured
Population Fitted Values
Within-group Fitted Values

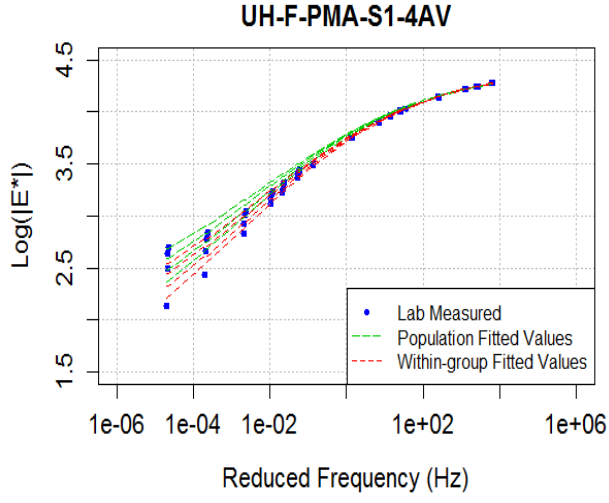
UH-F-PMA-S1-4AV
Log(|E*|)
Reduced Frequency (Hz)
Lab Measured
Population Fitted Values
Within-group Fitted Values

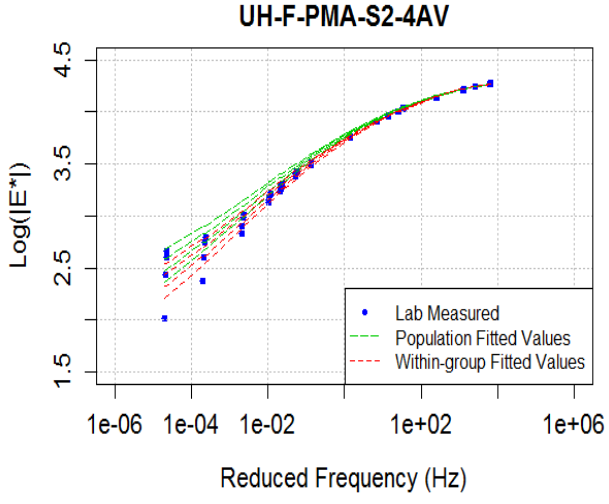
UH-F-PMA-S2-4AV
Log(|E*|)
Reduced Frequency (Hz)
Lab Measured
Population Fitted Values
Within-group Fitted Values

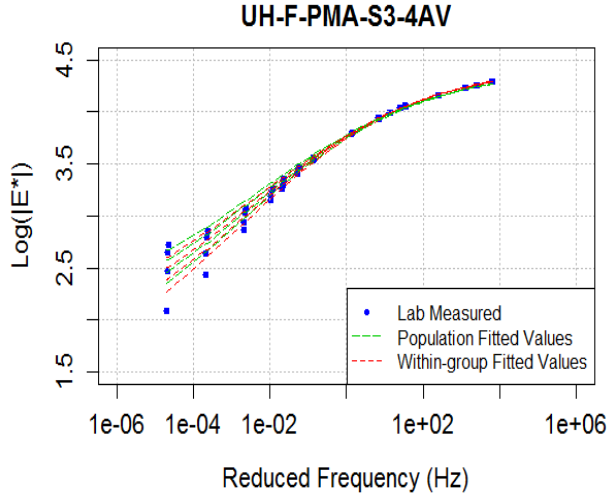
UH-F-PMA-S3-4AV
Log(|E*|)
Reduced Frequency (Hz)
Lab Measured
Population Fitted Values
Within-group Fitted Values

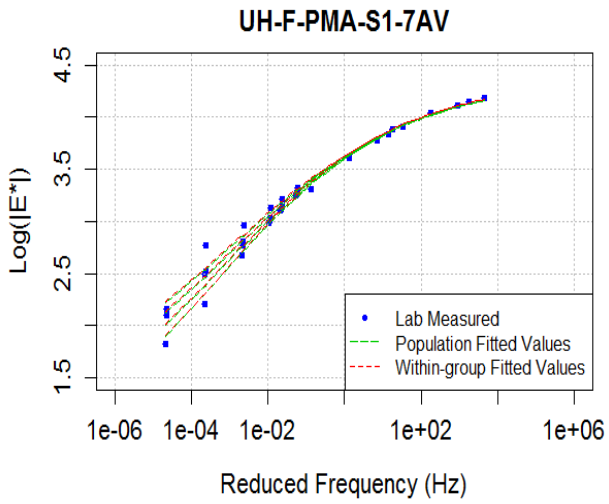
UH-F-PMA-S1-7AV
Log(|E*|)
Reduced Frequency (Hz)
Lab Measured
Population Fitted Values
Within-group Fitted Values

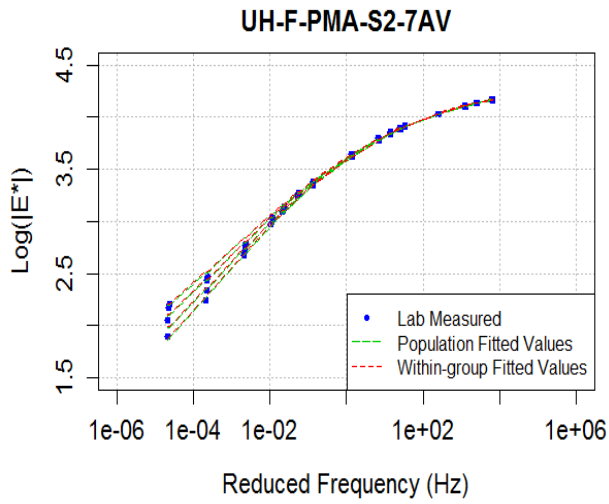
UH-F-PMA-S2-7AV
Log(|E*|)
Reduced Frequency (Hz)
Lab Measured
Population Fitted Values
Within-group Fitted Values

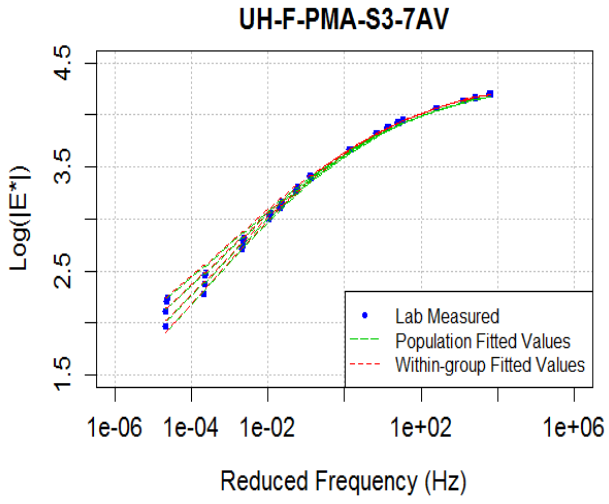
UH-F-PMA-S3-7AV
Log(|E*|)
Reduced Frequency (Hz)
Lab Measured
Population Fitted Values
Within-group Fitted Values

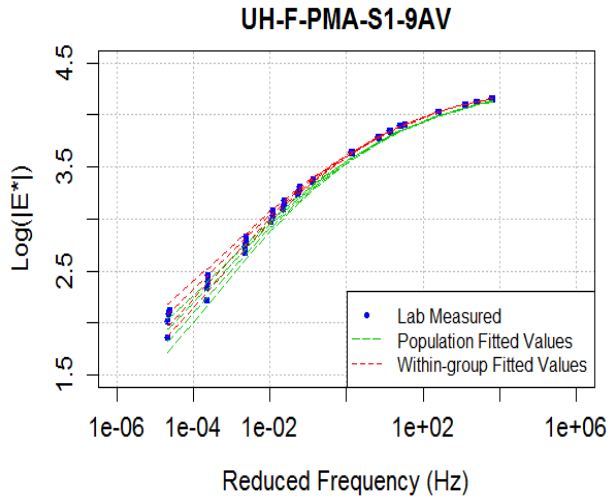
UH-F-PMA-S1-9AV
Log(|E*|)
Reduced Frequency (Hz)
Lab Measured
Population Fitted Values
Within-group Fitted Values

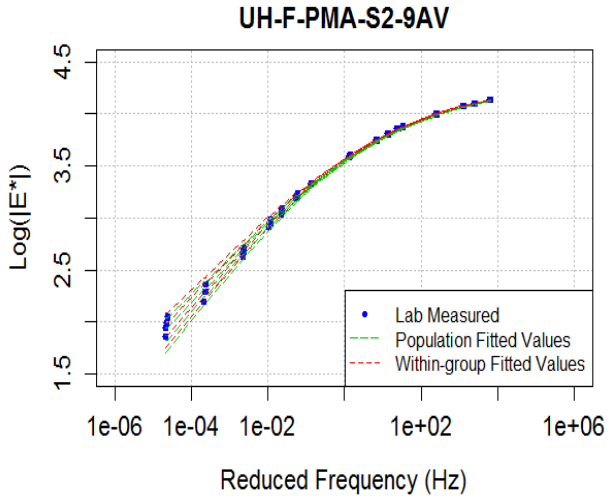
UH-F-PMA-S2-9AV
Log(|E*|)
Reduced Frequency (Hz)
Lab Measured
Population Fitted Values
Within-group Fitted Values

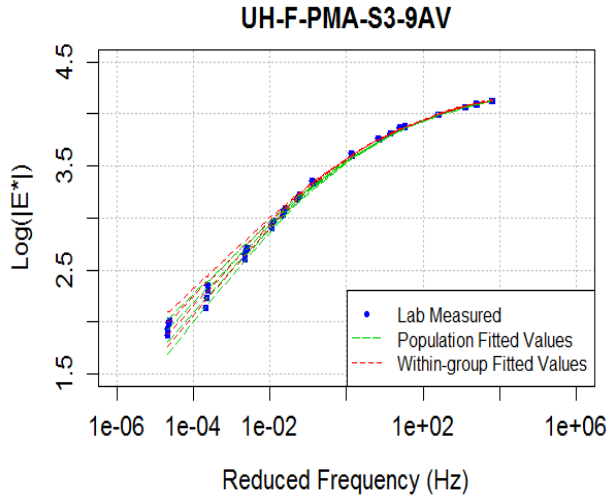
UH-F-PMA-S3-9AV
Log(|E*|)
Reduced Frequency (Hz)
Lab Measured
Population Fitted Values
Within-group Fitted Values

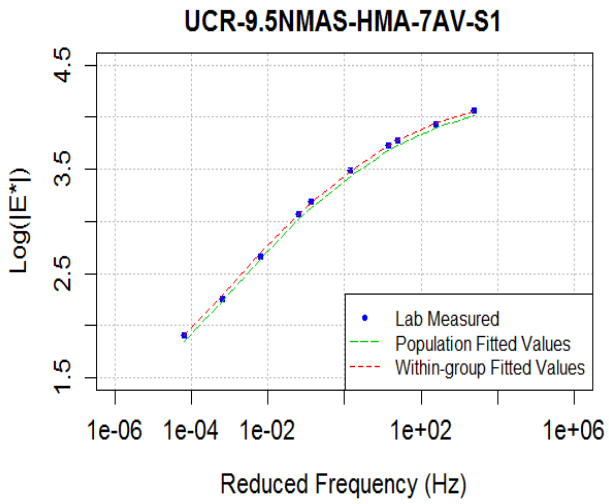
UCR-9.5NMAS-HMA-7AV-S1
Log(|E*|)
1.5
2.5
3.5
4.5
1e-06
1e-04
1e-02
1e+02
1e+06
Reduced Frequency (Hz)
Lab Measured
Population Fitted Values
Within-group Fitted Values

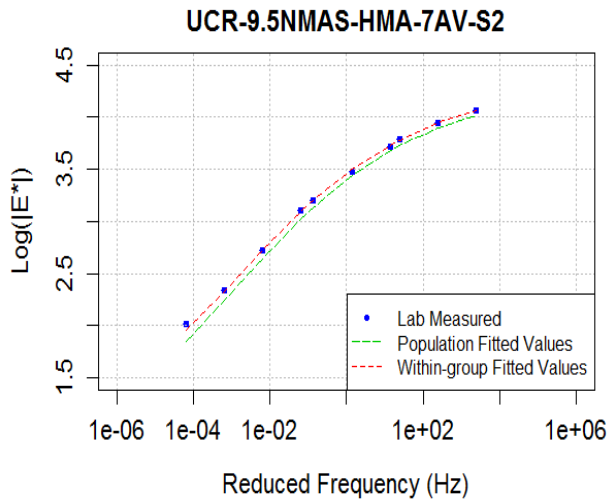
UCR-9.5NMAS-HMA-7AV-S2
Log(|E*|)
1.5
2.5
3.5
4.5
1e-06
1e-04
1e-02
1e+02
1e+06
Reduced Frequency (Hz)
Lab Measured
Population Fitted Values
Within-group Fitted Values

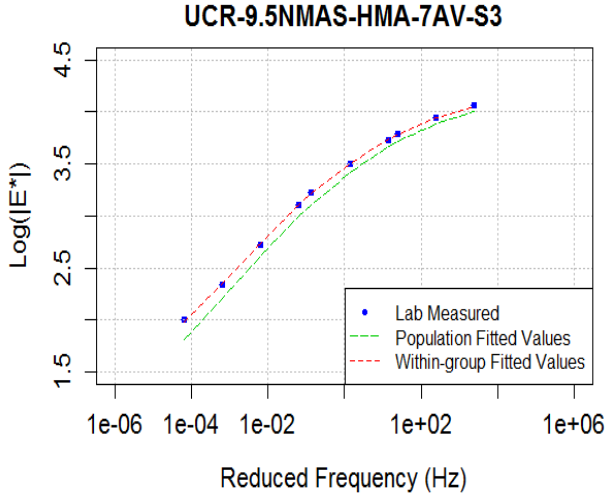
UCR-9.5NMAS-HMA-7AV-S3
Log(|E*|)
1.5
2.5
3.5
4.5
1e-06
1e-04
1e-02
1e+02
1e+06
Reduced Frequency (Hz)
Lab Measured
Population Fitted Values
Within-group Fitted Values

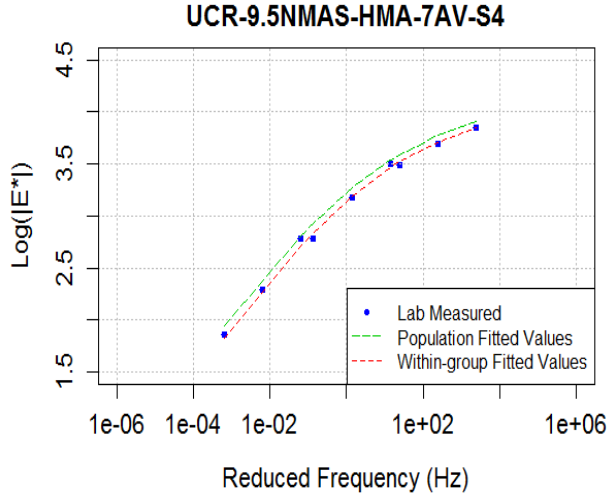
UCR-9.5NMAS-HMA-7AV-S4
Log(|E*|)
1.5
2.5
3.5
4.5
1e-06
1e-04
1e-02
1e+02
1e+06
Reduced Frequency (Hz)
Lab Measured
Population Fitted Values
Within-group Fitted Values

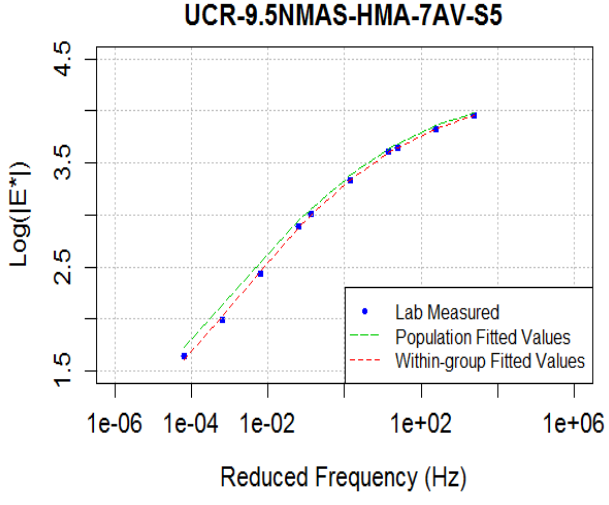
UCR-9.5NMAS-HMA-7AV-S5
Log(|E*|)
1.5
2.5
3.5
4.5
1e-06
1e-04
1e-02
1e+02
1e+06
Reduced Frequency (Hz)
Lab Measured
Population Fitted Values
Within-group Fitted Values

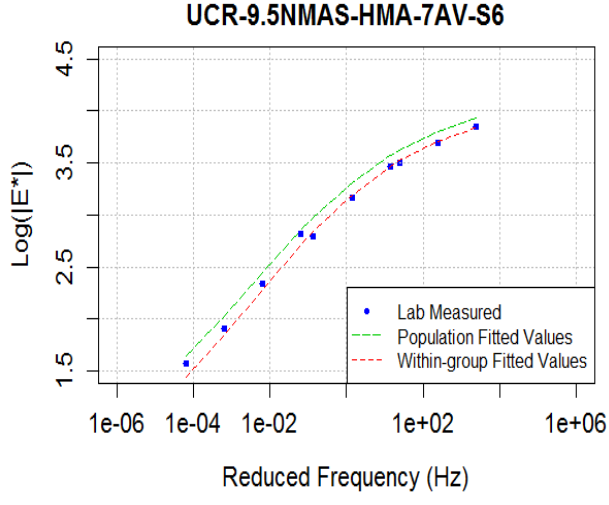
UCR-9.5NMAS-HMA-7AV-S6
Log(|E*|)
1.5
2.5
3.5
4.5
1e-06
1e-04
1e-02
1e+02
1e+06
Reduced Frequency (Hz)
Lab Measured
Population Fitted Values
Within-group Fitted Values

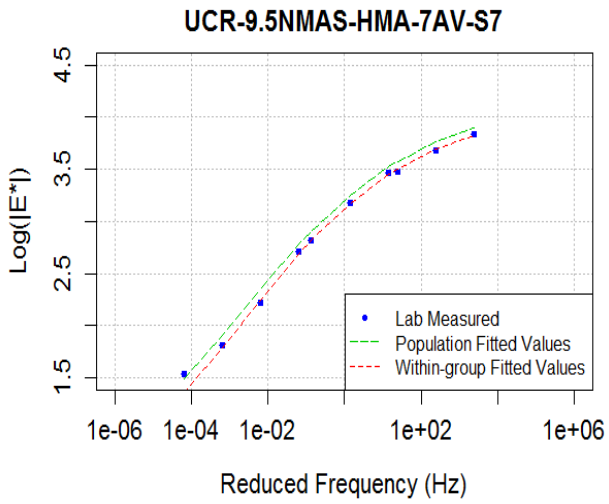
UCR-9.5NMAS-HMA-7AV-S7
Log(|E*|)
4.5
3.5
2.5
1.5
1e-06
1e-04
1e-02
1e+02
1e+06
Reduced Frequency (Hz)
Lab Measured
Population Fitted Values
Within-group Fitted Values

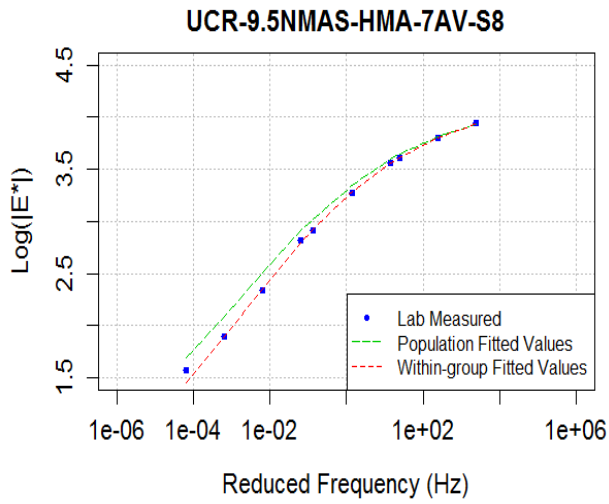
UCR-9.5NMAS-HMA-7AV-S8
Log(|E*|)
4.5
3.5
2.5
1.5
1e-06
1e-04
1e-02
1e+02
1e+06
Reduced Frequency (Hz)
Lab Measured
Population Fitted Values
Within-group Fitted Values

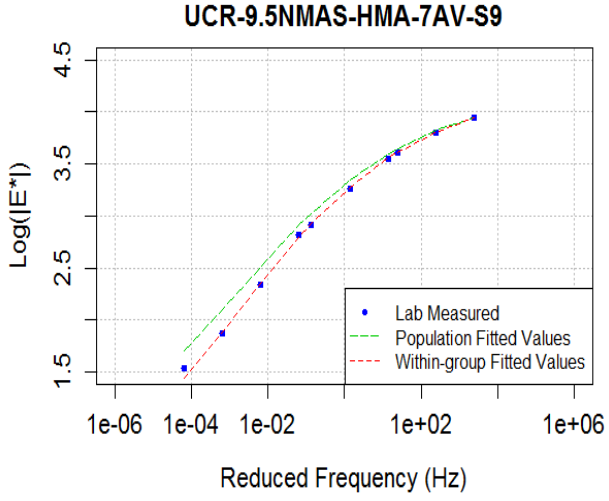
UCR-9.5NMAS-HMA-7AV-S9
Log(|E*|)
4.5
3.5
2.5
1.5
1e-06
1e-04
1e-02
1e+02
1e+06
Reduced Frequency (Hz)
Lab Measured
Population Fitted Values
Within-group Fitted Values

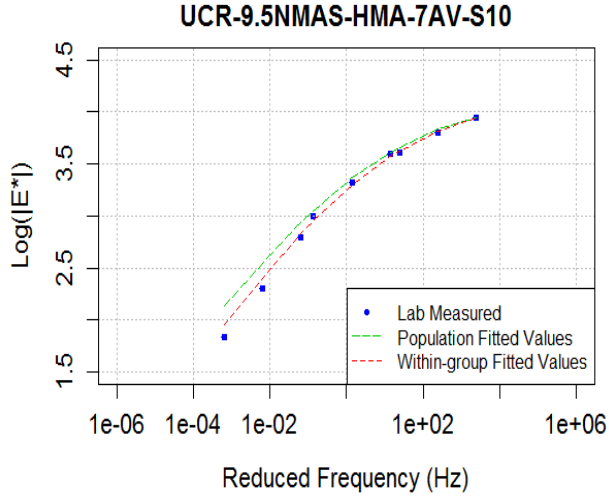
UCR-9.5NMAS-HMA-7AV-S10
Log(|E*|)
4.5
3.5
2.5
1.5
1e-06
1e-04
1e-02
1e+02
1e+06
Reduced Frequency (Hz)
Lab Measured
Population Fitted Values
Within-group Fitted Values

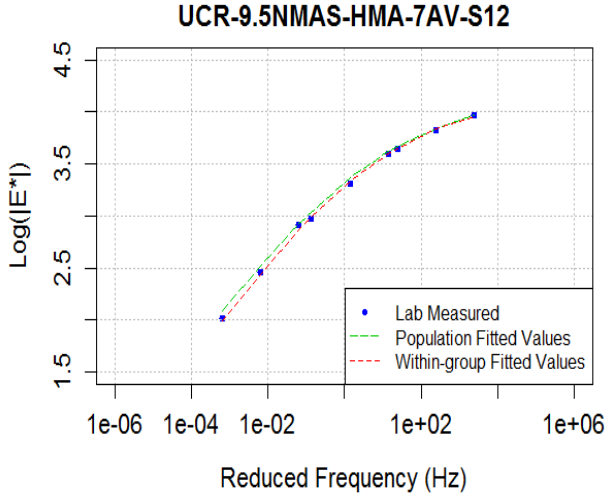
UCR-9.5NMAS-HMA-7AV-S12
Log(|E*|)
4.5
3.5
2.5
1.5
1e-06
1e-04
1e-02
1e+02
1e+06
Reduced Frequency (Hz)
Lab Measured
Population Fitted Values
Within-group Fitted Values

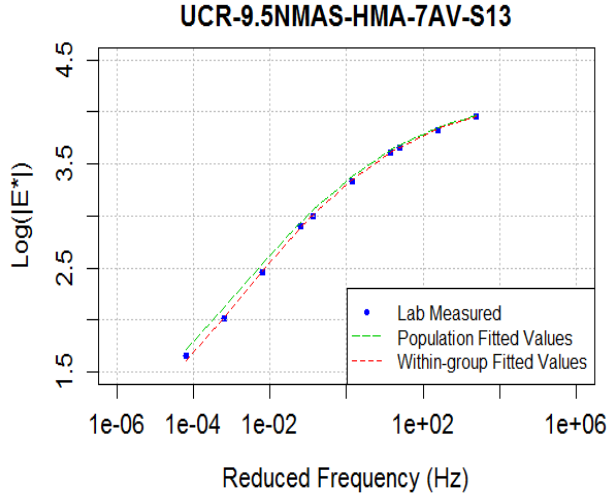
UCR-9.5NMAS-HMA-7AV-S13
Log(|E*|)
4.5
3.5
2.5
1.5
1e-06
1e-04
1e-02
1e+02
1e+06
Reduced Frequency (Hz)
Lab Measured
Population Fitted Values
Within-group Fitted Values

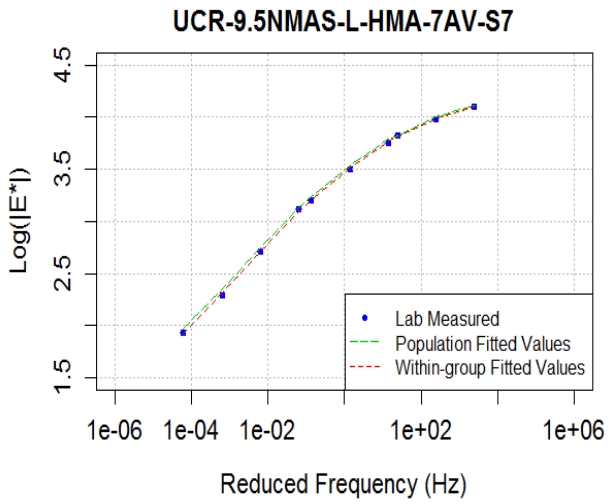
UCR-9.5NMAS-L-HMA-7AV-S7
Log(|E*|)
4.5
3.5
2.5
1.5
1e-06
1e-04
1e-02
1e+02
1e+06
Reduced Frequency (Hz)
Lab Measured
Population Fitted Values
Within-group Fitted Values

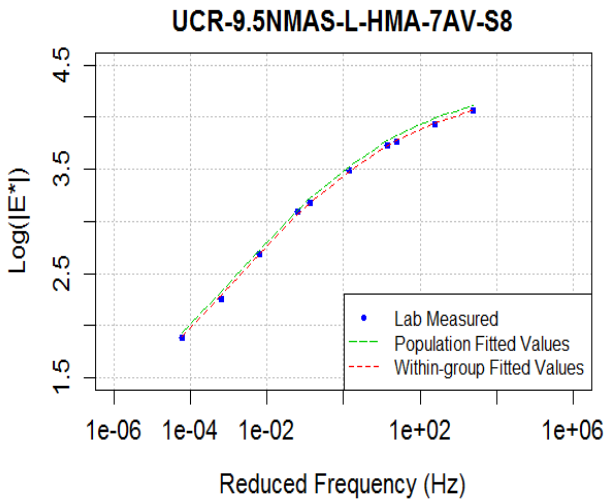
UCR-9.5NMAS-L-HMA-7AV-S8
Log(|E*|)
4.5
3.5
2.5
1.5
1e-06
1e-04
1e-02
1e+02
1e+06
Reduced Frequency (Hz)
Lab Measured
Population Fitted Values
Within-group Fitted Values

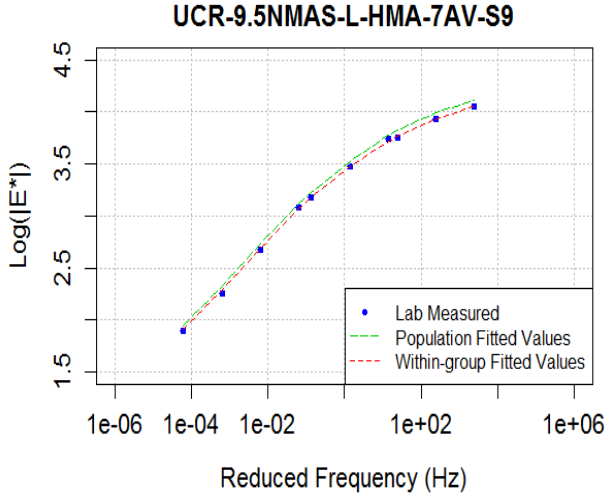
UCR-9.5NMAS-L-HMA-7AV-S9
Log(|E*|)
4.5
3.5
2.5
1.5
1e-06
1e-04
1e-02
1e+02
1e+06
Reduced Frequency (Hz)
Lab Measured
Population Fitted Values
Within-group Fitted Values

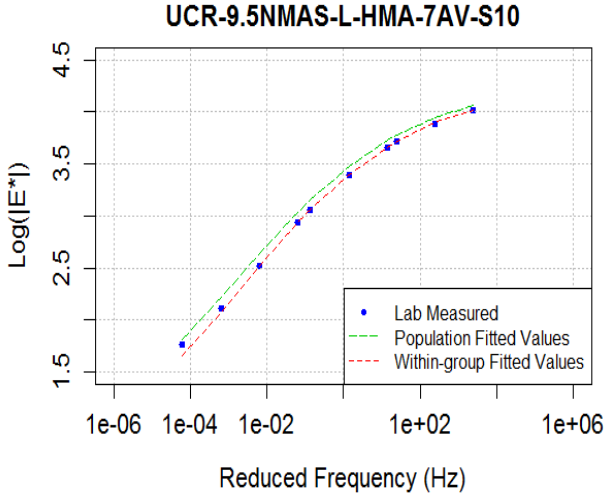
UCR-9.5NMAS-L-HMA-7AV-S10
Log(|E*|)
4.5
3.5
2.5
1.5
1e-06
1e-04
1e-02
1e+02
1e+06
Reduced Frequency (Hz)
Lab Measured
Population Fitted Values
Within-group Fitted Values

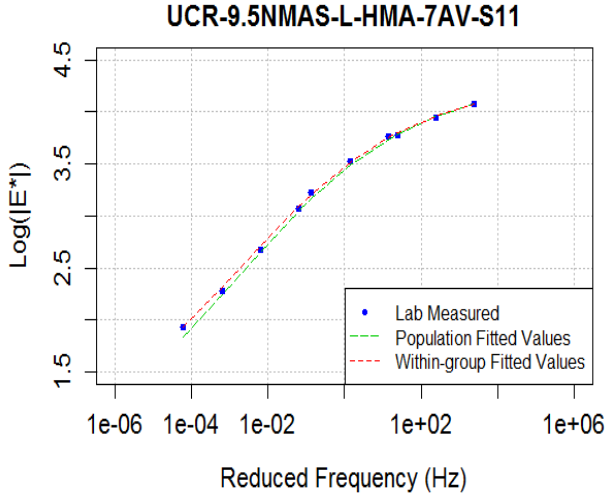
UCR-9.5NMAS-L-HMA-7AV-S11
Log(|E*|)
4.5
3.5
2.5
1.5
1e-06
1e-04
1e-02
1e+02
1e+06
Reduced Frequency (Hz)
Lab Measured
Population Fitted Values
Within-group Fitted Values

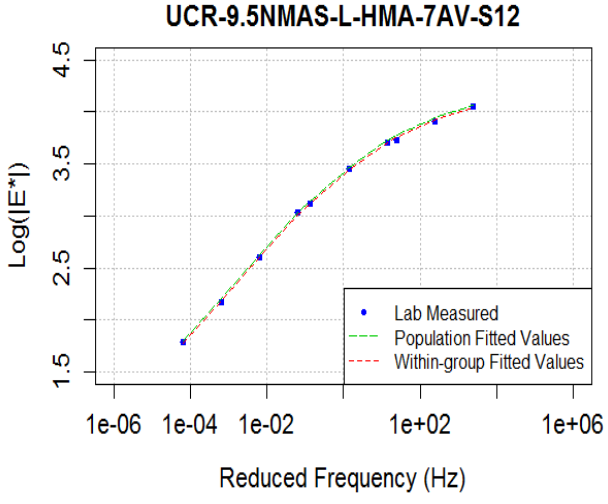
UCR-9.5NMAS-L-HMA-7AV-S12
Log(|E*|)
4.5
3.5
2.5
1.5
1e-06
1e-04
1e-02
1e+02
1e+06
Reduced Frequency (Hz)
Lab Measured
Population Fitted Values
Within-group Fitted Values

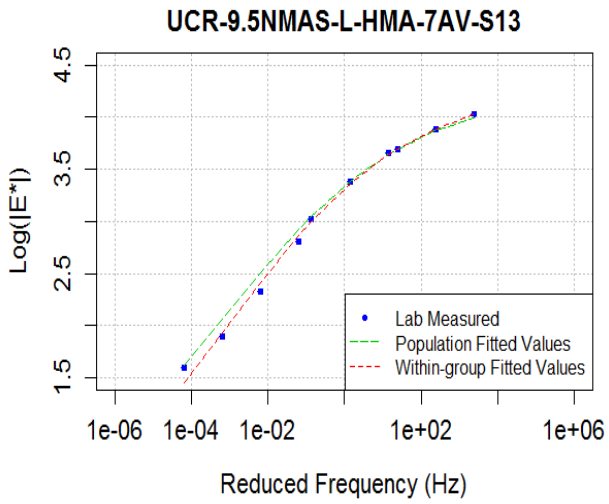
UCR-9.5NMAS-L-HMA-7AV-S13
Log(|E*|)
Reduced Frequency (Hz)
Lab Measured
Population Fitted Values
Within-group Fitted Values

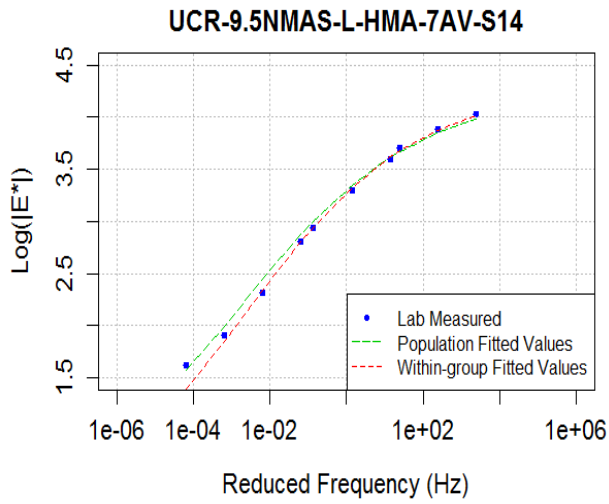
UCR-9.5NMAS-L-HMA-7AV-S14
Log(|E*|)
Reduced Frequency (Hz)
Lab Measured
Population Fitted Values
Within-group Fitted Values

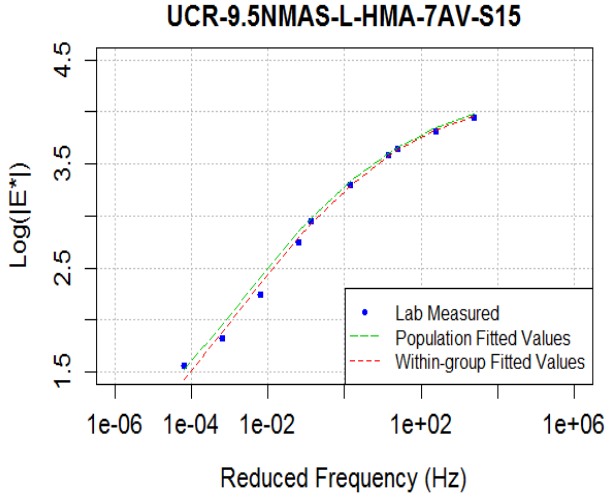
UCR-9.5NMAS-L-HMA-7AV-S15
Log(|E*|)
Reduced Frequency (Hz)
Lab Measured
Population Fitted Values
Within-group Fitted Values

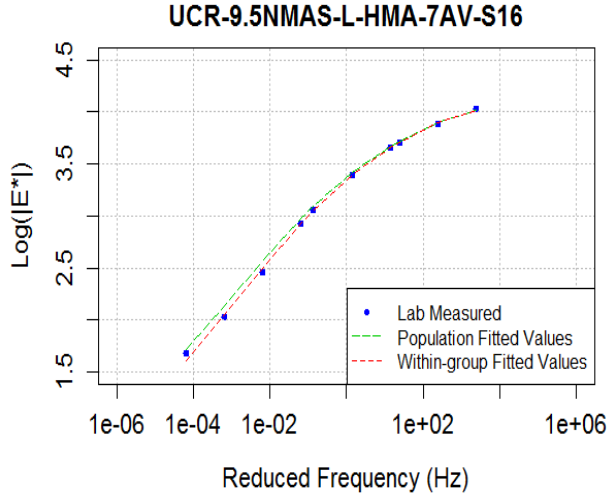
UCR-9.5NMAS-L-HMA-7AV-S16
Log(|E*|)
Reduced Frequency (Hz)
Lab Measured
Population Fitted Values
Within-group Fitted Values

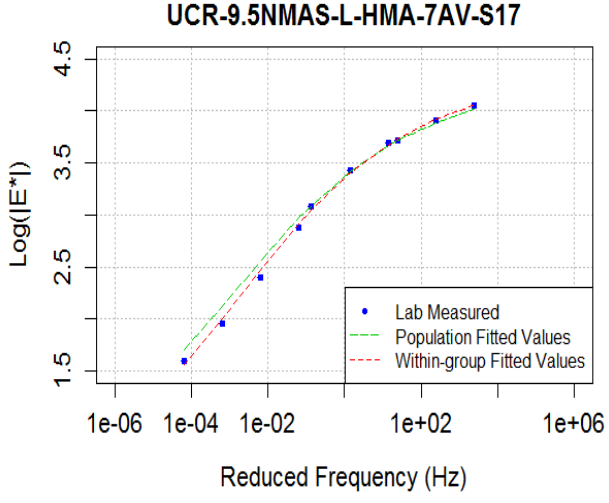
UCR-9.5NMAS-L-HMA-7AV-S17
Log(|E*|)
Reduced Frequency (Hz)
Lab Measured
Population Fitted Values
Within-group Fitted Values

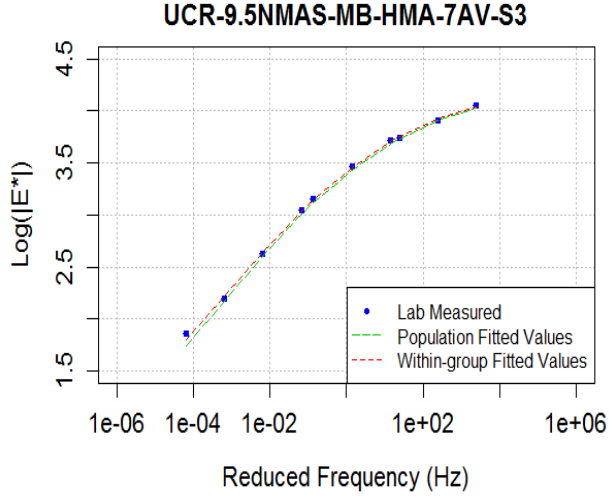
UCR-9.5NMAS-MB-HMA-7AV-S3
Log(|E*|)
Reduced Frequency (Hz)
Lab Measured
Population Fitted Values
Within-group Fitted Values

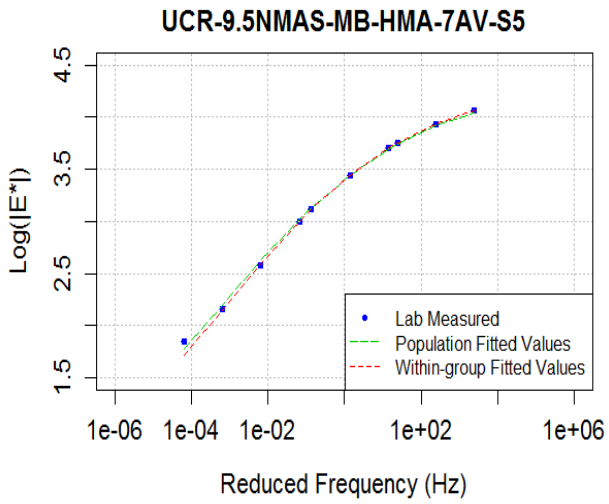
UCR-9.5NMAS-MB-HMA-7AV-S5
Log(|E*|)
4.5
3.5
2.5
1.5
1e-06
1e-04
1e-02
1e+02
1e+06
Reduced Frequency (Hz)
Lab Measured
Population Fitted Values
Within-group Fitted Values

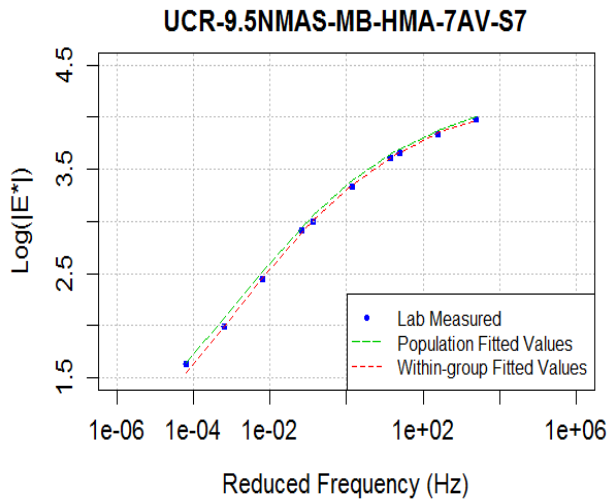
UCR-9.5NMAS-MB-HMA-7AV-S7
Log(|E*|)
4.5
3.5
2.5
1.5
1e-06
1e-04
1e-02
1e+02
1e+06
Reduced Frequency (Hz)
Lab Measured
Population Fitted Values
Within-group Fitted Values

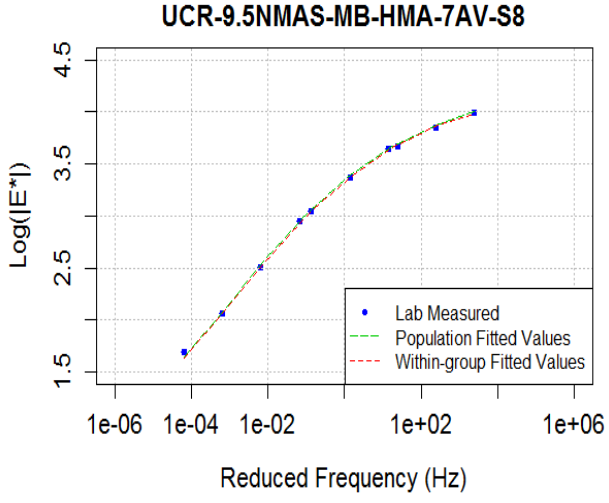
UCR-9.5NMAS-MB-HMA-7AV-S8
Log(|E*|)
4.5
3.5
2.5
1.5
1e-06
1e-04
1e-02
1e+02
1e+06
Reduced Frequency (Hz)
Lab Measured
Population Fitted Values
Within-group Fitted Values

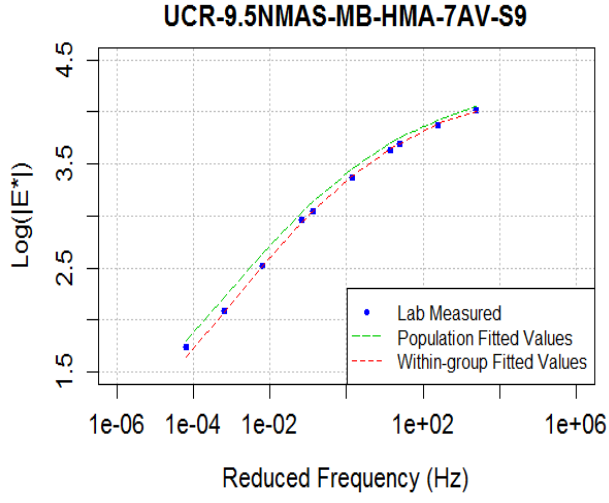
UCR-9.5NMAS-MB-HMA-7AV-S9
Log(|E*|)
4.5
3.5
2.5
1.5
1e-06
1e-04
1e-02
1e+02
1e+06
Reduced Frequency (Hz)
Lab Measured
Population Fitted Values
Within-group Fitted Values

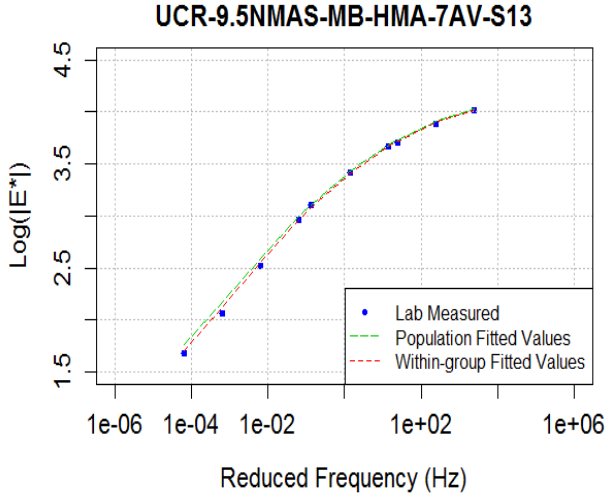
UCR-9.5NMAS-MB-HMA-7AV-S13
Log(|E*|)
4.5
3.5
2.5
1.5
1e-06
1e-04
1e-02
1e+02
1e+06
Reduced Frequency (Hz)
Lab Measured
Population Fitted Values
Within-group Fitted Values

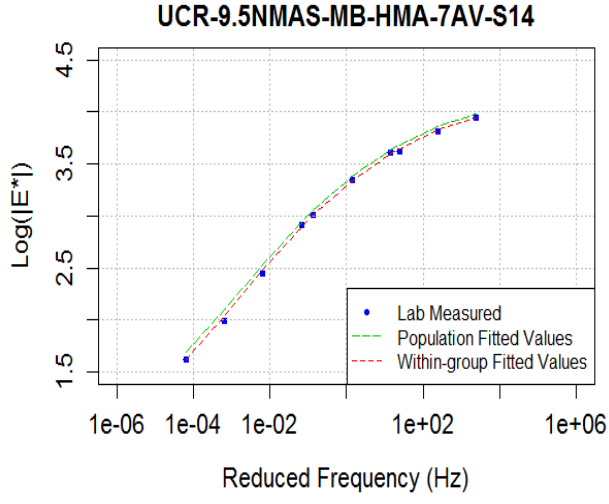
UCR-9.5NMAS-MB-HMA-7AV-S14
Log(|E*|)
4.5
3.5
2.5
1.5
1e-06
1e-04
1e-02
1e+02
1e+06
Reduced Frequency (Hz)
Lab Measured
Population Fitted Values
Within-group Fitted Values

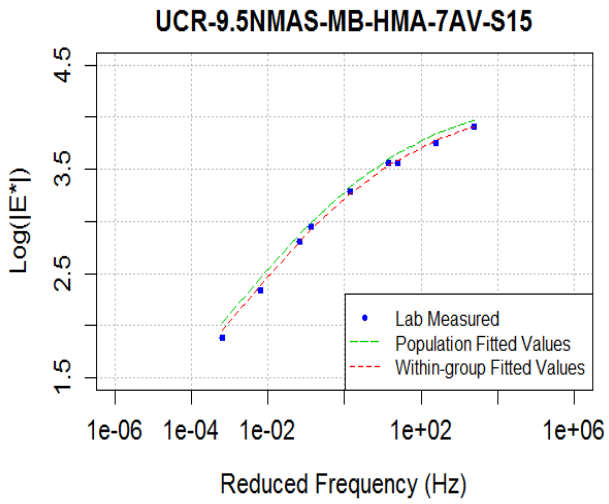
UCR-9.5NMAS-MB-HMA-7AV-S15
Log(|E*|)
Reduced Frequency (Hz)
Lab Measured
Population Fitted Values
Within-group Fitted Values

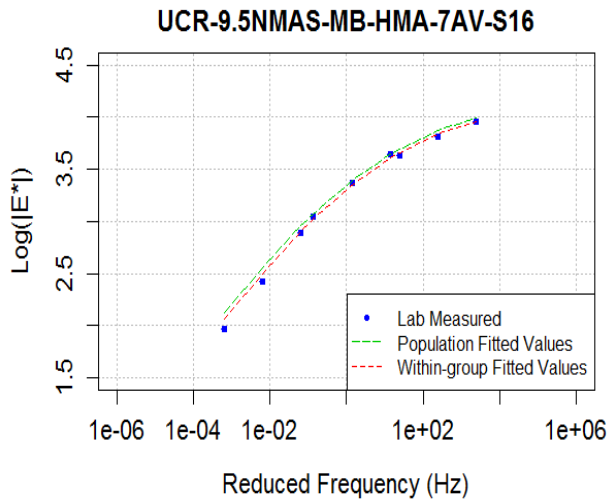
UCR-9.5NMAS-MB-HMA-7AV-S16
Log(|E*|)
Reduced Frequency (Hz)
Lab Measured
Population Fitted Values
Within-group Fitted Values

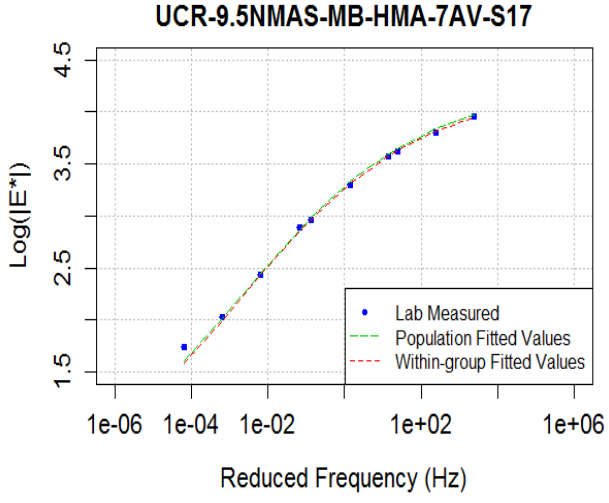
UCR-9.5NMAS-MB-HMA-7AV-S17
Log(|E*|)
Reduced Frequency (Hz)
Lab Measured
Population Fitted Values
Within-group Fitted Values

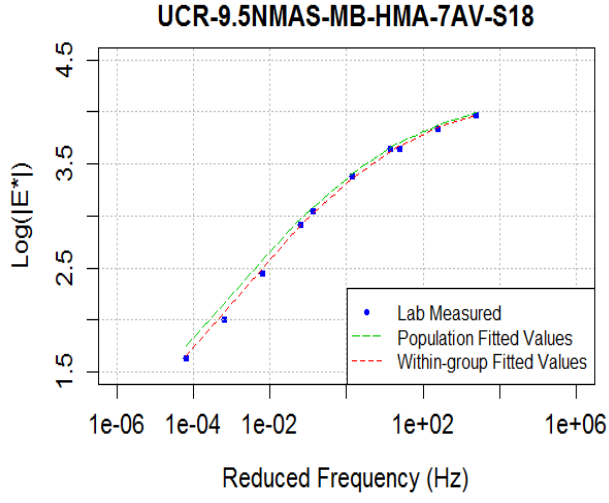
UCR-9.5NMAS-MB-HMA-7AV-S18
Log(|E*|)
Reduced Frequency (Hz)
Lab Measured
Population Fitted Values
Within-group Fitted Values

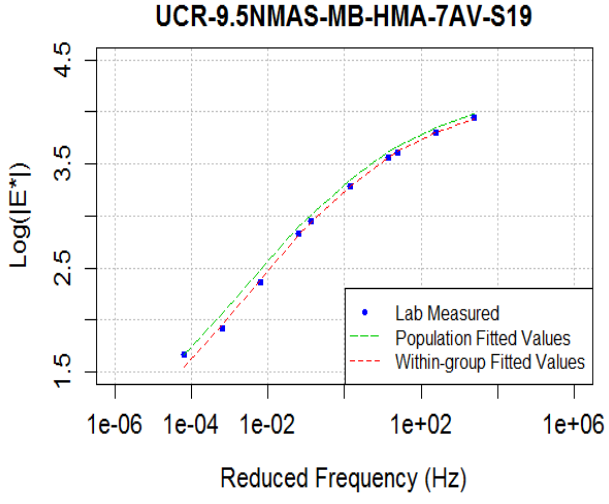
UCR-9.5NMAS-MB-HMA-7AV-S19
Log(|E*|)
Reduced Frequency (Hz)
Lab Measured
Population Fitted Values
Within-group Fitted Values

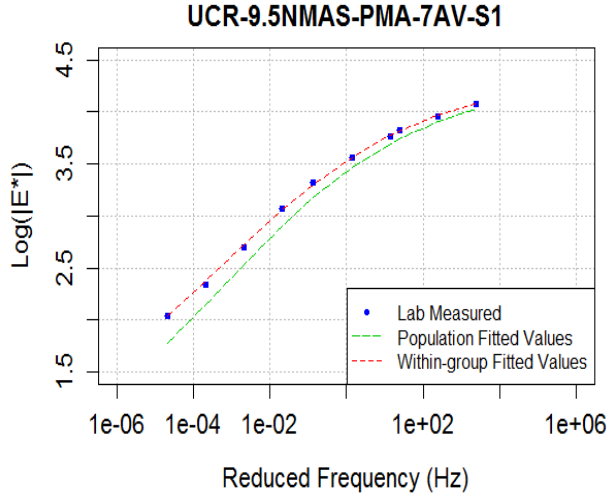
UCR-9.5NMAS-PMA-7AV-S1
Log(|E*|)
Reduced Frequency (Hz)
Lab Measured
Population Fitted Values
Within-group Fitted Values

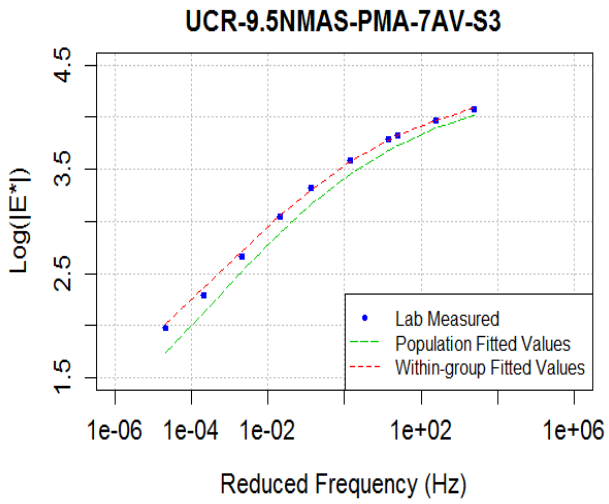
UCR-9.5NMAS-PMA-7AV-S3
Log(|E*|)
4.5
3.5
2.5
1.5
1e-06
1e-04
1e-02
1e+02
1e+06
Reduced Frequency (Hz)
Lab Measured
Population Fitted Values
Within-group Fitted Values

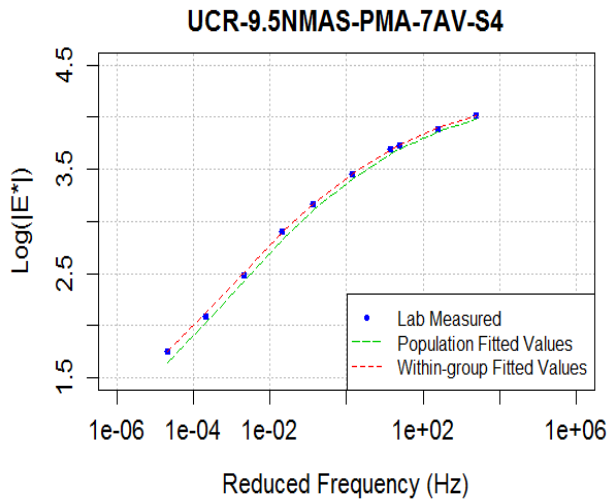
UCR-9.5NMAS-PMA-7AV-S4
Log(|E*|)
4.5
3.5
2.5
1.5
1e-06
1e-04
1e-02
1e+02
1e+06
Reduced Frequency (Hz)
Lab Measured
Population Fitted Values
Within-group Fitted Values

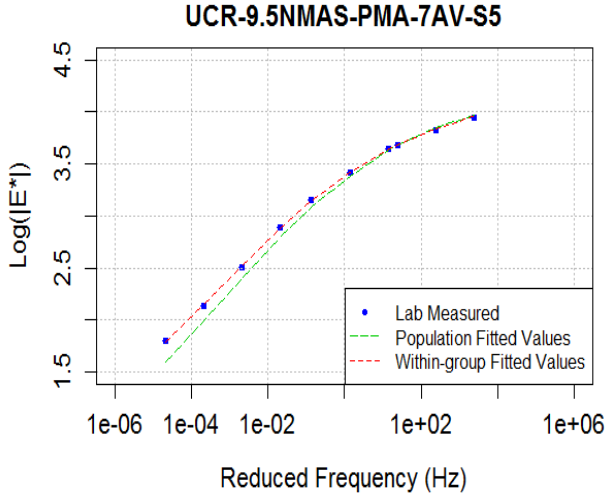
UCR-9.5NMAS-PMA-7AV-S5
Log(|E*|)
4.5
3.5
2.5
1.5
1e-06
1e-04
1e-02
1e+02
1e+06
Reduced Frequency (Hz)
Lab Measured
Population Fitted Values
Within-group Fitted Values

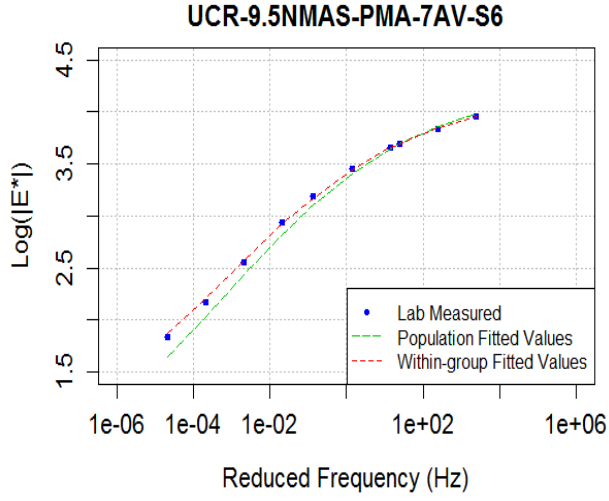
UCR-9.5NMAS-PMA-7AV-S6
Log(|E*|)
4.5
3.5
2.5
1.5
1e-06
1e-04
1e-02
1e+02
1e+06
Reduced Frequency (Hz)
Lab Measured
Population Fitted Values
Within-group Fitted Values

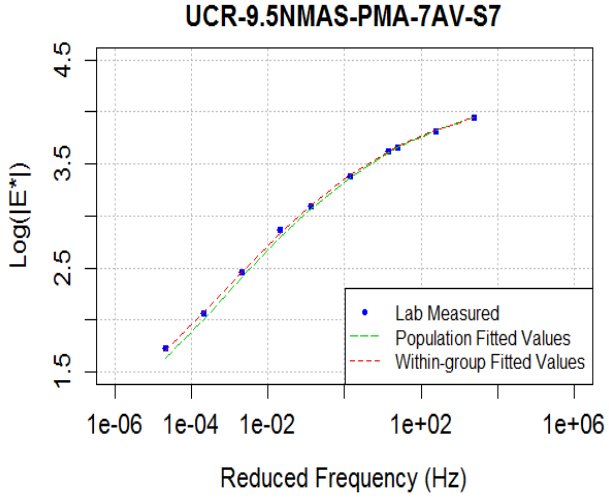
UCR-9.5NMAS-PMA-7AV-S7
Log(|E*|)
4.5
3.5
2.5
1.5
1e-06
1e-04
1e-02
1e+02
1e+06
Reduced Frequency (Hz)
Lab Measured
Population Fitted Values
Within-group Fitted Values

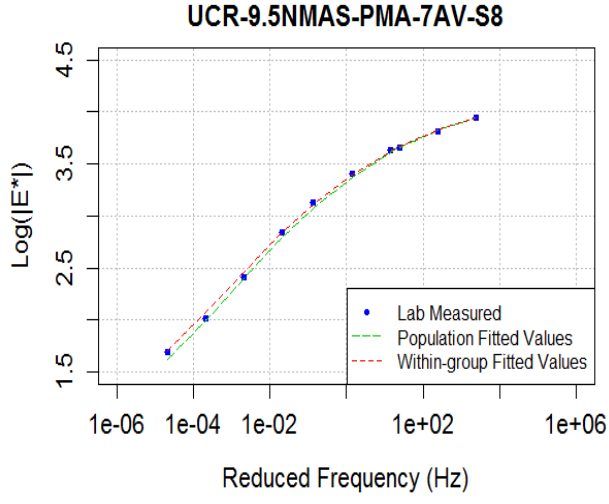
UCR-9.5NMAS-PMA-7AV-S8
Log(|E*|)
4.5
3.5
2.5
1.5
1e-06
1e-04
1e-02
1e+02
1e+06
Reduced Frequency (Hz)
Lab Measured
Population Fitted Values
Within-group Fitted Values

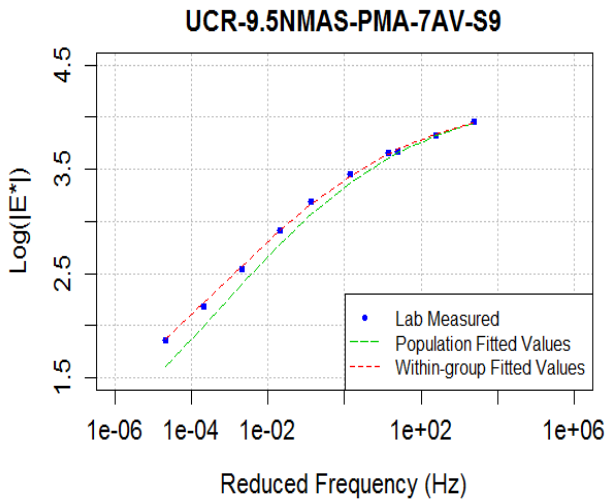
UCR-9.5NMAS-PMA-7AV-S9
Log(|E*|)
1.5
2.5
3.5
4.5
1e-06
1e-04
1e-02
1e+02
1e+06
Reduced Frequency (Hz)
Lab Measured
Population Fitted Values
Within-group Fitted Values

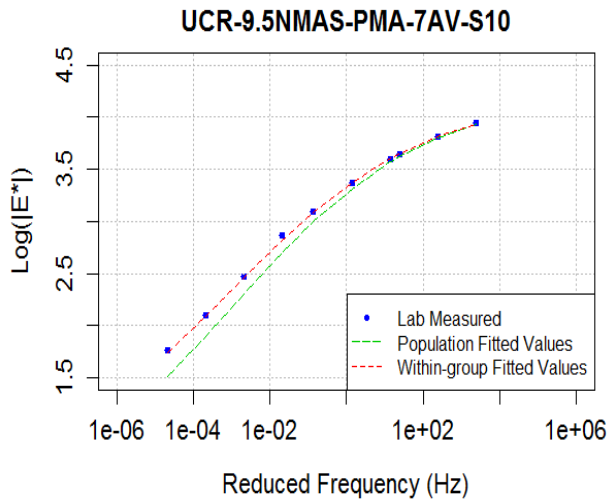
UCR-9.5NMAS-PMA-7AV-S10
Log(|E*|)
1.5
2.5
3.5
4.5
1e-06
1e-04
1e-02
1e+02
1e+06
Reduced Frequency (Hz)
Lab Measured
Population Fitted Values
Within-group Fitted Values

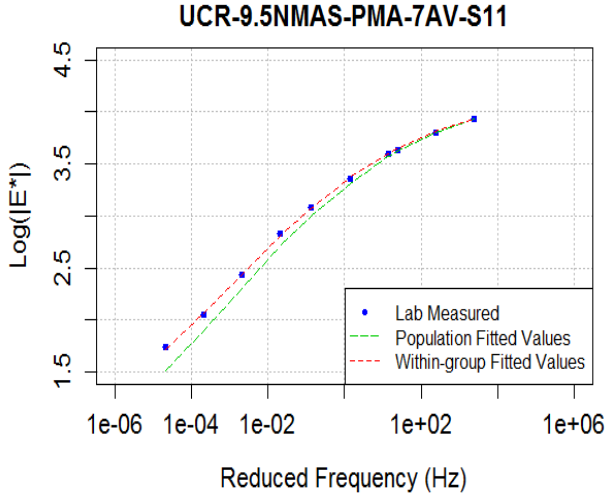
UCR-9.5NMAS-PMA-7AV-S11
Log(|E*|)
1.5
2.5
3.5
4.5
1e-06
1e-04
1e-02
1e+02
1e+06
Reduced Frequency (Hz)
Lab Measured
Population Fitted Values
Within-group Fitted Values

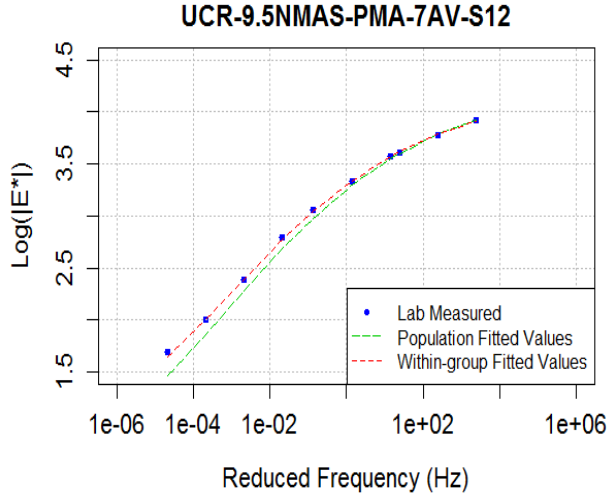
UCR-9.5NMAS-PMA-7AV-S12
Log(|E*|)
1.5
2.5
3.5
4.5
1e-06
1e-04
1e-02
1e+02
1e+06
Reduced Frequency (Hz)
Lab Measured
Population Fitted Values
Within-group Fitted Values

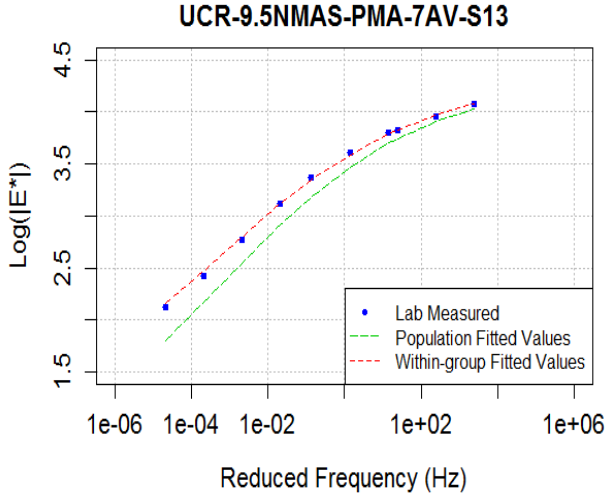
UCR-9.5NMAS-PMA-7AV-S13
Log(|E*|)
1.5
2.5
3.5
4.5
1e-06
1e-04
1e-02
1e+02
1e+06
Reduced Frequency (Hz)
Lab Measured
Population Fitted Values
Within-group Fitted Values

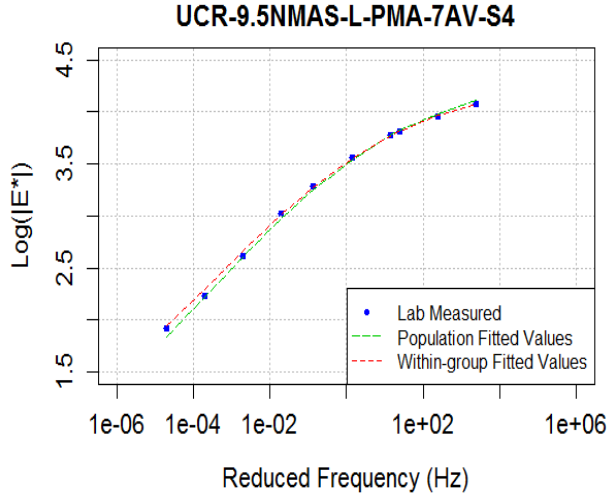
UCR-9.5NMAS-L-PMA-7AV-S4
Log(|E*|)
1.5
2.5
3.5
4.5
1e-06
1e-04
1e-02
1e+02
1e+06
Reduced Frequency (Hz)
Lab Measured
Population Fitted Values
Within-group Fitted Values

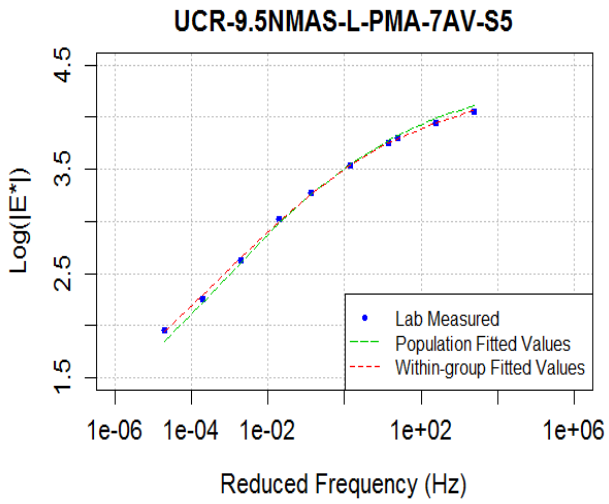
UCR-9.5NMAS-L-PMA-7AV-S5
Log(|E*|)
1.5
2.5
3.5
4.5
1e-06
1e-04
1e-02
1e+02
1e+06
Reduced Frequency (Hz)
Lab Measured
Population Fitted Values
Within-group Fitted Values

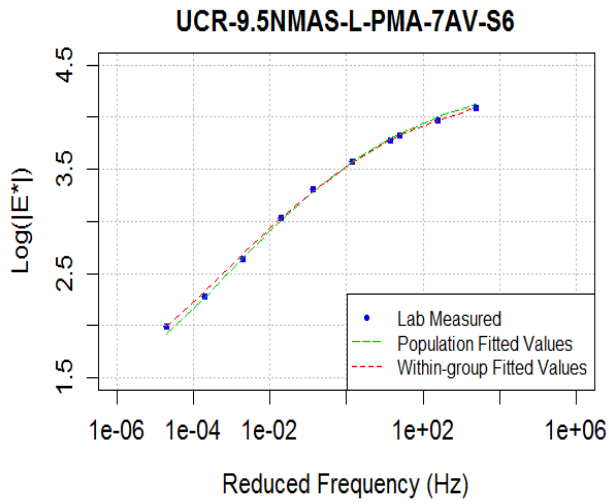
UCR-9.5NMAS-L-PMA-7AV-S6
Log(|E*|)
1.5
2.5
3.5
4.5
1e-06
1e-04
1e-02
1e+02
1e+06
Reduced Frequency (Hz)
Lab Measured
Population Fitted Values
Within-group Fitted Values

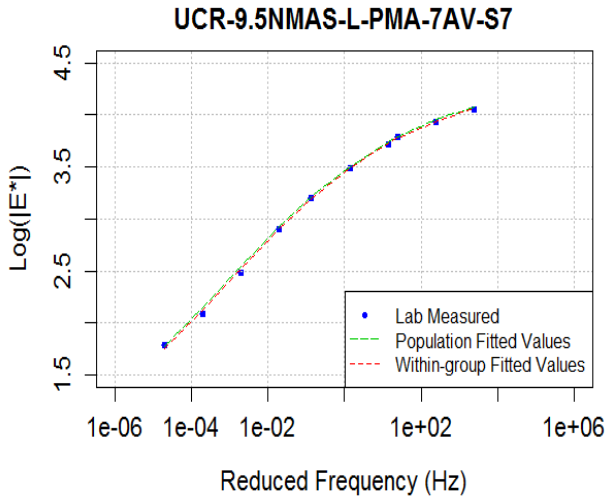
UCR-9.5NMAS-L-PMA-7AV-S7
Log(|E*|)
1.5
2.5
3.5
4.5
1e-06
1e-04
1e-02
1e+02
1e+06
Reduced Frequency (Hz)
Lab Measured
Population Fitted Values
Within-group Fitted Values

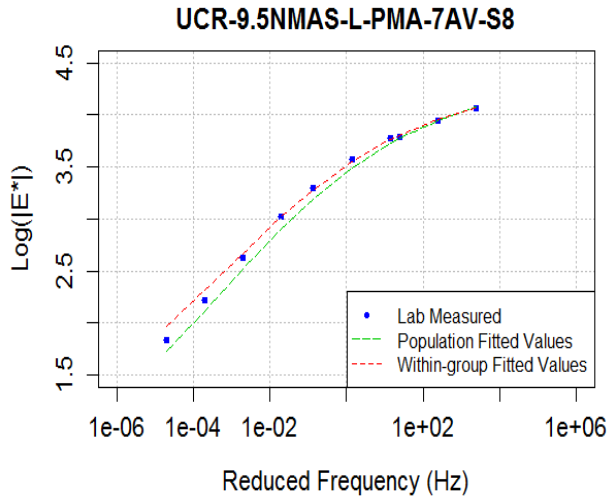
UCR-9.5NMAS-L-PMA-7AV-S8
Log(|E*|)
1.5
2.5
3.5
4.5
1e-06
1e-04
1e-02
1e+02
1e+06
Reduced Frequency (Hz)
Lab Measured
Population Fitted Values
Within-group Fitted Values

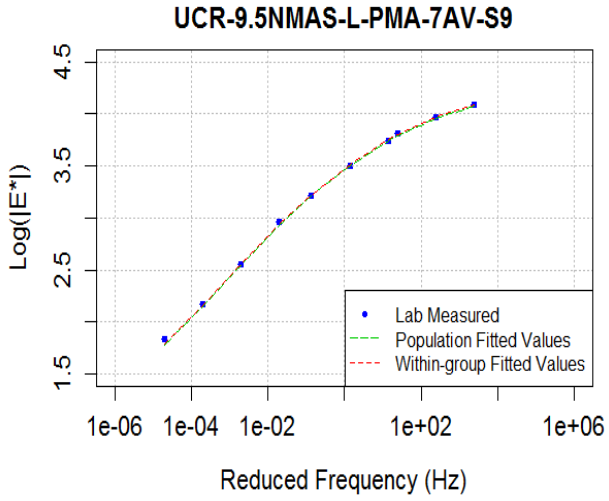
UCR-9.5NMAS-L-PMA-7AV-S9
Log(|E*|)
1.5
2.5
3.5
4.5
1e-06
1e-04
1e-02
1e+02
1e+06
Reduced Frequency (Hz)
Lab Measured
Population Fitted Values
Within-group Fitted Values

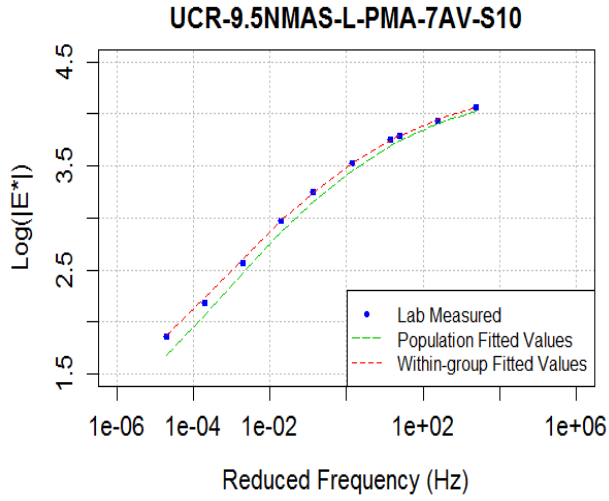
UCR-9.5NMAS-L-PMA-7AV-S10
Log(|E*|)
1.5
2.5
3.5
4.5
1e-06
1e-04
1e-02
1e+02
1e+06
Reduced Frequency (Hz)
Lab Measured
Population Fitted Values
Within-group Fitted Values

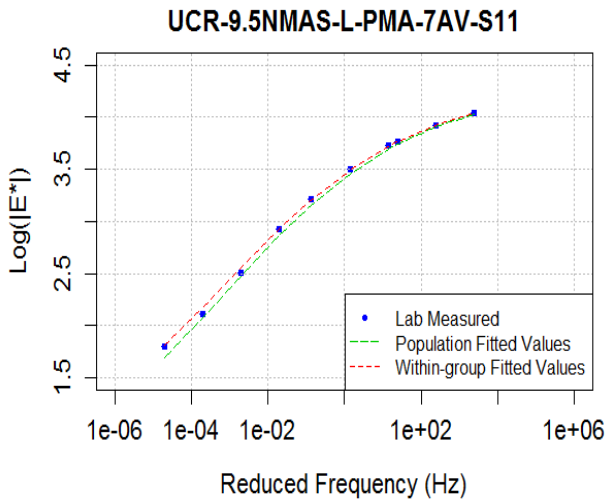
UCR-9.5NMAS-L-PMA-7AV-S11
Log(|E*|)
4.5
3.5
2.5
1.5
1e-06
1e-04
1e-02
1e+02
1e+06
Reduced Frequency (Hz)
Lab Measured
Population Fitted Values
Within-group Fitted Values

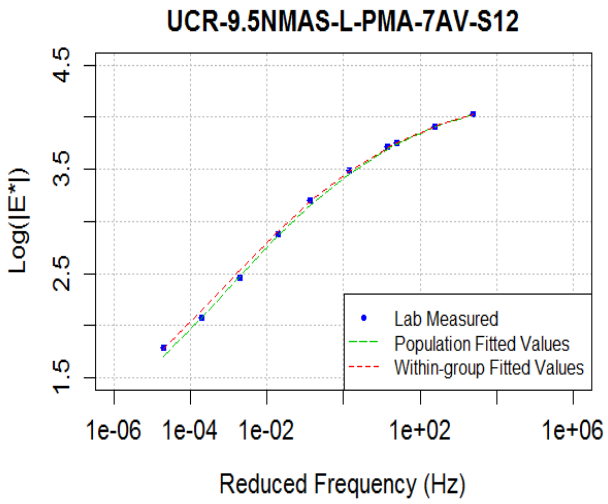
UCR-9.5NMAS-L-PMA-7AV-S12
Log(|E*|)
4.5
3.5
2.5
1.5
1e-06
1e-04
1e-02
1e+02
1e+06
Reduced Frequency (Hz)
Lab Measured
Population Fitted Values
Within-group Fitted Values

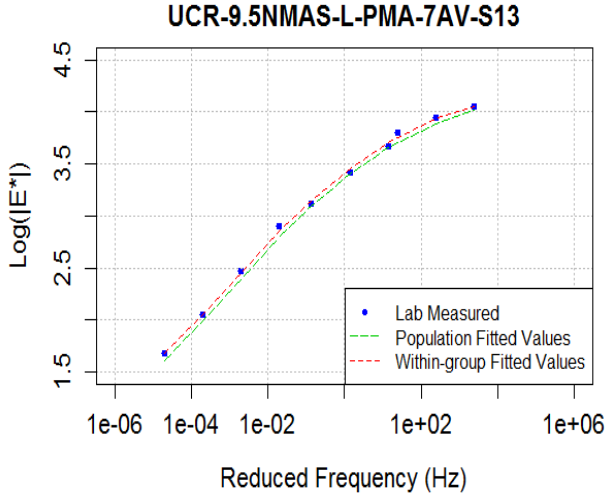
UCR-9.5NMAS-L-PMA-7AV-S13
Log(|E*|)
4.5
3.5
2.5
1.5
1e-06
1e-04
1e-02
1e+02
1e+06
Reduced Frequency (Hz)
Lab Measured
Population Fitted Values
Within-group Fitted Values

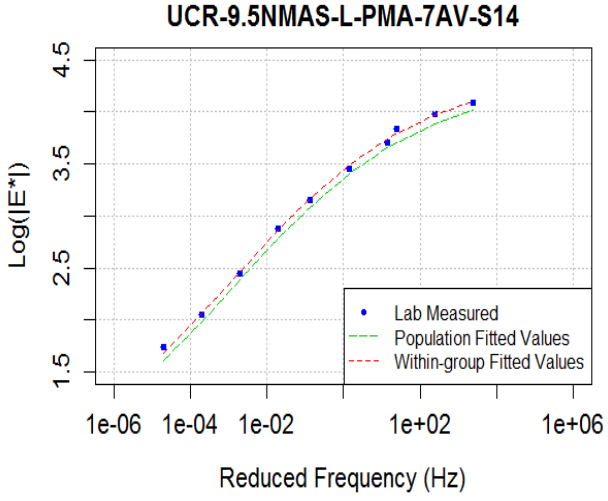
UCR-9.5NMAS-L-PMA-7AV-S14
Log(|E*|)
4.5
3.5
2.5
1.5
1e-06
1e-04
1e-02
1e+02
1e+06
Reduced Frequency (Hz)
Lab Measured
Population Fitted Values
Within-group Fitted Values

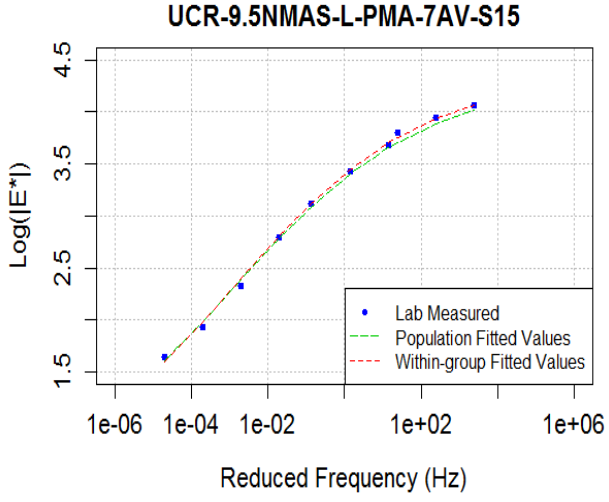
UCR-9.5NMAS-L-PMA-7AV-S15
Log(|E*|)
4.5
3.5
2.5
1.5
1e-06
1e-04
1e-02
1e+02
1e+06
Reduced Frequency (Hz)
Lab Measured
Population Fitted Values
Within-group Fitted Values

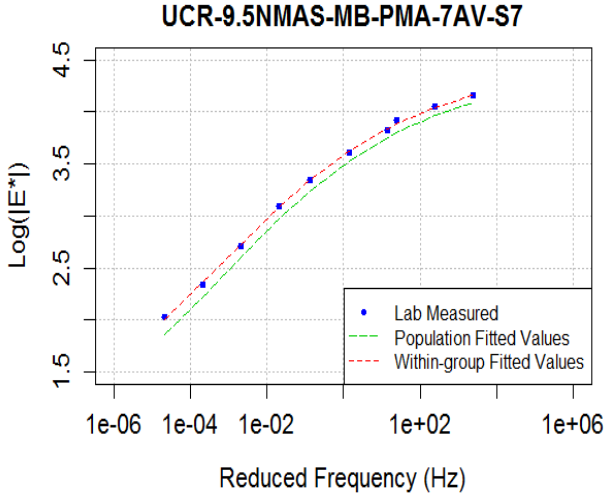
UCR-9.5NMAS-MB-PMA-7AV-S7
Log(|E*|)
4.5
3.5
2.5
1.5
1e-06
1e-04
1e-02
1e+02
1e+06
Reduced Frequency (Hz)
Lab Measured
Population Fitted Values
Within-group Fitted Values

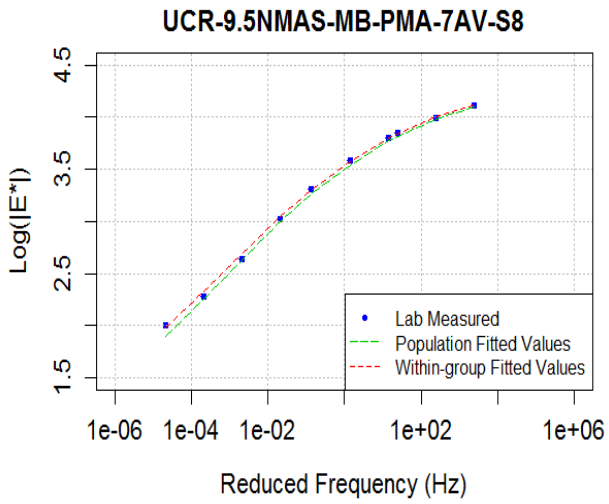
UCR-9.5NMAS-MB-PMA-7AV-S8
Log(|E*|)
4.5
3.5
2.5
1.5
1e-06
1e-04
1e-02
1e+02
1e+06
Reduced Frequency (Hz)
Lab Measured
Population Fitted Values
Within-group Fitted Values

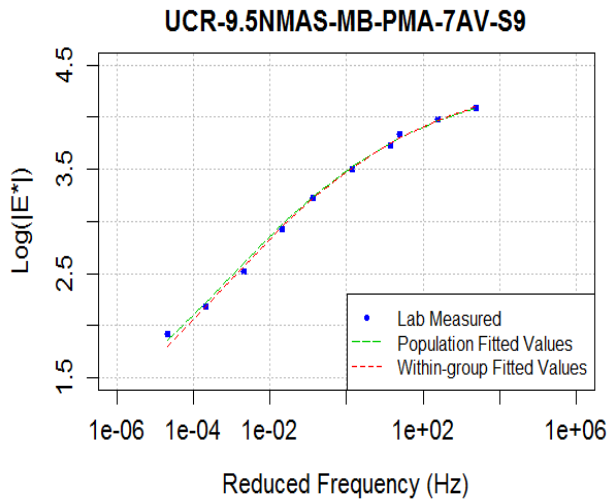
UCR-9.5NMAS-MB-PMA-7AV-S9
Log(|E*|)
4.5
3.5
2.5
1.5
1e-06
1e-04
1e-02
1e+02
1e+06
Reduced Frequency (Hz)
Lab Measured
Population Fitted Values
Within-group Fitted Values

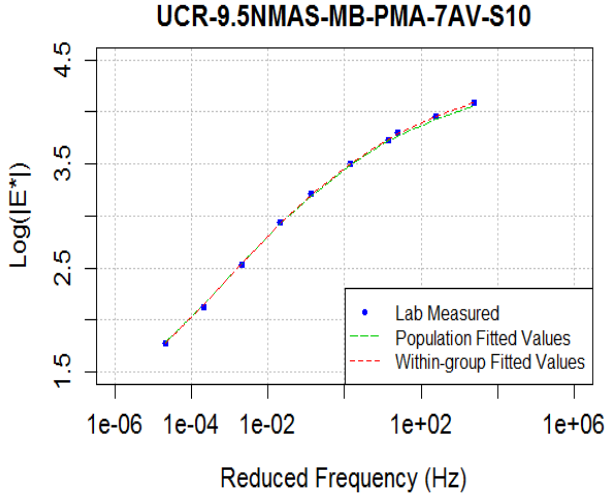
UCR-9.5NMAS-MB-PMA-7AV-S10
Log(|E*|)
4.5
3.5
2.5
1.5
1e-06
1e-04
1e-02
1e+02
1e+06
Reduced Frequency (Hz)
Lab Measured
Population Fitted Values
Within-group Fitted Values

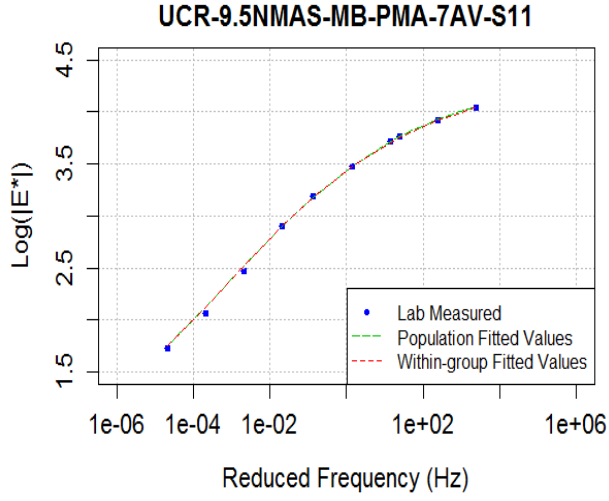
UCR-9.5NMAS-MB-PMA-7AV-S11
Log(|E*|)
4.5
3.5
2.5
1.5
1e-06
1e-04
1e-02
1e+02
1e+06
Reduced Frequency (Hz)
Lab Measured
Population Fitted Values
Within-group Fitted Values

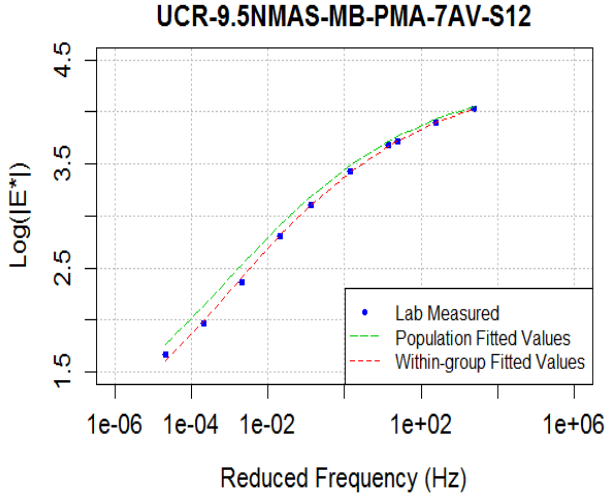
UCR-9.5NMAS-MB-PMA-7AV-S12
Log(|E*|)
4.5
3.5
2.5
1.5
1e-06
1e-04
1e-02
1e+02
1e+06
Reduced Frequency (Hz)
Lab Measured
Population Fitted Values
Within-group Fitted Values

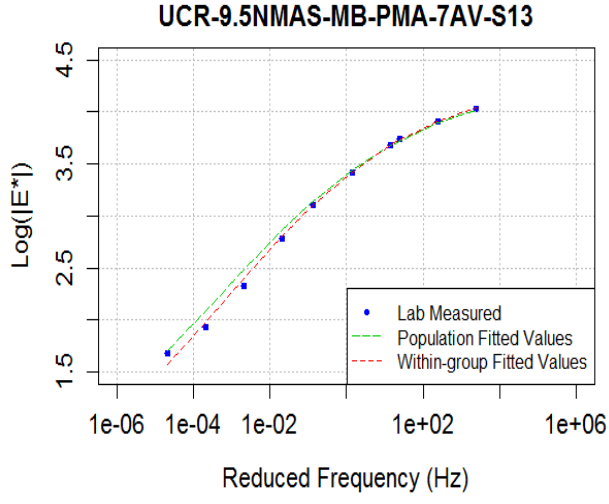
UCR-9.5NMAS-MB-PMA-7AV-S13
Log(|E*|)
4.5
3.5
2.5
1.5
1e-06
1e-04
1e-02
1e+02
1e+06
Reduced Frequency (Hz)
Lab Measured
Population Fitted Values
Within-group Fitted Values

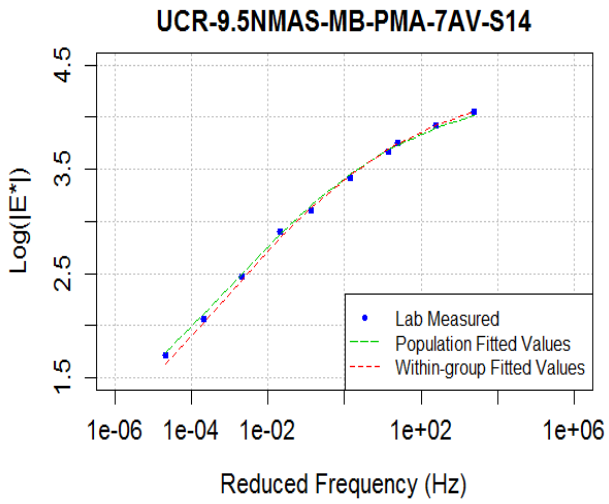
UCR-9.5NMAS-MB-PMA-7AV-S14
Log(|E*|)
1.5
2.5
3.5
4.5
1e-06
1e-04
1e-02
1e+02
1e+06
Reduced Frequency (Hz)
Lab Measured
Population Fitted Values
Within-group Fitted Values

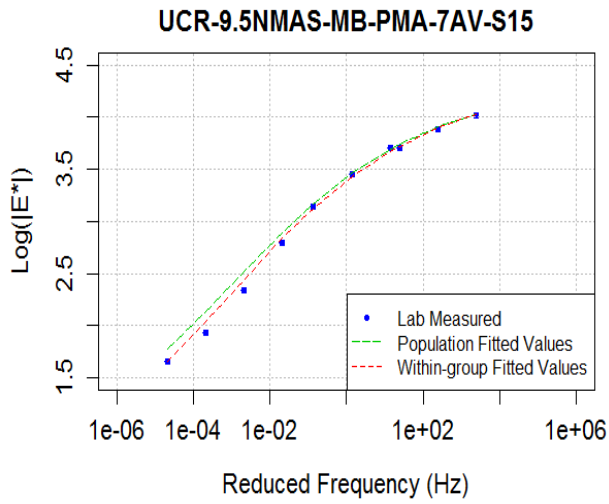
UCR-9.5NMAS-MB-PMA-7AV-S15
Log(|E*|)
1.5
2.5
3.5
4.5
1e-06
1e-04
1e-02
1e+02
1e+06
Reduced Frequency (Hz)
Lab Measured
Population Fitted Values
Within-group Fitted Values

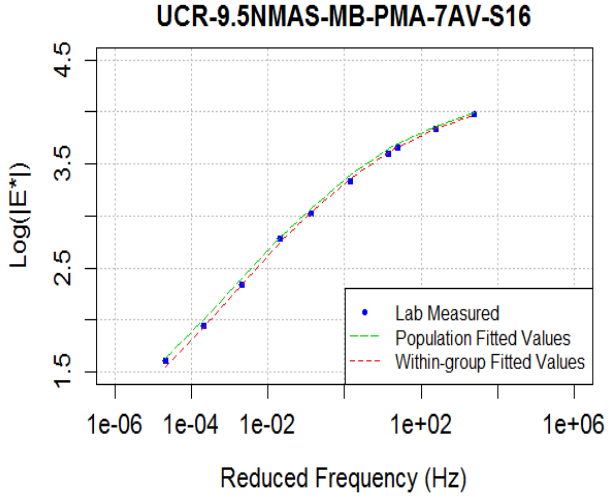
UCR-9.5NMAS-MB-PMA-7AV-S16
Log(|E*|)
1.5
2.5
3.5
4.5
1e-06
1e-04
1e-02
1e+02
1e+06
Reduced Frequency (Hz)
Lab Measured
Population Fitted Values
Within-group Fitted Values

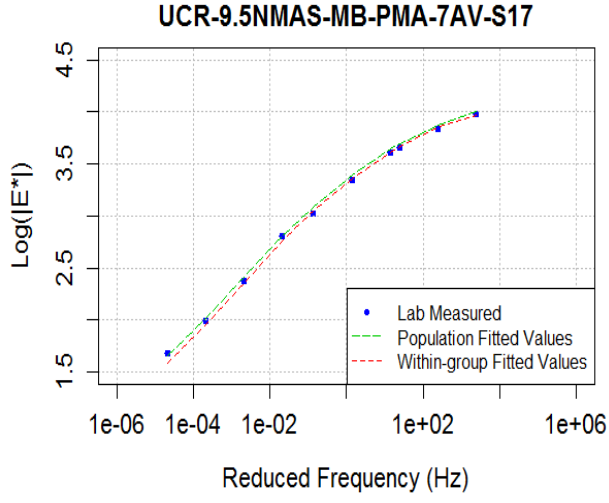
UCR-9.5NMAS-MB-PMA-7AV-S17
Log(|E*|)
1.5
2.5
3.5
4.5
1e-06
1e-04
1e-02
1e+02
1e+06
Reduced Frequency (Hz)
Lab Measured
Population Fitted Values
Within-group Fitted Values

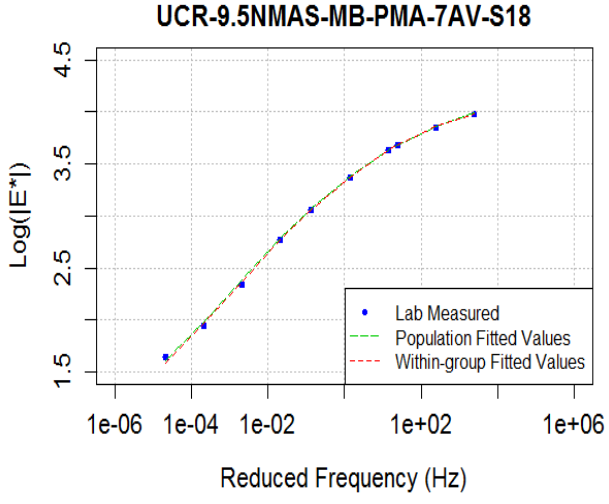
UCR-9.5NMAS-MB-PMA-7AV-S18
Log(|E*|)
1.5
2.5
3.5
4.5
1e-06
1e-04
1e-02
1e+02
1e+06
Reduced Frequency (Hz)
Lab Measured
Population Fitted Values
Within-group Fitted Values

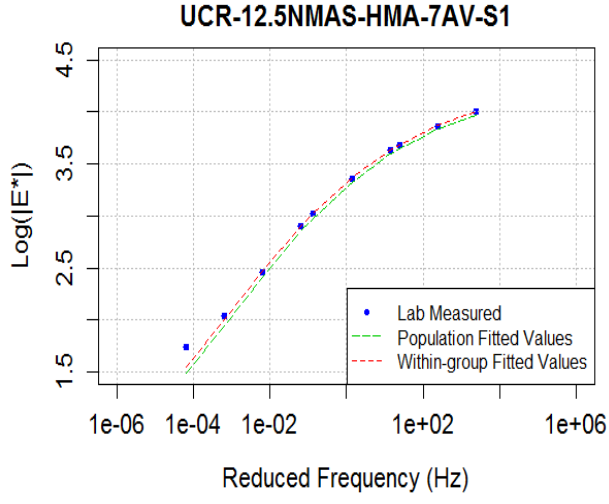
UCR-12.5NMAS-HMA-7AV-S1
Log(|E*|)
1.5
2.5
3.5
4.5
1e-06
1e-04
1e-02
1e+02
1e+06
Reduced Frequency (Hz)
Lab Measured
Population Fitted Values
Within-group Fitted Values

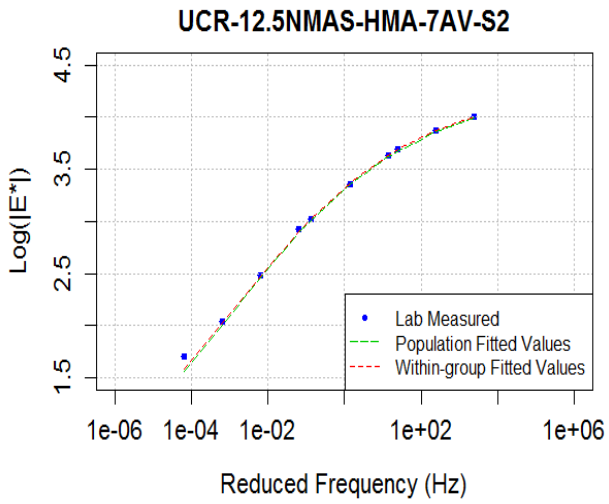
UCR-12.5NMAS-HMA-7AV-S2
Log(|E*|)
4.5
3.5
2.5
1.5
1e-06
1e-04
1e-02
1e+02
1e+06
Reduced Frequency (Hz)
Lab Measured
Population Fitted Values
Within-group Fitted Values

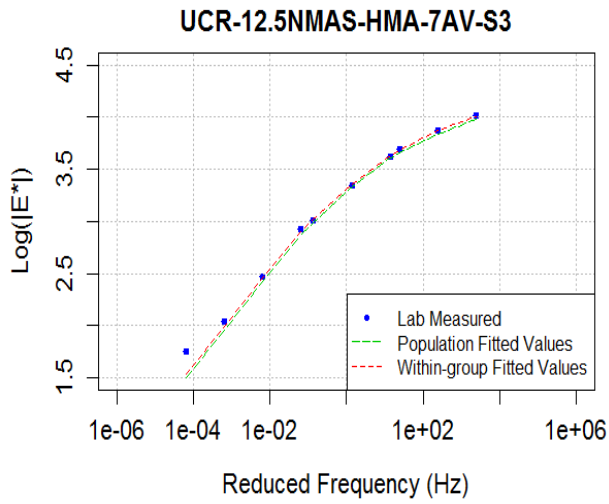
UCR-12.5NMAS-HMA-7AV-S3
Log(|E*|)
4.5
3.5
2.5
1.5
1e-06
1e-04
1e-02
1e+02
1e+06
Reduced Frequency (Hz)
Lab Measured
Population Fitted Values
Within-group Fitted Values

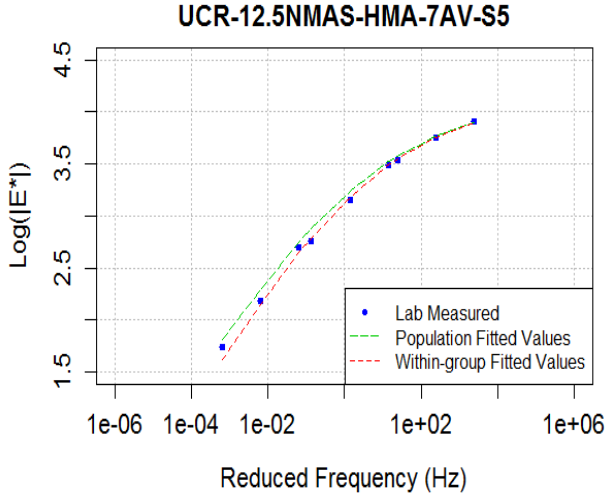
UCR-12.5NMAS-HMA-7AV-S5
Log(|E*|)
4.5
3.5
2.5
1.5
1e-06
1e-04
1e-02
1e+02
1e+06
Reduced Frequency (Hz)
Lab Measured
Population Fitted Values
Within-group Fitted Values

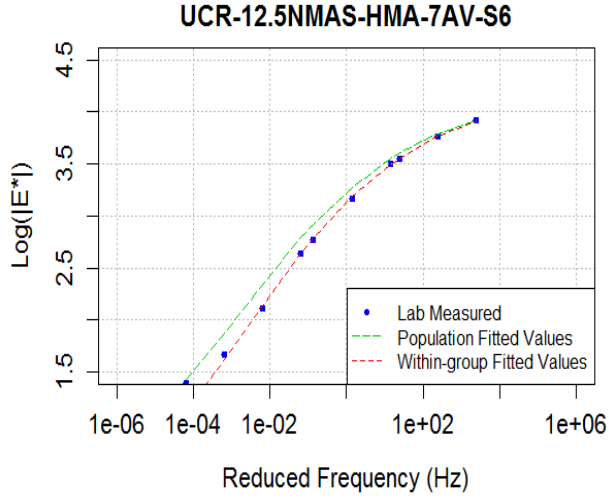
UCR-12.5NMAS-HMA-7AV-S6
Log(|E*|)
4.5
3.5
2.5
1.5
1e-06
1e-04
1e-02
1e+02
1e+06
Reduced Frequency (Hz)
Lab Measured
Population Fitted Values
Within-group Fitted Values

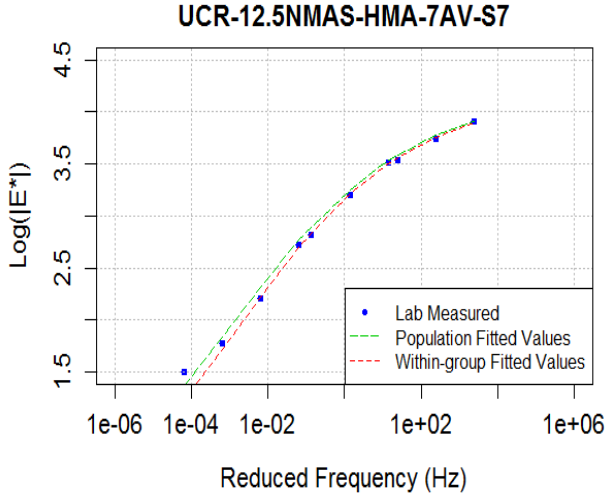
UCR-12.5NMAS-HMA-7AV-S7
Log(|E*|)
4.5
3.5
2.5
1.5
1e-06
1e-04
1e-02
1e+02
1e+06
Reduced Frequency (Hz)
Lab Measured
Population Fitted Values
Within-group Fitted Values

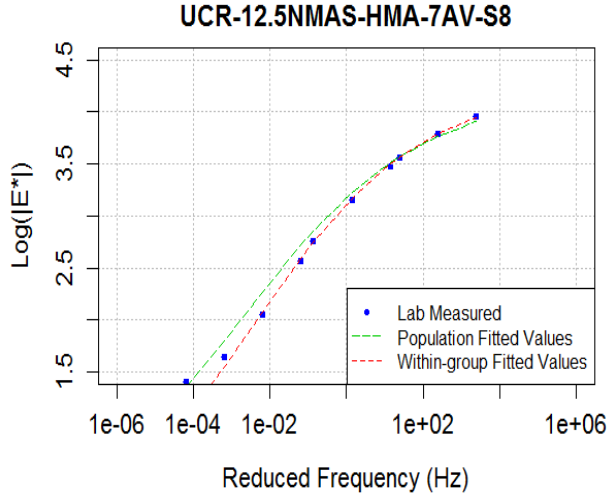
UCR-12.5NMAS-HMA-7AV-S8
Log(|E*|)
4.5
3.5
2.5
1.5
1e-06
1e-04
1e-02
1e+02
1e+06
Reduced Frequency (Hz)
Lab Measured
Population Fitted Values
Within-group Fitted Values

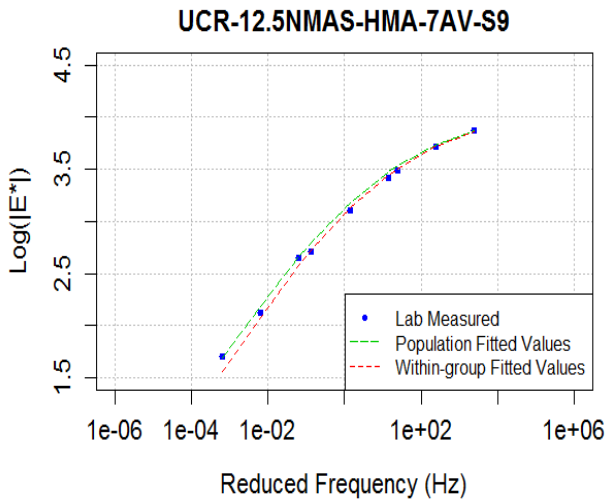
UCR-12.5NMAS-HMA-7AV-S9
Log(|E*|)
Reduced Frequency (Hz)
Lab Measured
Population Fitted Values
Within-group Fitted Values

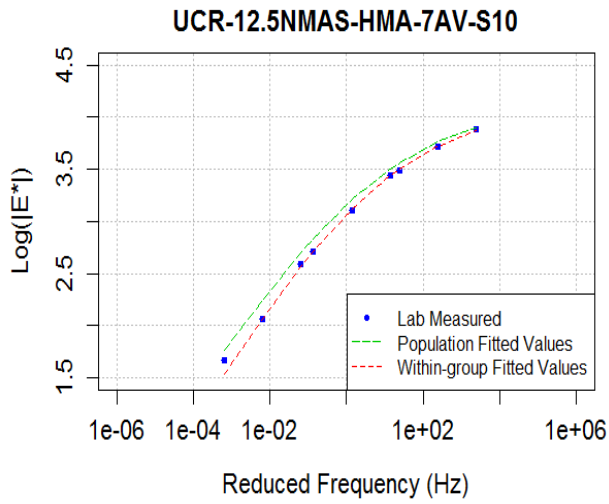
UCR-12.5NMAS-HMA-7AV-S10
Log(|E*|)
Reduced Frequency (Hz)
Lab Measured
Population Fitted Values
Within-group Fitted Values

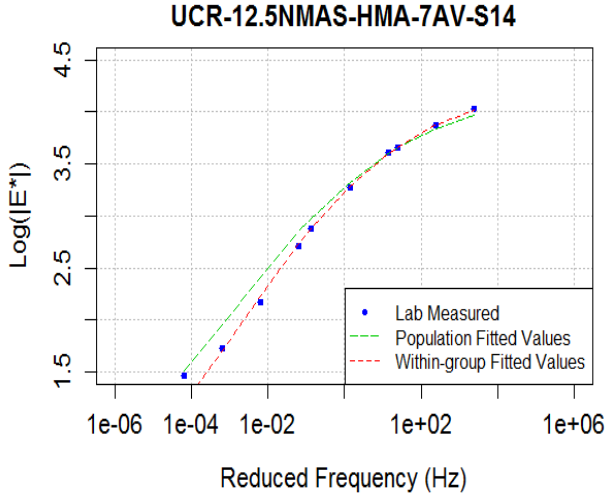
UCR-12.5NMAS-HMA-7AV-S14
Log(|E*|)
Reduced Frequency (Hz)
Lab Measured
Population Fitted Values
Within-group Fitted Values

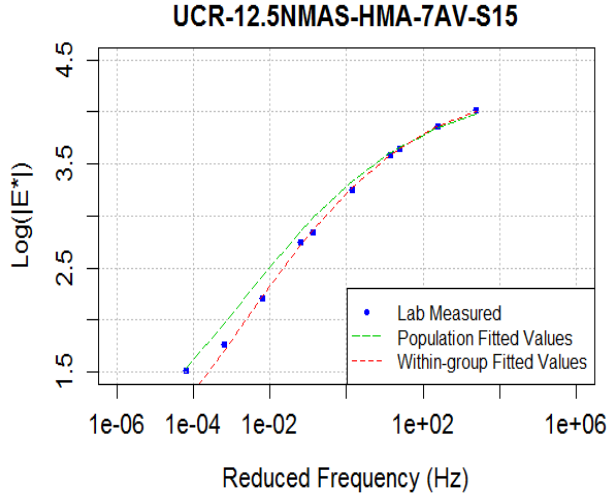
UCR-12.5NMAS-HMA-7AV-S15
Log(|E*|)
Reduced Frequency (Hz)
Lab Measured
Population Fitted Values
Within-group Fitted Values

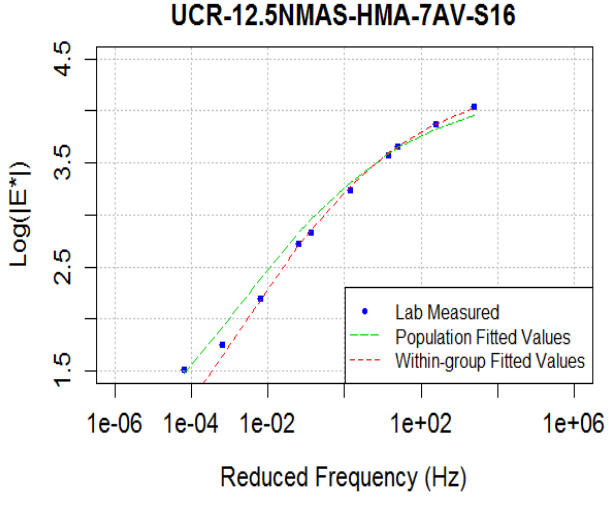
UCR-12.5NMAS-HMA-7AV-S16
Log(|E*|)
Reduced Frequency (Hz)
Lab Measured
Population Fitted Values
Within-group Fitted Values

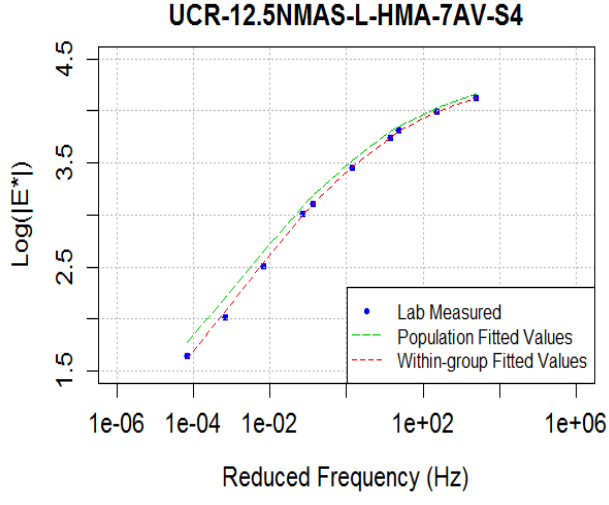
UCR-12.5NMAS-L-HMA-7AV-S4
Log(|E*|)
Reduced Frequency (Hz)
Lab Measured
Population Fitted Values
Within-group Fitted Values

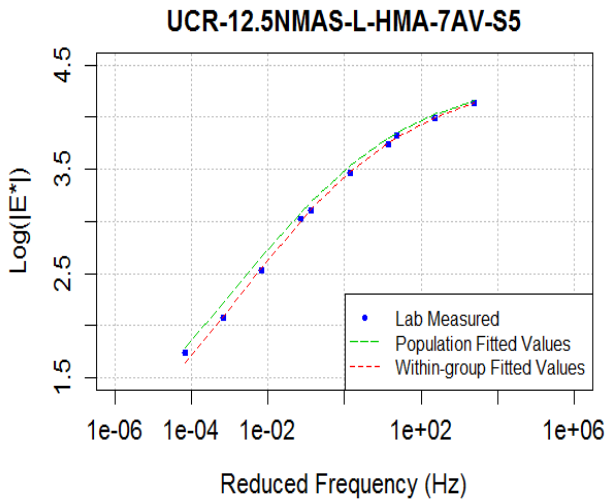
UCR-12.5NMAS-L-HMA-7AV-S5
Log(|E*|)
Reduced Frequency (Hz)
Lab Measured
Population Fitted Values
Within-group Fitted Values

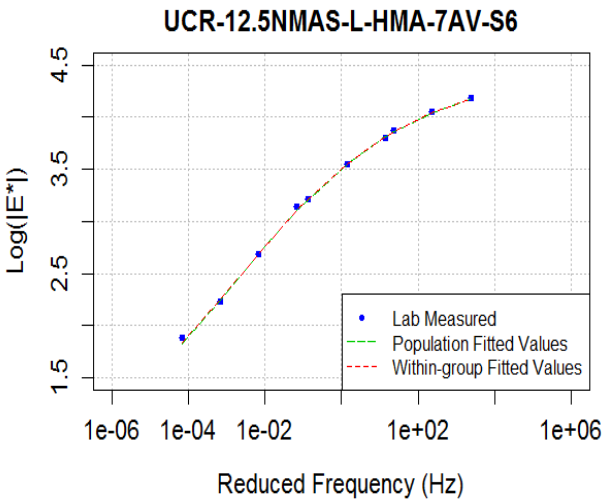
UCR-12.5NMAS-L-HMA-7AV-S6
Log(|E*|)
Reduced Frequency (Hz)
Lab Measured
Population Fitted Values
Within-group Fitted Values

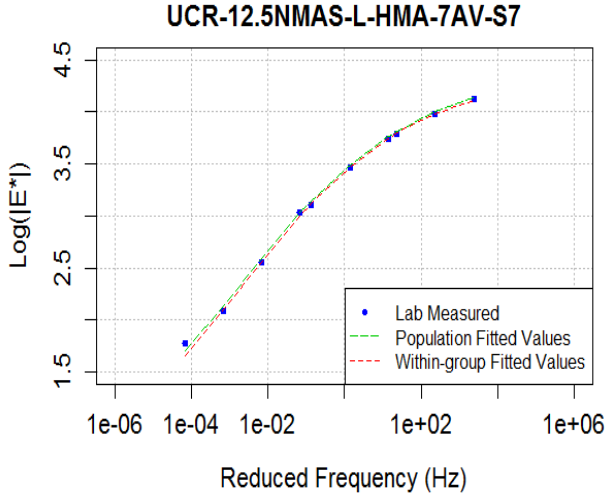
UCR-12.5NMAS-L-HMA-7AV-S7
Log(|E*|)
Reduced Frequency (Hz)
Lab Measured
Population Fitted Values
Within-group Fitted Values

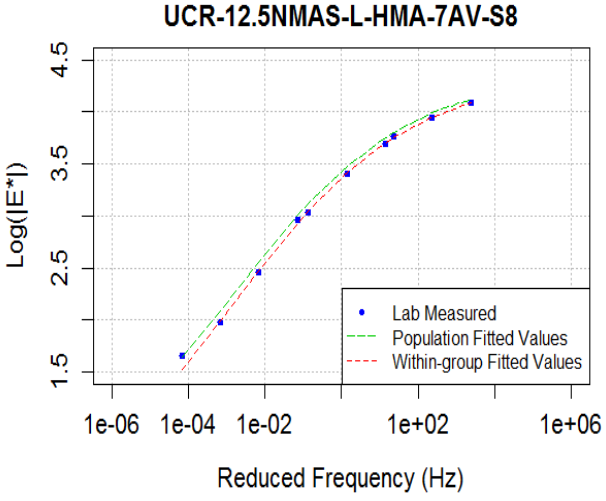
UCR-12.5NMAS-L-HMA-7AV-S8
Log(|E*|)
Reduced Frequency (Hz)
Lab Measured
Population Fitted Values
Within-group Fitted Values

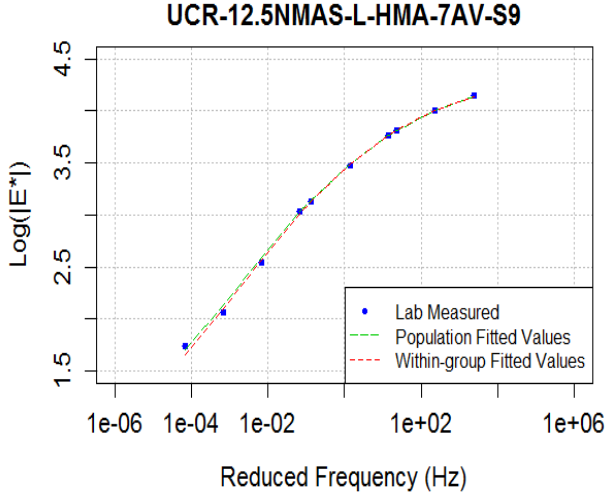
UCR-12.5NMAS-L-HMA-7AV-S9
Log(|E*|)
Reduced Frequency (Hz)
Lab Measured
Population Fitted Values
Within-group Fitted Values

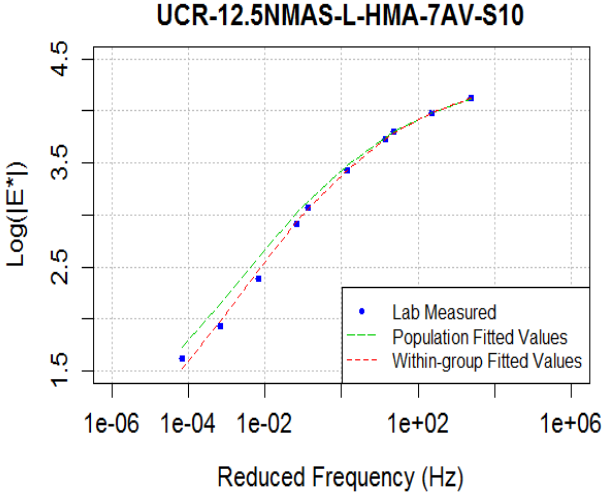
UCR-12.5NMAS-L-HMA-7AV-S10
Log(|E*|)
Reduced Frequency (Hz)
Lab Measured
Population Fitted Values
Within-group Fitted Values

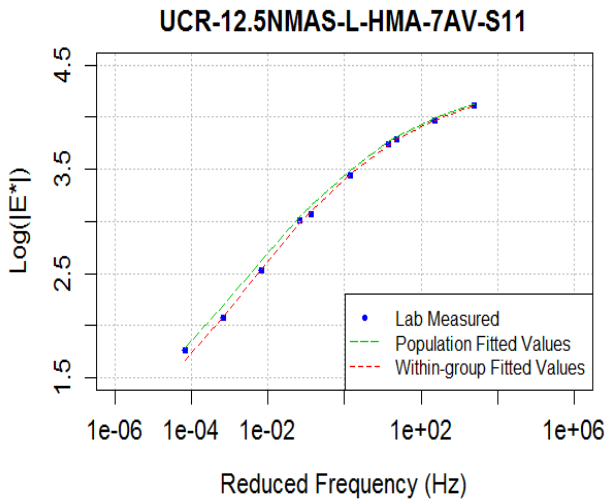
UCR-12.5NMAS-L-HMA-7AV-S11
Log(|E*|)
Reduced Frequency (Hz)
Lab Measured
Population Fitted Values
Within-group Fitted Values

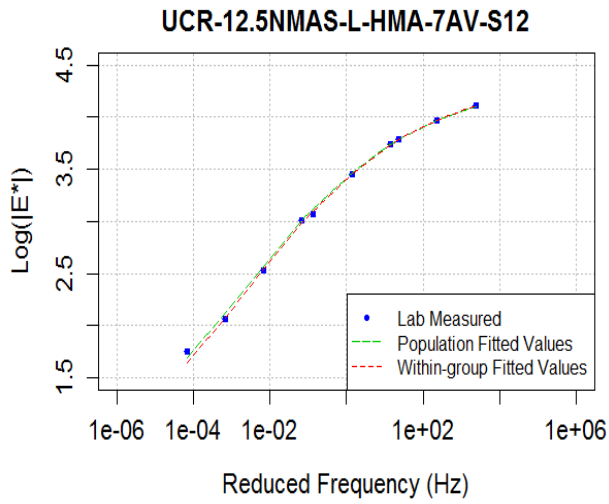
UCR-12.5NMAS-L-HMA-7AV-S12
Log(|E*|)
Reduced Frequency (Hz)
Lab Measured
Population Fitted Values
Within-group Fitted Values

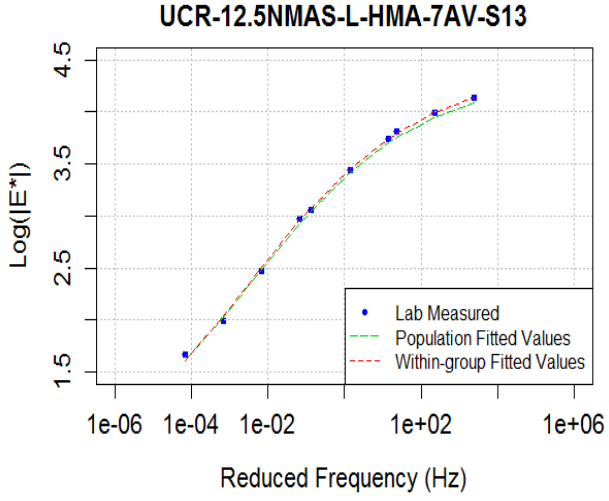
UCR-12.5NMAS-L-HMA-7AV-S13
Log(|E*|)
Reduced Frequency (Hz)
Lab Measured
Population Fitted Values
Within-group Fitted Values

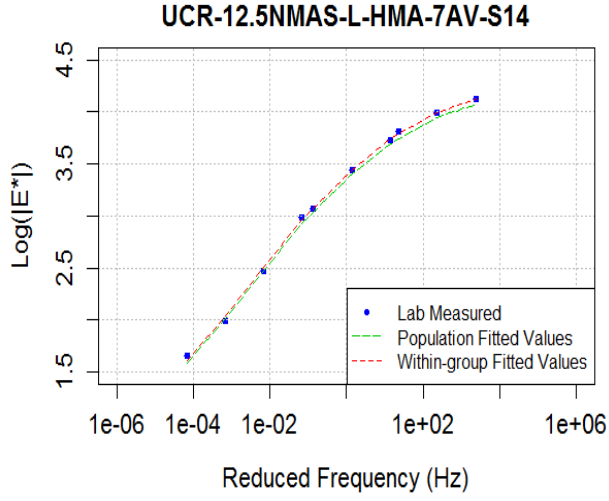
UCR-12.5NMAS-L-HMA-7AV-S14
Log(|E*|)
Reduced Frequency (Hz)
Lab Measured
Population Fitted Values
Within-group Fitted Values

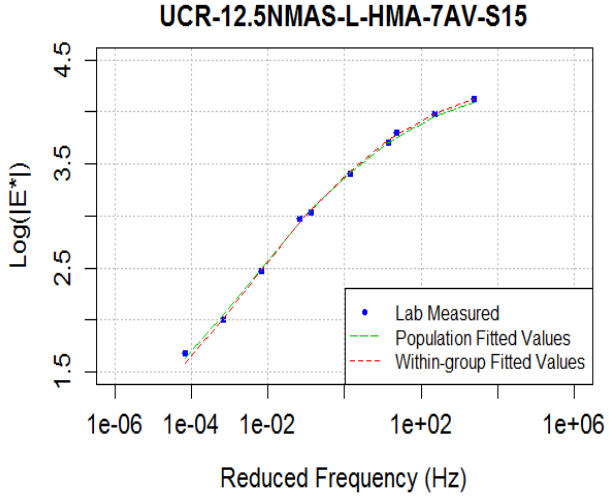
UCR-12.5NMAS-L-HMA-7AV-S15
Log(|E*|)
Reduced Frequency (Hz)
Lab Measured
Population Fitted Values
Within-group Fitted Values

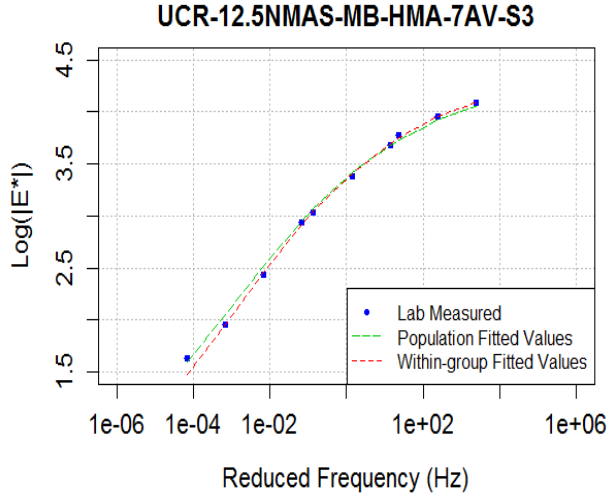
UCR-12.5NMAS-MB-HMA-7AV-S3
Log(|E*|)
Reduced Frequency (Hz)
Lab Measured
Population Fitted Values
Within-group Fitted Values

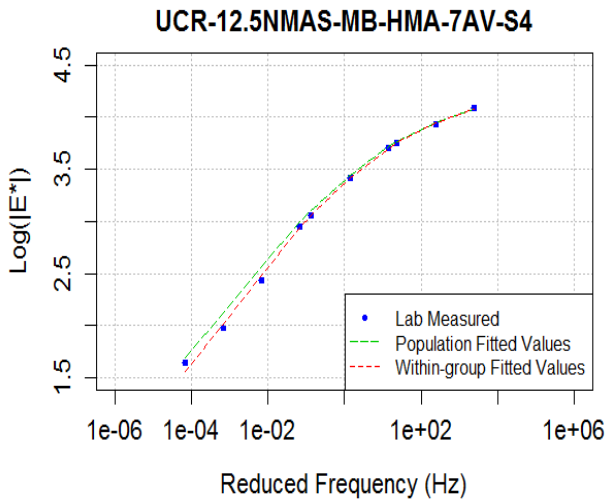
UCR-12.5NMAS-MB-HMA-7AV-S4
Log(|E*|)
Reduced Frequency (Hz)
Lab Measured
Population Fitted Values
Within-group Fitted Values

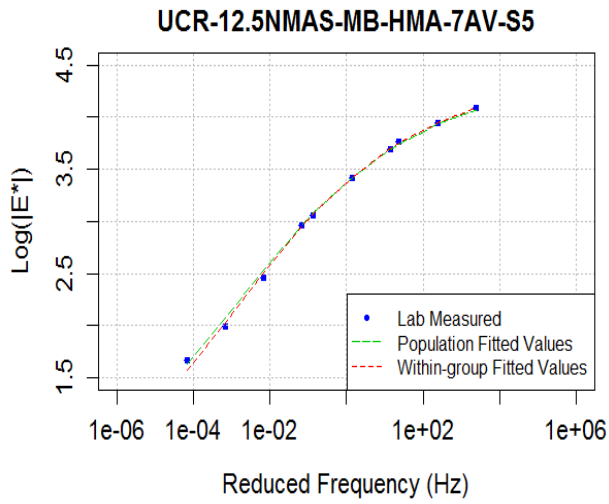
UCR-12.5NMAS-MB-HMA-7AV-S5
Log(|E*|)
Reduced Frequency (Hz)
Lab Measured
Population Fitted Values
Within-group Fitted Values

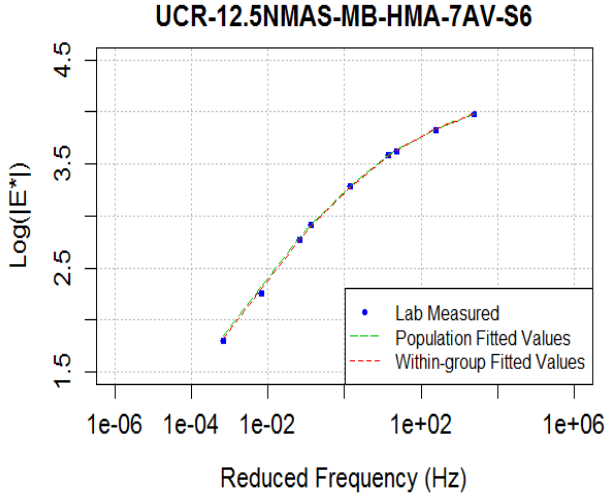
UCR-12.5NMAS-MB-HMA-7AV-S6
Log(|E*|)
Reduced Frequency (Hz)
Lab Measured
Population Fitted Values
Within-group Fitted Values

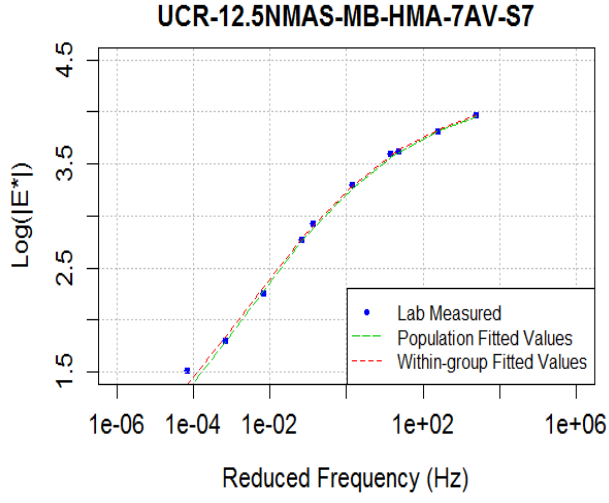
UCR-12.5NMAS-MB-HMA-7AV-S7
Log(|E*|)
Reduced Frequency (Hz)
Lab Measured
Population Fitted Values
Within-group Fitted Values

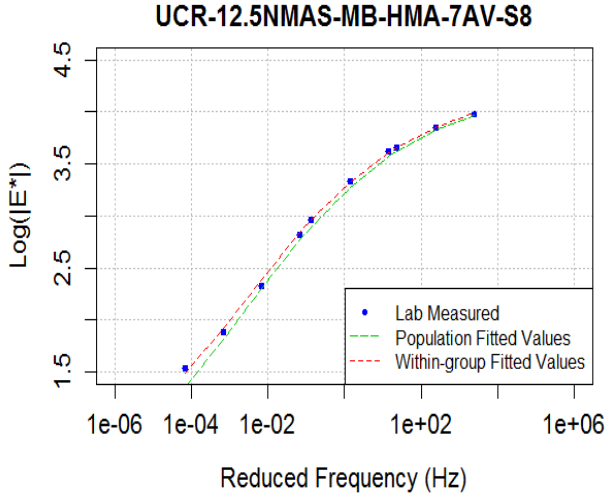
UCR-12.5NMAS-MB-HMA-7AV-S8
Log(|E*|)
Reduced Frequency (Hz)
Lab Measured
Population Fitted Values
Within-group Fitted Values

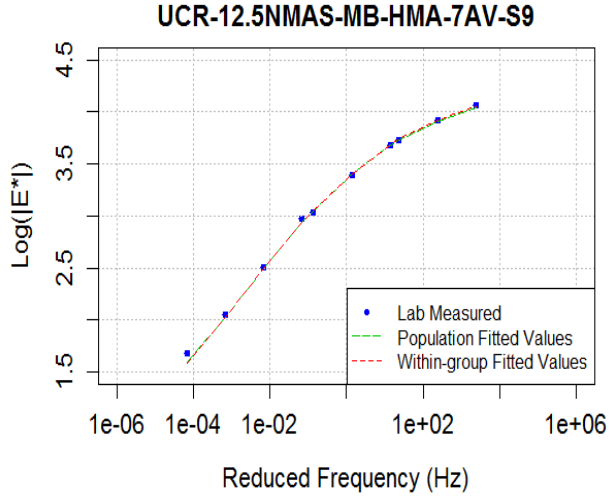
UCR-12.5NMAS-MB-HMA-7AV-S9
Log(|E*|)
Reduced Frequency (Hz)
Lab Measured
Population Fitted Values
Within-group Fitted Values

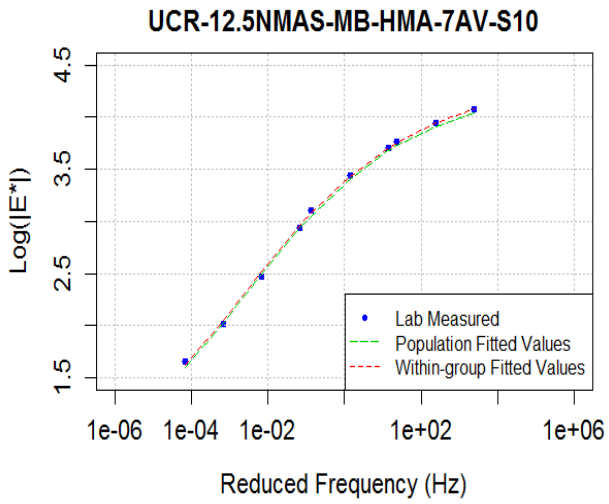
UCR-12.5NMAS-MB-HMA-7AV-S10
Log(|E*|)
Reduced Frequency (Hz)
Lab Measured
Population Fitted Values
Within-group Fitted Values

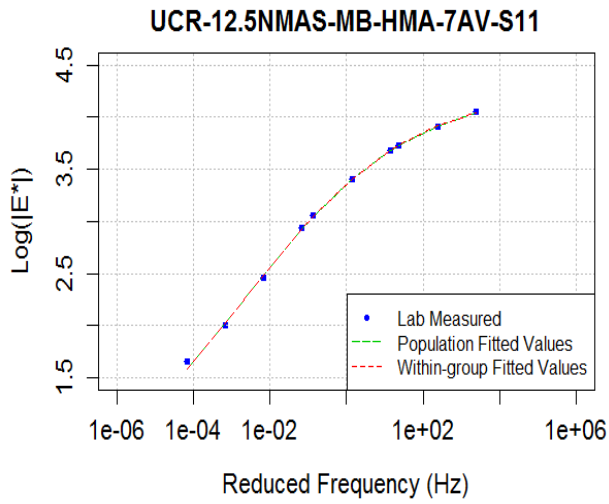
UCR-12.5NMAS-MB-HMA-7AV-S11
Log(|E*|)
Reduced Frequency (Hz)
Lab Measured
Population Fitted Values
Within-group Fitted Values

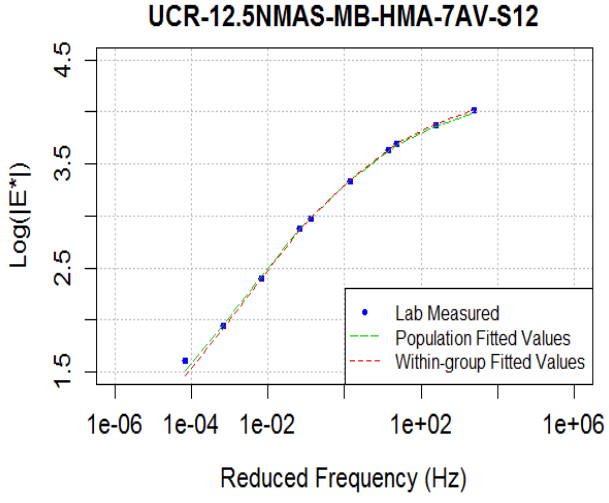
UCR-12.5NMAS-MB-HMA-7AV-S12
Log(|E*|)
Reduced Frequency (Hz)
Lab Measured
Population Fitted Values
Within-group Fitted Values

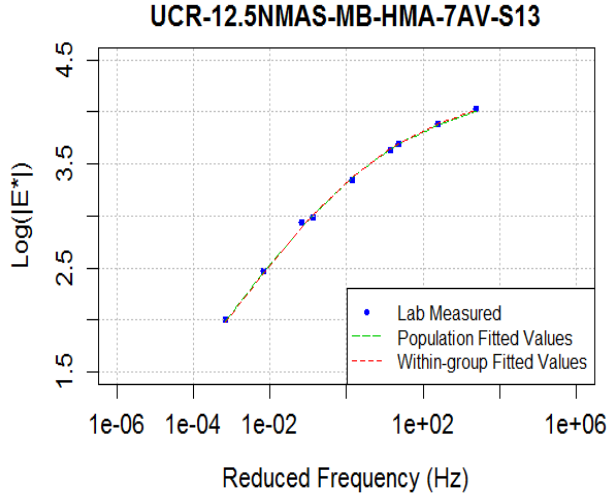
UCR-12.5NMAS-MB-HMA-7AV-S13
Log(|E*|)
Reduced Frequency (Hz)
Lab Measured
Population Fitted Values
Within-group Fitted Values

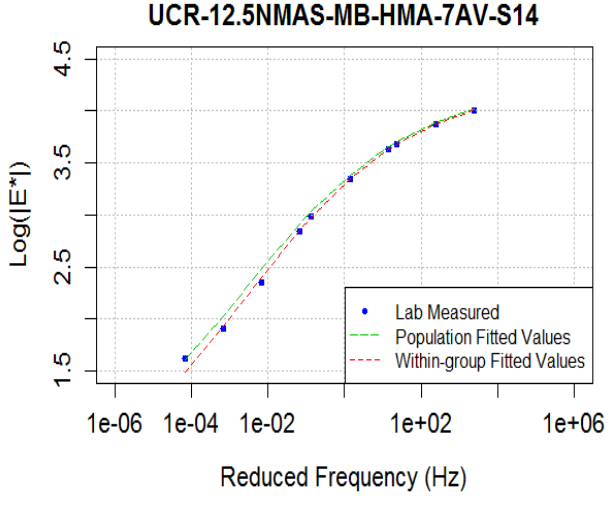
UCR-12.5NMAS-MB-HMA-7AV-S14
Log(|E*|)
Reduced Frequency (Hz)
Lab Measured
Population Fitted Values
Within-group Fitted Values

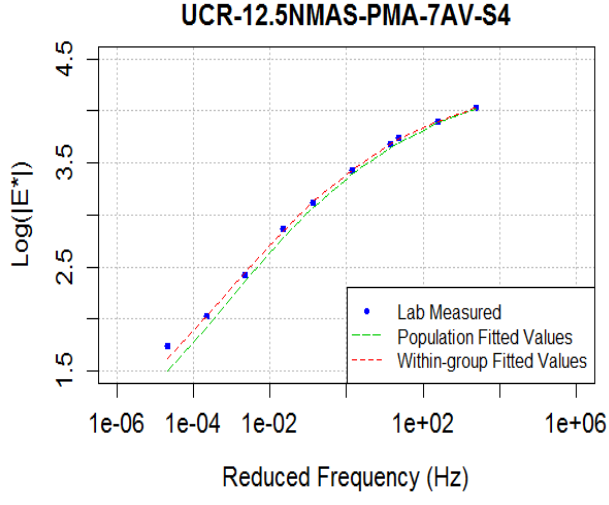
UCR-12.5NMAS-PMA-7AV-S4
Log(|E*|)
Reduced Frequency (Hz)
Lab Measured
Population Fitted Values
Within-group Fitted Values

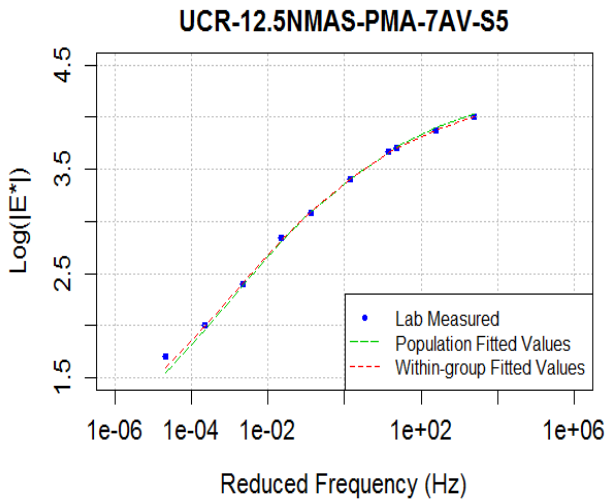
UCR-12.5NMAS-PMA-7AV-S5
Log(|E*|)
Reduced Frequency (Hz)
Lab Measured
Population Fitted Values
Within-group Fitted Values

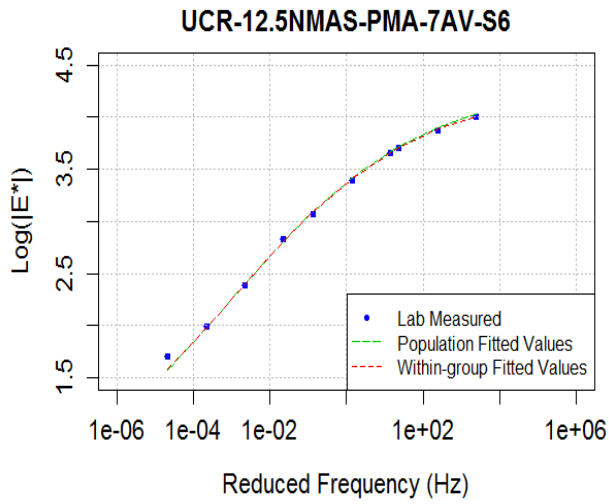
UCR-12.5NMAS-PMA-7AV-S6
Log(|E*|)
Reduced Frequency (Hz)
Lab Measured
Population Fitted Values
Within-group Fitted Values

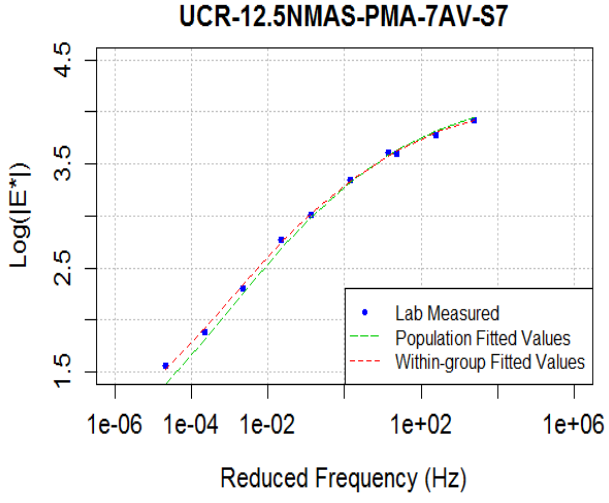
UCR-12.5NMAS-PMA-7AV-S7
Log(|E*|)
Reduced Frequency (Hz)
Lab Measured
Population Fitted Values
Within-group Fitted Values

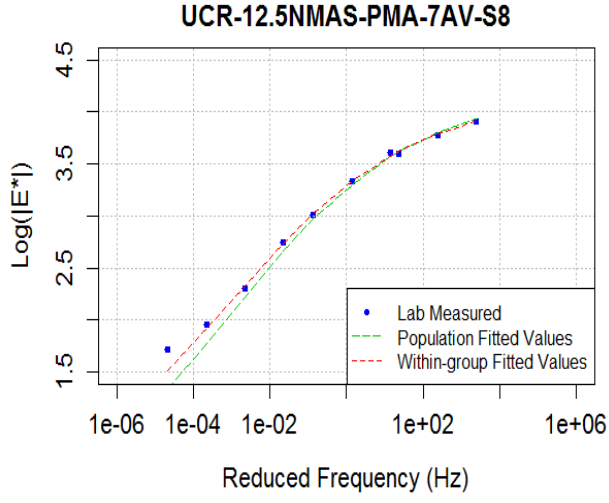
UCR-12.5NMAS-PMA-7AV-S8
Log(|E*|)
Reduced Frequency (Hz)
Lab Measured
Population Fitted Values
Within-group Fitted Values

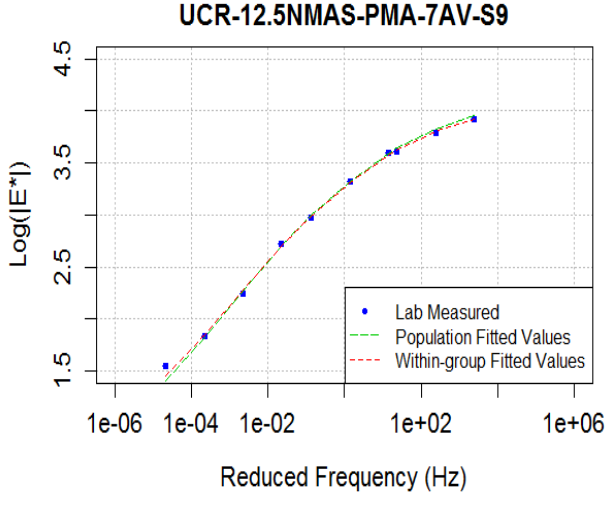
UCR-12.5NMAS-PMA-7AV-S9
Log(|E*|)
Reduced Frequency (Hz)
Lab Measured
Population Fitted Values
Within-group Fitted Values

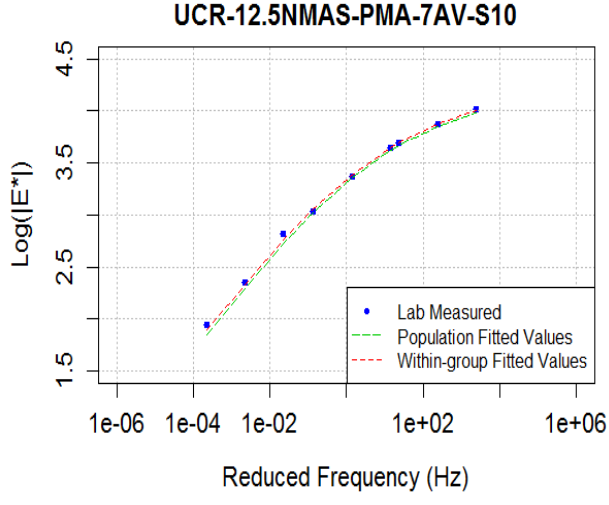
UCR-12.5NMAS-PMA-7AV-S10
Log(|E*|)
Reduced Frequency (Hz)
Lab Measured
Population Fitted Values
Within-group Fitted Values

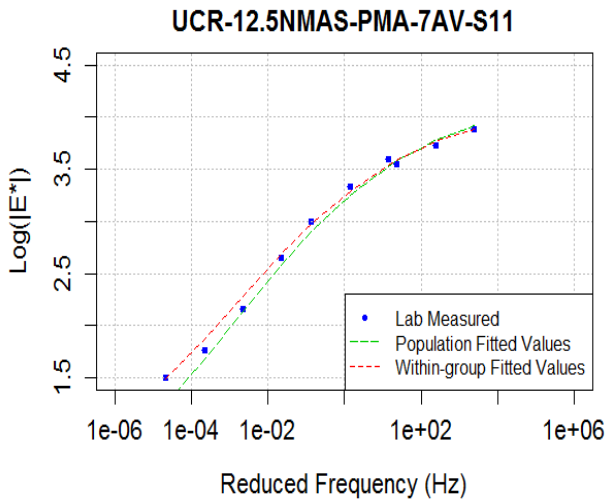
UCR-12.5NMAS-PMA-7AV-S11
Log(|E*|)
Reduced Frequency (Hz)
Lab Measured
Population Fitted Values
Within-group Fitted Values

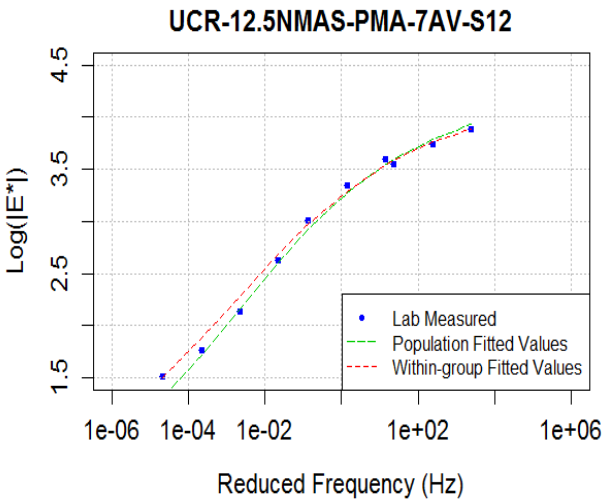
UCR-12.5NMAS-PMA-7AV-S12
Log(|E*|)
Reduced Frequency (Hz)
Lab Measured
Population Fitted Values
Within-group Fitted Values

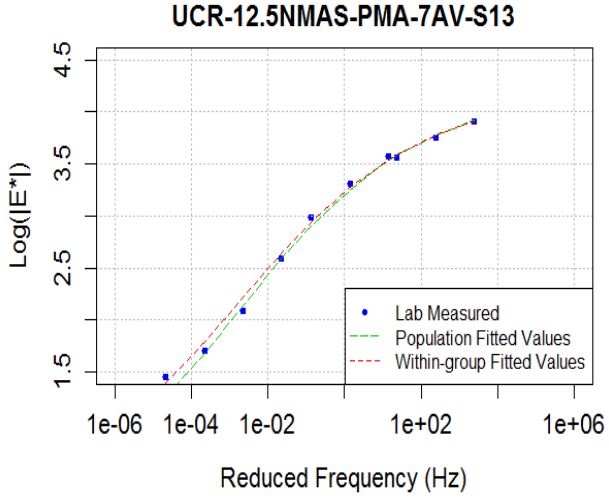
UCR-12.5NMAS-PMA-7AV-S13
Log(|E*|)
Reduced Frequency (Hz)
Lab Measured
Population Fitted Values
Within-group Fitted Values

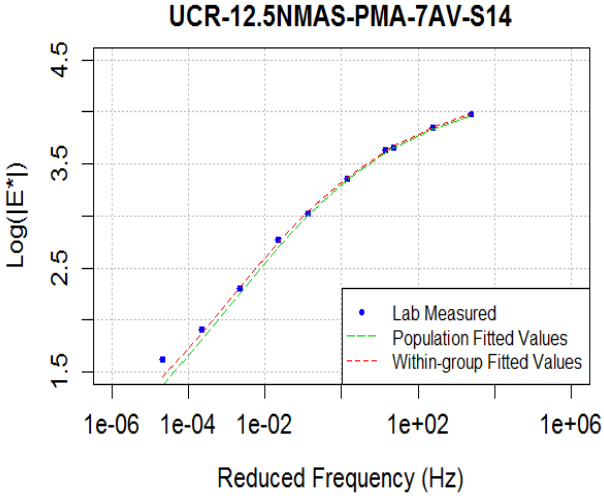
UCR-12.5NMAS-PMA-7AV-S14
Log(|E*|)
Reduced Frequency (Hz)
Lab Measured
Population Fitted Values
Within-group Fitted Values

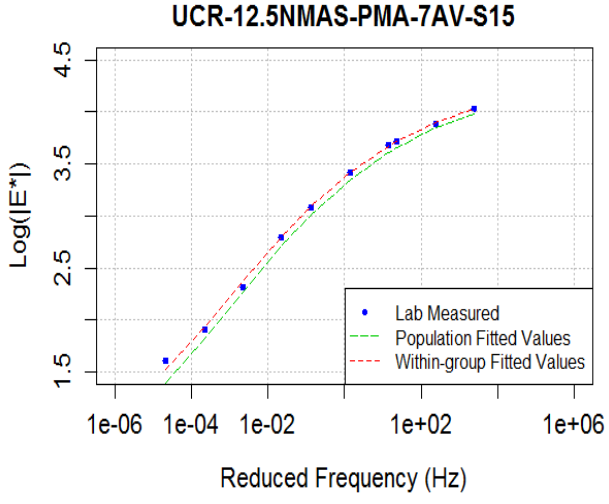
UCR-12.5NMAS-PMA-7AV-S15
Log(|E*|)
Reduced Frequency (Hz)
Lab Measured
Population Fitted Values
Within-group Fitted Values

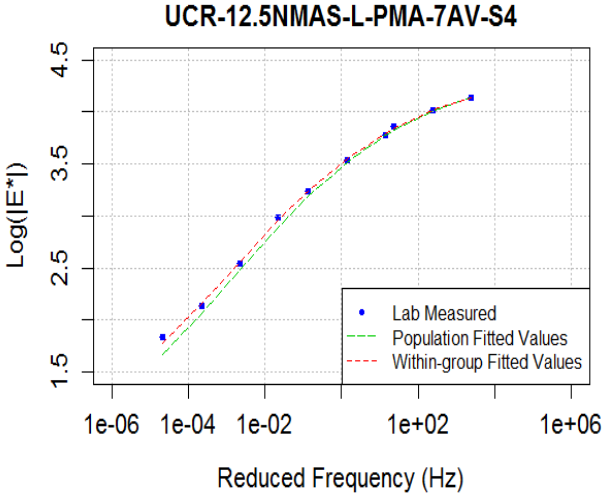
UCR-12.5NMAS-L-PMA-7AV-S4
Log(|E*|)
Reduced Frequency (Hz)
Lab Measured
Population Fitted Values
Within-group Fitted Values

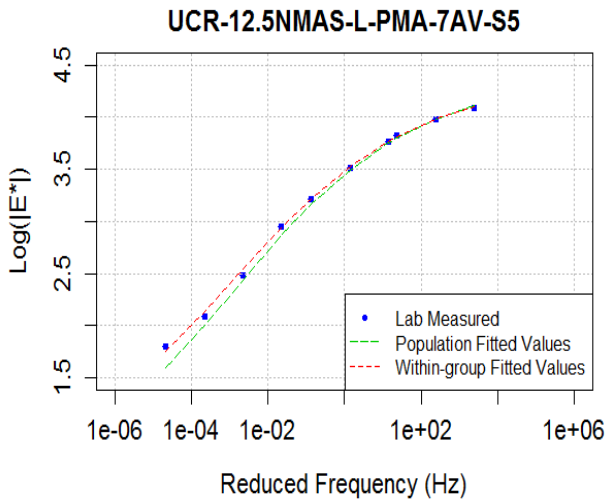
UCR-12.5NMAS-L-PMA-7AV-S5
Log(|E*|)
4.5
3.5
2.5
1.5
1e-06
1e-04
1e-02
1e+02
1e+06
Reduced Frequency (Hz)
Lab Measured
Population Fitted Values
Within-group Fitted Values

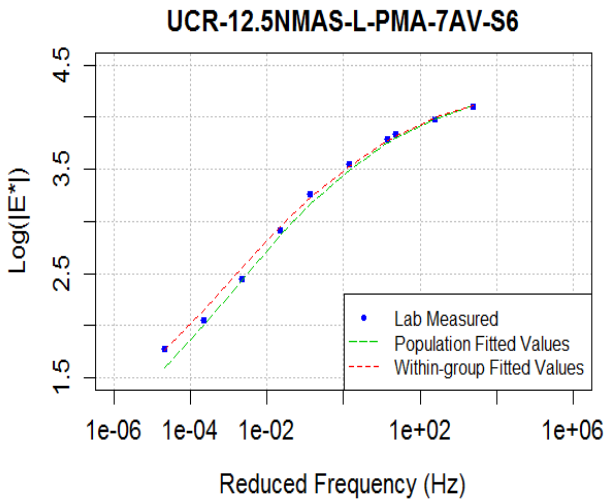
UCR-12.5NMAS-L-PMA-7AV-S6
Log(|E*|)
4.5
3.5
2.5
1.5
1e-06
1e-04
1e-02
1e+02
1e+06
Reduced Frequency (Hz)
Lab Measured
Population Fitted Values
Within-group Fitted Values

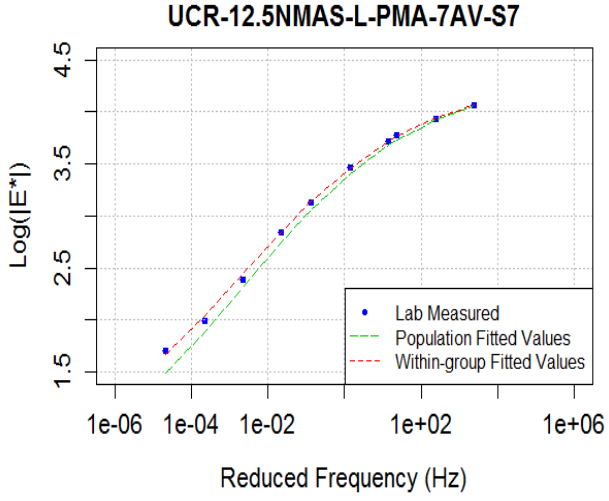
UCR-12.5NMAS-L-PMA-7AV-S7
Log(|E*|)
4.5
3.5
2.5
1.5
1e-06
1e-04
1e-02
1e+02
1e+06
Reduced Frequency (Hz)
Lab Measured
Population Fitted Values
Within-group Fitted Values

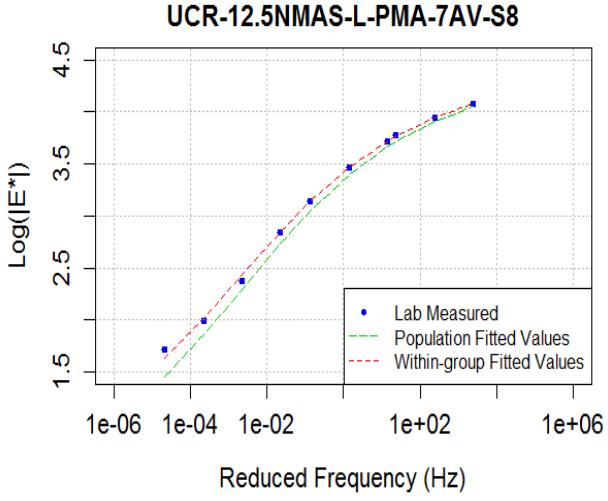
UCR-12.5NMAS-L-PMA-7AV-S8
Log(|E*|)
4.5
3.5
2.5
1.5
1e-06
1e-04
1e-02
1e+02
1e+06
Reduced Frequency (Hz)
Lab Measured
Population Fitted Values
Within-group Fitted Values

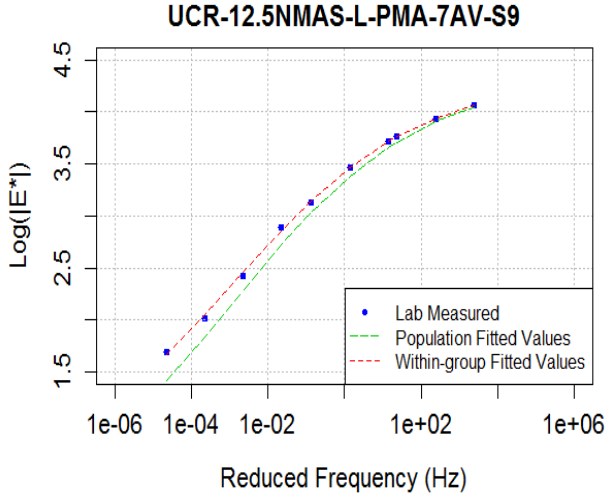
UCR-12.5NMAS-L-PMA-7AV-S9
Log(|E*|)
4.5
3.5
2.5
1.5
1e-06
1e-04
1e-02
1e+02
1e+06
Reduced Frequency (Hz)
Lab Measured
Population Fitted Values
Within-group Fitted Values

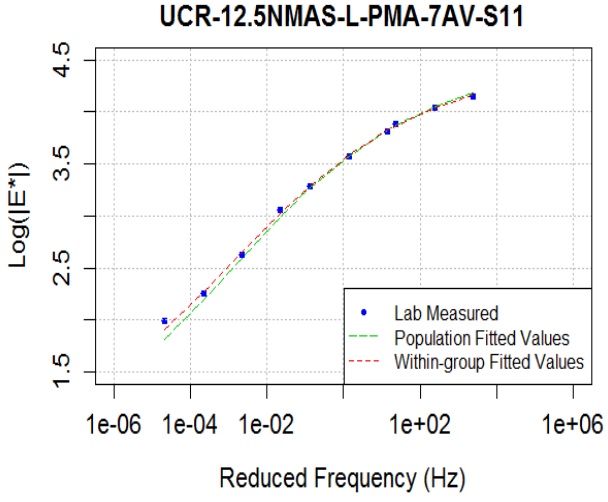
UCR-12.5NMAS-L-PMA-7AV-S11
Log(|E*|)
4.5
3.5
2.5
1.5
1e-06
1e-04
1e-02
1e+02
1e+06
Reduced Frequency (Hz)
Lab Measured
Population Fitted Values
Within-group Fitted Values

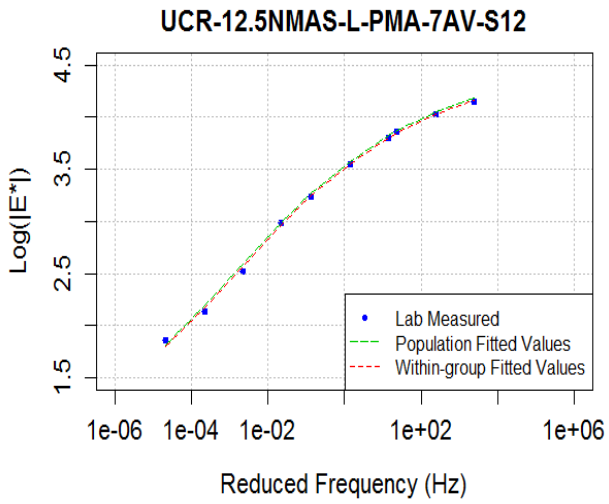
UCR-12.5NMAS-L-PMA-7AV-S12
Log(|E*|)
Reduced Frequency (Hz)
Lab Measured
Population Fitted Values
Within-group Fitted Values

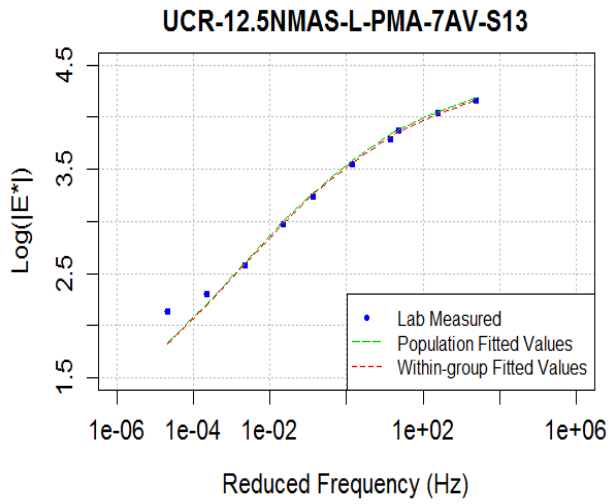
UCR-12.5NMAS-L-PMA-7AV-S13
Log(|E*|)
Reduced Frequency (Hz)
Lab Measured
Population Fitted Values
Within-group Fitted Values

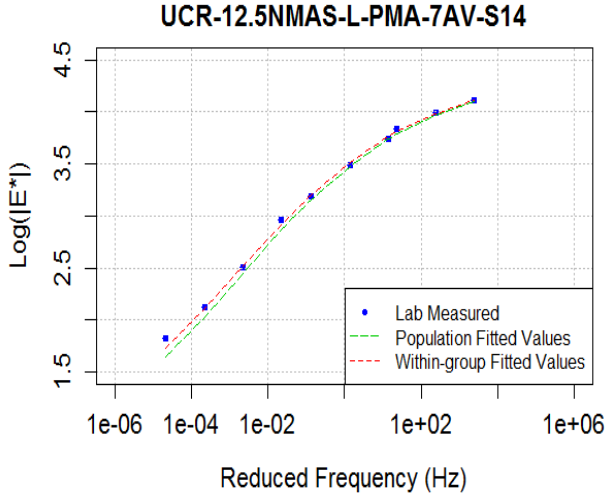
UCR-12.5NMAS-L-PMA-7AV-S14
Log(|E*|)
Reduced Frequency (Hz)
Lab Measured
Population Fitted Values
Within-group Fitted Values

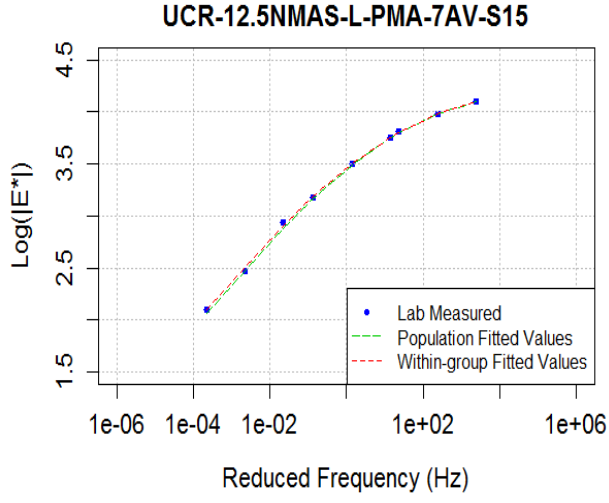
UCR-12.5NMAS-L-PMA-7AV-S15
Log(|E*|)
Reduced Frequency (Hz)
Lab Measured
Population Fitted Values
Within-group Fitted Values

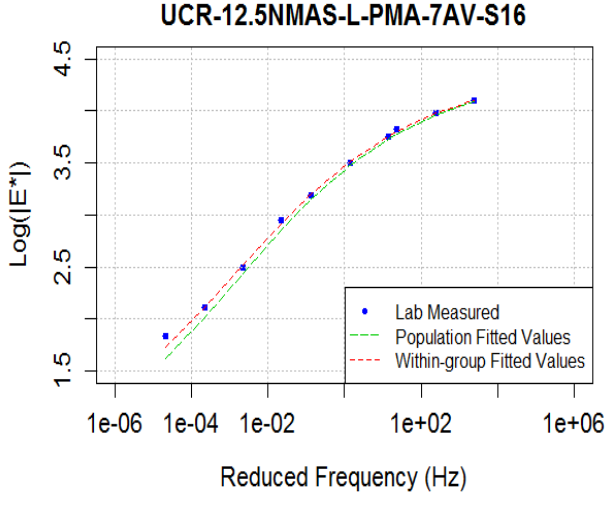
UCR-12.5NMAS-L-PMA-7AV-S16
Log(|E*|)
Reduced Frequency (Hz)
Lab Measured
Population Fitted Values
Within-group Fitted Values

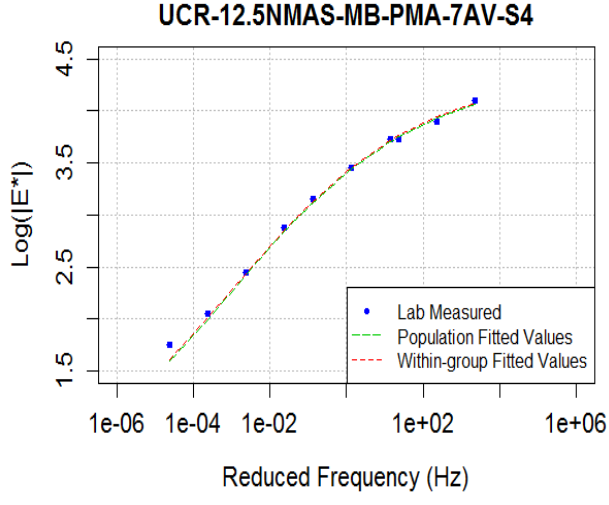
UCR-12.5NMAS-MB-PMA-7AV-S4
Log(|E*|)
Reduced Frequency (Hz)
Lab Measured
Population Fitted Values
Within-group Fitted Values

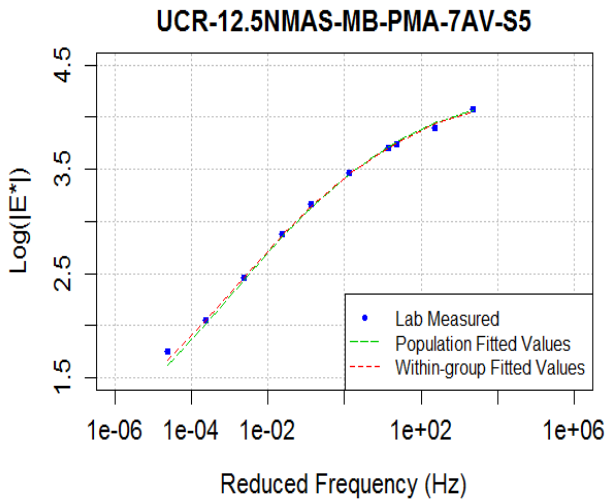
UCR-12.5NMAS-MB-PMA-7AV-S5
Log(|E*|)
1.5
2.5
3.5
4.5
1e-06
1e-04
1e-02
1e+02
1e+06
Reduced Frequency (Hz)
Lab Measured
Population Fitted Values
Within-group Fitted Values

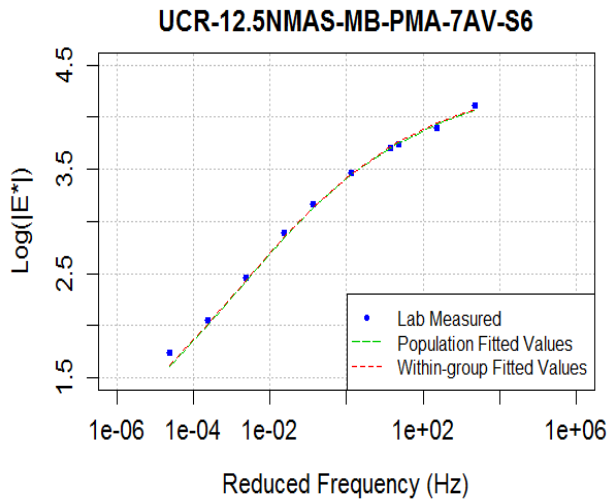
UCR-12.5NMAS-MB-PMA-7AV-S6
Log(|E*|)
1.5
2.5
3.5
4.5
1e-06
1e-04
1e-02
1e+02
1e+06
Reduced Frequency (Hz)
Lab Measured
Population Fitted Values
Within-group Fitted Values

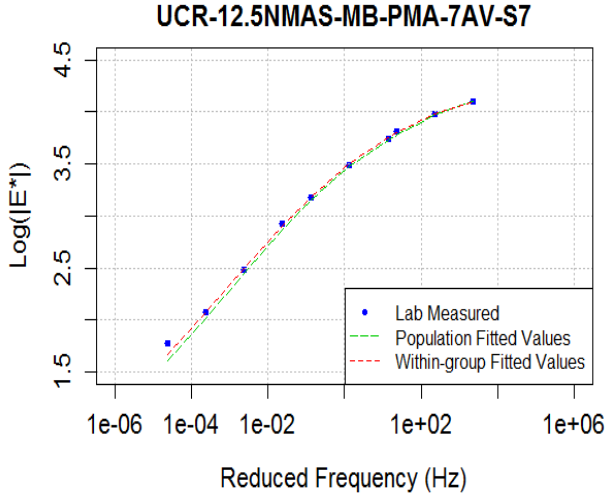
UCR-12.5NMAS-MB-PMA-7AV-S7
Log(|E*|)
1.5
2.5
3.5
4.5
1e-06
1e-04
1e-02
1e+02
1e+06
Reduced Frequency (Hz)
Lab Measured
Population Fitted Values
Within-group Fitted Values

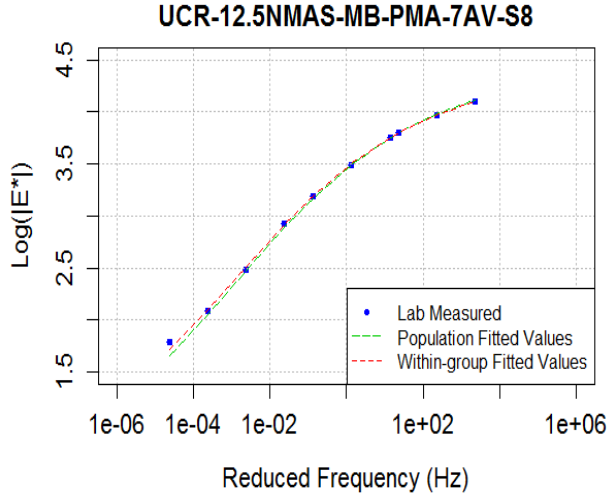
UCR-12.5NMAS-MB-PMA-7AV-S8
Log(|E*|)
1.5
2.5
3.5
4.5
1e-06
1e-04
1e-02
1e+02
1e+06
Reduced Frequency (Hz)
Lab Measured
Population Fitted Values
Within-group Fitted Values

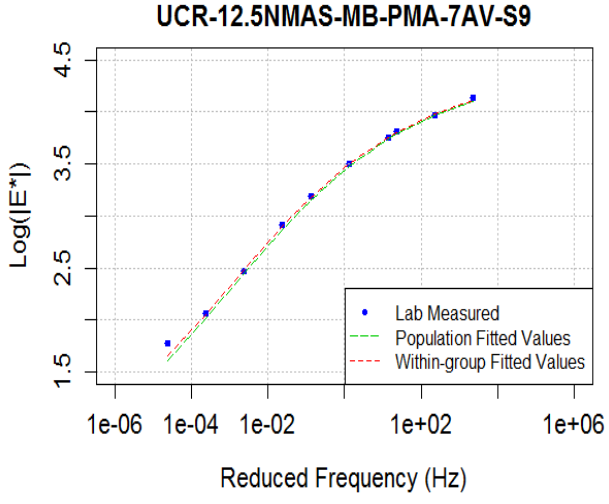
UCR-12.5NMAS-MB-PMA-7AV-S9
Log(|E*|)
1.5
2.5
3.5
4.5
1e-06
1e-04
1e-02
1e+02
1e+06
Reduced Frequency (Hz)
Lab Measured
Population Fitted Values
Within-group Fitted Values

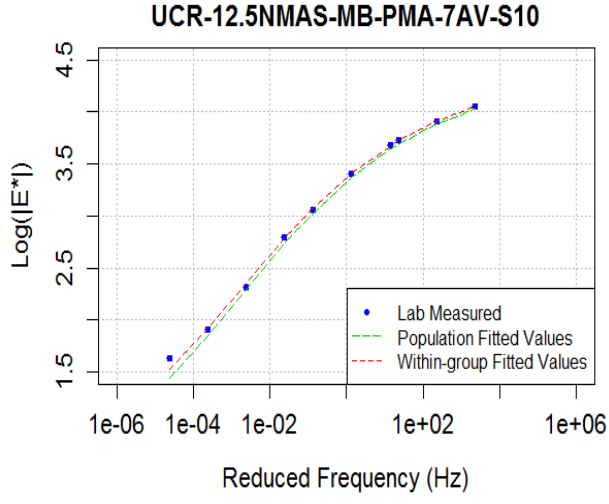
UCR-12.5NMAS-MB-PMA-7AV-S10
Log(|E*|)
1.5
2.5
3.5
4.5
1e-06
1e-04
1e-02
1e+02
1e+06
Reduced Frequency (Hz)
Lab Measured
Population Fitted Values
Within-group Fitted Values

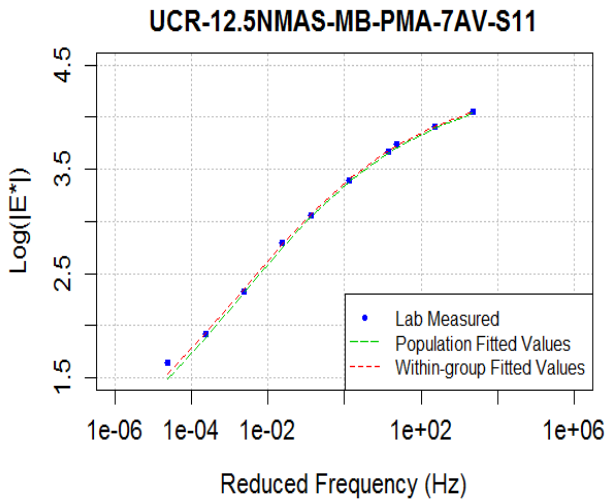
UCR-12.5NMAS-MB-PMA-7AV-S11
Log(|E*|)
1.5
2.5
3.5
4.5
1e-06
1e-04
1e-02
1e+02
1e+06
Reduced Frequency (Hz)
Lab Measured
Population Fitted Values
Within-group Fitted Values

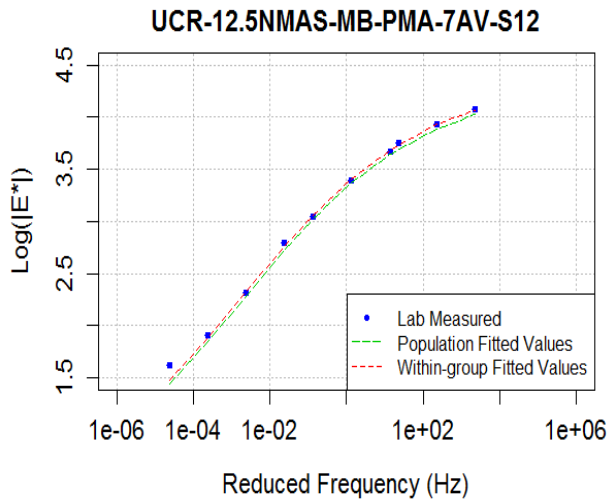
UCR-12.5NMAS-MB-PMA-7AV-S12
Log(|E*|)
1.5
2.5
3.5
4.5
1e-06
1e-04
1e-02
1e+02
1e+06
Reduced Frequency (Hz)
Lab Measured
Population Fitted Values
Within-group Fitted Values

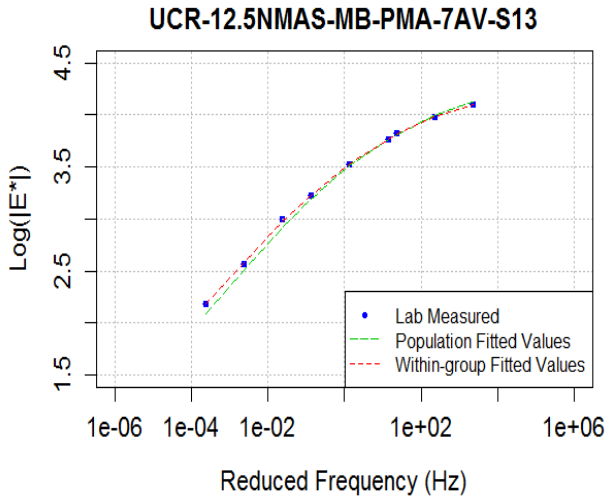
UCR-12.5NMAS-MB-PMA-7AV-S13
Log(|E*|)
1.5
2.5
3.5
4.5
1e-06
1e-04
1e-02
1e+02
1e+06
Reduced Frequency (Hz)
Lab Measured
Population Fitted Values
Within-group Fitted Values

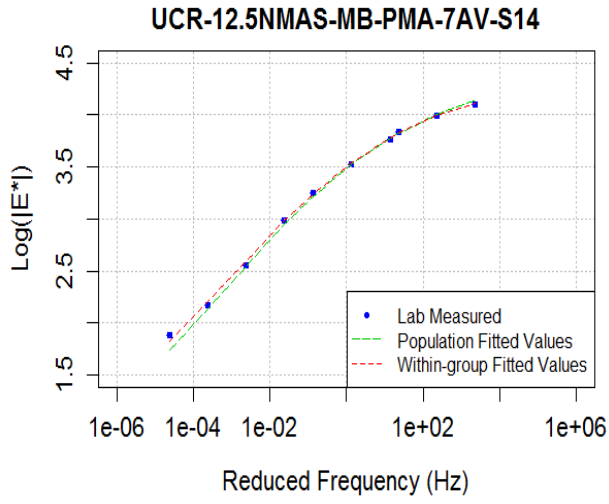
UCR-12.5NMAS-MB-PMA-7AV-S14
Log(|E*|)
1.5
2.5
3.5
4.5
1e-06
1e-04
1e-02
1e+02
1e+06
Reduced Frequency (Hz)
Lab Measured
Population Fitted Values
Within-group Fitted Values

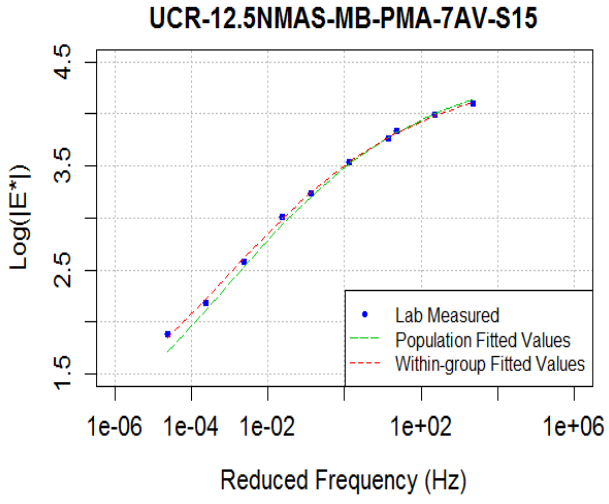
UCR-12.5NMAS-MB-PMA-7AV-S15
Log(|E*|)
1.5
2.5
3.5
4.5
1e-06
1e-04
1e-02
1e+02
1e+06
Reduced Frequency (Hz)
Lab Measured
Population Fitted Values
Within-group Fitted Values

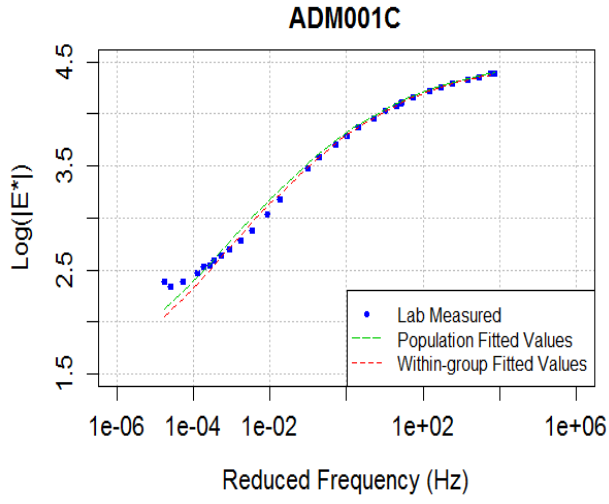
ADM001C
Log(|E*|)
1.5
2.5
3.5
4.5
1e-06
1e-04
1e-02
1e+02
1e+06
Reduced Frequency (Hz)
Lab Measured
Population Fitted Values
Within-group Fitted Values

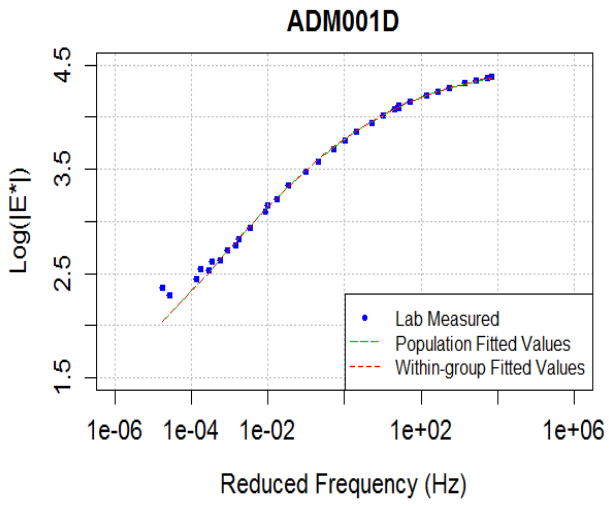
ADM001D
Log(|E*|)
4.5
3.5
2.5
1.5
1e-06
1e-04
1e-02
1e+02
1e+06
Reduced Frequency (Hz)
Lab Measured
Population Fitted Values
Within-group Fitted Values

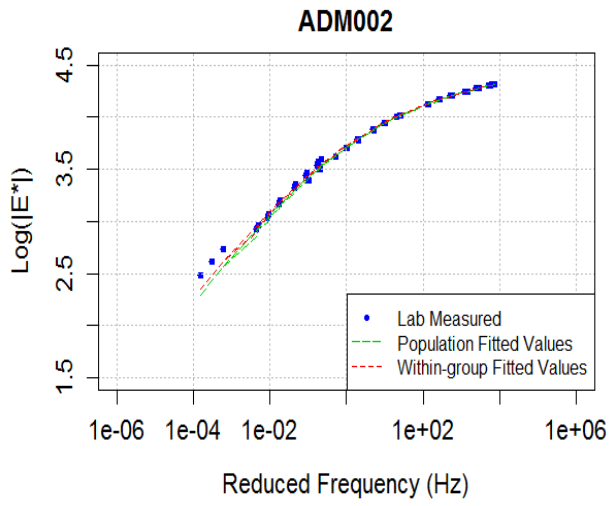
ADM002
Log(|E*|)
4.5
3.5
2.5
1.5
1e-06
1e-04
1e-02
1e+02
1e+06
Reduced Frequency (Hz)
Lab Measured
Population Fitted Values
Within-group Fitted Values

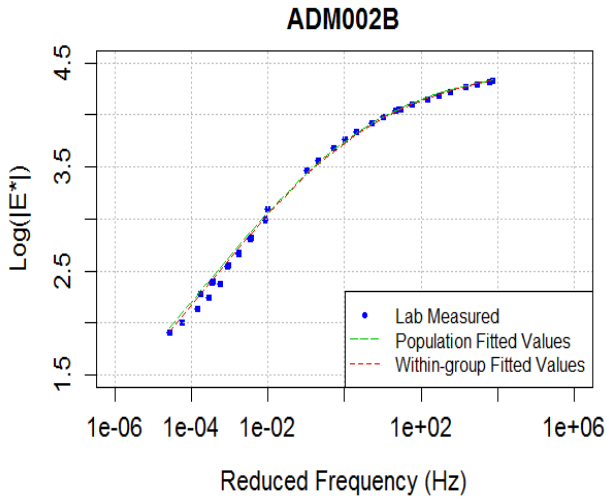
ADM002B
Log(|E*|)
4.5
3.5
2.5
1.5
1e-06
1e-04
1e-02
1e+02
1e+06
Reduced Frequency (Hz)
Lab Measured
Population Fitted Values
Within-group Fitted Values

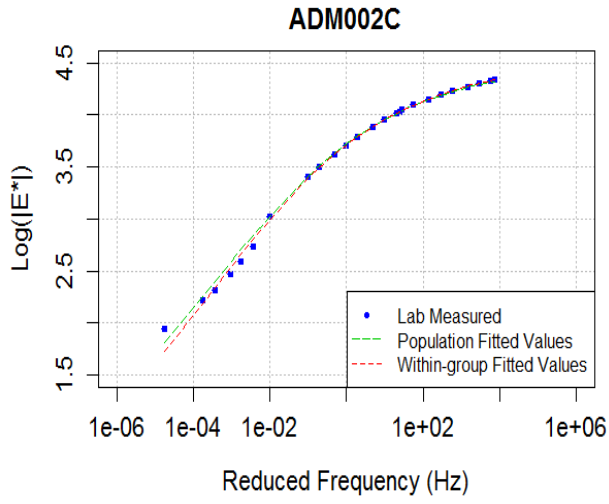
ADM002C
Log(|E*|)
4.5
3.5
2.5
1.5
1e-06
1e-04
1e-02
1e+02
1e+06
Reduced Frequency (Hz)
Lab Measured
Population Fitted Values
Within-group Fitted Values

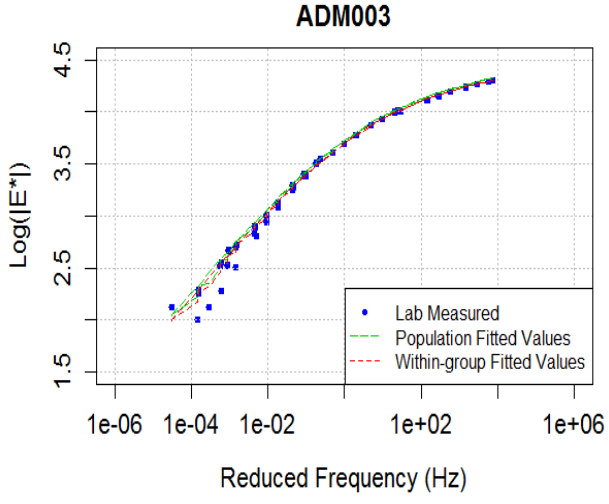
ADM003
Log(|E*|)
4.5
3.5
2.5
1.5
1e-06
1e-04
1e-02
1e+02
1e+06
Reduced Frequency (Hz)
Lab Measured
Population Fitted Values
Within-group Fitted Values

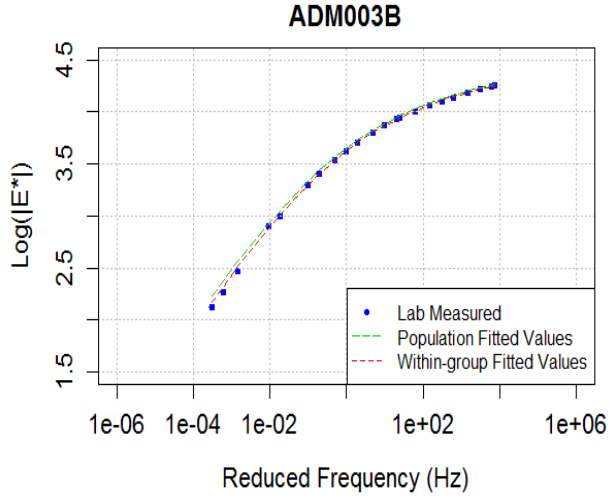
ADM003B
Log(|E*|)
4.5
3.5
2.5
1.5
1e-06
1e-04
1e-02
1e+02
1e+06
Reduced Frequency (Hz)
Lab Measured
Population Fitted Values
Within-group Fitted Values

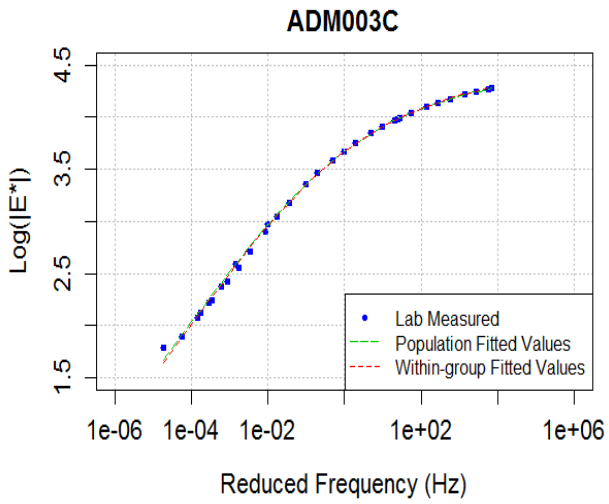
ADM003C
Log(|E*|)
4.5
3.5
2.5
1.5
1e-06
1e-04
1e-02
1e+02
1e+06
Reduced Frequency (Hz)
Lab Measured
Population Fitted Values
Within-group Fitted Values

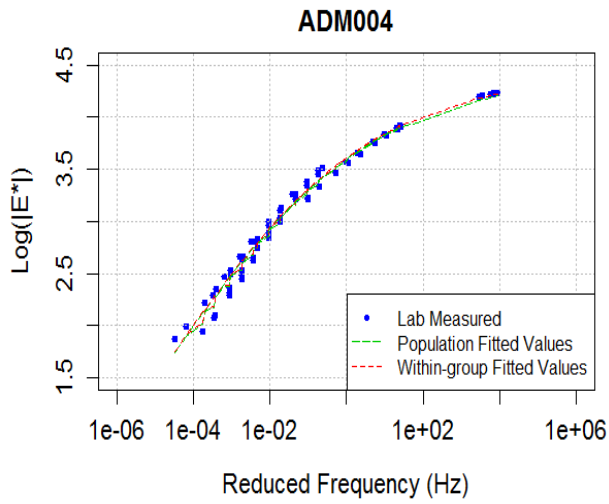
ADM004
Log(|E*|)
4.5
3.5
2.5
1.5
1e-06
1e-04
1e-02
1e+02
1e+06
Reduced Frequency (Hz)
Lab Measured
Population Fitted Values
Within-group Fitted Values

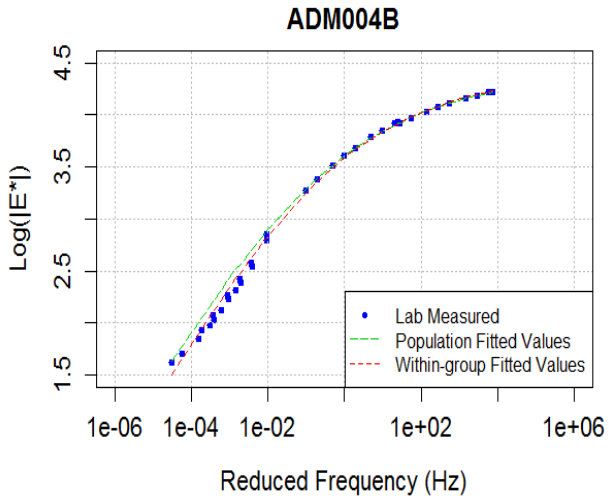
ADM004B
Log(|E*|)
4.5
3.5
2.5
1.5
1e-06
1e-04
1e-02
1e+02
1e+06
Reduced Frequency (Hz)
Lab Measured
Population Fitted Values
Within-group Fitted Values

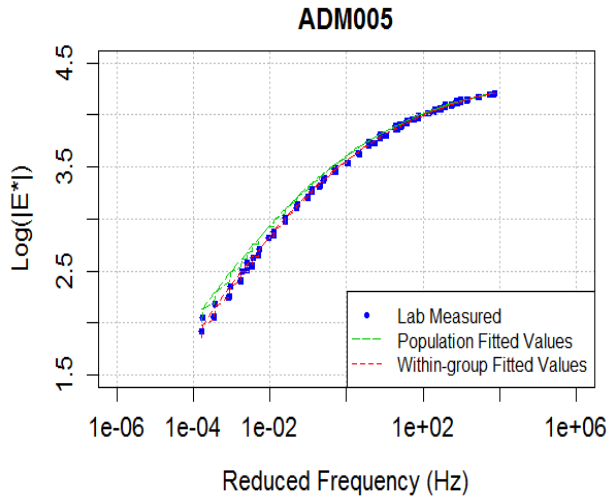
ADM005
Log(|E*|)
4.5
3.5
2.5
1.5
1e-06
1e-04
1e-02
1e+02
1e+06
Reduced Frequency (Hz)
Lab Measured
Population Fitted Values
Within-group Fitted Values

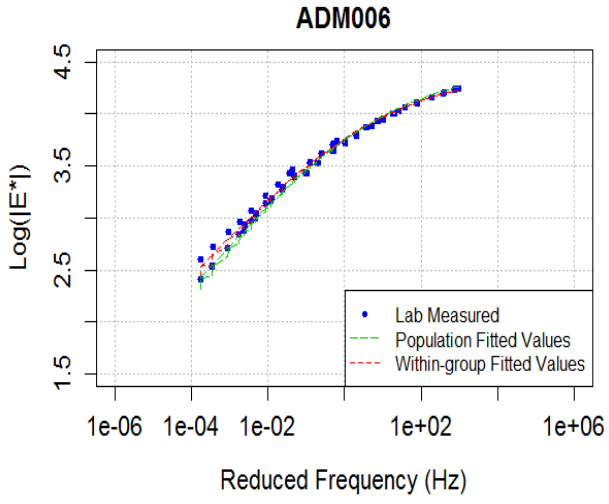
ADM006
Log(|E*|)
4.5
3.5
2.5
1.5
1e-06
1e-04
1e-02
1e+02
1e+06
Reduced Frequency (Hz)
Lab Measured
Population Fitted Values
Within-group Fitted Values

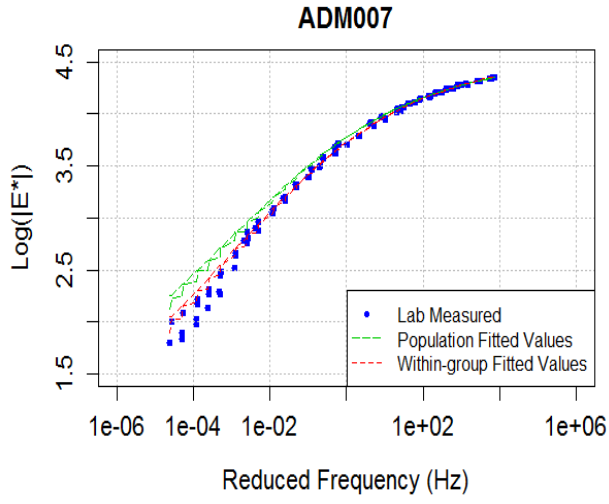
ADM007
Log(|E*|)
4.5
3.5
2.5
1.5
1e-06
1e-04
1e-02
1e+02
1e+06
Reduced Frequency (Hz)
Lab Measured
Population Fitted Values
Within-group Fitted Values

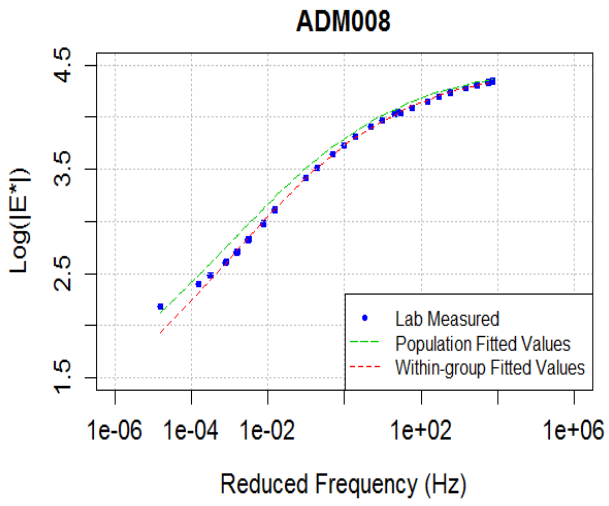
ADM008
Log(|E*|)
4.5
3.5
2.5
1.5
1e-06
1e-04
1e-02
1e+02
1e+06
Reduced Frequency (Hz)
Lab Measured
Population Fitted Values
Within-group Fitted Values

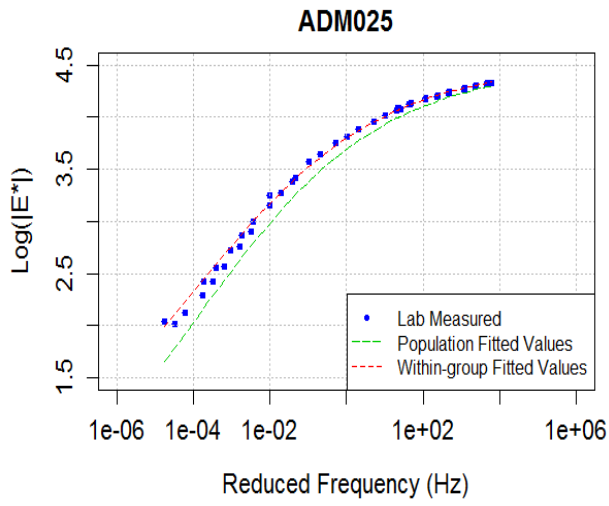
ADM025
Log(|E*|)
4.5
3.5
2.5
1.5
1e-06
1e-04
1e-02
1e+02
1e+06
Reduced Frequency (Hz)
Lab Measured
Population Fitted Values
Within-group Fitted Values

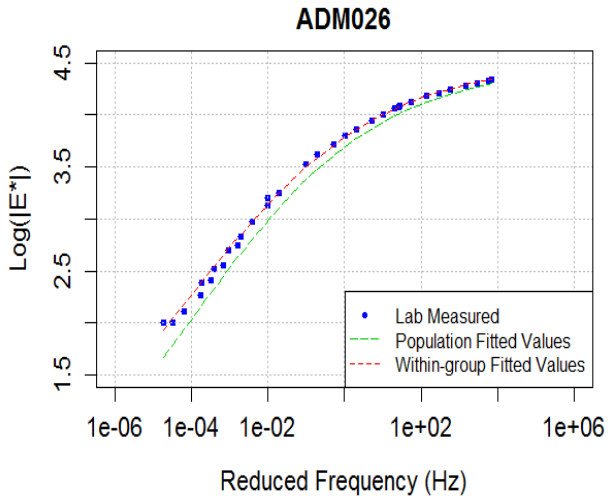
ADM026
Log(|E*|)
4.5
3.5
2.5
1.5
1e-06
1e-04
1e-02
1e+02
1e+06
Reduced Frequency (Hz)
Lab Measured
Population Fitted Values
Within-group Fitted Values

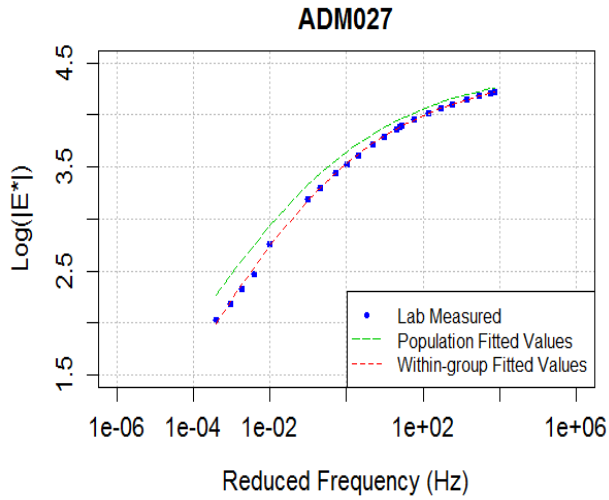
ADM027
Log(|E*|)
4.5
3.5
2.5
1.5
1e-06
1e-04
1e-02
1e+02
1e+06
Reduced Frequency (Hz)
Lab Measured
Population Fitted Values
Within-group Fitted Values

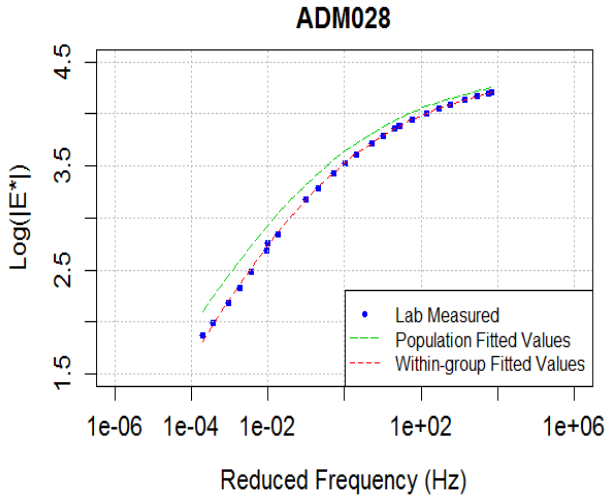
ADM028
Log(|E*|)
4.5
3.5
2.5
1.5
1e-06
1e-04
1e-02
1e+02
1e+06
Reduced Frequency (Hz)
Lab Measured
Population Fitted Values
Within-group Fitted Values

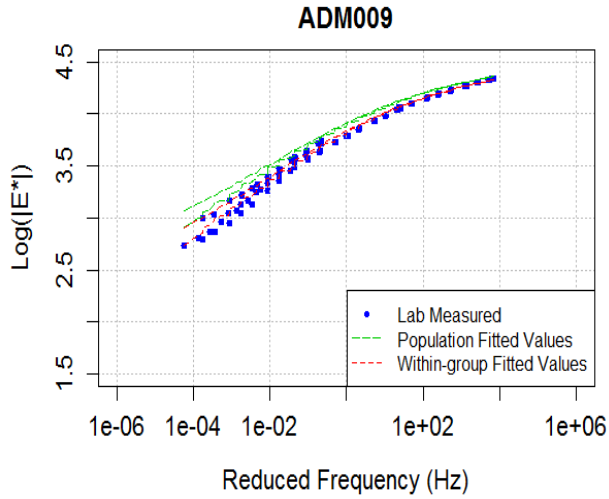
ADM009
Log(|E*|)
4.5
3.5
2.5
1.5
1e-06
1e-04
1e-02
1e+02
1e+06
Reduced Frequency (Hz)
Lab Measured
Population Fitted Values
Within-group Fitted Values

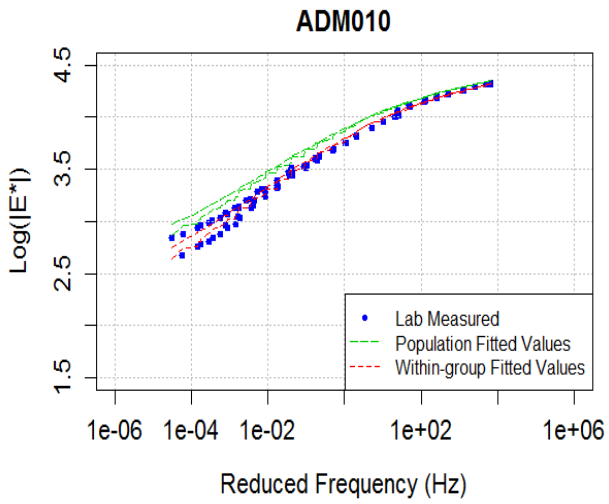
ADM010
Log(|E*|)
4.5
3.5
2.5
1.5
1e-06
1e-04
1e-02
1e+02
1e+06
Reduced Frequency (Hz)
Lab Measured
Population Fitted Values
Within-group Fitted Values

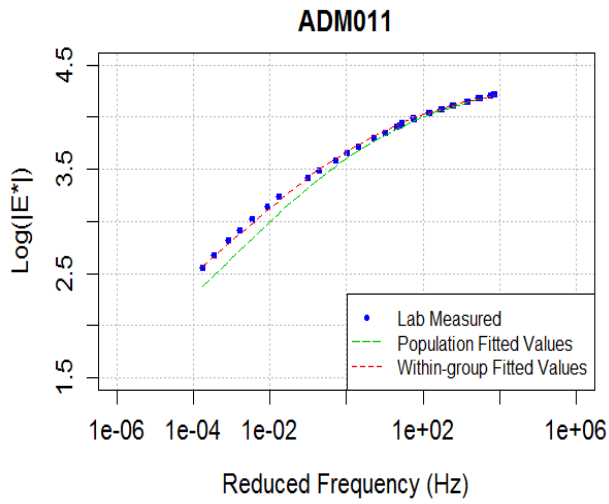
ADM011
Log(|E*|)
4.5
3.5
2.5
1.5
1e-06
1e-04
1e-02
1e+02
1e+06
Reduced Frequency (Hz)
Lab Measured
Population Fitted Values
Within-group Fitted Values

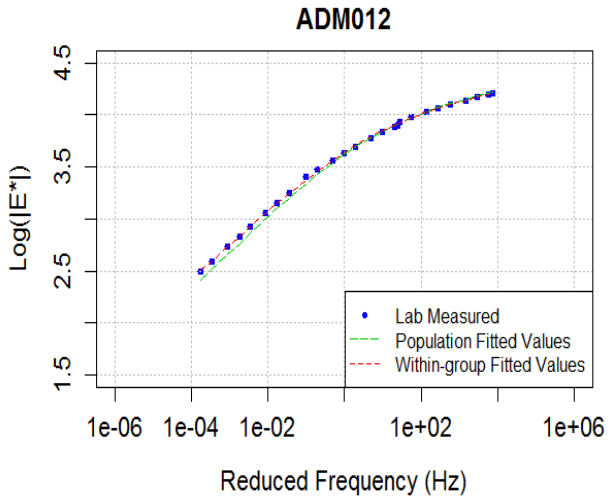
ADM012
Log(|E*|)
4.5
3.5
2.5
1.5
1e-06
1e-04
1e-02
1e+02
1e+06
Reduced Frequency (Hz)
Lab Measured
Population Fitted Values
Within-group Fitted Values

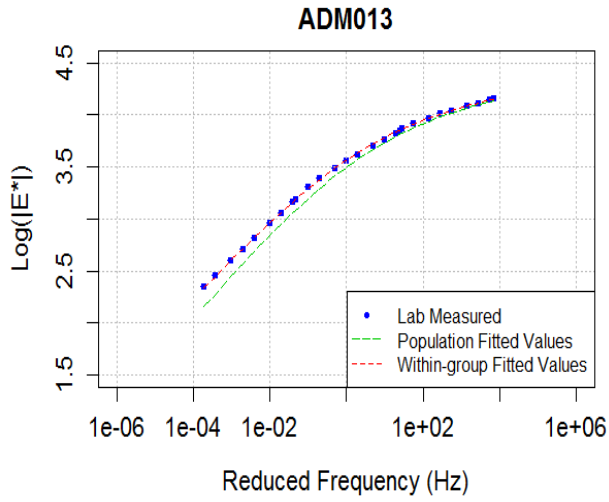
ADM013
Log(|E*|)
4.5
3.5
2.5
1.5
1e-06
1e-04
1e-02
1e+02
1e+06
Reduced Frequency (Hz)
Lab Measured
Population Fitted Values
Within-group Fitted Values

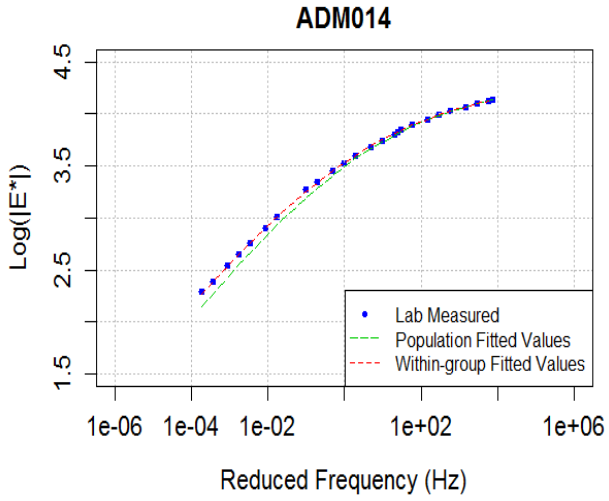
ADM014
Log(|E*|)
4.5
3.5
2.5
1.5
1e-06
1e-04
1e-02
1e+02
1e+06
Reduced Frequency (Hz)
Lab Measured
Population Fitted Values
Within-group Fitted Values

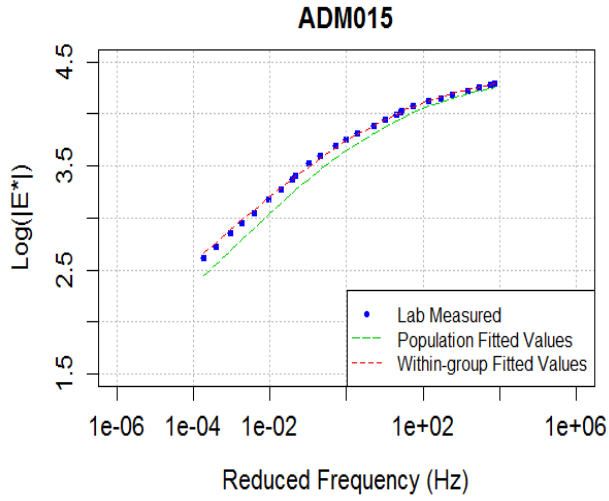
ADM015
Log(|E*|)
4.5
3.5
2.5
1.5
1e-06
1e-04
1e-02
1e+02
1e+06
Reduced Frequency (Hz)
Lab Measured
Population Fitted Values
Within-group Fitted Values

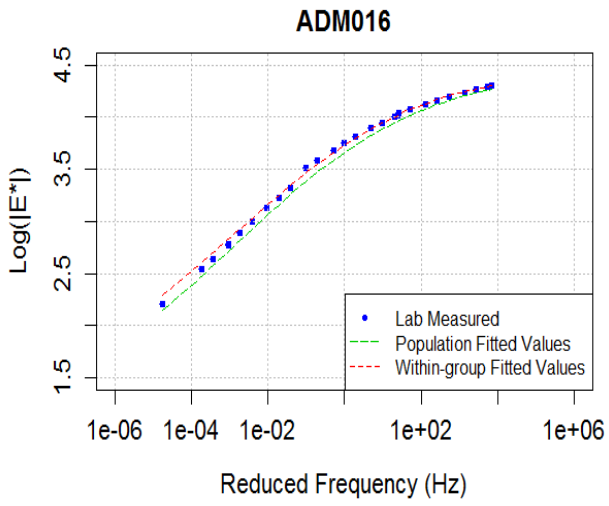
ADM016
Log(|E*|)
4.5
3.5
2.5
1.5
1e-06
1e-04
1e-02
1e+02
1e+06
Reduced Frequency (Hz)
Lab Measured
Population Fitted Values
Within-group Fitted Values

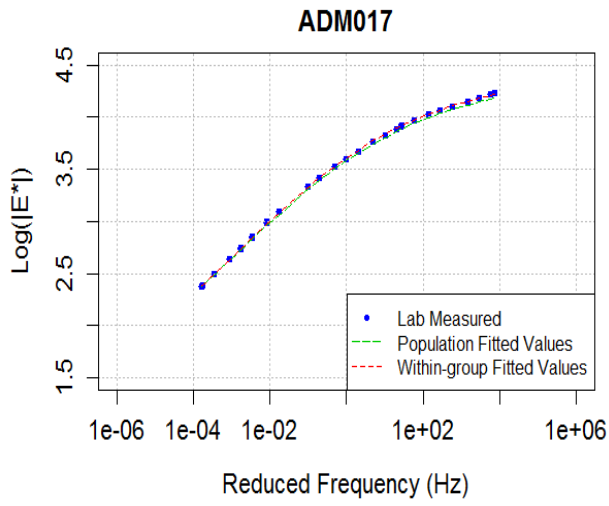
ADM017
Log(|E*|)
4.5
3.5
2.5
1.5
1e-06
1e-04
1e-02
1e+02
1e+06
Reduced Frequency (Hz)
Lab Measured
Population Fitted Values
Within-group Fitted Values

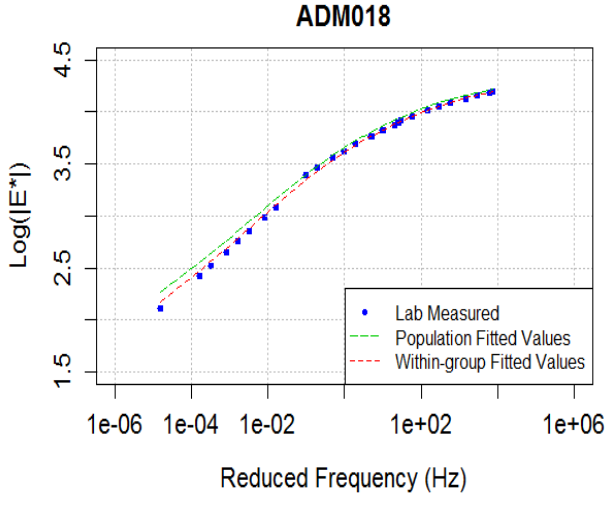
ADM018
Log(|E*|)
4.5
3.5
2.5
1.5
1e-06
1e-04
1e-02
1e+02
1e+06
Reduced Frequency (Hz)
Lab Measured
Population Fitted Values
Within-group Fitted Values

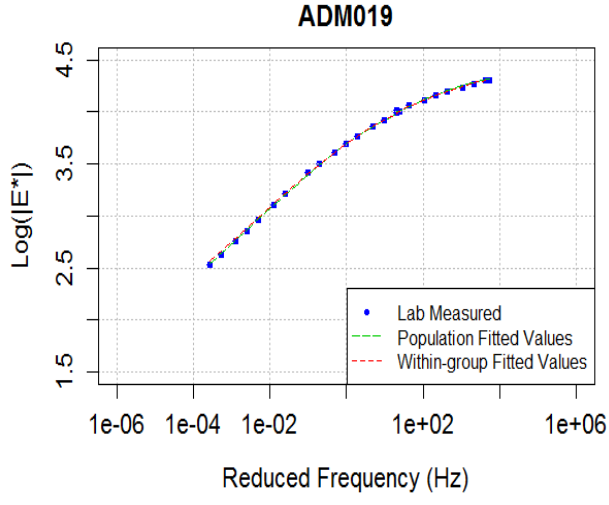
ADM019
Log(|E*|)
4.5
3.5
2.5
1.5
1e-06
1e-04
1e-02
1e+02
1e+06
Reduced Frequency (Hz)
Lab Measured
Population Fitted Values
Within-group Fitted Values

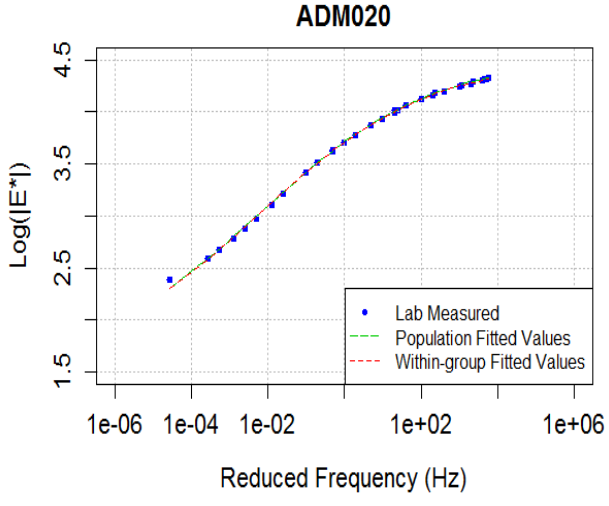
ADM020
Log(|E*|)
4.5
3.5
2.5
1.5
1e-06
1e-04
1e-02
1e+02
1e+06
Reduced Frequency (Hz)
Lab Measured
Population Fitted Values
Within-group Fitted Values

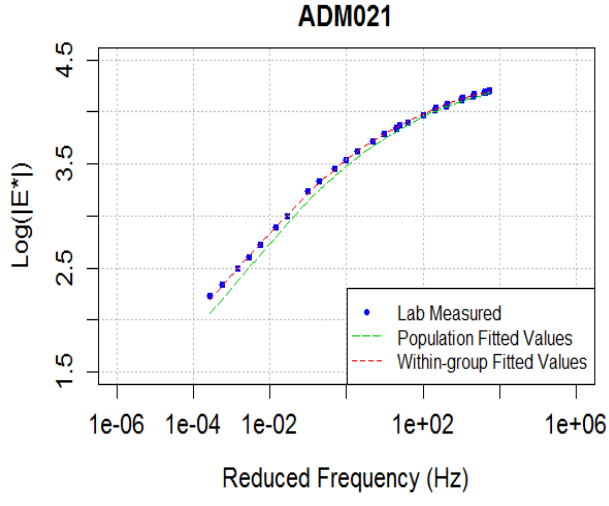
ADM021
Log(|E*|)
4.5
3.5
2.5
1.5
1e-06
1e-04
1e-02
1e+02
1e+06
Reduced Frequency (Hz)
Lab Measured
Population Fitted Values
Within-group Fitted Values

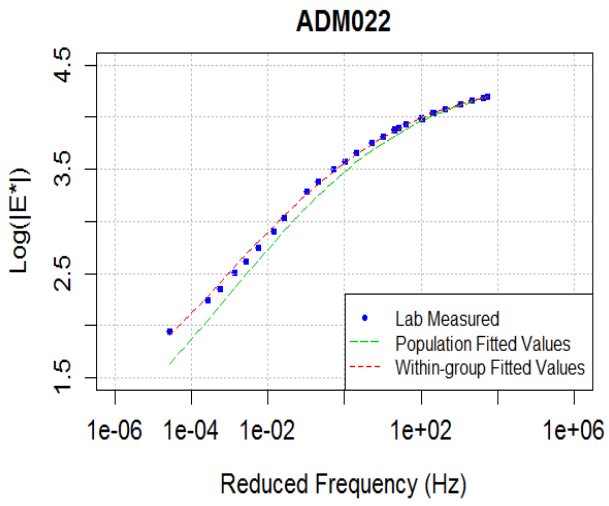
ADM022
Log(|E*|)
4.5
3.5
2.5
1.5
1e-06
1e-04
1e-02
1e+02
1e+06
Reduced Frequency (Hz)
Lab Measured
Population Fitted Values
Within-group Fitted Values

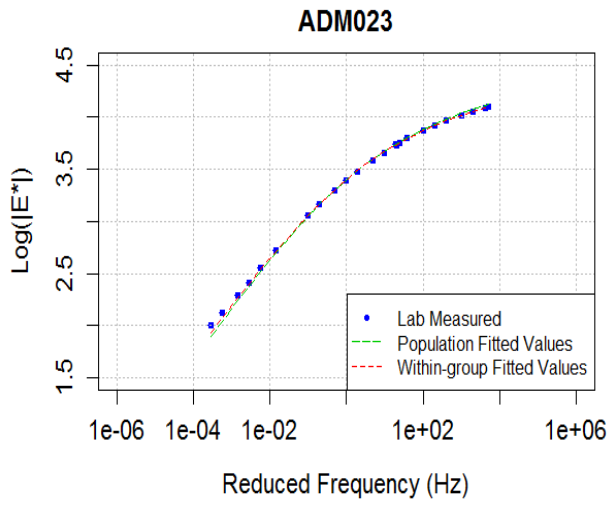
ADM023
Log(|E*|)
4.5
3.5
2.5
1.5
1e-06
1e-04
1e-02
1e+02
1e+06
Reduced Frequency (Hz)
Lab Measured
Population Fitted Values
Within-group Fitted Values

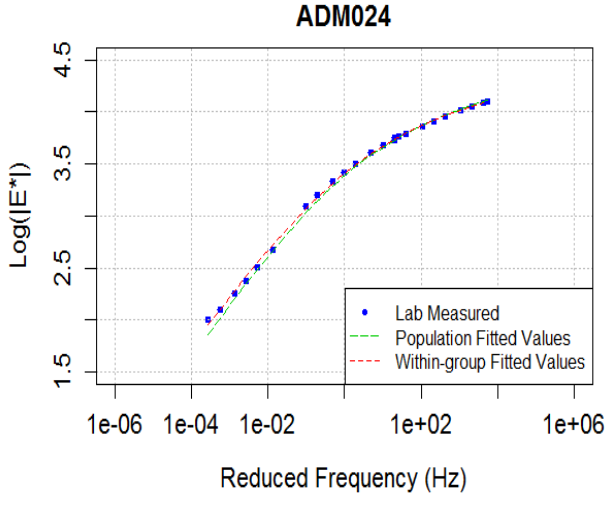
ADM024
Log(|E*|)
4.5
3.5
2.5
1.5
1e-06
1e-04
1e-02
1e+02
1e+06
Reduced Frequency (Hz)
Lab Measured
Population Fitted Values
Within-group Fitted Values

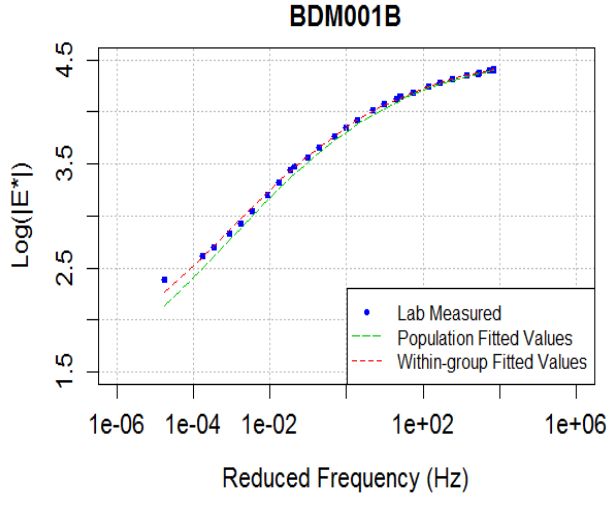
BDM001B
Log(|E*|)
4.5
3.5
2.5
1.5
1e-06
1e-04
1e-02
1e+02
1e+06
Reduced Frequency (Hz)
Lab Measured
Population Fitted Values
Within-group Fitted Values

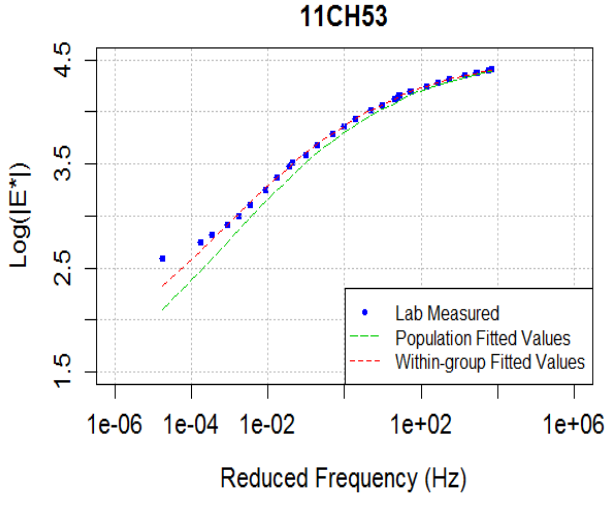
11CH53
Log(|E*|)
4.5
3.5
2.5
1.5
1e-06
1e-04
1e-02
1e+02
1e+06
Reduced Frequency (Hz)
Lab Measured
Population Fitted Values
Within-group Fitted Values

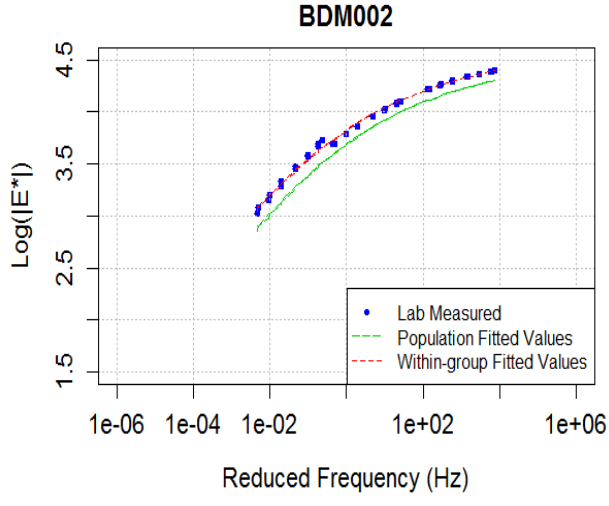
BDM002
Log(|E*|)
4.5
3.5
2.5
1.5
1e-06
1e-04
1e-02
1e+02
1e+06
Reduced Frequency (Hz)
Lab Measured
Population Fitted Values
Within-group Fitted Values

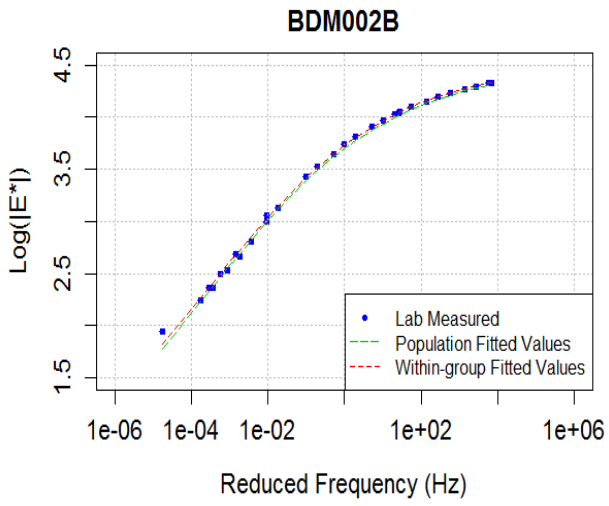
BDM002B
Log(|E*|)
4.5
3.5
2.5
1.5
1e-06
1e-04
1e-02
1e+02
1e+06
Reduced Frequency (Hz)
Lab Measured
Population Fitted Values
Within-group Fitted Values

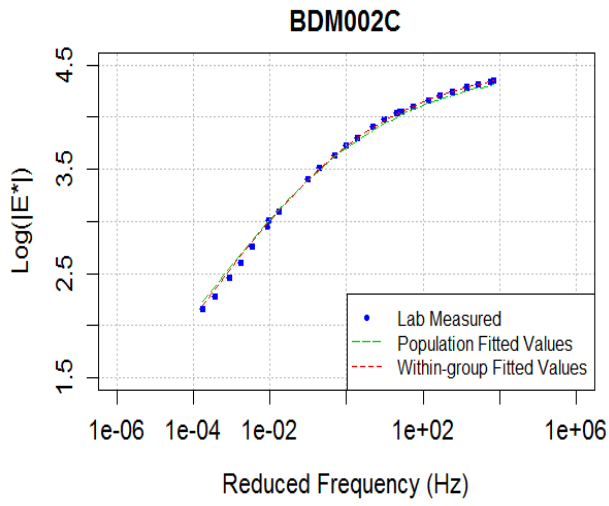
BDM002C
Log(|E*|)
4.5
3.5
2.5
1.5
1e-06
1e-04
1e-02
1e+02
1e+06
Reduced Frequency (Hz)
Lab Measured
Population Fitted Values
Within-group Fitted Values

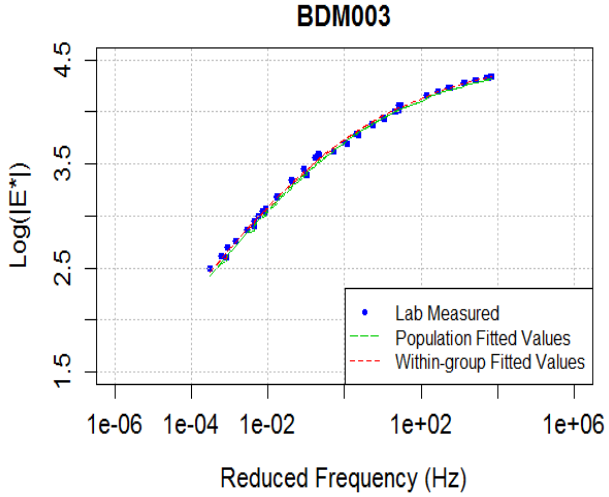
BDM003
Log(|E*|)
4.5
3.5
2.5
1.5
1e-06
1e-04
1e-02
1e+02
1e+06
Reduced Frequency (Hz)
Lab Measured
Population Fitted Values
Within-group Fitted Values

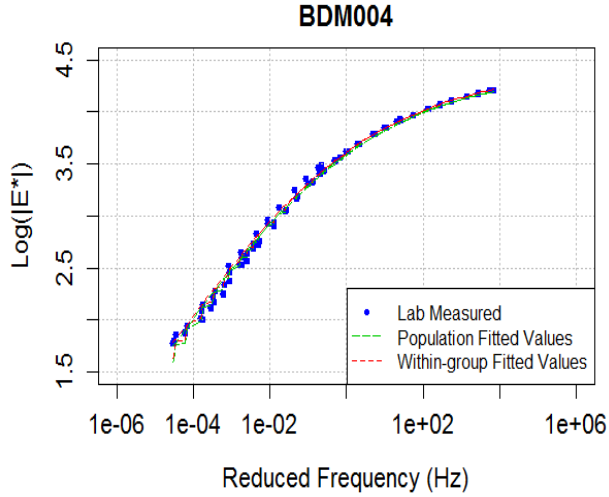
BDM004
Log(|E*|)
4.5
3.5
2.5
1.5
1e-06
1e-04
1e-02
1e+02
1e+06
Reduced Frequency (Hz)
Lab Measured
Population Fitted Values
Within-group Fitted Values

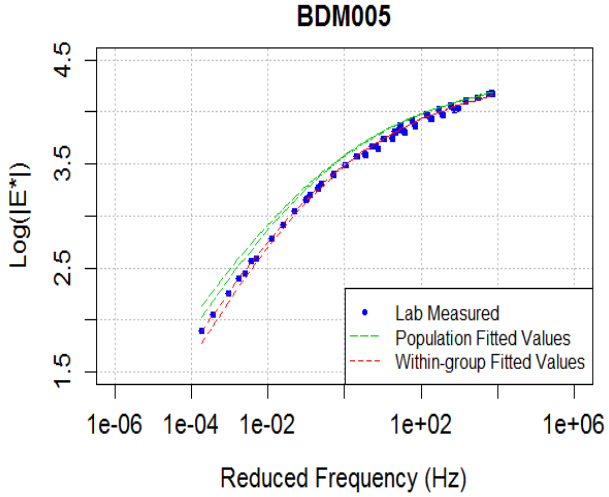
BDM005
Log(|E*|)
4.5
3.5
2.5
1.5
1e-06
1e-04
1e-02
1e+02
1e+06
Reduced Frequency (Hz)
Lab Measured
Population Fitted Values
Within-group Fitted Values

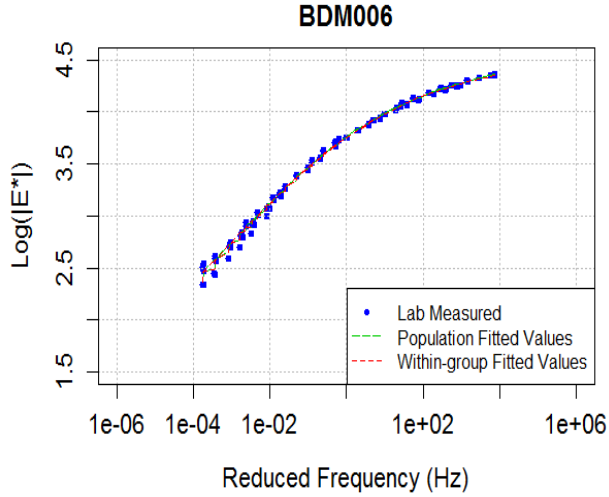
BDM006
Log(|E*|)
4.5
3.5
2.5
1.5
1e-06
1e-04
1e-02
1e+02
1e+06
Reduced Frequency (Hz)
Lab Measured
Population Fitted Values
Within-group Fitted Values

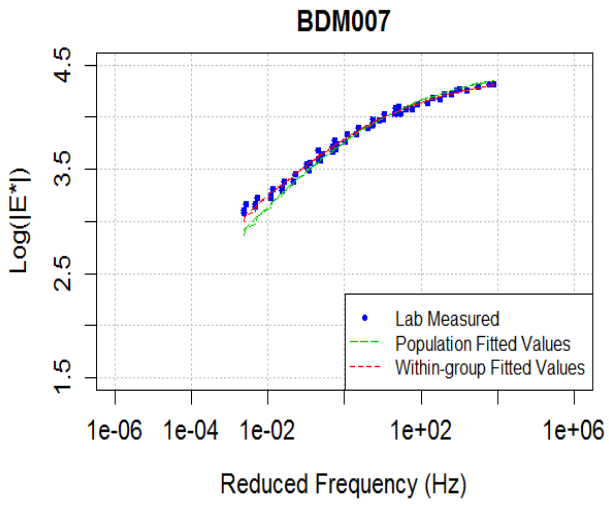
BDM007
Log(|E*|)
4.5
3.5
2.5
1.5
1e-06
1e-04
1e-02
1e+02
1e+06
Reduced Frequency (Hz)
Lab Measured
Population Fitted Values
Within-group Fitted Values

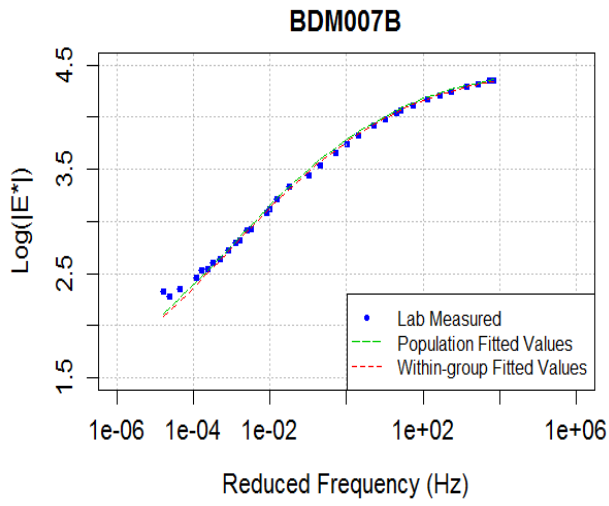
BDM007B
Log(|E*|)
4.5
3.5
2.5
1.5
1e-06
1e-04
1e-02
1e+02
1e+06
Reduced Frequency (Hz)
Lab Measured
Population Fitted Values
Within-group Fitted Values

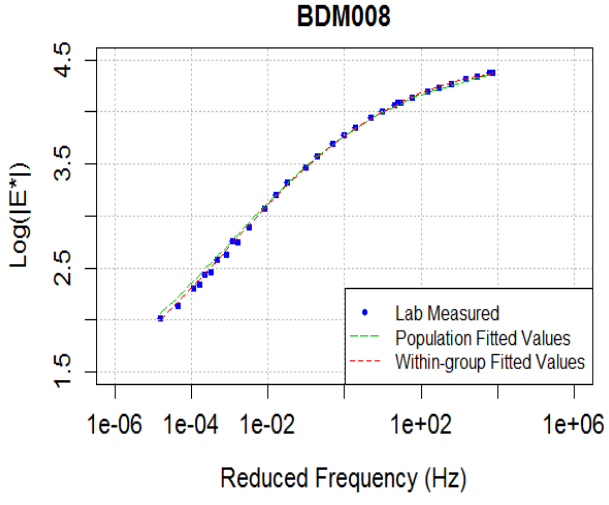
BDM008
Log(|E*|)
4.5
3.5
2.5
1.5
1e-06
1e-04
1e-02
1e+02
1e+06
Reduced Frequency (Hz)
Lab Measured
Population Fitted Values
Within-group Fitted Values

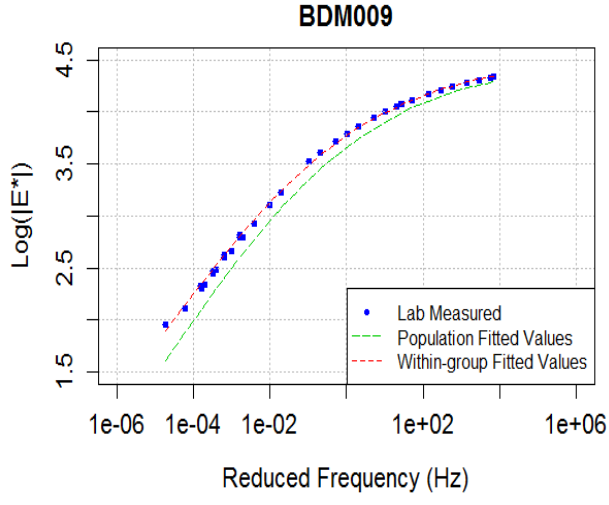
BDM009
Log(|E*|)
4.5
3.5
2.5
1.5
1e-06
1e-04
1e-02
1e+02
1e+06
Reduced Frequency (Hz)
Lab Measured
Population Fitted Values
Within-group Fitted Values

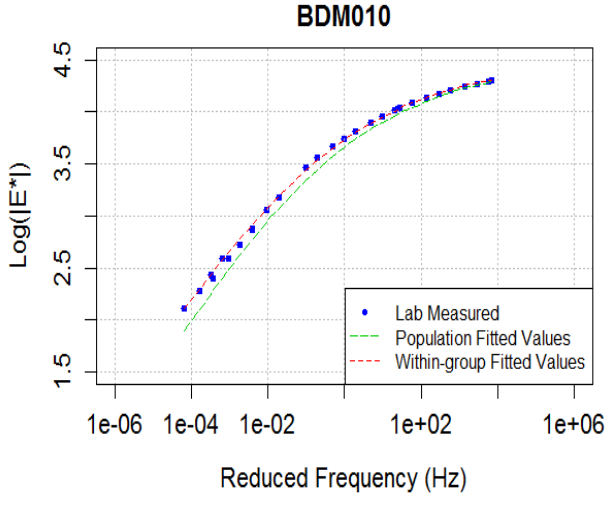
BDM010
Log(|E*|)
4.5
3.5
2.5
1.5
1e-06
1e-04
1e-02
1e+02
1e+06
Reduced Frequency (Hz)
Lab Measured
Population Fitted Values
Within-group Fitted Values

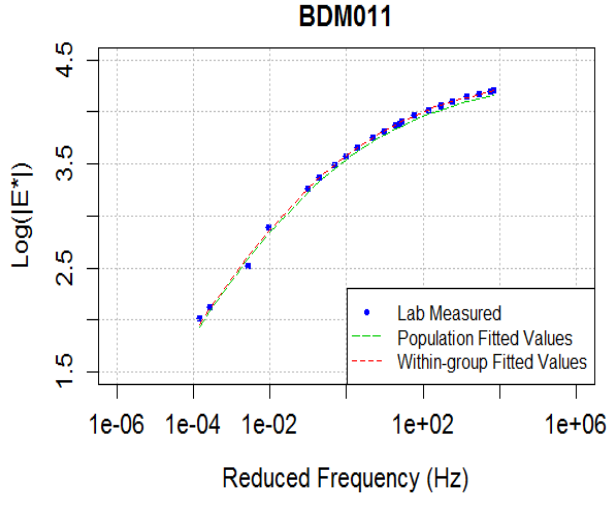
BDM011
Log(|E*|)
4.5
3.5
2.5
1.5
1e-06
1e-04
1e-02
1e+02
1e+06
Reduced Frequency (Hz)
Lab Measured
Population Fitted Values
Within-group Fitted Values

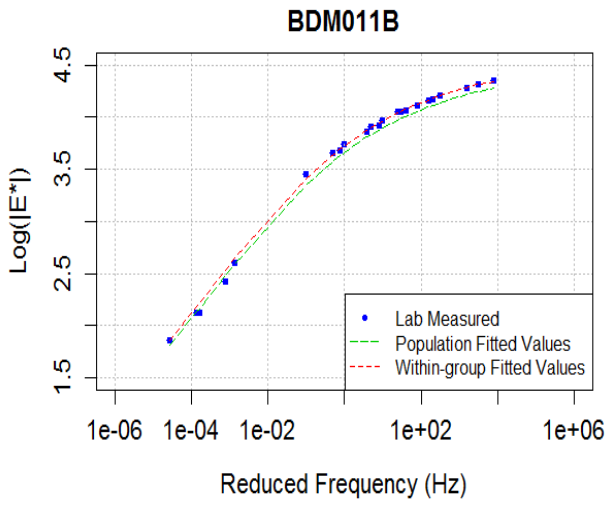
BDM011B
Log(|E*|)
4.5
3.5
2.5
1.5
1e-06
1e-04
1e-02
1e+02
1e+06
Reduced Frequency (Hz)
Lab Measured
Population Fitted Values
Within-group Fitted Values

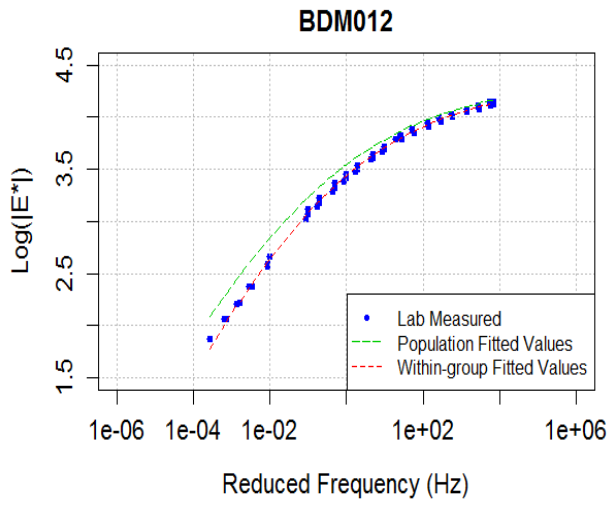
BDM012
Log(|E*|)
4.5
3.5
2.5
1.5
1e-06
1e-04
1e-02
1e+02
1e+06
Reduced Frequency (Hz)
Lab Measured
Population Fitted Values
Within-group Fitted Values

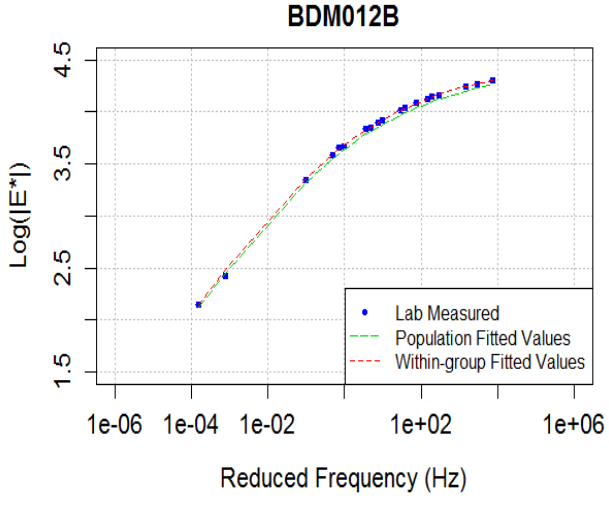
BDM012B
Log(|E*|)
4.5
3.5
2.5
1.5
1e-06
1e-04
1e-02
1e+02
1e+06
Reduced Frequency (Hz)
Lab Measured
Population Fitted Values
Within-group Fitted Values

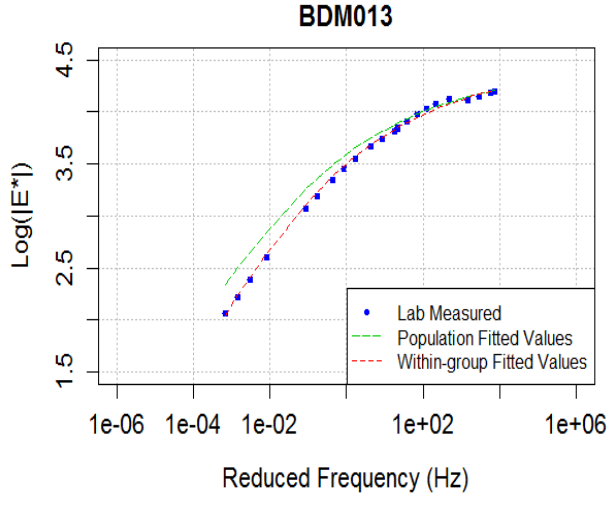
BDM013
Log(|E*|)
4.5
3.5
2.5
1.5
1e-06
1e-04
1e-02
1e+02
1e+06
Reduced Frequency (Hz)
Lab Measured
Population Fitted Values
Within-group Fitted Values

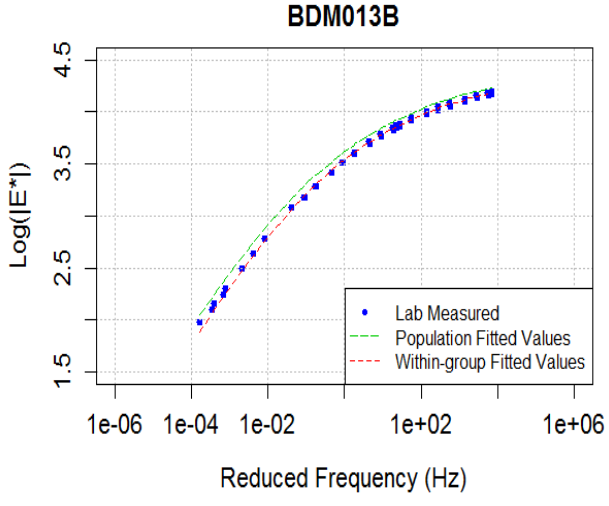
BDM013B
Log(|E*|)
4.5
3.5
2.5
1.5
1e-06
1e-04
1e-02
1e+02
1e+06
Reduced Frequency (Hz)
Lab Measured
Population Fitted Values
Within-group Fitted Values

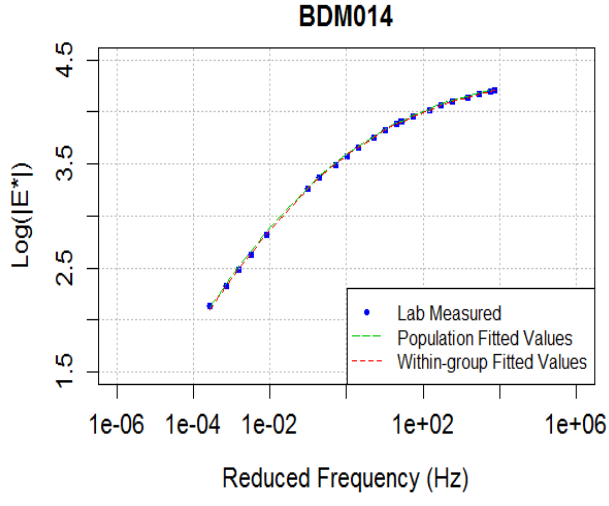
BDM014
Log(|E*|)
4.5
3.5
2.5
1.5
1e-06
1e-04
1e-02
1e+02
1e+06
Reduced Frequency (Hz)
Lab Measured
Population Fitted Values
Within-group Fitted Values

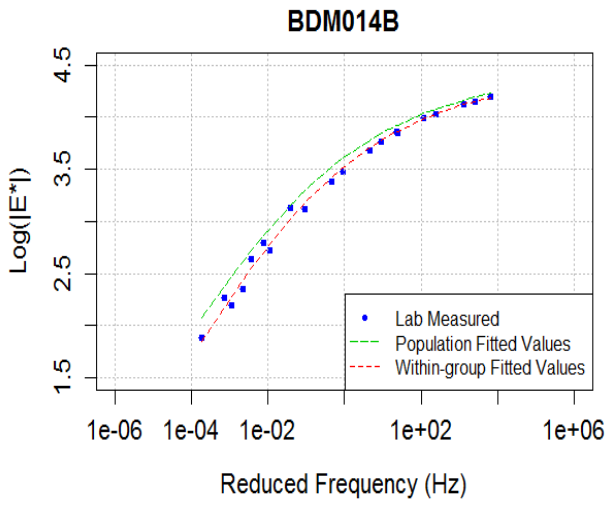
BDM014B
Log(|E*|)
4.5
3.5
2.5
1.5
1e-06
1e-04
1e-02
1e+02
1e+06
Reduced Frequency (Hz)
Lab Measured
Population Fitted Values
Within-group Fitted Values

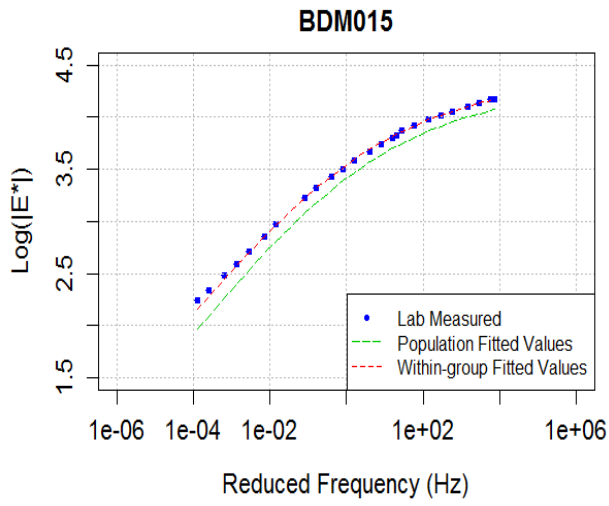
BDM015
Log(|E*|)
4.5
3.5
2.5
1.5
1e-06
1e-04
1e-02
1e+02
1e+06
Reduced Frequency (Hz)
Lab Measured
Population Fitted Values
Within-group Fitted Values

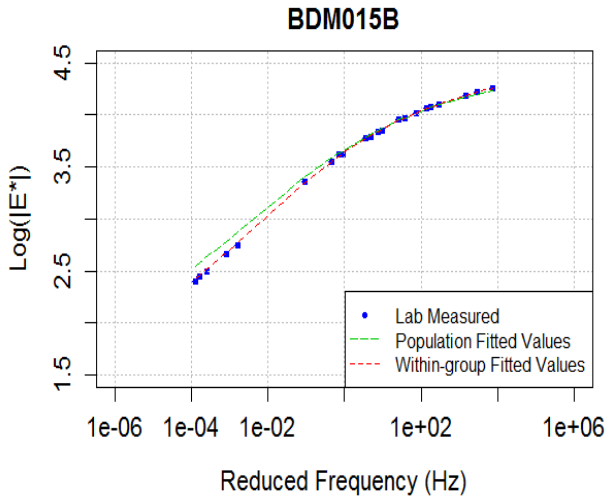
BDM015B
Log(|E*|)
4.5
3.5
2.5
1.5
1e-06
1e-04
1e-02
1e+02
1e+06
Reduced Frequency (Hz)
Lab Measured
Population Fitted Values
Within-group Fitted Values

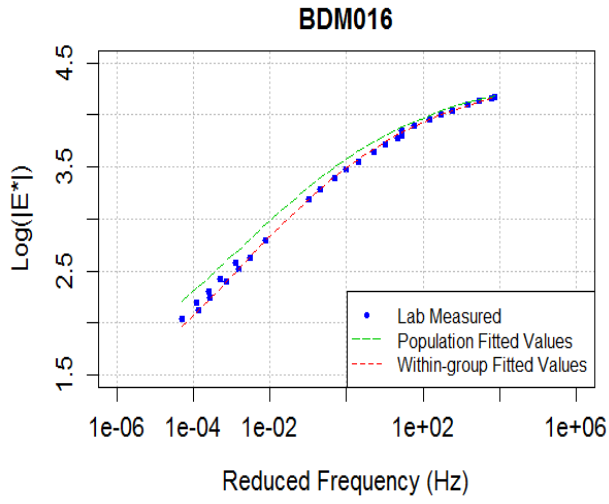
BDM016
Log(|E*|)
4.5
3.5
2.5
1.5
1e-06
1e-04
1e-02
1e+02
1e+06
Reduced Frequency (Hz)
Lab Measured
Population Fitted Values
Within-group Fitted Values

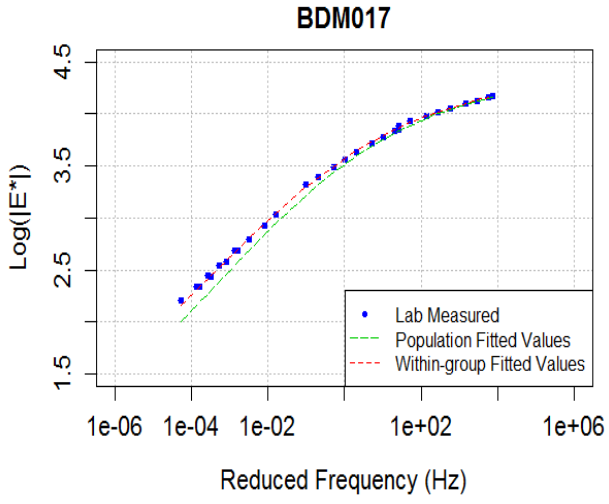
BDM017
Log(|E*|)
4.5
3.5
2.5
1.5
1e-06
1e-04
1e-02
1e+02
1e+06
Reduced Frequency (Hz)
Lab Measured
Population Fitted Values
Within-group Fitted Values

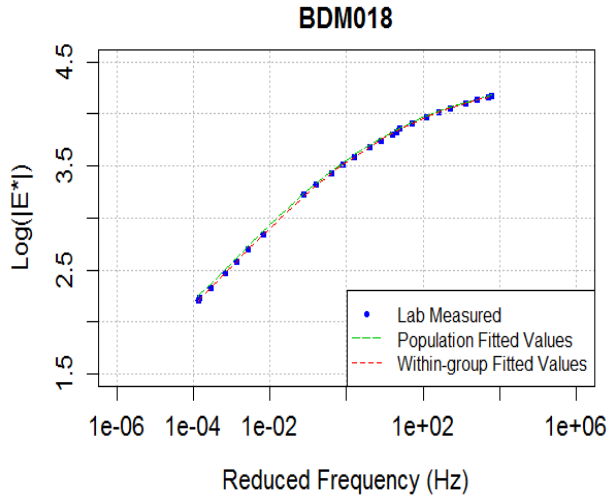
BDM018
Log(|E*|)
4.5
3.5
2.5
1.5
1e-06
1e-04
1e-02
1e+02
1e+06
Reduced Frequency (Hz)
Lab Measured
Population Fitted Values
Within-group Fitted Values

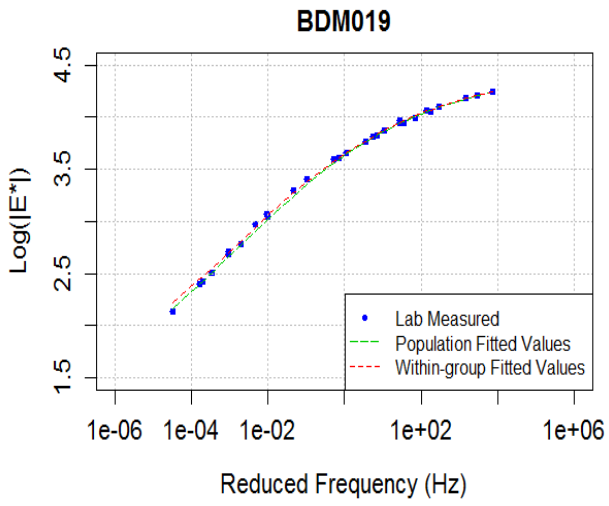
BDM019
Log(|E*|)
4.5
3.5
2.5
1.5
1e-06
1e-04
1e-02
1e+02
1e+06
Reduced Frequency (Hz)
Lab Measured
Population Fitted Values
Within-group Fitted Values

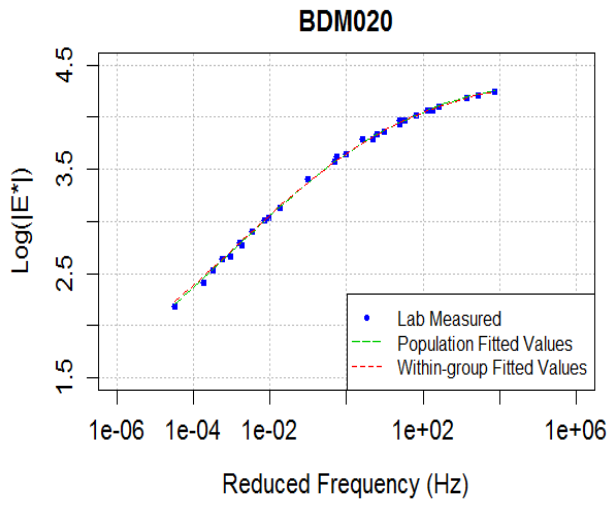
BDM020
Log(|E*|)
4.5
3.5
2.5
1.5
1e-06
1e-04
1e-02
1e+02
1e+06
Reduced Frequency (Hz)
Lab Measured
Population Fitted Values
Within-group Fitted Values

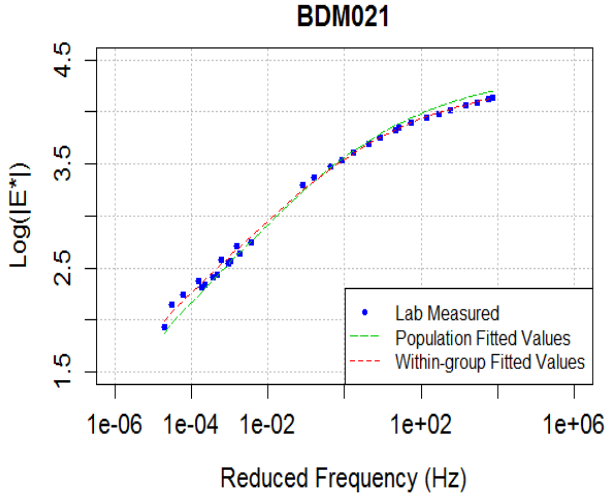
BDM021
Log(|E*|)
4.5
3.5
2.5
1.5
1e-06
1e-04
1e-02
1e+02
1e+06
Reduced Frequency (Hz)
Lab Measured
Population Fitted Values
Within-group Fitted Values

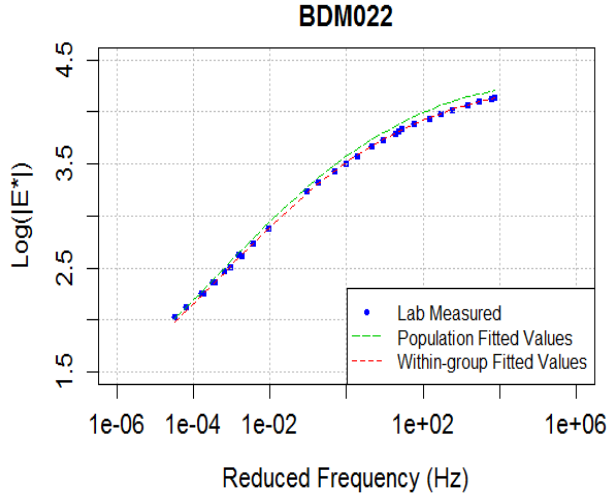
BDM022
Log(|E*|)
4.5
3.5
2.5
1.5
1e-06
1e-04
1e-02
1e+02
1e+06
Reduced Frequency (Hz)
Lab Measured
Population Fitted Values
Within-group Fitted Values

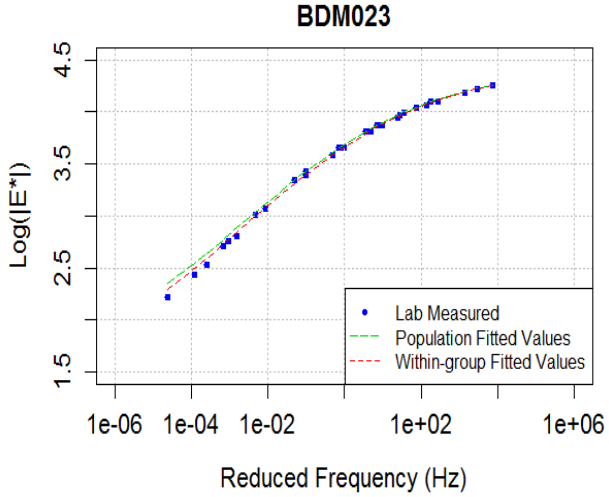
BDM023
Log(|E*|)
4.5
3.5
2.5
1.5
1e-06
1e-04
1e-02
1e+02
1e+06
Reduced Frequency (Hz)
Lab Measured
Population Fitted Values
Within-group Fitted Values

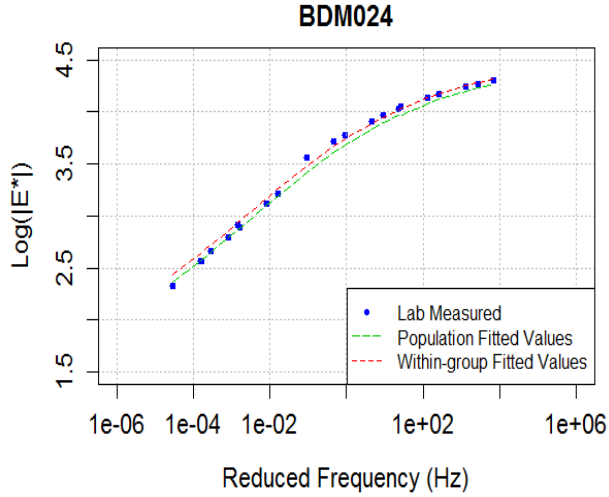
BDM024
Log(|E*|)
4.5
3.5
2.5
1.5
1e-06
1e-04
1e-02
1e+02
1e+06
Reduced Frequency (Hz)
Lab Measured
Population Fitted Values
Within-group Fitted Values

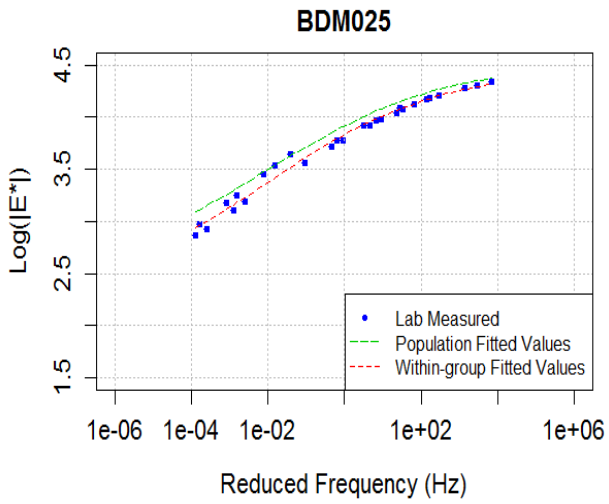
BDM025
Log(|E*|)
4.5
3.5
2.5
1.5
1e-06
1e-04
1e-02
1e+02
1e+06
Reduced Frequency (Hz)
Lab Measured
Population Fitted Values
Within-group Fitted Values

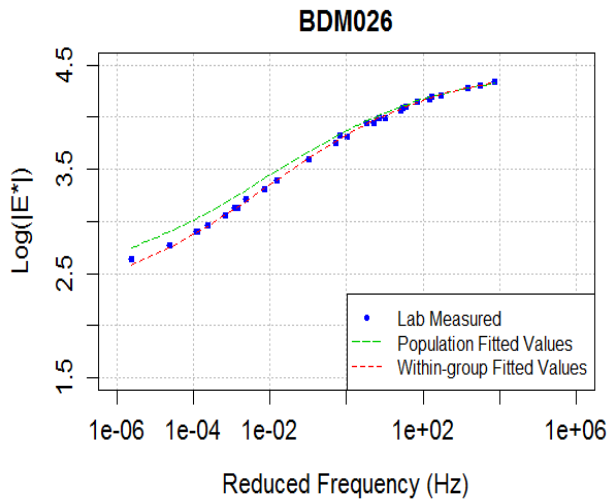
BDM026
Log(|E*|)
4.5
3.5
2.5
1.5
1e-06
1e-04
1e-02
1e+02
1e+06
Reduced Frequency (Hz)
Lab Measured
Population Fitted Values
Within-group Fitted Values

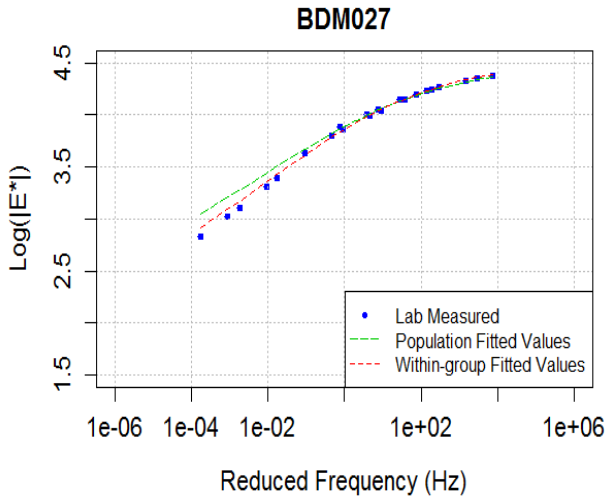
BDM027
Log(|E*|)
4.5
3.5
2.5
1.5
1e-06
1e-04
1e-02
1e+02
1e+06
Reduced Frequency (Hz)
Lab Measured
Population Fitted Values
Within-group Fitted Values

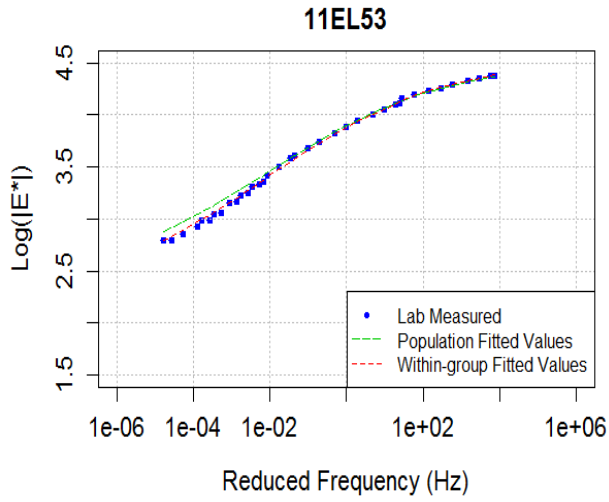
11EL53
Log(|E*|)
4.5
3.5
2.5
1.5
1e-06
1e-04
1e-02
1e+02
1e+06
Reduced Frequency (Hz)
Lab Measured
Population Fitted Values
Within-group Fitted Values

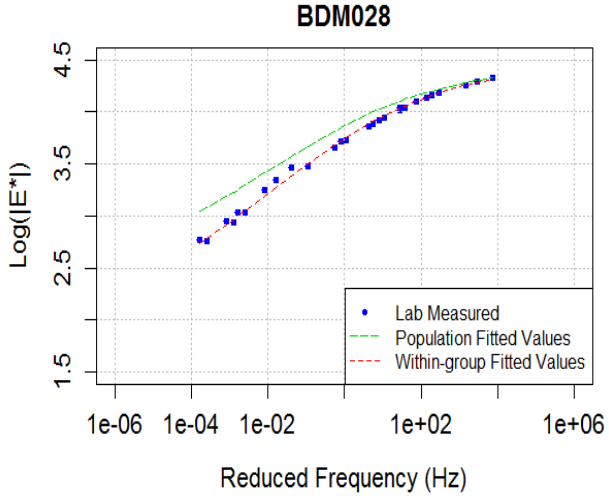
BDM028
Log(|E*|)
4.5
3.5
2.5
1.5
1e-06
1e-04
1e-02
1e+02
1e+06
Reduced Frequency (Hz)
Lab Measured
Population Fitted Values
Within-group Fitted Values

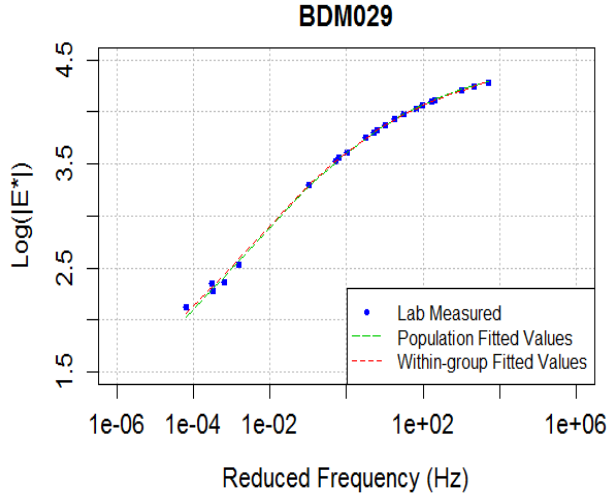
BDM029
Log(|E*|)
4.5
3.5
2.5
1.5
1e-06
1e-04
1e-02
1e+02
1e+06
Reduced Frequency (Hz)
Lab Measured
Population Fitted Values
Within-group Fitted Values

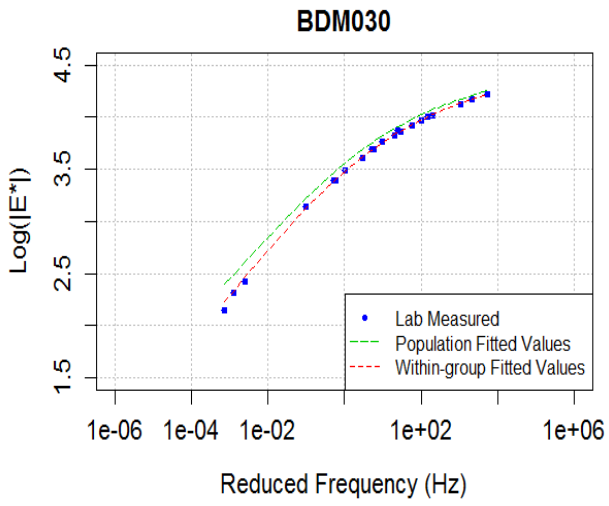
BDM030
Log(|E*|)
4.5
3.5
2.5
1.5
1e-06
1e-04
1e-02
1e+02
1e+06
Reduced Frequency (Hz)
Lab Measured
Population Fitted Values
Within-group Fitted Values

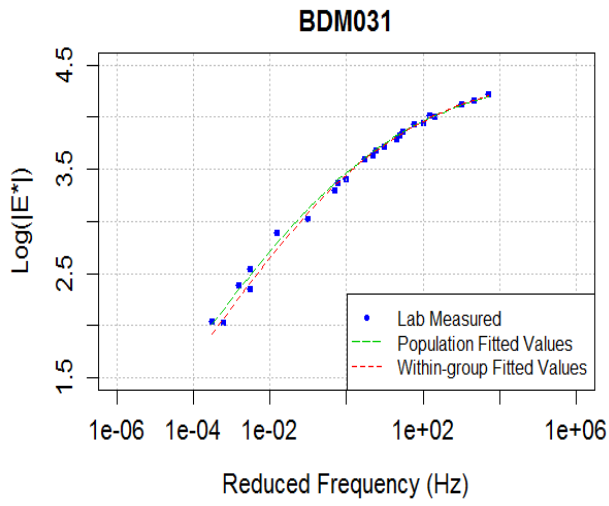
BDM031
Log(|E*|)
4.5
3.5
2.5
1.5
1e-06
1e-04
1e-02
1e+02
1e+06
Reduced Frequency (Hz)
Lab Measured
Population Fitted Values
Within-group Fitted Values

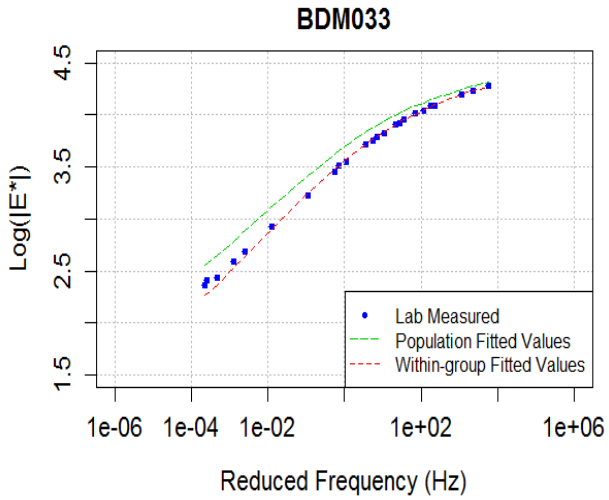
BDM033
Log(|E*|)
4.5
3.5
2.5
1.5
1e-06
1e-04
1e-02
1e+02
1e+06
Reduced Frequency (Hz)
Lab Measured
Population Fitted Values
Within-group Fitted Values

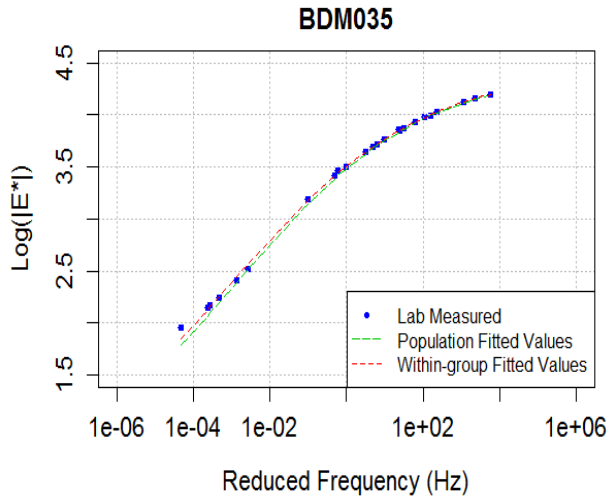
BDM035
Log(|E*|)
4.5
3.5
2.5
1.5
1e-06
1e-04
1e-02
1e+02
1e+06
Reduced Frequency (Hz)
Lab Measured
Population Fitted Values
Within-group Fitted Values

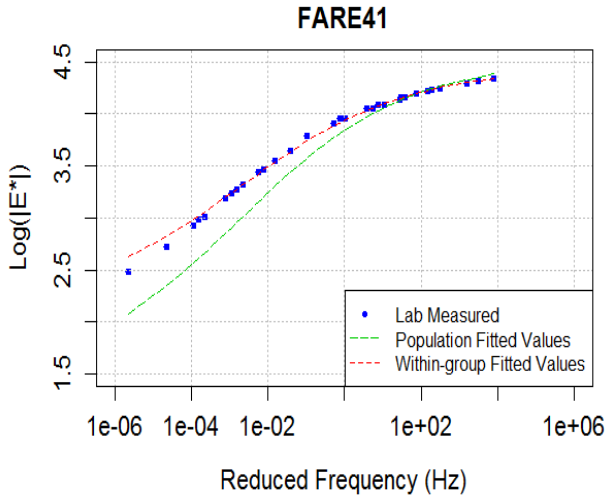
FARE41
Log(|E*|)
4.5
3.5
2.5
1.5
1e-06
1e-04
1e-02
1e+02
1e+06
Reduced Frequency (Hz)
Lab Measured
Population Fitted Values
Within-group Fitted Values

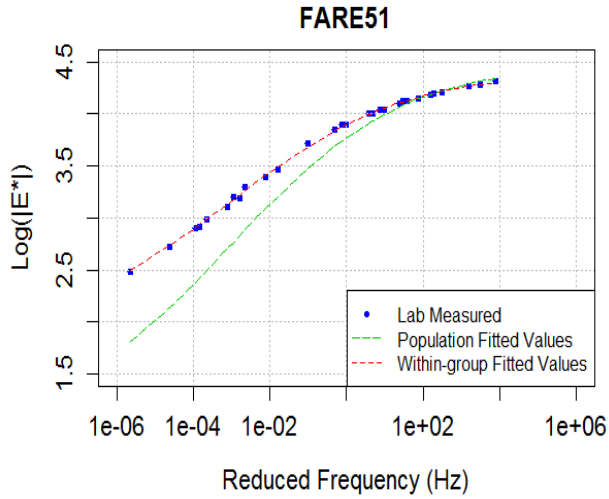
FARE51
Log(|E*|)
4.5
3.5
2.5
1.5
1e-06
1e-04
1e-02
1e+02
1e+06
Reduced Frequency (Hz)
Lab Measured
Population Fitted Values
Within-group Fitted Values

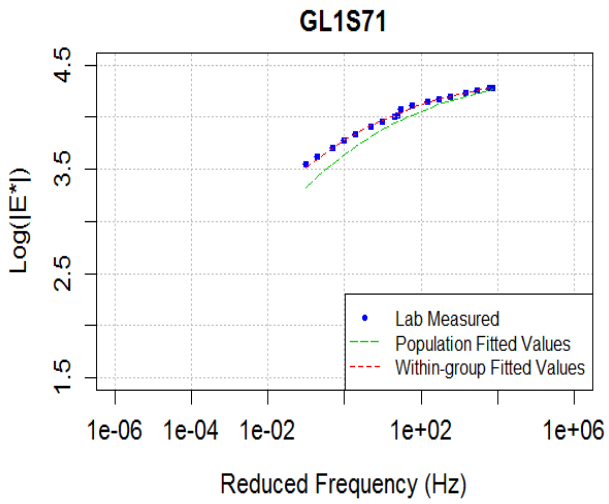
GL1S71
Log(|E*|)
4.5
3.5
2.5
1.5
1e-06
1e-04
1e-02
1e+02
1e+06
Reduced Frequency (Hz)
Lab Measured
Population Fitted Values
Within-group Fitted Values

REFERENCES

AASHTO Guide for Design of Pavement Structures. (1993). American Association of State Highway and Transportation Officials. Washington, D.C

AASHTO. (2016). Standard Specifications for Transportation Materials and Methods of Sampling and Testing, 35th Edition and AASHTO Provisional Standards.

Andrei, D., Witczak, M.W., and Mirza, M.W. (1999). Development of a Revised Predictive Model for the Dynamic (Complex) Modulus of Asphalt Mixtures. NCHRP 1-37A Interim Team Report, University of Maryland.

Apeagyei, A.K., Diefenderfer, B. K., Diefenderfer, S.D. (2012). "Development of Dynamic Modulus Master Curves for Hot Mix Asphalt with Abbreviated Testing Temperatures," International Journal of Pavement Engineering, 13(2). p. 98-109.

ARA, Inc., ERES Consultants Division. (2004). Guide for Mechanistic–Empirical Design of New and Rehabilitated Pavement Structures. Final report, NCHRP Project 1-37A. Transportation Research Board of the National Academies, Washington, D.C.

Archilla, A.R. (2000). Development of Rutting Progression Models by Combining Data from Multiple Sources. Ph.D dissertation, University of California at Berkeley, Berkeley, CA.

Archilla, A.R., and Madanat, S.M. (2001). Estimation of Rutting Models by Combining data from Different Sources. Journal of Transportation Engineering, Volume 127(5), pp 379-389.

Archilla, A.R., Ooi, P.S.K., and Sandefur, K.G. (2007). Estimation of a Resilient Modulus Model for Cohesive Soils Using Joint Estimation and Mixed Effects. Journal of Geotechnical and Geoenvironmental Engineering. Volume 133(8), pp 984-994.

Archilla, A.R. (2010). Developing Master Curve Models for the Local Conditions: A Case Study for Hawaii. Journal of the Association of Asphalt Paving Technologists (AAPT), Vol 79, pp 278-308.

Archilla, A.R. Ooi, P.S. and Diaz-Vasquez L.G. (2014). Update of the State Pavement Management Systems and Implementation of the Mechanistic-Empirical Pavement Design Guide. Final Report. FHWA/HI-15-53463. Honolulu, HI.

Asphalt Institute (2008). MS-1 Thickness Design for Highways and Streets. Lexington, Ky. Ninth edition, reprint.

Bahia, H.U., Hanson, D.I., Zeng, M., Zhai, H., Khatri, M.A. and Anderson, R.M. (2001). Characteristics of modified asphalt binders in Superpave mix design. NCHRP Report 459. Transportation Research Board – National Research Council. Washington, D.C.

Bari, J., Witczak, M.W. (2006). Development of a New Revised Version of the Witczak E* Predictive Model for Hot Mix Asphalt Mixtures. Journal of the Association of Asphalt Paving Technologists (AAPT), Vol 75, pp 381-424.

Ben-Akiva, M., Lerman, S. (1985). Discrete Choice Analysis: Theory and Application to Travel Demand. The MIT Press. Cambridge, Massachusetts.

Bennert, T. (2012). Advanced characterization testing of Forta-FI fiber reinforced high performance thin overlay (HPTO). Proposal for FORTA Corporation. Center for Advanced Infrastructure and Transportation. Rodgers Univerity. Piscataway, New Jersey.

Bennert, T. (2012). Forta-Fi mixture evaluation. Report for the New Jersey Department of Transportation (NJDOT). Center for Advanced Infrastructure and Transportation. Rodgers University. Piscataway, New Jersey.

Bonaquist, R. (2011). Mix design practices for warm mix asphalt. NCHRP Report 691. Transportation Research Board – National Research Council. Washington, D.C.

Bueno, B. S., Silva, W. R., Lima, D. C., and Minete, E. (2003). "Engineering Properties of Fiber Reinforced Cold Asphalt Mixes. Technical Note," J. Environ. Eng.,Vol. 129, No. 10 pp. 952-955.

Ceylan, Halil, K. Gopalakrishnan, S. Kim (2008). Advanced Approaches to Hot-Mix Asphalt Dynamic Modulus Prediction. Canadian Journal of Civil Engineering, Vol. 35, n 7, pp. 699-707.

Christensen Jr, D.W., Pelinen, T., Bonaquist, R.F. (2003). Hirsch Model for Estimating the Modulus of Asphalt Concrete. Journal of the Association of Asphalt Paving Technologists. Vol.72. p. 97-121

Cooper, S.B. (2009). Evaluation of HMA mixtures containing Sasobit®. Technical Assistance Report No. 06-ITA. State Project No. 064-90-0081. Louisiana Transportation Research Center. Baton Rouge, Louisiana.

Corrales-Azofeifa, J., Archilla, A.R. (2016). Effects of Confinement on the Dynamic Modulus of Hot Asphalt Mixtures and Interaction with Binder/Fiber Combinations and Air Voids. Presented at the 95th Annual Meeting of the Transportation Research Board(TRB). Washington. D.C.

Davidian, M. and Giltinan, D.M. (1995). Nonlinear Models for Repeated Measurement Data. Chapman & Hall. Great Britain.

Epps, J.A., Sebaaly, P.E., Penaranda, J., Maher, M.R., McCann, M.B. and Hand, A.J. (2000). Compatibility of a test for moisture-induced damage with Superpave volumetric mix design. NCHRP Report 444. Transportation Research Board – National Research Council. Washington, D.C.

Giambelluca, T.W., Q. Chen, A.G. Frazier, J.P. Price, Y.-L. Chen, P.-S. Chu, J.K. Eischeid, and D.M. Delparte (2013): Online Rainfall Atlas of Hawai'i. Bull. Amer. Meteor. Soc. 94, 313-316, doi: 10.1175/BAMS-D-11-00228.1.

Gibson, N. and X., Li. (2015). Cracking Characterization of Asphalt Mixtures with Fiber Reinforcement Using Cyclic Fatigue and Direct Tension Strength Tests, TRB 94th Annual Meeting Compendium of Papers, Transportation Research Board Annual Meeting, Paper #15-4306.

Hicks, G.R., Santucci, L. and Aschenbrener, T. (2003). Introduction to Seminar Objectives. Moisture Sensitivity of Asphalt Pavements – A National Seminar. San Diego, California.

Highway Research Board. (1961). The AASHO Road Test: Report 1, History and Description of the Project. Special Report 61A. National Academy of Sciences. Washington, D.C

Hveem, F.N. and Carmany, R.M. (1949). The Factors Underlying the Rational Design of Pavements Proceedings of the 28th Annual Meeting of the Highway Research Board, Washington, D.C. Vol. 28 pp. 101-136. December 7-10, 1948.

Jamshidi, A., Hamzah, M.O. and Aman, M.Y. (2012). Effects of Sasobit ® content on the rheological characteristics of unaged and aged asphalt binders at high and intermediate temperatures. Mat Res., Sao Carlos, Vol 15, number 4, pp. 628-638.

Kaloush, K.E., K.P. Biligiri, W.A. Zeiada, M.C. Rodenzo, and J.X. Reed. (2010). Evaluation of Fiber-Reinforced Asphalt Mixtures Using Advanced Materials Characterization Tests, Journal of Testing and Evaluation, Vol. 38, No. 4, pp. 1–12.

Kanabar, N. (2010). Comparison of ethylene terpolymer, styrene butadiene, and polyphosphoric acid type modifiers for asphalt cement. Master of Science thesis. Queen's University. Kingston, Ontario, Canada.

Kim, Y., Guddati, M., Underwood, B., Yun, T., y Savadatti, V. (2009). Development of a multiaxial viscoelastoplastic continuum damage model for asphalt mixtures. FHWA Publication No. DTFH61-05-H-00019, Federal Highway Administration, McLean, VA., 2009.

Kim, Y. and Lutif, J.S. (2006). Material selection and design consideration for moisture damage of asphalt pavements. Technical Report P564. University of Nebraska-Lincoln, Nebraska.

Kluttz, B. (2012). Introduction to asphalt modification. Presented at the Nebraska Asphalt Paving Conference. Association of Modified Asphalt Procedures. Nebraska.

Kridan, F.A., Arshad, A.K. and Rahman, M.Y. (2011). The effect of warm mix asphalt additive (Sasobit®) on determination of optimum bitumen content. International Journal of Research & Reviews in Applied Sciences. Vol. 6, Issue 4, pp 400-406.

Lacroix, A., Underwood, B.S., y Kim, R. (2011). Reduced Testing Protocol for Measuring the Confined Dynamic Modulus of Asphalt Mixtures. In Transportation Research Record: Journal of the Transportation Research Board, No. 2210, Transportation Research Board of the National Academies, Washington, D.C., pp. 20-29.

Lee, S. J., Rust, J. P., Hamouda, H., Kim, Y. R., and Borden, R. H. (2005). Fatigue Cracking Resistance of Fiber-Reinforced Asphalt Concrete. Text. Res. J., Vol. 75, No. 2, pp. 123–128.

Leiva-Villacorta, F., Loria-Salazar, L., Aguiar-Moya, J.P. (2013). Development of an improved and more effective dynamic modulus E* model for mixtures in Costa Rica by means of artificial neural networks. In Transportation Research Record 92nd Annual Meeting Compendium of Papers 13-2176. Washington, D.C.

Little, D.N. and Jones IV, D.R. (2003). Chemical and Mechanical Processes of Moisture Damage in Hot-Mix Asphalt Pavements. Moisture Sensitivity of Asphalt Pavements – A National Seminar. San Diego, California.

McDaniel, R.S. (2015). Fiber Additives in Asphalt Mixtures, NCHRP Synthesis 475, National Cooperative Highway Research Program, Transportation Research Board, Washington, D.C.

Morikawa, T., Ben-Akiva, M., and Yamada, K. (1991). Forecasting intercity rail ridership using revealed preference and stated preference data. Transportation Research Record, 1328, Transportation Research Board, National Research Council, Washington, D.C., pp 30-35.

Nadkarni, A. A., K. E. Kaloush, W. A. Zeiada, and K. P. Biligiri. (2009). Using Dynamic Modulus Test to Evaluate Moisture Susceptibility of Asphalt Mixtures. In Transportation Research Record: Journal of the Transportation Research Board, No. 2127, Transportation Research Board of the National Academies, Washington, D.C., pp. 29–35.

Panabaker, H. (2009). DuPont innovative asphalt modifiers. North Central Asphalt User/Producer Goup Meeting. Monona Terrace, Madison, Wyoming.

Pellinen, T. K., Witczak, M.W., Marasteanu, M., Chehab, G., Alavi, S., y Dongre, R. (2002). Stress-Dependent Master Curve Construction for Dynamic (Complex) Modulus. Journal of the Association of Asphalt Paving Technologists, Vol. 71, pp. 281-309.

Pierce, L.M. and McGovern, G. (2014). Implementation of the AASHTO Mechanistic-Empirical Pavement Design Guide and Software. NCHRP Synthesis 457. Transportation Research Board of the National Academies, Washington, D.C.

Pierce, L.M. (2011). Handbook for Pavement Design, Construction, and Management. NCHRP01-46. Transportation Research Board of the National Academies, Washington, D.C.

Pyndyck, R.S., Rubinfeld, D.L. (1991). Econometric Models and Economic Forecasts. Third Edition. McGraw-Hill, Inc. New York.

Pinheiro, J.A., and Bates, D.M. (2000). Mixed-Effects models in S and S-Plus, Springer, New York.

Prozzi, J.A., and Madanat, S.M. (2004). Development of Pavement Performance Models by Combining Experimental and Field Data. Journal of Infrastructure Systems. Volume 10(1), pp 9-22.

Qin, Q., Farrar, M., Turner, T.F. and Planche J. (2015). Characterization of the effects of wax (Sasobit®) on asphalt binder. Fundamental properties of asphalts and modified asphalts III product: FP 13. Western Research Institute. Laramie Wyoming

Rae Hunter, E. and Ksaibati, K. (2002). Evaluating moisture susceptibility of asphalt mixes. Univeristy of Wyoming. Thesis Report. Laramie, Wyoming.

Sebaaly, P., Little, D.N. and Epps, J.A. (2006). The benefits of hydrated lime in hot mix asphalt. Report for the National Lime Association (NLA).

Shenoy, A., y Romero, P. (2002). Standardized Procedure for Analysis of Dynamic Modulus |E*| Data to Predict Asphalt Pavement Distresses. In Transportation Research Record: Journal of the Transportation Research Board, No. 1789, Transportation Research Board of the National Academies, Washington, D.C. pp. 173-182.

Solaimanian, M., D. Fedor, R. Bonaquist, A. Soltani, and V. Tandon. (2006). Simple Performance Test for Moisture Damage Prediction in Asphalt Concrete. Journal of Association of Asphalt Paving Technologists, Vol. 75, pp. 345–380.

Solaimanian, M., J. Harvey, M. Tahmoressi, and V. Tandon. (2003). Test Methods to Predict Moisture Sensitivity of Hot-Mix Asphalt Pavements. Moisture Sensitivity of Asphalt Pavements – A National Seminar. San Diego, California.

Sotil, A., Kaloush, K., y Witczak, M.W. (2004). Reduced Confined Dynamic Modulus Testing Protocol for Asphalt Mixtures. In Transportation Research Record: Journal of the Transportation Research Board, No. 1891, Transportation Research Board of the National Academies, Washington, D.C., pp. 153-162.

Tarefder, R. and Arifuzzman, M. (2011). A study of moisture damage in plastomeric polymer modified asphalt binder using functionalized AFM tips. Journal of Systemics, Cybernetics and Informatics. Vol. 9, Number 6, pp. 20-29.

Vargas Nordcbeck, A. Leiva-Villacorta, F. Aguiar-Moya, J.P. and Loria-Salazar, L. (2016). Evaluating moisture susceptibility of asphalt concrete mixtures through simple performance tests. In Transportation Research Record: Journal of the Transportation Research Board, No. 2575, Transportation Research Board of the National Academies, Washington, D.C., pp. 70-78.

Von Quintus, H. L., Mallela, J. and Jiang, J. (2003). Quantification of the Effects of Polymer-Modified Asphalt to Enhancing HMA Performance, Report Number 5504-2/1, Affiliate Committee, Asphalt Institute; Lexington, Kentucky.

Walker, D. (2014). The benefits of modified asphalts. Asphalt Institute Magazine. Vol. 29 Issue 1. Pp 13-19.

World Bank. (2016). World development indicators: Agricultural inputs. Table 3.2 Accessed Online: http://wdi.worldbank.org/table/3.2# (June 2016)

Zeiada, W.A., Kaloush, K.E., Underwood, B.S., and Mamlouk, M.E. (2014). Improved Method of Considering Air Void and Asphalt Content on Long-Term Performance of Asphalt Concrete Pavements. International Journal of Pavement Engineering. Vol 15(8), pp 718-730.

Zeiada, W., Kaloush, K., Biligiri, K., Reed, J., y Stempihar, J. (2011). Significance of confined dynamic modulus laboratory testing for asphalt concrete: Conventional, gap-graded and open-graded mixtures. In Transportation Research Record: Journal of the Transportation Research Board, No. 2210, TRB Transportation Research Board of the National Academies, Washington, D.C., pp. 9-19.

Zhao, Y., Tang, J., y Liu, L. (2012). Construction of triaxial dynamic modulus master curve for asphalt mixtures. Construction and Building Materials, Vol 37, pp. 21-26.